

AFIT/GAE/ENY/92D-20

**AD-A258 909**



**EFFECT OF THICKNESS AND PLY LAYUP ON THE  
COLLAPSE CHARACTERISTICS OF CYLINDRICAL  
COMPOSITE SHELLS WITH LARGE CUTOUTS**

**THESIS**

**JAMES C. HATFIELD**  
Captain, USAF

AFIT/GAE/ENY/92D-20

**DTIC**  
**S** **E** **D**  
ELECTE  
JAN 07 1993

Approved for public release; distribution unlimited



93-00047

205  
ps

EFFECT OF THICKNESS AND PLY LAYUP ON THE COLLAPSE  
CHARACTERISTICS OF CYLINDRICAL COMPOSITE SHELLS  
WITH LARGE CUTOUTS

THESIS

Presented to the Faculty of the School of Engineering  
of the Air Force Institute of Technology

Air University

In Partial Fulfillment of the  
Requirements for the Degree of  
Master of Science in Aeronautical Engineering

James C. Hatfield, B.S.

Captain, USAF

December 1992

Accession For	
NTIS CRA&I	<input checked="checked" type="checkbox"/>
DTIC TAB	<input type="checkbox"/>
Unannounced	<input type="checkbox"/>
Justification .....	
By .....	
Distribution /	
Availability Codes	
Dist	Avail and/or Special
A-1	

Approved for public release; distribution unlimited

DTIC QUALITY INSPECTED 1.

## **ACKNOWLEDGEMENTS**

The success of this research project would not have been possible without the guidance and support of many people. I would especially like to thank my wife, Kathy, and daughters, Shari and Michelle, for providing the inspiration and at numerous times the stamina required to finish a project of this magnitude. Many other friends and family provided invaluable support during this time especially Carlos and Louise Crain, John Hatfield, and Pete "Salty" Clarke.

I would also like to acknowledge the Flight Dynamics Laboratory for sponsoring this research, in particular, Dr. R.S. Sandhu for his kindness and technical/administrative support. The professionals with whom I worked with at FIBCA are second to none. From the beginning, Mr. Chuck Ramsey accepted me as part of his group and provided the Macintosh computer/laser printer which were instrumental in publishing a professional final product. The impetus for getting the shell panels fabricated and the experiments off the ground was a direct result of the expertise and dedication of Mr. Doug Dolvin and Mr. Jack Smith. In particular, Mr. Smith's timely advice and unsolicited support kept me from going down too many dead ends.

Thanks also to Captains Ben Wham, Steve Creaghan, Jim Greer, and Scott Schimmels, as well as, Dr. Greg Schoeppner for their help in mastering the SHELL computer code and the SuperMac. I also greatly appreciated the expertise and unrelenting support Mr. Don Cook and Mr. Larry Bates provided during the numerous tests and retests, and I wish them the best of luck with my successors.

Finally, a very special thanks to my mentor Dr. Anthony Palazotto who patiently taught me how to tackle the complexities of shell theory. It was exciting to work with a person who is truly an expert in the field of nonlinear collapse of shell structures, and I wish him the best in his future explorations into the unknown.

## TABLE OF CONTENTS

	Page
Acknowledgements_____	ii
List of Figures_____	v
List of Tables _____	xi
Symbols_____	xii
Abstract_____	xiii
I. Introduction_____	1
1. Background_____	1
2. Objective_____	5
3. Scope_____	6
II. Theory_____	7
1. Classical Laminated Plate Theory (CLPT) _____	7
2. SHELL Theory_____	14
1) SHELL's Geometry and Contracted Notation_____	17
2) SHELL's Constitutive Development_____	19
3) SHELL's Strain-Displacement Relations_____	24
III. Experimental Methods_____	27
1. Manufacturing_____	27
2. Axial Compression_____	30
IV. Finite Element Modeling_____	33
V. Results and Discussion_____	40
1. Introduction_____	40
2. Analysis of the Numerical Data from SHELL_____	40
1) Quasi-Isotropic Shell Panels_____	44
2) Cross-Ply Shell Panels_____	57
3. Experimental Results_____	69
4. Experimental Difficulties_____	93
VI. Conclusions_____	111
Bibliography_____	114

Appendix A, Experimental Test Plan	117
Appendix B, Additional Numerical / Experimental Axial Load versus Displacement Curves	129
Appendix C, Sample Input Decks Used in the SHELL Finite-Element Program	176
Vita	190

## LIST OF FIGURES

Figure	Page
1. Fiber Orientation With Respect to Global Coordinates_____	8
2. Definition of Angle $\theta$ _____	10
3. Geometry of an N-Layered Laminate_____	11
4. Axial Load versus Top Edge Displacement Curves for Typical Cylindrical Shell_____	16
5. Shell Panel Geometry With Ply Orientation Angle $\theta$ _____	18
6. Point M Located in 3-D Space by Position Vector $\bar{r}$ _____	23
7. Schematic of Curved-Panel Cutting Support_____	29
8. Experimental Setup, Axial Compression Fixture_____	31
9. Finite-Element Mesh Used For 12" X 12" Shell Panels_____	35
10. Finite-Element Mesh Used For 12" X 20" Shell Panels_____	36
11. SHELL 36 Degree-of-Freedom Element_____	37
12. Comparison of Collapse Response for 8-Ply Quasi-Isotropic Shells, With and Without Cutouts (12" X 20")_____	50
13. Comparison of Collapse Response for 16-Ply Quasi-Isotropic Shells, With and Without Cutouts (12" X 20")_____	51
14. Comparison of Collapse Response for 24-Ply Quasi-Isotropic Shells, With and Without Cutouts (12" X 20")_____	52
15. Comparison of Load vs. Top Edge Displacement Curves, For Quasi-Isotropic Shells with No Cutouts (12" X 20")_____	53
16. Comparison of Load vs. Top Edge Displacement Curves, For Quasi-Isotropic Shells with Cutouts (12" X 20")_____	54
17. Collapse Load vs. Shell Thickness (Quasi-Isotropic, No Cutouts) (12" X 20")_____	55
18. Collapse Load vs. Shell Thickness (Quasi-Isotropic, 4" Cutouts) (12" X 20")_____	56

Figure	Page
19. Comparison of Collapse Response for 8-Ply Cross-Ply Shells, With and Without Cutouts (12" X 20")	60
20. Comparison of Collapse Response for 16-Ply Cross-Ply Shells, With and Without Cutouts (12" X 20")	61
21. Comparison of Collapse Response for 24-Ply Cross-Ply Shells, With and Without Cutouts (12" X 20")	62
22. Comparison of Load vs. Top Edge Displacement Curves, For Cross-Ply Shells with No Cutouts (12" X 20")	65
23. Comparison of Load vs. Top Edge Displacement Curves, For Cross-Ply Shells with Cutouts (12" X 20")	66
24. Collapse Load vs. Shell Thickness (Cross-Ply, No Cutouts) (12" X 20")	67
25. Collapse Load vs. Shell Thickness (Cross-Ply, 4" Cutouts) (12" X 20")	68
26. Load vs. Top Edge Displacement, [0/90] <sub>2s</sub> , 4" Cutout (12" X 12")	74
27. Load vs. Radial Displacement, [0/90] <sub>2s</sub> , 4" Cutout (12" X 12")	75
28. Load vs. Radial Displacement, [0/90] <sub>2s</sub> , 4" Cutout (12" X 12")	76
29. Load vs. Top Edge Displacement, [0/90] <sub>2s</sub> , 4" Cutout (12" X 20")	77
30. Load vs. Radial Displacement, [0/90] <sub>2s</sub> , 4" Cutout (12" X 20")	78
31. Load vs. Radial Displacement, [0/90] <sub>2s</sub> , 4" Cutout (12" X 20")	79
32. Load vs. Top Edge Displacement, [0/+45/-45/90] <sub>s</sub> , 4" Cutout (12" X 20")	80
33. Load vs. Radial Displacement, [0/+45/-45/90] <sub>s</sub> , 4" Cutout (12" X 20")	81
34. Load vs. Radial Displacement, [0/+45/-45/90] <sub>s</sub> , 4" Cutout (12" X 20")	82
35. Load vs. Top Edge Displacement, [0/+45/-45/90] <sub>2s</sub> , 4" Cutout (12" X 20")	83
36. Load vs. Radial Displacement, [0/+45/-45/90] <sub>2s</sub> , 4" Cutout (12" X 20")	84
37. Load vs. Radial Displacement, [0/+45/-45/90] <sub>2s</sub> , 4" Cutout (12" X 20")	85
38. Load vs. Top Edge Displacement, [0/+45/-45/90] <sub>3s</sub> , 4" Cutout (12" X 20")	86

Figure	Page
39. Load vs. Radial Displacement, [0/+45/-45/90] <sub>3s</sub> , 4" Cutout (12" X 20")	87
40. Load vs. Radial Displacement, [0/+45/-45/90] <sub>3s</sub> , 4" Cutout (12" X 20")	88
41. Load vs. Top Edge Displacement, [0/90] <sub>6s</sub> , 4" Cutout (12" X 20")	89
42. Load vs. Radial Displacement, [0/90] <sub>6s</sub> , 4" Cutout (12" X 20")	90
43. Load vs. Radial Displacement, [0/90] <sub>6s</sub> , 4" Cutout (12" X 20")	91
44. Photograph Showing Method Used for Clamping the Horizontal Panel Edges	94
45. Photograph of [0/90] <sub>6s</sub> with a 4" X 4" Cutout, Just After Collapse	97
46. Load vs. Radial Displacement, [0/+45/-45/90] <sub>3s</sub> , No Cutout (12" X 20")	99
47. Load vs. Radial Displacement, [0/+45/-45/90] <sub>3s</sub> , No Cutout (12" X 20")	100
48. Load vs. Radial Displacement, [0/90] <sub>6s</sub> , No Cutout (12" X 20")	101
49. Load vs. Radial Displacement, [0/90] <sub>6s</sub> , No Cutout (12" X 20")	102
50. Load vs. Radial Displacement, [0/90] <sub>2s</sub> , No Cutout (12" X 12")	103
51. Load vs. Radial Displacement, [0/90] <sub>2s</sub> , No Cutout (12" X 12")	104
52. Side View of [0/90] <sub>6s</sub> Solid Shell Panel, Depicting Asymmetrical Collapse	106
53. Load vs. Top Edge Displacement, [0/90] <sub>4s</sub> , 4" Cutout (12" X 20")	109
54. Load vs. Radial Displacement, [0/90] <sub>4s</sub> , 4" Cutout (12" X 20")	110
A1. Panel Size 12" X 13" Without Cutout	122
A2. Panel Size 12" X 21" Without Cutout	123
A3. Panel Size 12" X 13" With 4" X 4" Central Cutout	124
A4. Panel Size 12" X 21" With 4" X 4" Central Cutout	125
A5. Displacement Measurements Using LVDTs	126
A6. LVDT and Strain Gage Locations, Solid Panels	127



Figure	Page
A7. LVDT and Strain Gage Locations, Panels With Cutouts_____	128
55. Load vs. Top Edge Displacement, [0/+45/-45/90] <sub>s</sub> , 4" Cutout (12" X 12")_	130
56. Load vs. Radial Displacement, [0/+45/-45/90] <sub>s</sub> , 4" Cutout (12" X 12")_____	131
57. Load vs. Radial Displacement, [0/+45/-45/90] <sub>s</sub> , 4" Cutout (12" X 12")_____	132
58. Load vs. Radial Displacement, [0/+45/-45/90] <sub>s</sub> , 4" Cutout (12" X 12")_____	133
59. Load vs. Radial Displacement, [0/90] <sub>2s</sub> , 4" Cutout (12" X 12")_____	134
60. Load vs. Top Edge Displacement, [0/+45/-45/90] <sub>s</sub> , No Cutout (12" X 12")_	135
61. Load vs. Radial Displacement, [0/+45/-45/90] <sub>s</sub> , No Cutout (12" X 12")_____	136
62. Load vs. Radial Displacement, [0/+45/-45/90] <sub>s</sub> , No Cutout (12" X 12")_____	137
63. Load vs. Radial Displacement, [0/+45/-45/90] <sub>s</sub> , No Cutout (12" X 12")_____	138
64. Load vs. Radial Displacement, [0/+45/-45/90] <sub>s</sub> , No Cutout (12" X 12")_____	139
65. Load vs. Top Edge Displacement, [0/90] <sub>2s</sub> , No Cutout (12" X 12")_____	140
66. Load vs. Radial Displacement, [0/90] <sub>2s</sub> , No Cutout (12" X 12")_____	141
67. Load vs. Radial Displacement, [0/90] <sub>2s</sub> , No Cutout (12" X 12")_____	142
68. Load vs. Radial Displacement, [0/+45/-45/90] <sub>s</sub> , 4" Cutout (12" X 20")_____	143
69. Load vs. Radial Displacement, [0/90] <sub>2s</sub> , 4" Cutout (12" X 20")_____	144
70. Load vs. Top Edge Displacement, [0/+45/-45/90] <sub>s</sub> , No Cutout (12" X 20")_	145
71. Load vs. Radial Displacement, [0/+45/-45/90] <sub>s</sub> , No Cutout (12" X 20")_____	146
72. Load vs. Radial Displacement, [0/+45/-45/90] <sub>s</sub> , No Cutout (12" X 20")_____	147
73. Load vs. Radial Displacement, [0/+45/-45/90] <sub>s</sub> , No Cutout (12" X 20")_____	148
74. Load vs. Radial Displacement, [0/+45/-45/90] <sub>s</sub> , No Cutout (12" X 20")_____	149
75. Load vs. Top Edge Displacement, [0/90] <sub>2s</sub> , No Cutout (12" X 20")_____	150
76. Load vs. Radial Displacement, [0/90] <sub>2s</sub> , No Cutout (12" X 20")_____	151
77. Load vs. Radial Displacement, [0/90] <sub>2s</sub> , No Cutout (12" X 20")_____	152
78. Load vs. Radial Displacement, [0/90] <sub>2s</sub> , No Cutout (12" X 20")_____	153

Figure	Page
79. Load vs. Radial Displacement, [0/90] <sub>2s</sub> , No Cutout (12" X 20")	154
80. Load vs. Radial Displacement, [0/+45/-45/90] <sub>2s</sub> , 4" Cutout (12" X 20")	155
81. Load vs. Radial Displacement, [0/90] <sub>4s</sub> , 4" Cutout (12" X 20")	156
82. Load vs. Radial Displacement, [0/90] <sub>4s</sub> , 4" Cutout (12" X 20")	157
83. Load vs. Top Edge Displacement, [0/+45/-45/90] <sub>2s</sub> , No Cutout (12" X 20")	158
84. Load vs. Radial Displacement, [0/+45/-45/90] <sub>2s</sub> , No Cutout (12" X 20")	159
85. Load vs. Radial Displacement, [0/+45/-45/90] <sub>2s</sub> , No Cutout (12" X 20")	160
86. Load vs. Radial Displacement, [0/+45/-45/90] <sub>2s</sub> , No Cutout (12" X 20")	161
87. Load vs. Radial Displacement, [0/+45/-45/90] <sub>2s</sub> , No Cutout (12" X 20")	162
88. Load vs. Top Edge Displacement, [0/90] <sub>4s</sub> , No Cutout (12" X 20")	163
89. Load vs. Radial Displacement, [0/90] <sub>4s</sub> , No Cutout (12" X 20")	164
90. Load vs. Radial Displacement, [0/90] <sub>4s</sub> , No Cutout (12" X 20")	165
91. Load vs. Radial Displacement, [0/90] <sub>4s</sub> , No Cutout (12" X 20")	166
92. Load vs. Radial Displacement, [0/90] <sub>4s</sub> , No Cutout (12" X 20")	167
93. Load vs. Radial Displacement, [0/+45/-45/90] <sub>3s</sub> , 4" Cutout (12" X 20")	168
94. Load vs. Radial Displacement, [0/90] <sub>6s</sub> , 4" Cutout (12" X 20")	169
95. Load vs. Top Edge Displacement, [0/+45/-45/90] <sub>3s</sub> , No Cutout (12" X 20")	170
96. Load vs. Radial Displacement, [0/+45/-45/90] <sub>3s</sub> , No Cutout (12" X 20")	171
97. Load vs. Radial Displacement, [0/+45/-45/90] <sub>3s</sub> , No Cutout (12" X 20")	172
98. Load vs. Top Edge Displacement, [0/90] <sub>6s</sub> , No Cutout (12" X 20")	173

Figure	Page
99. Load vs. Radial Displacement, $[0/90]_{6s}$ , No Cutout (12" X 20")	174
100. Load vs. Radial Displacement, $[0/90]_{6s}$ , No Cutout (12" X 20")	175

## LIST OF TABLES

Table	Page
1. SHELL Contracted Notation_____	19
2. Summary of Experimental Test Plan_____	27
3. Basic Material Properties of AS4/3501-6 Graphite/Epoxy_____	28
4. Panel Thickness_____	34
5. Numerical Global Collapse Characteristics_____	45
6. Numerical Local Collapse Characteristics_____	46
7. Numerical Maximum Bending Rotations/ Transverse Shear Strains_____	47
8. Comparison Between Experimental and Numerical Collapse Loads_____	71

## SYMBOLS

$\sigma$	Normal Stress
$\tau$	Shear Stress
$\theta$	Lamina Orientation Angle With Global System
$Q_{ij}$	Reduced Stiffnesses
$\bar{Q}_{ij}$	Transformed Reduced Stiffnesses
$\epsilon$	Normal Strain
$\gamma$	Shear Strain
$G_{12}$	In-Plane Shear Modulus of Elasticity
$G_{13}, G_{23}$	Transverse Shear Moduli of Elasticity
$E_1$	Longitudinal Modulus of Elasticity
$E_2, E_3$	Transverse Moduli of Elasticity
$\nu$	Poisson's Ratio
$\kappa_x, \kappa_y, \kappa_{xy}$	Curvatures at the Midplane Surface
$u, v, w$	Displacements in X, S, and Z Directions
$N_x, N_y, N_{xy}$	Resultant Forces
$M_x, M_y, M_{xy}$	Resultant Moments
$A_{ij}$	Extensional Stiffnesses
$B_{ij}$	Coupling Stiffnesses
$D_{ij}$	Bending Stiffnesses
$\Pi_p$	Potential Energy in a Body
$U$	Internal Strain Energy
$W$	Work Done by Applied Forces
$R$	Radius of Curvature
$\psi$	Rotation of Elastic Curve Due to Bending

### ABSTRACT

This study involved a numerical and experimental investigation of the geometric instability (collapse loads/displacements) of vertically unsupported graphite/epoxy cylindrical shell panels undergoing axial compression. The test specimens, with effective dimensions of either 12" X 12" or 12" X 20", were fabricated using the Hercules AS4/3501-6 material system and had 12" radii of curvature. Symmetric quasi-isotropic and cross-ply laminates, with and without 4" X 4" centralized cutouts, were investigated for three different thicknesses: 8, 16, and 24 plies. The experimental data was compared to results from SHELL, a geometrically nonlinear finite-element computer program which incorporates a parabolic transverse shear strain distribution through the thickness.

Good correlation was obtained for shells with large cutouts between the SHELL numerical data and the experimental results. The best correlation between numerically-derived and experimental collapse loads occurred with the 16-ply shell panels. This research verified that the SHELL finite-element program will provide good predictions of the collapse characteristics of shell structures undergoing large displacements and moderately large rotations.

It was found that the largest surface bending rotations, radial displacements, and transverse shear strains occurred along unsupported vertical edges and around the four corners of a square cutout. In addition, the magnitudes of transverse shear strain increased with increasing panel thickness and increased significantly when a large cutout was placed in a shell.

There were indications that under large displacement and moderately large rotation conditions, the collapse of cross-ply shells was more affected by transverse shear strain than the collapse of quasi-isotropic shells. In addition, when a large cutout was present, the cross-ply shells responded more flexibly than the quasi-isotropic shells.

# **EFFECT OF THICKNESS AND PLY LAYUP ON THE COLLAPSE CHARACTERISTICS OF CYLINDRICAL COMPOSITE SHELLS WITH LARGE CUTOUTS**

## **1. INTRODUCTION**

### **1.1 *Background***

The use of composite materials in aircraft structures has increased significantly during the last decade. In particular, the material used most often is graphite/epoxy. This material is composed of graphite (carbon) fibers held together by an epoxy matrix. Aircraft designers use composite materials to increase the overall structure's strength-to-weight ratio and to enhance a particular component's stiffness. Composite materials provide the aircraft designer with the capability of tailoring the material properties of a structure to withstand the anticipated load environment. This material tailoring leads to lighter structural components than similar metal structures which is critical in aerospace design. An overall lighter aircraft, with no loss of internal volume, equates to an increase in cargo capacity (passengers, weapons, supplies) with no increase in fuel consumption.

Due to the required aerodynamic shapes of aircraft fuselages and wings, graphite/epoxy shell structures are often used. These structural components may be used in either reinforced or unreinforced forms. In addition, it is occasionally necessary to cut square holes in these structures for access ports. These holes or structural discontinuities change the collapse characteristics of the structure, which affects how and when a component will no longer be able to support increased loading. Therefore, a greater understanding of the geometric collapse characteristics of graphite/epoxy shell structures, with and without cutouts, needs to be achieved. Due to the geometric nature of curved

cylindrical shells, the study of these structures requires nonlinear analysis whenever compressive loading is applied. This nonlinearity is even more pronounced as the thickness of the shell panel and the area of the cutout region increases [7].

The nonlinear behavior of axially compressed graphite/epoxy shells with cutouts has been studied primarily by the Air Force Institute of Technology (AFIT) and the National Aeronautics and Space Administration (NASA). Geometric instability (collapse) analysis of cylindrical shell panels has been performed experimentally and then modeled with computer codes using finite-element theory. Analytical shell models developed in the past, using flat moderate-rotation elements have accurately predicted panel response except for geometries with large cutouts (greater than 10 percent of panel area) [28]. Structural analysis using finite-element programs to determine collapse states has been difficult and expensive, with limited accuracy. With the advent of higher-speed computers, more accurate programs involving cylindrically-shaped elements can be employed.

The term collapse, with regard to a structure, refers to a sudden material failure causing irreparable damage which affects the strength of the component. Collapse can be caused by impact, fracture, creep, etc.; but the research in this study will focus on the collapse phenomena due to loss of stability. This type of research involves the computation of the nonlinear relationship between applied loads and the resulting deformations or displacements. Finite-element computer codes, which model the thru-the-thickness transverse shear stress distribution, have proven to be the most accurate [6, 25, 26]. Whenever a new finite-element algorithm is developed, the data the program produces must be checked experimentally while using the same loading method and boundary conditions. This enables understanding of the code's strengths, as well as, its limitations.

The majority of previous research related to shells has dealt with geometrically linear problems. Geometrical nonlinearities, of interest in this research, can result from large displacements and rotations of the fibers of a differential volume element that has



undergone a transformation from some original configuration. Other than the recently published book by Palazotto and Dennis [20], few references were found that addressed collapse of composite shell structures with large cutouts, which requires a nonlinear analysis. Of those found that dealt with cutouts, most were experiments and computer analyses of shell panels with circular holes [13, 22]. In contrast, numerous studies have been published on isotropic plates and cylindrical shell panels without cutouts.

One of the more comprehensive research publications available on the collapse characteristics of composite cylindrical shell panels with large square cutouts was authored by Scott A. Schimmels, which included results of the research he performed for his master's degree thesis [25]. Schimmels summarized the significant findings of AFIT and NASA researchers, where most work of this nature has occurred. From these organizations, some of the more published researchers in this area include N.F. Knight, J.H. Starnes, S.T. Dennis, and A.N. Palazotto. A summary of their research findings, along with other AFIT researchers, is included in the remaining paragraphs of this section and the published works are noted in the bibliography.

The collapse characteristics of composite shells are dependent upon the ply layup and the size of the cutout [11]. As the surface area of the cutout is increased, the collapse loads decrease and the nonlinear effects become more pronounced [15]. In fact, larger cutouts (greater than 3 percent of the panel surface area) induce nonlinear load/displacement responses throughout most of the loading range [28]. Up to this size of cutout, good agreement is consistently achieved between experimental data and commercially available finite-element programs. During Tisler's study [28], the analytical response obtained from Lockheed's Structural Analysis for General Shells (STAGSC-1) computer code for shells with a 4" X 4" cutout was less stiff than the experimental response. This disagrees with the expected stiffer analytical response, which is normally obtained from similar displacement-based finite-element formulations. Dennis and Palazotto concluded that the

magnitude of the panel-surface rotations around the cutout, measured experimentally at approximately 10 degrees, may have exceeded the intermediate nonlinear capabilities of the STAGSC-1 finite-element program [7]. This conclusion is consistent with similar findings by Knight and Starnes in their research of axially compressed composite panels with larger circular holes [13].

Dennis and Palazotto developed a theory to address the limitations found in the STAGSC-1 formulation [8]. Their theory can handle the large displacements and moderately large rotations caused by geometric nonlinearities in small strain situations (no plasticity). In addition, the theory includes a parabolic transverse shear stress and strain formulation throughout the shell thickness. This part of the theory is critical in order to accurately predict collapse loads for thicker panels on the order of 16 and 24 plies. This theory has been incorporated into a finite-element computer code developed at AFIT called SHELL. SHELL employs a modified Newton-Raphson (MNR) iterative technique, which traces the equilibrium path up to and through the collapse load. The MNR method differs from the Newton-Raphson method in that the tangent-stiffness matrix is not updated or is updated infrequently [5]. Thus, for problems involving numerous degrees of freedom, expensive repetitions of forming and reducing the tangent-stiffness matrix can be avoided. However, more iterative cycles are needed in order to reach a reasonably prescribed convergence tolerance. In addition, Bergan [4] stated that the Newton-Raphson technique, without modifications, is not used because in addition to the already mentioned inefficiency, it is sometimes unreliable due to solution divergence problems. The SHELL computer algorithm uses cylindrically-curved finite elements as opposed to the traditional flat elements used in STAGSC-1, in order to capture the shell bending-membrane coupling. Initial comparisons by Schimmels and Palazotto [26] between experimental data on quasi-isotropic cylindrical shells with orientations of  $[0/+45/-45/90]_s$  and the SHELL computer analysis showed good agreement. However, more extensive experimental research is

needed in order to verify the SHELL program's accuracy in predicting collapse loads and displacements for a wider range of shell panel configurations, panel thicknesses, and composite ply layups.

## 1.2 *Objective*

The objective of this research was to study the instability of graphite/epoxy shell panels, which have cylindrical shell geometry. A collapse analysis (loads/displacements) was performed on panels, with and without large (either 7% or 11% of the planform area) square cutouts (centrally located), while the panels underwent axial compression. The test specimens were fabricated using the AS4/3501-6 graphite/epoxy material system, which is commonly used in the aerospace industry. The experimental data was collected to check the accuracy of the SHELL computer program, which was developed at AFIT by Scott T. Dennis as part of his dissertation [6].

Another objective of this research effort was to analyze the effects of increased panel thickness on the collapse characteristics. Previous studies of this nature involved fairly thin shells (up to eight laminate plies) where the effects of thru-the-thickness shear was not a major factor. This study involved experiments and computer analyses of thicker shells (16 and 24 plies), where the deformations are increasingly dominated by the transverse shear stresses. These shear stresses contribute to larger panel-surface rotations and severe bending gradients near the cutouts and at unsupported edges.

Finally, this research investigated the collapse responses of longer (in axial length) panels which more closely model actual fuselage/wing structural components. The laminate orientations studied were the cross-ply  $[0/90]_{2s}$ ,  $[0/90]_{4s}$ ,  $[0/90]_{6s}$ ; and the quasi-isotropics  $[0/+45/-45/90]_s$ ,  $[0/+45/-45/90]_{2s}$ , and  $[0/+45/-45/90]_{3s}$ . These types of laminates are often used in aerospace design.

### 1.3 *Scope*

A total of 16 different panel configurations were tested and compared with results from the SHELL finite-element program. Half of the shell panels investigated had 4" X 4" centralized square cutouts, while the remaining were solid (no cutouts) panels. Analysis was performed on eight configurations dealing with fairly thin (0.04") cylindrical shells. The remaining eight configurations investigated thicker shell collapse behavior. At this time, no known research efforts have been directed at analyzing the collapse behavior of thicker (greater than 0.06") composite shells with square cutouts. In addition to the three panel thicknesses investigated, two different ply layups (cross-ply and quasi-isotropic) and two different axial lengths (12" and 20") were studied to determine how each affected panel collapse.

## 2. THEORY

### 2.1 Classical Laminated Plate Theory (CLPT)

In order to understand the global behavior of composite cylindrical shells undergoing axial compression, the basic constitutive relations for each individual lamina (or ply) must first be understood. The research in this thesis assumes linearly-elastic (small strain,  $\epsilon < 0.03$ ) material response; however, complexity in laminate response arises due to the non-uniform orientation of the plies. A review of classical laminated plate theory will aid in an understanding of the affect ply orientations have on the laminate's stress-strain relations. The reader may want to review reference [12] for a more indepth development of these relations.

The stress-strain relations in principal material coordinates (see Fig. 1) for an orthotropic material, assuming plane-stress conditions ( $\sigma_3 = \sigma_4 = \sigma_5 = 0$ ), are given by:

$$\begin{Bmatrix} \sigma_1 \\ \sigma_2 \\ \tau_{12} \end{Bmatrix} = \begin{bmatrix} Q_{11} & Q_{12} & 0 \\ Q_{12} & Q_{22} & 0 \\ 0 & 0 & Q_{66} \end{bmatrix} \begin{Bmatrix} \epsilon_1 \\ \epsilon_2 \\ \gamma_{12} \end{Bmatrix} \quad (1)$$

where  $\epsilon_1$  and  $\epsilon_2$  are normal strains and  $\gamma_{12}$  is the shear strain in the 1-2 plane. Throughout this research effort, it is assumed that the material is transversely isotropic with respect to planes parallel to the 2-3 plane [29]. In other words,  $E_2 = E_3$  and  $G_{12} = G_{13}$ .

The  $Q_{ij}$ 's are the reduced stiffnesses in terms of engineering constants as follows:

$$\begin{aligned} Q_{11} &= E_1 / (1 - \nu_{12} \nu_{21}) \\ Q_{12} &= \nu_{12} E_2 / (1 - \nu_{12} \nu_{21}) = \nu_{21} E_1 / (1 - \nu_{12} \nu_{21}) \\ Q_{22} &= E_2 / (1 - \nu_{12} \nu_{21}) \\ Q_{66} &= G_{12} \end{aligned} \quad (2)$$

Where the  $E_1$  and  $E_2$  are Young's moduli in the 1 and 2 directions, respectively.  $\nu_{ij}$  is Poisson's ratio for transverse strain in the  $j$  direction when loaded in the  $i$  direction.  $G_{12}$  is the shear modulus in the 1-2 plane.

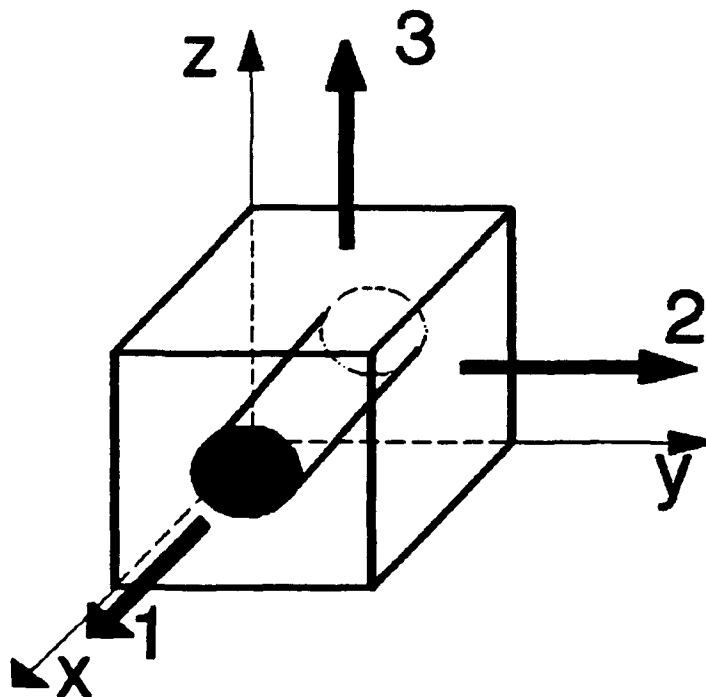


Figure 1. Fiber Orientation With Respect to Global Coordinates

The preceding stresses and strains were defined with respect to the principal material directions of an orthotropic material. If the principal directions of a certain lamina do not coincide with the global coordinate directions, then the stress-strain relations are defined in terms of transformed reduced stiffnesses, the  $\bar{Q}_{ij}$ 's. The  $\bar{Q}_{ij}$ 's are functions of the original  $Q_{ij}$ 's and an angle  $\theta$  from the global coordinate system as shown in Figure 2. Thus, the stress-strain relations with respect to the global X-Y coordinate system are:

$$\begin{Bmatrix} \sigma_x \\ \sigma_y \\ \tau_{xy} \end{Bmatrix} = \begin{bmatrix} \bar{Q}_{11} & \bar{Q}_{12} & \bar{Q}_{16} \\ \bar{Q}_{12} & \bar{Q}_{22} & \bar{Q}_{26} \\ \bar{Q}_{16} & \bar{Q}_{26} & \bar{Q}_{66} \end{bmatrix} \begin{Bmatrix} \epsilon_x \\ \epsilon_y \\ \gamma_{xy} \end{Bmatrix} \quad (3)$$

where the material coefficients,  $Q_{ij}$ , are symmetric and defined as:

$$\begin{aligned} \bar{Q}_{11} &= Q_{11}\cos^4\theta + 2(Q_{12} + 2Q_{66})\sin^2\theta \cos^2\theta + Q_{22}\sin^4\theta \\ \bar{Q}_{12} &= (Q_{11} + Q_{22} - 4Q_{66})\sin^2\theta \cos^2\theta + Q_{12}(\sin^4\theta + \cos^4\theta) \\ \bar{Q}_{22} &= Q_{11}\sin^4\theta + 2(Q_{12} + 2Q_{66})\sin^2\theta \cos^2\theta + Q_{22}\cos^4\theta \\ \bar{Q}_{16} &= (Q_{11} - Q_{12} - 2Q_{66})\sin\theta \cos^3\theta + (Q_{12} - Q_{22} + 2Q_{66})\sin^3\theta \cos\theta \\ \bar{Q}_{26} &= (Q_{11} - Q_{12} - 2Q_{66})\sin^3\theta \cos\theta + (Q_{12} - Q_{22} + 2Q_{66})\sin\theta \cos^3\theta \\ \bar{Q}_{66} &= (Q_{11} + Q_{22} - 2Q_{12} - 2Q_{66})\sin^2\theta \cos^2\theta + Q_{66}(\sin^4\theta + \cos^4\theta) \end{aligned} \quad (4)$$

For a more detailed derivation of the transformed reduced stiffnesses, see reference [12].

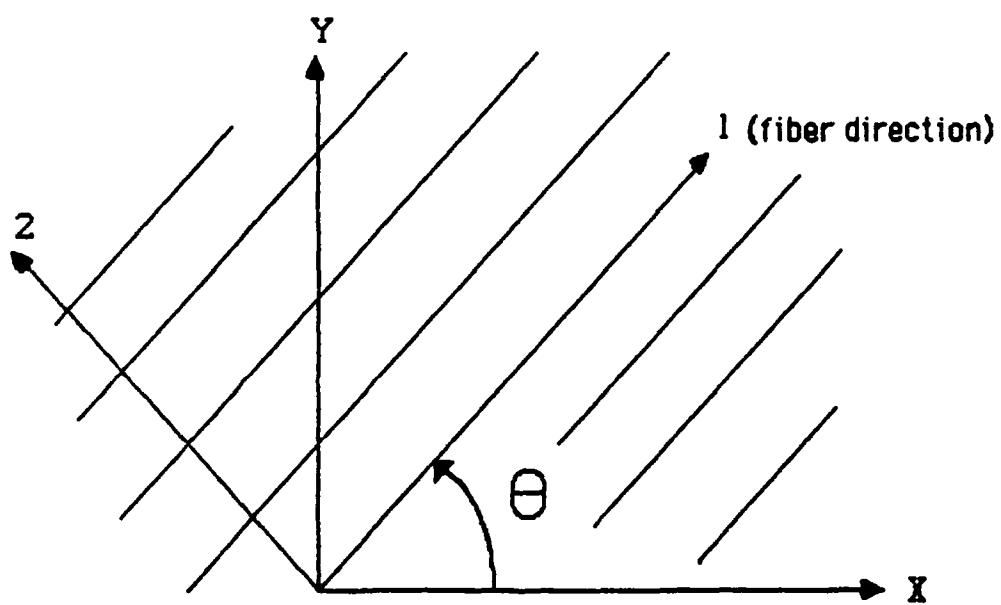


Figure 2. Definition of Angle  $\theta$



The above equations were derived for an individual ply. In order to determine the stress-strain behavior through the laminate thickness, each  $k$ th ply may be characterized by:

$$\{\sigma\}_k = [\bar{Q}_{ij}]_k \{\epsilon\}_k \quad (5)$$

where the  $k$ th ply is defined by its distance from the midplane of the laminate as shown in Figure 3.

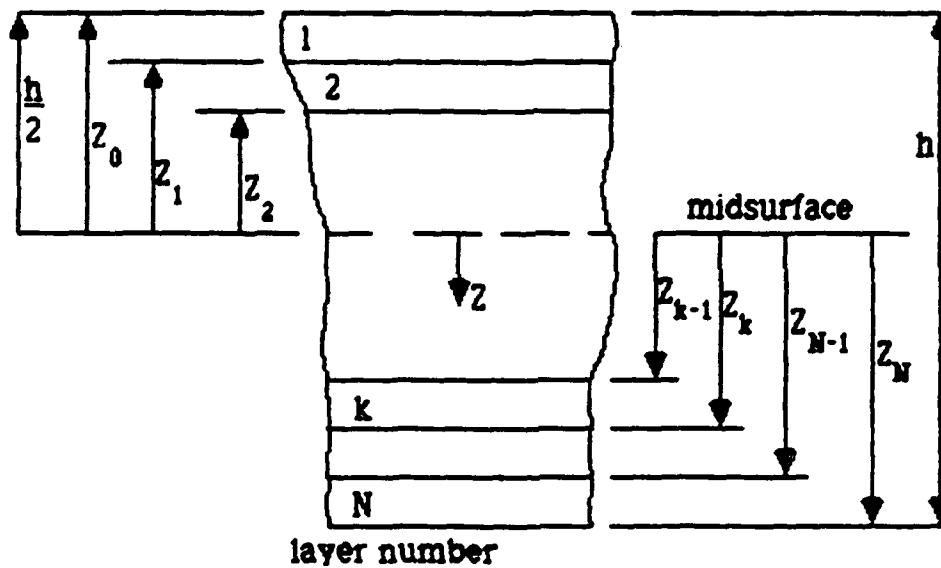


Figure 3. Geometry of an N-Layered Laminate

Certain assumptions must be made in order to extend the theory from single lamina to a multilayered laminate. First, each lamina can be characterized as an orthotropic material, whereby the individual properties of the composite constituents, fibers and matrix, are "smeared" together [6]. Second, the laminate is perfectly bonded between layers, whereby the interply adhesive is assumed to have infinitesimal thickness but infinite shear stiffness. This assumption eliminates concern with interlaminar shear effects and allows for continuous displacements within each lamina. Therefore, no lamina can slip relative to the other lamina. The final assumption involves the Kirchhoff-Love hypothesis for a thin laminate, which states that normal sections remain plane and normal to the midplane after bending.

By applying the Kirchhoff-Love hypothesis and knowing the midplane strains and curvatures ( $\epsilon_x^0, \epsilon_y^0, \gamma_{xy}^0, \kappa_x, \kappa_y, \kappa_{xy}$ ), the strain-curvature relationship for a laminate becomes:

$$\begin{Bmatrix} \epsilon_x \\ \epsilon_y \\ \gamma_{xy} \end{Bmatrix}_k = \begin{Bmatrix} \epsilon_x^0 \\ \epsilon_y^0 \\ \gamma_{xy}^0 \end{Bmatrix} + Z \begin{Bmatrix} \kappa_x \\ \kappa_y \\ \kappa_{xy} \end{Bmatrix} \quad (6)$$

where,

$$\begin{aligned} \epsilon_x^0 &= u_{0,x} \\ \epsilon_y^0 &= v_{0,y} \\ \gamma_{xy}^0 &= u_{0,y} + v_{0,x} \end{aligned} \quad (7)$$

and,

$$\begin{aligned} \kappa_x &= -w_{0,xx} \\ \kappa_y &= -w_{0,yy} \\ \kappa_{xy} &= -2w_{0,xy} \end{aligned} \quad (8)$$

The stress in the kth ply can be determined by substituting Eq (6) back into Eq (5). Then, the resultant forces and moments acting on the laminate can be obtained by

integrating the stresses through each ply thickness and summing the contributions over the entire laminate ( $k = 1$  to  $k = N$ ). Since the stiffness matrix  $[\bar{Q}_{ij}]$  is constant throughout each ply, the equations for the resultant forces  $\{N_{ij}\}$  and the resultant moments  $\{M_{ij}\}$  become:

$$\begin{Bmatrix} N_X \\ N_Y \\ N_{XY} \end{Bmatrix} = \begin{bmatrix} A_{11} & A_{12} & A_{16} \\ A_{12} & A_{22} & A_{26} \\ A_{16} & A_{26} & A_{66} \end{bmatrix} \begin{Bmatrix} \epsilon_x^0 \\ \epsilon_y^0 \\ \gamma_{xy}^0 \end{Bmatrix} + \begin{bmatrix} B_{11} & B_{12} & B_{16} \\ B_{12} & B_{22} & B_{26} \\ B_{16} & B_{26} & B_{66} \end{bmatrix} \begin{Bmatrix} \kappa_x \\ \kappa_y \\ \kappa_{xy} \end{Bmatrix} \quad (9)$$

$$\begin{Bmatrix} M_X \\ M_Y \\ M_{XY} \end{Bmatrix} = \begin{bmatrix} B_{11} & B_{12} & B_{16} \\ B_{12} & B_{22} & B_{26} \\ B_{16} & B_{26} & B_{66} \end{bmatrix} \begin{Bmatrix} \epsilon_x^0 \\ \epsilon_y^0 \\ \gamma_{xy}^0 \end{Bmatrix} + \begin{bmatrix} D_{11} & D_{12} & D_{16} \\ D_{12} & D_{22} & D_{26} \\ D_{16} & D_{26} & D_{66} \end{bmatrix} \begin{Bmatrix} \kappa_x \\ \kappa_y \\ \kappa_{xy} \end{Bmatrix}$$

The  $[A_{ij}]$ ,  $[D_{ij}]$ , and  $[B_{ij}]$  matrices are referred to as the extensional stiffness matrix, bending stiffness matrix, and coupling stiffness matrix, respectively. The extensional stiffness terms relate the resultant forces to the midplane strains, while the bending stiffness terms relate the resultant moments to the laminate curvatures. The coupling stiffness terms exist if the laminate layup is not symmetric with respect to the midplane. An unsymmetrical layup will lead to a coupling between the bending and extension of a laminate. In other words, for a specimen with nonzero  $B_{ij}$  terms, application of a normal tensile load could produce twisting as well as the expected extensional and shear deformation. Unsymmetrical laminates are also prone to warping during the curing cycle. For this research effort, only symmetric laminates were investigated, and therefore the  $B_{ij}$  terms were always equal to zero.

## 2.2 SHELL Theory

The analysis involved in this research effort is concerned with static loading, and thus the problem is one of solving the equation of static equilibrium, namely,  $\Sigma \text{ Forces} = 0$ . During static equilibrium (when the displacements of the structure are those of the equilibrium state), the potential energy ( $\Pi_p$ ) of deformation must be at a minimum, and the first variation of potential energy ( $\delta\Pi_p$ ) will be zero [23]. This yields the equilibrium equation. For geometric instability analysis (either linear or nonlinear), the second variation ( $\delta^2\Pi_p$ ) is also zero at the collapse point. The nonlinear studies considered in this work seek a limit point in the loading curve. Curved cylindrical shell panels undergo post buckling at decreased loads only, so the first limit point is the actual collapse load, as seen in Figure 4.

As shown in Figure 4, the solution derived by linear bifurcation analysis may be either higher or lower than the actual solution [2]. For a cylindrical shell panel without cutouts, the bifurcation value is too high. While for panels with large cutouts, the bifurcation values become too low [28]. Thus, the use of a bifurcation analysis is limited and will not be used in this thesis.

In considering the classical laminated theory, it is possible to obtain certain features of a potential energy approach. Thus, some detail involving this functional approach is included. The total potential energy in a body is the internal strain energy minus the work of the applied forces, or:

$$\Pi_p = U - W \quad (10)$$

Both  $U$  and  $W$  can be calculated based upon the displacement field using:

$$U = \frac{1}{2} \int \int \{\epsilon^0\}^T [N] \{\epsilon^0\} dA \quad (11)$$

where,

$$\{\epsilon^0\} = \begin{Bmatrix} \epsilon_x^0 \\ \epsilon_y^0 \\ \gamma_{xy}^0 \\ \kappa_x \\ \kappa_y \\ 2\kappa_{xy} \end{Bmatrix} \quad (12)$$

and,

$$[N] = \begin{bmatrix} [A] & [B] \\ [B] & [D] \end{bmatrix} \quad (13)$$

The work done by the applied forces is represented by:

$$W = \{d\}^T \{F\} \quad (14)$$

where,  $\{d\}$  is the vector of displacements

$\{F\}$  is the vector of externally applied forces

For applied displacements, the SHELL finite-element program calculates the loads required to achieve the specified top edge displacements (U). The SHELL algorithm was developed at AFIT in 1988 by Scott T. Dennis as part of his Ph.D. dissertation [6]. SHELL's primary capability is in the analysis of nonlinear behavior of thin cylindrical-shell structures undergoing large displacements and moderately large rotations, with the added feature of incorporating a parabolic distribution for transverse shear strain through the shell's thickness. The basic finite element used in SHELL is a cylindrically curved element that can exactly match the curvature of the shell surface. The nonlinear analysis is based upon either the Donnell approximations (similar to Von Karman plate relations but with curvature incorporated within the kinematic equations) or the exact nonlinear kinematic

relations. The computer runs involved in this research employed the more exact nonlinear option in order to more accurately capture the moderately large rotations (on the order of 9-12 degrees). According to research performed by Silva [27], as the magnitude of the rotations approach 15 degrees, the Donnell solution becomes appreciably stiffer than the SHELL solution. In fact, the Donnell equations develop significant inaccuracy when rotations exceed 15 degrees.

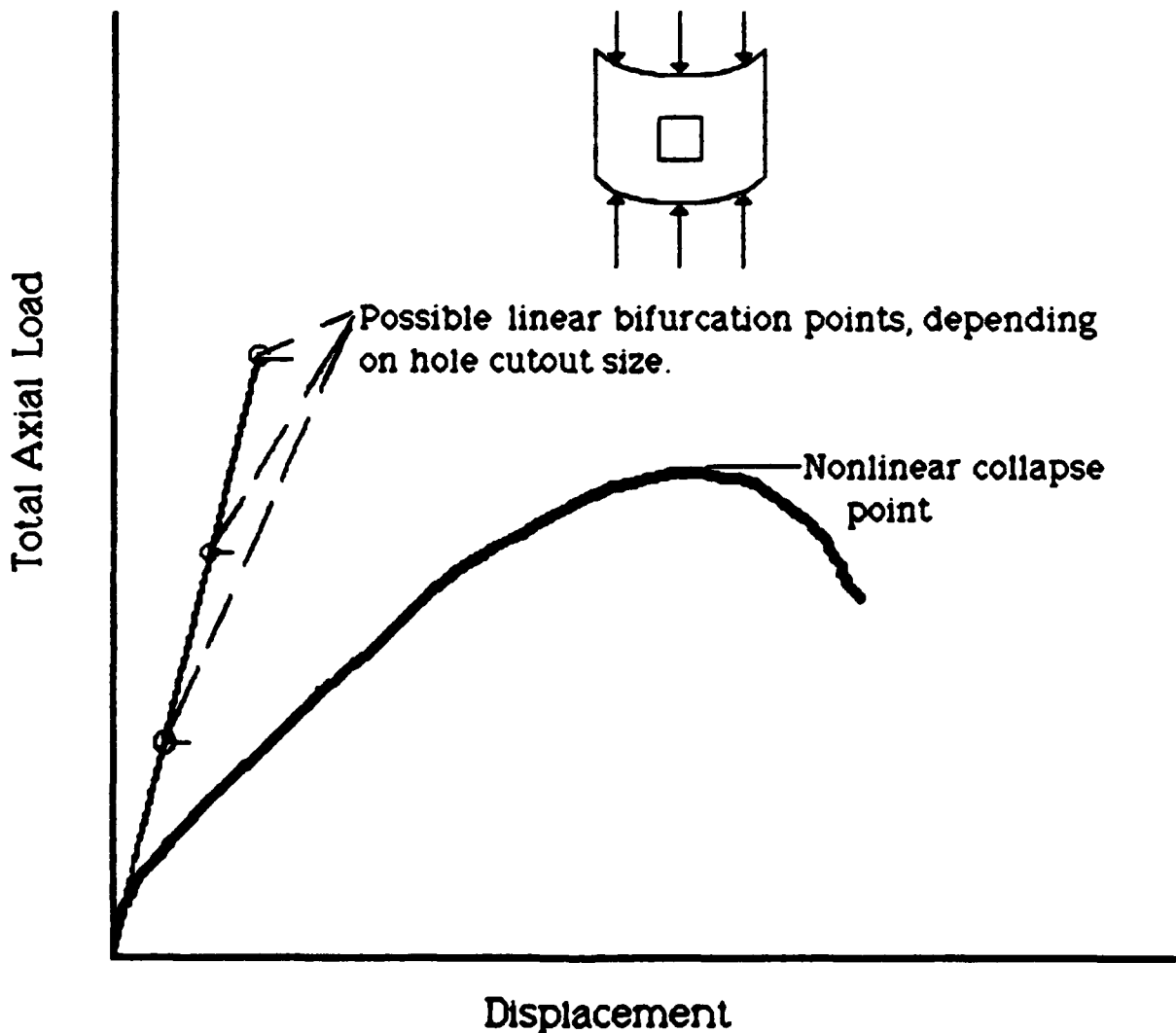


Figure 4. Axial Load versus Top Edge Displacement Curves for Typical Cylindrical Shell

The SHELL code has not been developed beyond the research phase and is therefore limited to flat plate and cylindrical shell geometries, while using only rectangular elements. In addition, material linearity is assumed in the element formulation. However, incorporation of thru-the-thickness shear while maintaining a two-dimensional analysis, allows for consistently more reliable results with fairly reasonable computer run times by ensuring no spurious zero-energy modes exist [3]. SHELL's transverse shear formulation becomes even more important in accurately predicting experimental results for thicker shells.

#### 2.2.1 *SHELL's Geometry and Contracted Notation*

The curvilinear orthogonal coordinate system used in the SHELL formulation is shown in Figure 5. The X-axis lies along the axial length of the shell structure, the S-axis follows the circumference, and the Z-axis is positive in the direction of the center of curvature and everywhere normal to the shell's midplane. The plane formed by the X and S axes lies in the center of the panel's thickness dimension, so that the laminate thickness coordinate (Z) is negative on the outer surface and positive on the inner surface. Displacements along the X, S, and Z axes are  $u$ ,  $v$ , and  $w$  respectively. Subscripts denoting the stress and strain orientation are summarized in Table 1 (also refer to Figure 1 for clarification).

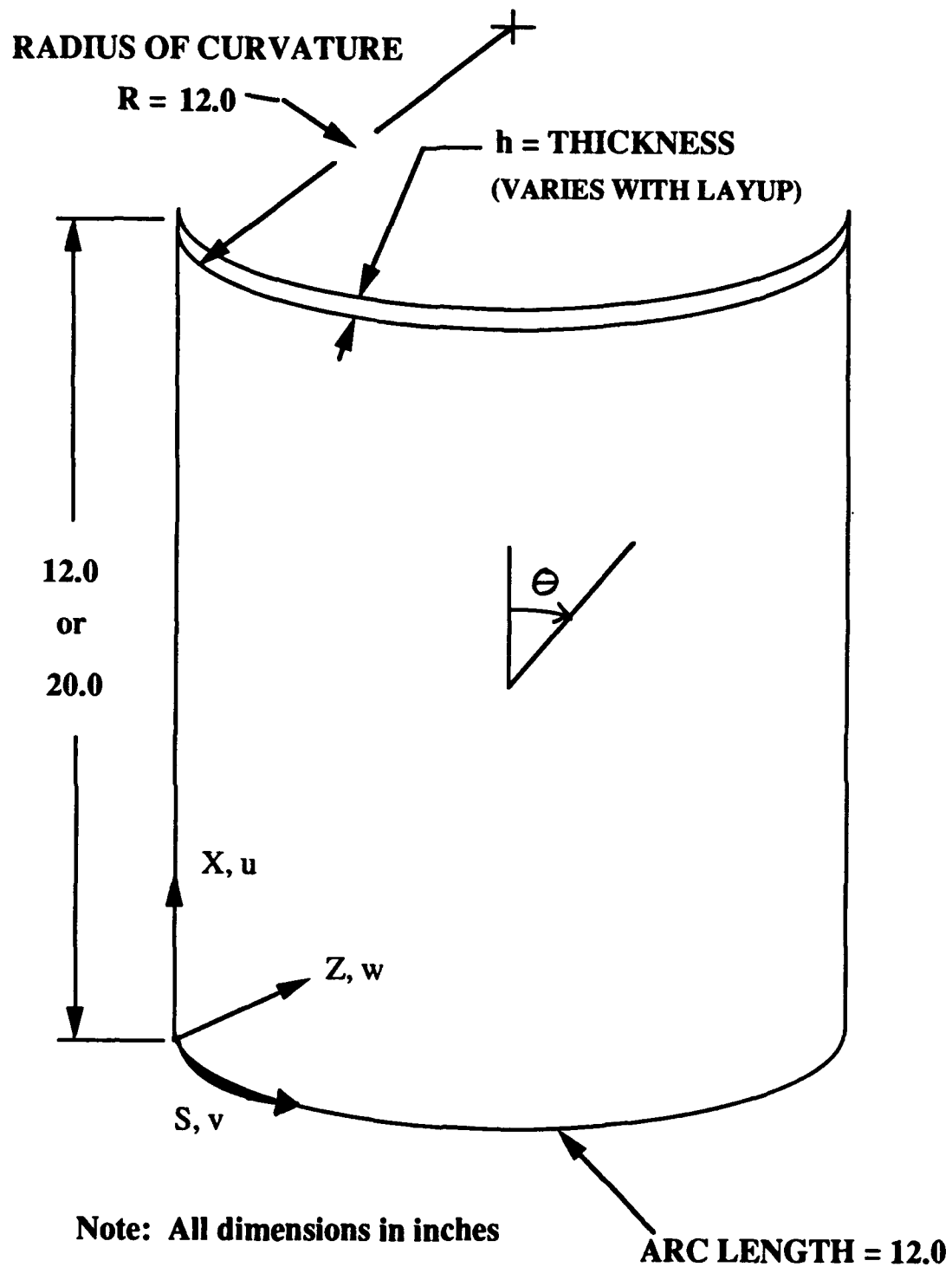


Figure 5. Shell Panel Geometry With Ply Orientation Angle  $\theta$



*Table 1. SHELL Contracted Notation [ 25]*

<u>Stress</u>	<u>Strain</u>	<u>Cylindrical Coordinates</u>
$\sigma_{11} = \sigma_1$	$\epsilon_{11} = \epsilon_1$	X = 1
$\sigma_{22} = \sigma_2$	$\epsilon_{22} = \epsilon_2$	S = 2
$\sigma_{33} = \sigma_3$	$\epsilon_{33} = \epsilon_3$	Z = 3
$\sigma_{23} = \sigma_4$	$\epsilon_{23} = \epsilon_4$	S - Z = 4
$\sigma_{13} = \sigma_5$	$\epsilon_{13} = \epsilon_5$	X - Z = 5
$\sigma_{12} = \sigma_6$	$\epsilon_{12} = \epsilon_6$	X - S = 6

### 2.2.2 SHELL's Constitutive Development

In developing the constitutive relations for SHELL, a modified plane stress condition is assumed. This modified condition allows  $\sigma_3 = 0$  (as expected) but it assumes  $\sigma_4$  and  $\sigma_5$  are not equal to zero, thereby incorporating nonzero thru-the-thickness shear stress into the finite-element code [6]. Thus, the reduced stiffness constitutive relations become [1]:

$$\begin{Bmatrix} \sigma_1 \\ \sigma_2 \\ \sigma_6 \\ \sigma_4 \\ \sigma_5 \end{Bmatrix} = \begin{bmatrix} Q_{11} & Q_{12} & 0 & 0 & 0 \\ Q_{12} & Q_{22} & 0 & 0 & 0 \\ 0 & 0 & Q_{66} & 0 & 0 \\ 0 & 0 & 0 & Q_{44} & 0 \\ 0 & 0 & 0 & 0 & Q_{55} \end{bmatrix} \begin{Bmatrix} \epsilon_1 \\ \epsilon_2 \\ \epsilon_6 \\ \epsilon_4 \\ \epsilon_5 \end{Bmatrix} \quad (15)$$

where, in terms of engineering constants the  $Q_{ij}$ 's are the same as in Eq (2), except for two additional terms:

$$Q_{44} = G_{23}$$

$$Q_{55} = G_{13}$$

The in-plane strains ( $\epsilon_1$ ,  $\epsilon_2$ , and  $\epsilon_6$ ) are developed by using the full nonlinear compliment of the Green's strain tensor, which includes all the nonlinear displacement terms in Eqs (16) and (17). Eq (16) represents the physical strains and the  $h_i / h_j$  are coordinate system scale factors based on the metric tensor. This metric tensor links the Cartesian coordinate system ( $X_1, X_2, X_3$ ) with an arbitrary orthogonal curvilinear coordinate system ( $Y_1, Y_2, Y_3$ ), through the invariant property of length (see Figure 6). However, the transverse shear strains ( $\epsilon_4$  and  $\epsilon_5$ ) are developed by using only the linear displacement terms in the Green's strain tensor components. Because the shell structure is relatively thin with respect to its planform dimensions, the nonlinear strain-displacement terms are considered as higher order for the transverse strains. According to Palazotto and Dennis [20], use of exact  $\epsilon_1$ ,  $\epsilon_2$ , and  $\epsilon_6$  along with linear  $\epsilon_4$  and  $\epsilon_5$  ( $\epsilon_3$  is considered negligible with the  $\sigma_3 = 0$  assumption) results in the following limits for the magnitudes of rotation. If  $\epsilon_4$  and  $\epsilon_5$  are negligible compared to  $\epsilon_1$ ,  $\epsilon_2$ , and  $\epsilon_6$  then this theory constitutes a large rotation theory since exact strain-displacement relations are assumed for the important strains. However, if  $\epsilon_4$  and  $\epsilon_5$  are not negligible compared to the in-plane strains, then the allowable rotations are limited to some degree. Librescu [17] shows that nonlinear (but not exact) in-plane strains coupled with linear transverse shear strains define a consistent moderate rotation theory. Therefore, the Palazotto and Dennis approach (which uses exact nonlinear in-plane strains) should always accurately follow rotations greater than what the moderate theories permit. Palazotto and Dennis refer to their approach as a large displacement and simplified large rotation (SLR) theory. It should be noted that the stresses in Eq (15) are components of the 2nd Piola-Kirchhoff stress tensor. Although the material properties ( $Q_{ij}$ 's) in Eq (15) were obtained with respect to the Eulerian or Cauchy coordinate system while the stress and strain tensors are Lagrangian formulations, the constitutive relations are assumed to be valid for cases which involve small strains, large

displacements, and moderately large rotations. This development is used in the SHELL algorithm.

$$\epsilon_{ij} = \gamma_{ij} / (h_i h_j) \quad (\text{no sum}) \quad (16)$$

$$\begin{aligned} \gamma_{11} &= h_1 \frac{\partial u_1}{\partial y_1} + \frac{h_1 u_2}{h_2} \frac{\partial h_1}{\partial y_2} + \frac{h_1 u_3}{h_3} \frac{\partial h_1}{\partial y_3} \\ &\quad + \frac{1}{2} \left( \frac{\partial u_1}{\partial y_1} + \frac{u_2}{h_2} \frac{\partial h_1}{\partial y_2} + \frac{u_3}{h_3} \frac{\partial h_1}{\partial y_3} \right)^2 \\ &\quad + \frac{1}{2} \left( \frac{\partial u_2}{\partial y_1} - \frac{u_1}{h_2} \frac{\partial h_1}{\partial y_2} \right)^2 + \frac{1}{2} \left( \frac{\partial u_3}{\partial y_1} - \frac{u_1}{h_3} \frac{\partial h_1}{\partial y_3} \right)^2 \\ \gamma_{22} &= h_2 \frac{\partial u_2}{\partial y_2} + \frac{h_2 u_3}{h_3} \frac{\partial h_2}{\partial y_3} + \frac{h_2 u_1}{h_1} \frac{\partial h_2}{\partial y_1} \\ &\quad + \frac{1}{2} \left( \frac{\partial u_2}{\partial y_2} + \frac{u_3}{h_3} \frac{\partial h_2}{\partial y_3} + \frac{u_1}{h_1} \frac{\partial h_2}{\partial y_1} \right)^2 \\ &\quad + \frac{1}{2} \left( \frac{\partial u_3}{\partial y_2} - \frac{u_2}{h_3} \frac{\partial h_2}{\partial y_3} \right)^2 + \frac{1}{2} \left( \frac{\partial u_1}{\partial y_2} - \frac{u_2}{h_1} \frac{\partial h_2}{\partial y_1} \right)^2 \\ \gamma_{33} &= h_3 \frac{\partial u_3}{\partial y_3} + \frac{h_3 u_1}{h_1} \frac{\partial h_3}{\partial y_1} + \frac{h_3 u_2}{h_2} \frac{\partial h_3}{\partial y_2} \\ &\quad + \frac{1}{2} \left( \frac{\partial u_3}{\partial y_3} + \frac{u_1}{h_1} \frac{\partial h_3}{\partial y_1} + \frac{u_2}{h_2} \frac{\partial h_3}{\partial y_2} \right)^2 \\ &\quad + \frac{1}{2} \left( \frac{\partial u_1}{\partial y_3} - \frac{u_3}{h_1} \frac{\partial h_3}{\partial y_1} \right)^2 + \frac{1}{2} \left( \frac{\partial u_2}{\partial y_3} - \frac{u_3}{h_2} \frac{\partial h_3}{\partial y_2} \right)^2 \end{aligned} \quad (17)$$

$$\begin{aligned}
\gamma_{12} &= \frac{1}{2} \left( h_1 \frac{\partial u_1}{\partial y_2} + h_2 \frac{\partial u_2}{\partial y_1} - u_2 \frac{\partial h_2}{\partial y_1} - u_1 \frac{\partial h_1}{\partial y_2} \right) \\
&+ \frac{1}{2} \left( \frac{\partial u_1}{\partial y_2} - \frac{u_2}{h_1} \frac{\partial h_2}{\partial y_1} \right) \left( \frac{\partial u_1}{\partial y_1} + \frac{u_2}{h_2} \frac{\partial h_1}{\partial y_2} + \frac{u_3}{h_3} \frac{\partial h_1}{\partial y_3} \right) \\
&+ \frac{1}{2} \left( \frac{\partial u_2}{\partial y_1} - \frac{u_1}{h_2} \frac{\partial h_1}{\partial y_2} \right) \left( \frac{\partial u_2}{\partial y_2} + \frac{u_1}{h_1} \frac{\partial h_2}{\partial y_1} + \frac{u_3}{h_3} \frac{\partial h_2}{\partial y_3} \right) \\
&+ \frac{1}{2} \left( \frac{\partial u_3}{\partial y_1} - \frac{u_1}{h_3} \frac{\partial h_1}{\partial y_3} \right) \left( \frac{\partial u_3}{\partial y_2} - \frac{u_2}{h_3} \frac{\partial h_2}{\partial y_3} \right) \\
\gamma_{13} &= \frac{1}{2} \left( h_3 \frac{\partial u_3}{\partial y_1} + h_1 \frac{\partial u_1}{\partial y_3} - u_1 \frac{\partial h_1}{\partial y_3} - u_3 \frac{\partial h_3}{\partial y_1} \right) \\
&+ \frac{1}{2} \left( \frac{\partial u_1}{\partial y_3} - \frac{u_3}{h_1} \frac{\partial h_3}{\partial y_1} \right) \left( \frac{\partial u_1}{\partial y_1} + \frac{u_3}{h_3} \frac{\partial h_1}{\partial y_3} + \frac{u_2}{h_2} \frac{\partial h_1}{\partial y_2} \right) \\
&+ \frac{1}{2} \left( \frac{\partial u_3}{\partial y_1} - \frac{u_1}{h_3} \frac{\partial h_1}{\partial y_3} \right) \left( \frac{\partial u_3}{\partial y_3} + \frac{u_1}{h_1} \frac{\partial h_3}{\partial y_1} + \frac{u_2}{h_2} \frac{\partial h_3}{\partial y_2} \right) \\
&+ \frac{1}{2} \left( \frac{\partial u_2}{\partial y_1} - \frac{u_1}{h_2} \frac{\partial h_1}{\partial y_2} \right) \left( \frac{\partial u_2}{\partial y_3} - \frac{u_3}{h_2} \frac{\partial h_3}{\partial y_2} \right) \\
\gamma_{23} &= \frac{1}{2} \left( h_3 \frac{\partial u_3}{\partial y_2} + h_2 \frac{\partial u_2}{\partial y_3} - u_2 \frac{\partial h_2}{\partial y_3} - u_3 \frac{\partial h_3}{\partial y_2} \right) \\
&+ \frac{1}{2} \left( \frac{\partial u_2}{\partial y_3} - \frac{u_3}{h_2} \frac{\partial h_3}{\partial y_2} \right) \left( \frac{\partial u_2}{\partial y_2} + \frac{u_3}{h_3} \frac{\partial h_2}{\partial y_3} + \frac{u_1}{h_1} \frac{\partial h_2}{\partial y_1} \right) \\
&+ \frac{1}{2} \left( \frac{\partial u_3}{\partial y_2} - \frac{u_2}{h_3} \frac{\partial h_2}{\partial y_3} \right) \left( \frac{\partial u_3}{\partial y_3} + \frac{u_2}{h_2} \frac{\partial h_3}{\partial y_2} + \frac{u_1}{h_1} \frac{\partial h_3}{\partial y_1} \right) \\
&+ \frac{1}{2} \left( \frac{\partial u_1}{\partial y_2} - \frac{u_1}{h_1} \frac{\partial h_2}{\partial y_1} \right) \left( \frac{\partial u_1}{\partial y_3} - \frac{u_3}{h_1} \frac{\partial h_3}{\partial y_1} \right)
\end{aligned} \tag{17}$$

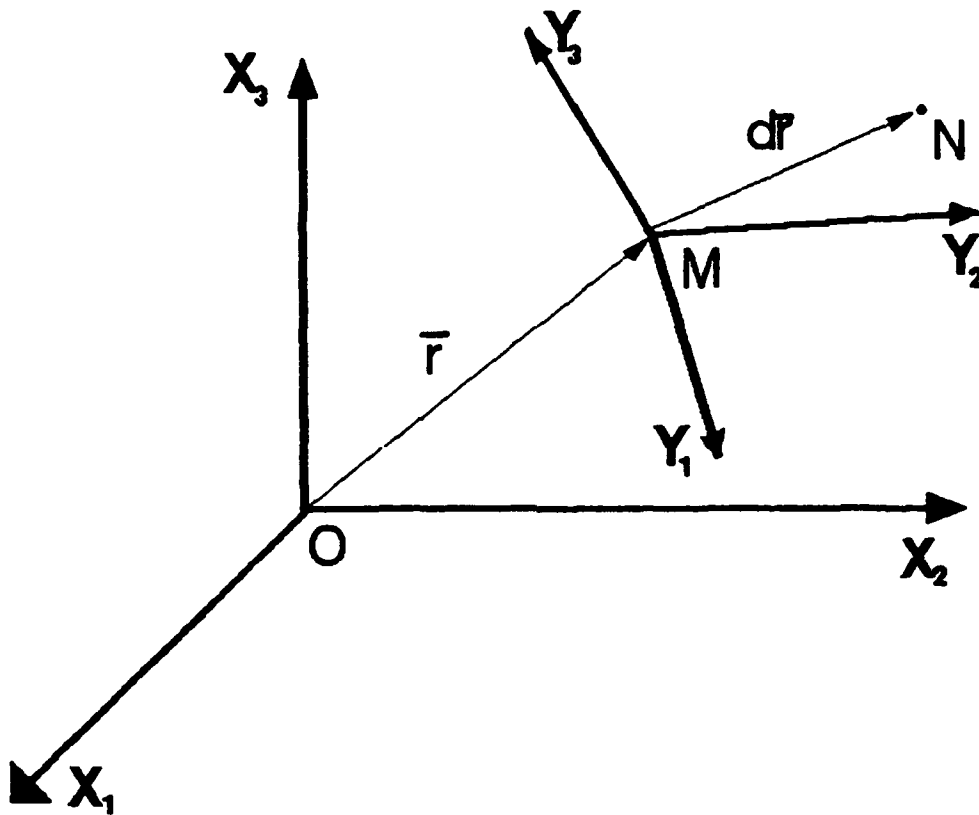


Figure 6. Point M Located in 3-D Space by Position Vector  $\bar{r}$

Finally, by expanding on the CLPT development from Section 2.1, the stress-strain relations for an N-ply laminate can be analyzed by referencing each ply to the global coordinate system using the following transformations:

$$\{\sigma_i\}_k = [T] [Q_{ij}]_k [T]^T \{\epsilon_i\}_k \quad (18)$$

where,

$$[T] = \begin{bmatrix} c^2 & s^2 & -2cs \\ s^2 & c^2 & 2cs \\ cs & -cs & (c^2 - s^2) \end{bmatrix} \quad \text{for} \quad \begin{bmatrix} Q_{11} & Q_{12} & 0 \\ Q_{12} & Q_{22} & 0 \\ 0 & 0 & Q_{66} \end{bmatrix} \quad (19)$$

and,

$$[T] = \begin{bmatrix} c & -s \\ s & c \end{bmatrix} \quad \text{for} \quad \begin{bmatrix} Q_{44} & 0 \\ 0 & Q_{55} \end{bmatrix} \quad (20)$$

with  $c = \cos\theta$  ,  $s = \sin\theta$

With these transformations, the constitutive relations become those in Eq (4) with the following three additional terms due to the modified plane stress condition [25]:

$$\begin{aligned} \overline{Q}_{44} &= Q_{44}\cos^4\theta + Q_{55}\sin^4\theta \\ \overline{Q}_{45} &= (Q_{44} - Q_{55})\cos\theta \sin\theta \\ \overline{Q}_{55} &= Q_{44}\sin^4\theta + Q_{55}\cos^4\theta \end{aligned} \quad (21)$$

### 2.2.3 SHELL's Strain - Displacement Relations

The shell panel's curvature creates a geometric nonlinearity which must be incorporated into the strain-displacement relations. Also here, thru-the-thickness shear effects are incorporated into the analysis. This development follows Dennis [6], who authored the SHELL computer code which employs these relations.

As already mentioned, parabolic transverse shear effects are incorporated into the analysis by assuming a modified state of plane stress for each lamina. The transverse shear stresses are assumed equal to zero on the top and bottom surfaces of each ply, and increase parabolically towards the midplane where they are maximum. Thus it follows that the associated strains will vary parabolically through the ply thickness.

The modified plane stress condition stipulates that  $\sigma_3 = 0$  and hence  $\epsilon_3 = 0$ . Furthermore, keeping just the linear (first order) displacement terms in the transverse shear strain expressions ( $\epsilon_4$  and  $\epsilon_5$ ) from Eqs (16) and (17) one obtains [23]:

$$\begin{aligned}\epsilon_4 &= (1/h_2) (u_{3,2} + h_2 u_{2,3} - u_2 h_{2,3}) \\ \epsilon_5 &= (1/h_1) (u_{3,1} + h_1 u_{1,3} - u_1 h_{1,3})\end{aligned}\quad (22)$$

Where the  $h_i$  terms are the coordinate system scale factors; for the cylindrical geometry used in this research,  $h_1 = 1$  and  $h_2 = 1 - (z/R)$ . Note:  $R$  = radius of curvature

The kinematic equations, in terms of the thickness variable  $z$ , and which enable the incorporation of the desired thru-the-thickness feature are [25]:

$$\begin{aligned}u(x, s, z) &= u_0 + z \psi_1 + z^2 \phi_1 + z^3 \gamma_1 + z^4 \theta_1 \\ v(x, s, z) &= v_0 [1 - (z/R)] + z \psi_2 + z^2 \phi_2 + z^3 \gamma_2 + z^4 \theta_2 \\ w(x, s) &= w\end{aligned}\quad (23)$$

Where  $u_0$ ,  $v_0$ ,  $w$ ,  $\psi_i$ ,  $\phi_i$ ,  $\gamma_i$ , and  $\theta_i$  are functions of the coordinates  $x$  and  $s$ .

The displacements  $u_0$  and  $v_0$  are located at the shell's midplane; transverse displacement  $w$  is constant throughout the thickness since the transverse normal strain is assumed to be negligible ( $\epsilon_3 \cong 0$ ). The  $\psi_i$  terms are rotations of the surface normals in the  $X$  and  $S$  planes, while the  $\phi_i$ ,  $\gamma_i$ , and  $\theta_i$  terms are found by applying the assumption that transverse shear stresses  $\sigma_4$  and  $\sigma_5$  are zero on the shell's top and bottom surfaces.

Solving for  $\epsilon_4$  and  $\epsilon_5$  in terms of  $w$  and rotations  $\psi_i$  (in the coordinate system of the SHELL algorithm), the details of which can be found in references [20, 25], produces:

$$\epsilon_4 = \{ 1 / [1 - (z/R)] \} (w,s + \psi_s) [1 - (4z^2/h)] \quad (24)$$

$$\epsilon_5 = (w,x + \psi_x) [1 - (4z^2/h)]$$

Where  $z$  is the distance from the midplane of the shell laminate,  $R$  is the shell's radius of curvature, and  $h$  is the shell's total thickness. Note that these resulting transverse shear strain expressions are parabolic with respect to the thickness variable ( $z$ ).

Again assuming zero transverse shear stress and associated zero strain on the shell's upper and lower surfaces [6], Eq (23) can be solved in terms of  $w$  and  $\psi_i$ , the details of which are provided in reference [25], yielding:

$$u(x, s, z) = u_0 + z \psi_x - (4/3h^2) z^3 (\psi_x + w,x) \quad (25)$$

$$v(x, s, z) = v_0 [1 - (z/R)] + z \psi_s - (4/3h^2) z^3 (\psi_s + w,s)$$

$$w(x, s) = w$$

The displacement functions now incorporate a thru-the-thickness shear strain distribution. Also, it should be noted that this formulation provides the seven degrees of freedom used in the SHELL computer code:  $u$  ;  $v$  ;  $w$  ;  $w,x$  ;  $w,s$  ;  $\psi_x$  ;  $\psi_s$ .



### 3. EXPERIMENTAL METHODS

#### 3.1 *Manufacturing*

A total of 32 specimens were fabricated for use in experiments involving axial compression of cylindrical shell panels with unsupported vertical edges. The experimental test plan (see Appendix A) provides a breakdown of the various geometries tested, the ply stacking sequences, and which panels had cutouts. Table 2 provides a summary of the different configurations tested.

*Table 2. Summary of Experimental Test Plan*

<u>Configurations</u>	<u>No. of Plies</u>	<u>Stacking Sequence</u>	<u>Effective Dimensions</u>
1 and 2	8	[0/90] <sub>2s</sub>	12" X 12"
3 and 4	8	[0/90] <sub>2s</sub>	12" X 20"
5 and 6	8	[0/+45/-45/90] <sub>s</sub>	12" X 12"
7 and 8	8	[0/+45/-45/90] <sub>s</sub>	12" X 20"
9 and 10	16	[0/90] <sub>4s</sub>	12" X 20"
11 and 12	16	[0/+45/-45/90] <sub>2s</sub>	12" X 20"
13 and 14	24	[0/90] <sub>6s</sub>	12" X 20"
15 and 16	24	[0/+45/-45/90] <sub>3s</sub>	12" X 20"

Note: Each of these configurations was tested with a 4" X 4" centered square cutout and without any cutout.

All 32 specimens were newly manufactured and had cylindrical shell geometry with radii of curvature of 12 inches, measured to the outside convex surface of the panel. The manufacturing process and material system (AS4/3501-6) were the same as used by

Horban [10], Tisler [28], Wilder [30], and Schimmels [25] for their studies. However, the material properties used in this study were slightly different from those used in their work. The properties used for this research were obtained by Dr. R. S. Sandhu of the Flight Dynamics Laboratory in more recent material properties tests [24]. Table 3 provides a summary of the material properties assumed valid for use in this research effort.

*Table 3. Basic Material Properties of AS4/3501-6 Graphite/Epoxy*

Elastic Modulus Along Fibers in Compression ( $E_1$ )	19.70 Msi
Elastic Moduli Transverse to Fibers in Compression ( $E_2 = E_3$ )	1.579 Msi
Major Poisson's Ratio in Compression ( $\nu_{12}$ )	0.276
Elastic Moduli in Shear ( $G_{12} = G_{13}$ )	0.925 Msi
Transverse Elastic Modulus in Shear ( $G_{23}$ )	0.462 Msi

All the panels were C-scanned after manufacturing to ensure no delaminations or internal defects were present. The thickness was measured at thirteen locations on each panel and the average thickness was recorded and used in the numerical part of this study. The average thickness variation within each panel was small ( $< 7\%$ ) and it was even smaller for panels within their respective group ( $< 2\%$ ).

A hole cutting process was developed during Tisler's work [28] to help alleviate damage caused by flattening of the panel during cutting. A wooden base, also with a radius of curvature of 12 inches, held the panel in its original shape during the cutting process. Fiberglass and rubber sheets helped reduce the possibility of vibration damage, while a steel template guided the router used for cutting. A schematic of the cutting setup is provided in Figure 7.

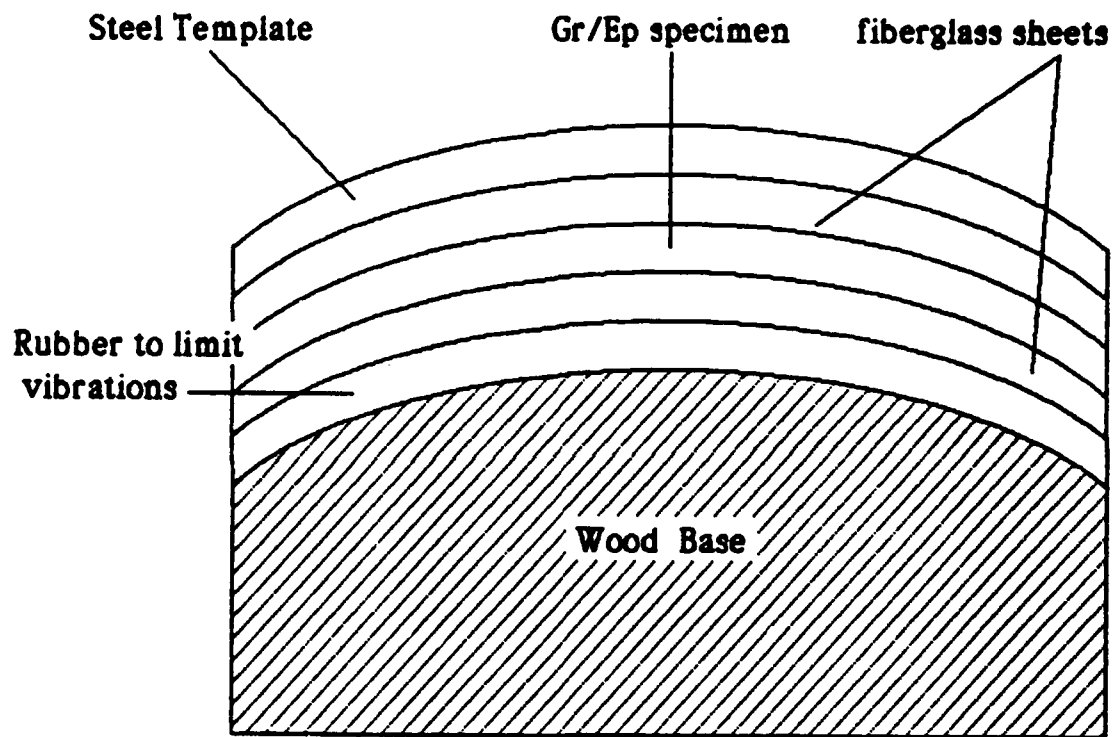


Figure 7. Schematic of Curved-Panel Cutting Support

The router was used to cut the square holes in the panels. This mechanism caused the corners of the square to be slightly rounded (about a 1/16 inch radius), which had the beneficial effect of removing stress singularities at the corners.

All the edges of the panels were cut the same way as done in previous studies [10, 25, 28, 30]. Specific tolerances (see test plan, Appendix A) were given to ensure that all edges, upper/lower and sides, were as close as possible to being parallel. This is critical to ensure evenly distributed loading and accurate assessment of radial displacements. The actual edge cutting procedure is explained in more detail by Horban [10].

In order for the specimens to be clamped into the loading fixture, along the top and bottom of the panel, the axial dimension had to be cut one inch longer to create a 1/2 inch holding tab at the panel's top and bottom edges. Thus, the effective axial dimension was one inch shorter than the actual fabricated panel specimen.

### 3.2 *Axial Compression*

The experimental fixture (see Figure 8) used for the axial compression tests, along with the curved panel clamping devices, is the same one used by Horban [10], Janisse [11], Tisler [28], Wilder [30], and Schimmels [25] for their studies. The specialized clamping devices are explained in more detail by Horban [10].

The top edge was clamped such that movement of the panel was fully constrained ( $u = v = w = 0, x = y, z = 0$ ), while the bottom edge of the panel could move vertically upward ( $u = \text{prescribed}, v = w = 0, x = y, z = 0$ ). The loading was applied by a 30,000 lb hydraulic compression machine, which incremented the loading via application of a uniform displacement of 0.05" per minute. Although the bottom platen was moving upward with the top platen fixed, the top edge was where the true applied loads took place. A load cell measured the total applied load. Each test was completed when the maximum collapse load was reached, at which point the panel continued to deform (bow outward) smoothly while the loading began to slowly drop off. To ensure the loading was uniform

across the top of the panel, two sets of back-to-back one-dimensional strain gages were used. See the test plan (Appendix A, Figures A6 and A7) for placement of these gages.



Figure 8. Experimental Setup, Axial Compression Fixture

Linear Variable Displacement Transducers (LVDTs) were used to measure the radial (out of plane, transverse to the loading direction) and axial displacements of the panels during compression. A vertically mounted LVDT in front of the panel (see Figure A5 of the test plan) was used to measure the top edge displacement ( $u$ ). On the other side of the panel, the radial displacements ( $w$ ) were measured by seven LVDTs (six for panels with cutouts) at locations specified in Figures A6 and A7 of the test plan. Since the largest radial displacements could occur near the cutout, they are of particular interest and will be compared to values obtained numerically using the SHELL finite-element program.

The data collected by the LVDTs and strain gages was saved on a VAX 11/780 computer, which allowed for generation of experimental load/displacement curves. The data collected from the strain gages was used to confirm the panel collapse loads because at the point of collapse, the load versus strain curves diverged dramatically.

For a more detailed discussion of the axial compression experimental procedure, including photographs and drawings of the holding fixtures, see [10, 11, 30].

#### **4. FINITE ELEMENT MODELING**

In structural mechanics, a problem is nonlinear if the stiffness matrix or the load vector depend on the displacements. In the general finite-element approach to nonlinear behavior analysis, the partial differential equations representing static equilibrium are linearized and solved by incremental/iterative methods [5]. In this approach, the continuum displacements of the equilibrium equations are approximated through interpolation functions; along with the values of displacements at discrete points (nodes) within the structural mesh. This mesh represents the domain and boundaries of the physical specimen. In the SHELL code, the nodes are placed on the midplane surface of the shell structure. This nodal placement will yield valid results if the shell is relatively thin with respect to the shell's other dimensions[6].

Two finite-element grids were constructed to model the two panel geometries studied, 12" X 12" and 12" X 20" ( see Figures 9 and 10). All panels had a radius of curvature of 12". The material properties in Table 3 were used for all the finite element computer runs using SHELL. However, the specimen thicknesses varied slightly from panel to panel, and this was taken into account in the input decks used. Since the SHELL algorithm models transverse thru-the-thickness shear, the program is very sensitive to thickness. A summary of the thicknesses used is shown in Table 4.

Based on Dennis' research [6], the 36 degree of freedom (DOF) element proved to be the best choice for use in the nonlinear analysis in SHELL. Schimmels [25, 26] confirmed this result and obtained good results using the element shown in Figure 11.

*Table 4. Panel Thickness*

<u>Panel Designator</u>	<u>Number of Plies</u>	<u>Average Ply Thickness (in)</u>
JH-1-0	8	0.00514
JH-3-4	8	0.00514
JH-4-0	8	0.005375
JH-6-4	8	0.005375
JH-7-0	8	0.00530
JH-9-4	8	0.00530
JH-10-0	8	0.00521
JH12-4	8	0.00521
JH-13-0	16	0.00535
JH-19-4	16	0.00530
JH-22-0	16	0.00527
JH-28-4	16	0.00532
JH-31-0	24	0.00540
JH-37-4	24	0.00535
JH-40-0	24	0.00545
JH-46-4	24	0.00542

Dennis [6] found that the 1/2" X 1/2" element was the optimal size to use in order to converge to an accurate solution while minimizing the CPU run time, in areas where large displacements and moderate rotations existed. It should be noted that in order to keep the computer run times from being too excessive and to minimize the memory usage, a mesh arrangement similar to the one used by Dennis in his dissertation [6: 275] was adopted for the larger 12" X 20" panels. Lee [15] performed a numerical analysis on the affects oblong elements (aspect ratios of 0.5 or 2) have on the determination of collapse



loads. She found that a safe distance from the cutout to use oblong elements of these aspect ratios is between 1.5 and 2.0 inches. For the 12" X 20" models used in this research effort, the oblong elements were at least 2" from the cutouts.

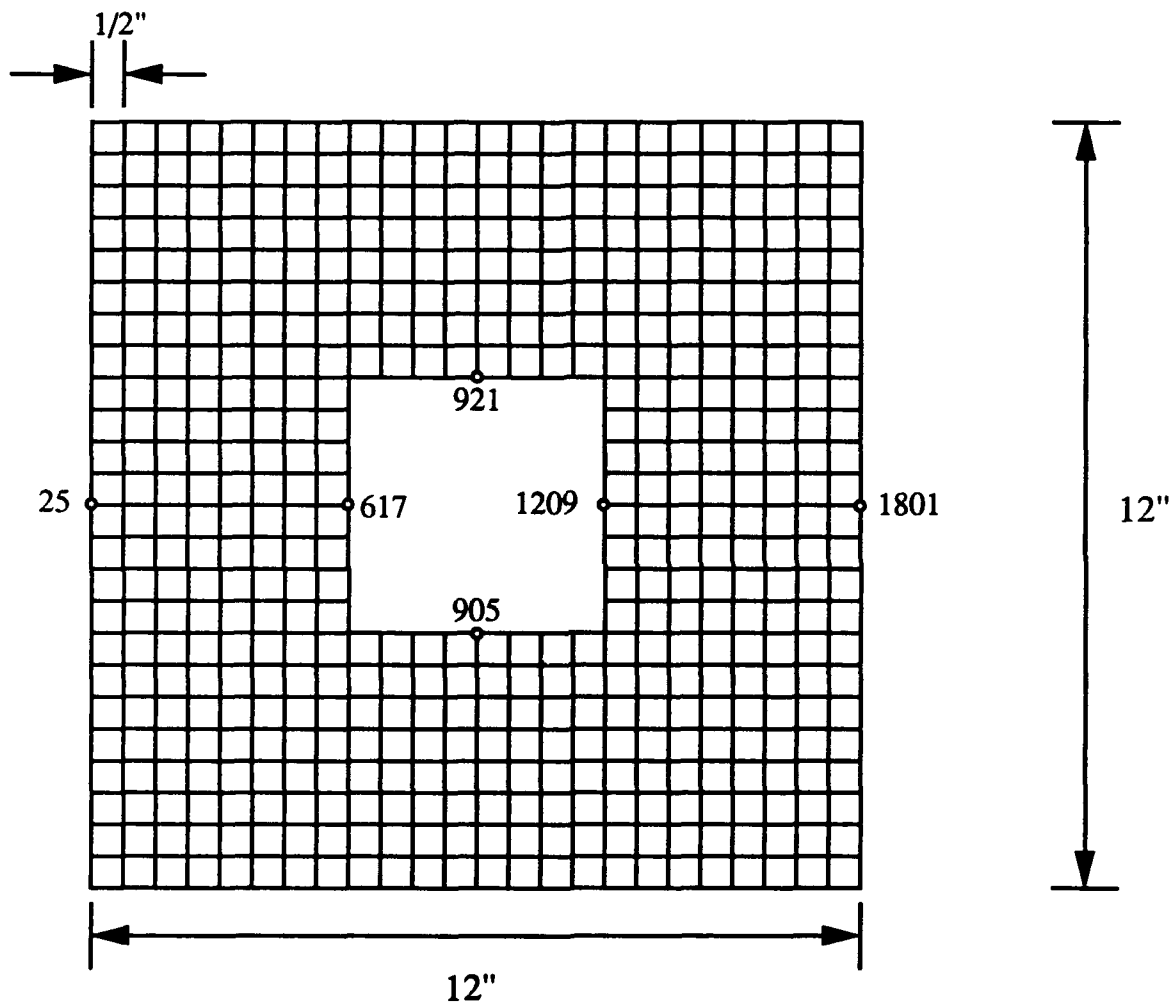


Figure 9. Finite-Element Mesh Used For 12" X 12" Shell Panels

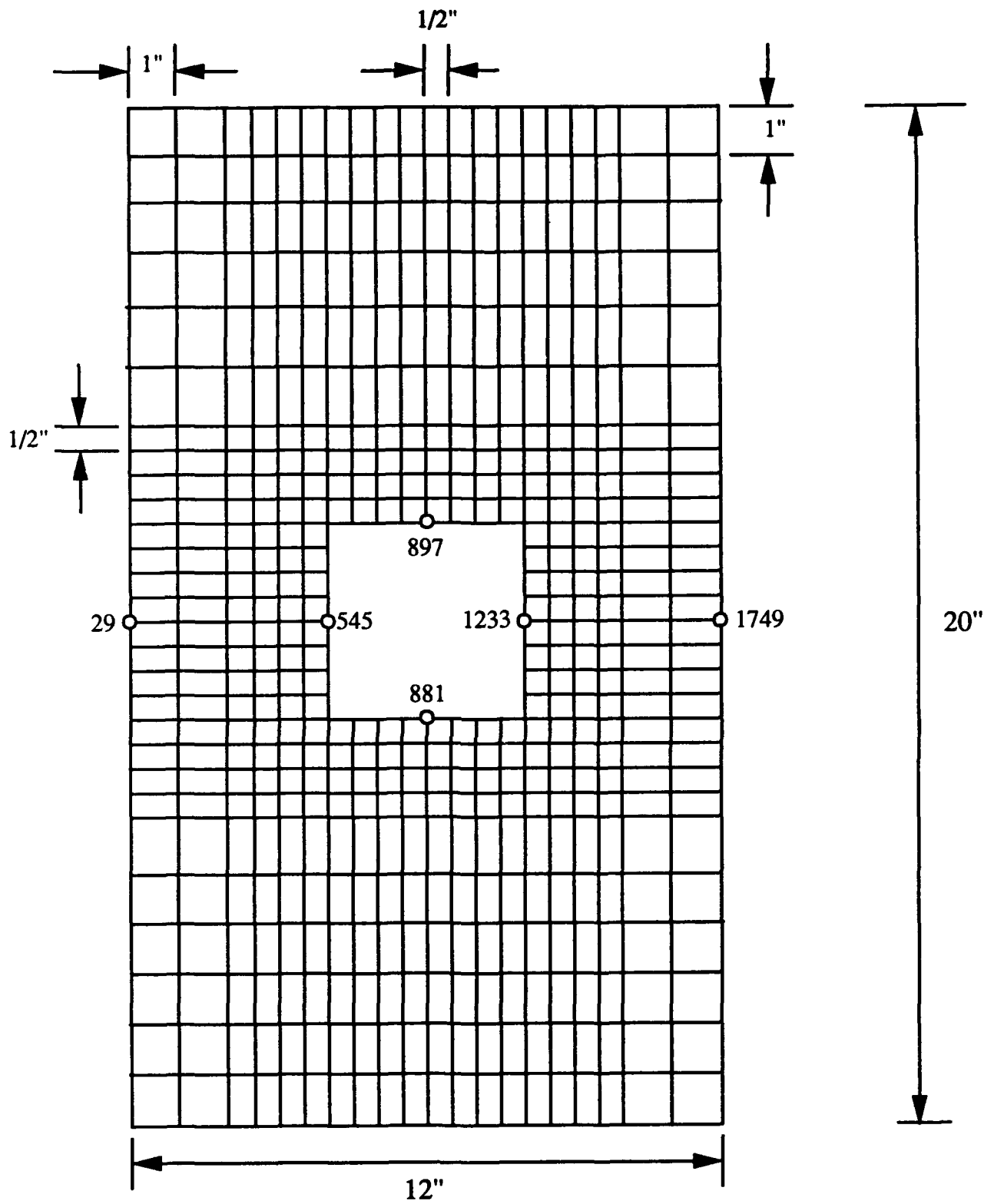


Figure 10. Finite-Element Mesh Used For 12" X 20" Shell Panels

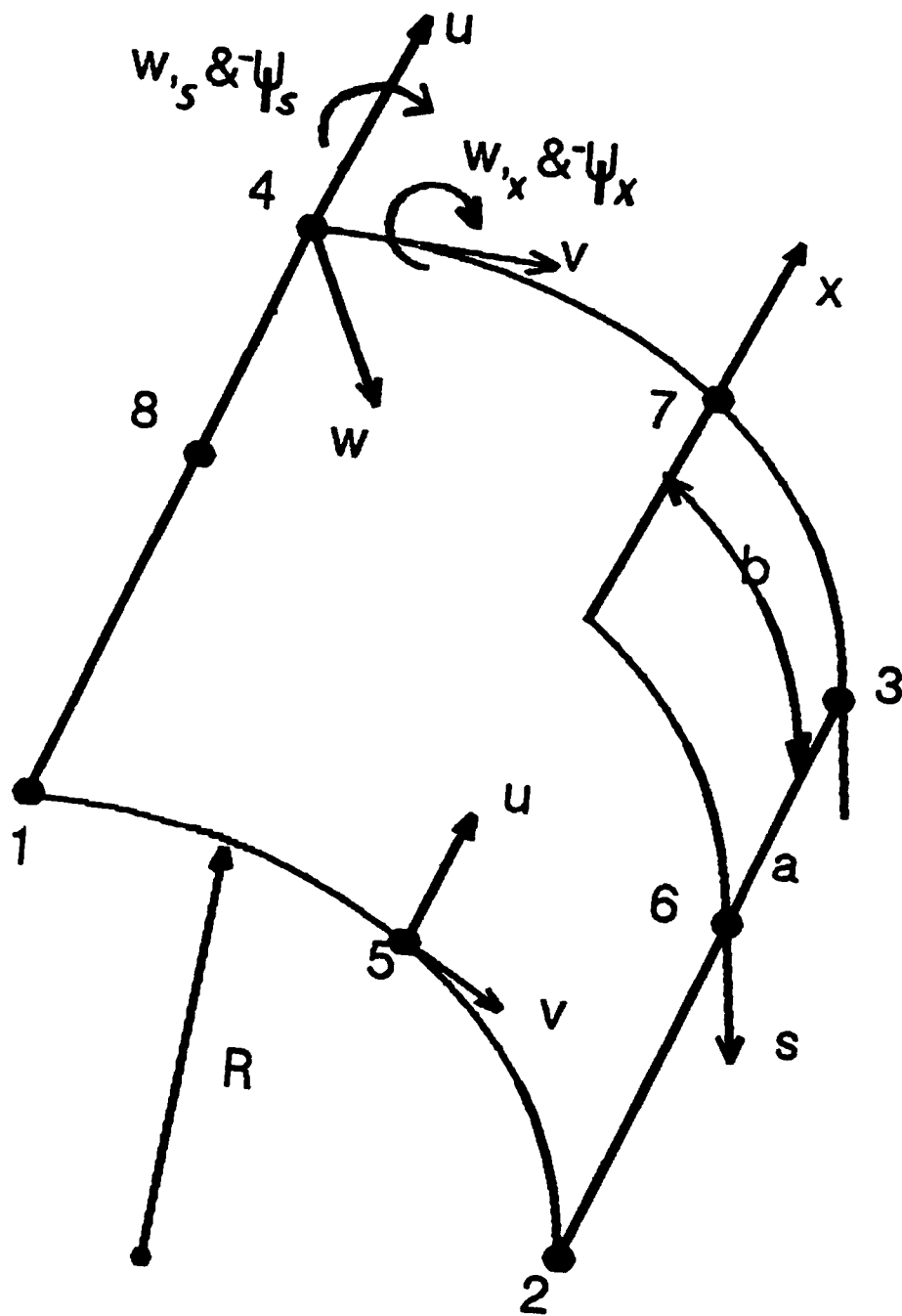


Figure 11. SHELL 36 Degree-of-Freedom Element

Although not shown in Figures 9 and 10, elements are actually present within the square cutout, but removed analytically. To do this, no stiffness is calculated for those elements within the cutout region [7]. This is done so that an automatic mesh generator can be used. Additionally, the nodes of those elements within the cutout, but not on the cutout border, must be constrained from movement.

When the experimental panels were cut, the router rounded off the corners of the square cutouts. By doing this, large stress concentrations would not form at the corners as the panels were experimentally loaded. Therefore, although the cutout corners of the analytical model are sharp, mesh refinement is not as severe as that normally required for a singularity. Thus, by keeping the mesh refinement relatively coarse, an analytical stress singularity cannot develop, hence representing the actual panels more accurately [7].

The nodal boundary conditions applied analytically had the bottom edge of the panel (at  $x = 0$ ) fully clamped ( $u = v = w = w_x = w_s = \psi_x = \psi_s = 0$ ). The top edge of the panel was also constrained from movement in six DOFs ( $v = w = w_x = w_s = \psi_x = \psi_s = 0$ ); while the axial displacement ( $u$ ) was prescribed, since the analytical load was input by a uniform displacement along the top edge (at  $x = 12$ ). The nodes along the vertical edges were allowed to displace freely since experimentally these edges were neither simply supported nor clamped.

Palazotto and Tisler [21] found that analytically applying a uniform displacement loading better resembled the actual test apparatus used in this study. In particular, they found that the distinction between uniform displacement and uniform loading along the top edge of the panel is very important for the panels with a larger cutout (greater than 2" X 2"). Therefore, for this study equal compressive displacements were incremented at each of the top edge nodes up to and through panel collapse. The SHELL program then calculated the loading required at each top edge node (41 total nodes for each model) in order to displace the particular node the prescribed displacement. Then, the total compressive load was

calculated from the 41 nodal loads. In addition, the SHELL algorithm also calculated displacements and rotations at the seven degrees of freedom for each node contained in the panel mesh (per each displacement increment).

The numerical calculations were performed on SUN SPARCstation 2 digital computers. The 12" X 12" panel mesh contained 576 elements and 1825 nodes, which equated to a calculated bandwidth of 289. The 12" X 20" panel mesh contained 560 elements and 1777 nodes, with a bandwidth of 333. It should be noted that the use of these refined grids, coupled with the dimensionality of the panel specimens, required large amounts of computer time (up to 260,000 CPU seconds in some cases) in order to reach the collapse loads. Samples of the input decks used for this research are contained in Appendix C.

## 5. RESULTS AND DISCUSSION

### 5.1 *Introduction*

This section documents the significant results obtained both numerically and experimentally during this research effort, which involved an investigation of the collapse characteristics of graphite/epoxy cylindrical shell panels under axial compression.

The behavior of symmetric quasi-isotropic and cross-ply laminated shells, with and without 4" X 4" centralized square cutouts, was analyzed for three different thicknesses: 8, 16, and 24 plies. During the experiments conducted by the Flight Dynamics Laboratory, panels with effective dimensions of 12" X 12" and 12" X 20" were placed under axial compression via application of uniform displacement increments along the top edge of the panels. The loads applied to the panels, as they progressed towards collapse, were recorded along with the corresponding top edge displacements and radial displacements (obtained at discrete points where the numerical data indicated the largest displacements occurred). After the panels reached the initial collapse load, observed when the loading dropped off even though the top edge continued to be displaced, the compressive loading was released. A total of 16 different shell panel configurations were tested and the results compared to data obtained numerically using the SHELL finite-element computer program. During the first part of this section, an analysis of the numerical data obtained from SHELL will be performed. Then in the latter part of the section, the experimental results will be compared to the numerical results. In addition, throughout the section, the results will be discussed in terms of the global and local behavior of laminated composite shells.

### 5.2 *Analysis of the Numerical Data from SHELL*

The SHELL finite-element computer program was used in this research effort to perform a nonlinear analysis on the geometric instability of unsupported graphite/epoxy shell panels undergoing axial compression. The sixteen different configurations

investigated included eight quasi-isotropic laminates with the following ply orientations:  $[0/+45/-45/90]_s$ ,  $[0/+45/-45/90]_{2s}$ , and  $[0/+45/-45/90]_{3s}$ ; and eight cross-ply laminates with these orientations:  $[0/90]_{2s}$ ,  $[0/90]_{4s}$ ,  $[0/90]_{6s}$ . For the 8-ply shells two dimensions were investigated, 12" X 12" and 12" X 20", while only 12" X 20" shell panels were analyzed for the 16 and 24 ply configurations. Half of the panels investigated had 4" X 4" cutouts, while the other half studied were solid panels (no cutouts). In analyzing the numerical data, it was observed in every configuration that the values of the nodal rotations and displacements maintained a symmetrical distribution with respect to both the horizontal and vertical panel centerlines.

Tables 5 and 6 represent the numerically-derived global and local collapse characteristics, respectively. Table 5 indicates the maximum load analytically applied to the shells just before the panels collapsed. Also displayed in this table is the panel top edge displacement (U) that is associated with the collapse load. Table 6 displays the magnitudes of the largest radial displacements (w) observed in each panel configuration, at the time of collapse. Although this table represents points of maximum radial displacement, similar orders of magnitude were observed distributed in the areas surrounding these points. In order to ensure valid comparisons between configurations, the data was collected at similar percentages of collapse load. Information pertaining to these tables will be analyzed in more detail in sections 5.2.1 and 5.2.2. However, a few overall comparisons will be made at this time.

The SHELL algorithm was designed to model shell structures undergoing large displacements and moderately large rotations (based on Palazotto and Dennis' simplified large rotation theory). One of the key features of the SHELL algorithm is that it incorporates a parabolic transverse shear strain distribution through the thickness of the shell. The presence of transverse shear decreases the global stiffness of the shell panel. This enhances the bending which occurs in the shell as it reaches the collapse load. A

comparison of the maximum bending rotations and transverse shear strains found in the shells during panel collapse is shown in Table 7. Again, even though the points chosen represent maximum values of rotation and transverse shear strain, the areas surrounding these points are similar in order of magnitude. The transverse shear strains at the midplane datum surface are defined as:

$$\epsilon_4 = |\psi_s| - |w,s| \quad (26)$$

$$\epsilon_5 = |\psi_x| - |w,x| \quad (27)$$

Where  $\psi_s$  and  $\psi_x$  are the rotations of the elastic curves due to bending and  $w,s$  and  $w,x$  are slopes of the elastic curves with respect to the S - Z plane and X - Z plane, respectively. These quantities are degrees of freedom calculated by SHELL and the difference between the magnitude of the bending rotation and the magnitude of the elastic curve slope must equal the rotation of the elastic curve due to the presence of transverse shear strain [20]. It was consistently observed, throughout the analysis of transverse shear strain in all the panels, that the magnitude of  $\epsilon_4$  greatly exceeded that of  $\epsilon_5$  at collapse. Therefore, since  $\epsilon_4$  contributes more significantly to the collapse of the shell panels, the analysis of the effect of transverse shear strain will be limited to studying transverse strain with respect to the S - Z plane. It should be noted that the  $0^\circ$  fiber's shear strength is the weakest in the S - Z plane, with  $G_{23}$  being half the magnitude of  $G_{12}$  and  $G_{13}$  (see Table 3).

Table 5 shows that for all cases (except one) involving the collapse of shell panels without cutouts, the quasi-isotropic panels globally behave more stiffly and collapse at higher loads than the cross-ply panels. The one exception involves the 12" X 12" solid 8-ply cross-ply shell panel. In this case, the cross-ply panel collapses at a load which is 38% higher than the quasi-isotropic collapse load. However, also note in Tables 6 and 7 that the bending rotations and radial displacements for this case are very small. This indicates that



very little bending is occurring and collapse of the panel is dictated by  $A_{11}$ , the axial stiffness of the panel. Since  $A_{11}$  is greater for the cross-ply laminate than the quasi-isotropic laminate, it follows that the solid quasi-isotropic shell panel would collapse at a lower load.

Table 6 verifies that a nonlinear theory of this nature is required for collapse of these types of shells undergoing axial compression. Note that the radial displacements for the three thickness categories range from being 3 - 7 times the shell thickness in the 24-ply cases, 6 - 7 times the shell thickness in the 16-ply cases, and to almost 12 times the shell thickness for the 12" X 20", 8-ply quasi-isotropic panel with cutout. In comparing the radial displacements in Table 6, some interesting differences are noted in the shell responses between quasi-isotropic and cross-ply panels, with and without cutouts. The cross-ply shell panels appear to locally respond more stiffly (comparatively smaller radial displacements) than the quasi-isotropic panels when no cutouts are present; but then respond more flexibly (comparatively larger radial displacements) than the quasi-isotropic shells when large cutouts are present. The most dramatic examples of this phenomena involve the 24-ply shells and the 8-ply, 12" X 12" shells; although to a lesser extent these trends were also observed in the 8-ply, 12" X 20" and the 16-ply shells. In the 24-ply case, where the collapse load for the quasi-isotropic shell with no cutout was similar to the cross-ply shell with no cutout, the cross-ply shell displayed radial displacements that were about 45% lower than the quasi-isotropic shell. Then after a large square was centrally placed in both types of 24-ply shells, significantly greater radial displacements (about 30%) were observed in the cross-ply laminated shells versus the quasi-isotropic shell panels.

Table 7 indicates that significantly greater bending rotations are occurring in the 24-ply quasi-isotropic shell panel with no cutout versus a similar cross-ply configuration, and yet globally the quasi-isotropic panel collapses at a higher load than the cross-ply panel. The cross-ply panels without cutouts are axially stiffer than the quasi-isotropic panels, with

the cross-ply having a 20% higher  $A_{11}$  stiffness term. Another difference in these two panel layups is the existence of  $\pm 45^\circ$  fiber laminae in the quasi-isotropic shells. This difference provides the quasi-isotropic panels with certain key bending stiffness terms which are significantly greater than similar terms for the cross-ply panels. For example,  $D_{66}$  (which directly relates to stiffening a laminate against in-plane twisting) is three times greater for the quasi-isotropic laminate than the cross-ply laminate. In addition the  $D_{16}$  and  $D_{26}$  stiffness terms, which are coupling terms between direct bending moments and the shear activity occurring in a structure, exist in quasi-isotropic laminates but are zero for cross-ply laminates. These  $D_{16}$  and  $D_{26}$  terms help to stiffen the quasi-isotropic panels against the bending curvatures caused by large rotations (which are nonlinear terms in this analysis), and thus act to hinder the  $M_x$  and  $M_y$  bending moments.

The presence of a large cutout may cause the shell panel to twist during axial compression. This twisting can enhance the radial displacements caused by the bending rotations present during compression. The much greater  $D_{66}$  stiffness of the quasi-isotropic panels compared to the cross-ply panels, enables the quasi-isotropic panels to resist to a greater extent the twisting action for similar magnitudes of rotation (see Table 7: 24-ply cases and 12" X 12", 8-ply cases), thus producing smaller values of radial displacements.

#### 5.2.1 *Quasi-Isotropic Shell Panels*

A common occurrence in all the numerical runs involving the quasi-isotropic shells, with and without cutouts, was that the largest radial displacements occurred along the unsupported vertical edges near the center of the panels. This would indicate that for quasi-isotropic shells, neither thickness nor the presence of large cutouts influence the location of the largest radial displacements in a panel undergoing axial compression. These displacements will occur along free edges and near the horizontal centerline of panels

during collapse. In addition, it was noted that the largest bending rotations usually were associated with areas where the largest radial displacements occurred.

*Table 5. Numerical Global Collapse Characteristics*

**QUASI-ISOTROPIC LAMINATED SHELLS**

<u>Number of Plies</u>	<u>Shell Type</u>	<u>Collapse Load (lbs)</u>	<u>U Displacement (in)</u>
8	12", NC	3387	0.012
8	12", Cutout	1418	0.011
8	20", NC	1971	0.010
8	20", Cutout	1100	0.017
16	20", NC	9218	0.030
16	20", Cutout	5131	0.030
24	20", NC	32,874	0.072
24	20", Cutout	12,959	0.040

**CROSS-PLY LAMINATED SHELLS**

<u>Number of Plies</u>	<u>Shell Type</u>	<u>Collapse Load (lbs)</u>	<u>U Displacement (in)</u>
8	12", NC	4683	0.012
8	12", Cutout	1333	0.010
8	20", NC	1654	0.006
8	20", Cutout	1200	0.014
16	20", NC	8439	0.020
16	20", Cutout	4896	0.027
24	20", NC	29,838	0.036
24	20", Cutout	12,346	0.040

Note: NC = No Cutout

Shells are either 12" X 12" or 12" X 20"

*Table 6. Numerical Local Collapse Characteristics*

**QUASI-ISOTROPIC LAMINATED SHELLS**

<u>Number of Plies</u>	<u>Shell Type</u>	<u>Collapse Load (%)</u>	<u>Maximum   w   (in)</u>
8	12", NC	100.0	0.20977
8	12", Cutout	99.1	0.27765
8	20", NC	96.5	0.32989
8	20", Cutout	98.4	0.46913
16	20", NC	100.0	0.50317
16	20", Cutout	99.3	0.55104
24	20", NC	100.0	0.65235
24	20", Cutout	98.1	0.55141

**CROSS-PLY LAMINATED SHELLS**

<u>Number of Plies</u>	<u>Shell Type</u>	<u>Collapse Load (%)</u>	<u>Maximum   w   (in)</u>
8	12", NC	100.0	0.070719
8	12", Cutout	98.3	0.278110
8	20", NC	98.9	0.212280
8	20", Cutout	99.9	0.440010
16	20", NC	93.4	0.499790
16	20", Cutout	96.7	0.584590
24	20", NC	88.2	0.357410
24	20", Cutout	96.4	0.714070

Note: NC = No Cutout

Shells are either 12" X 12" or 12" X 20"

**Table 7. Numerical Maximum Bending Rotations / Transverse Shear Strains**

<b>QUASI-ISOTROPIC LAMINATED SHELLS</b>				
<u>Number of Plies</u>	<u>Shell Type</u>	<u>Collapse Load (%)</u>	<u><math> \psi_s </math> (degrees)</u>	<u><math> \epsilon_4 </math> (radians)</u>
8	12", NC	100.0	5.8	0.0003344
8	12", Cutout	99.1	6.7	0.0008340
8	20", NC	96.5	7.6	0.0008700
8	20", Cutout	98.4	9.9	0.0022990
16	20", NC	100.0	9.2	0.0006200
16	20", Cutout	99.3	9.7	0.0027620
24	20", NC	100.0	11.5	0.0010919
24	20", Cutout	98.1	8.6	0.0052840
<b>CROSS-PLY LAMINATED SHELLS</b>				
<u>Number of Plies</u>	<u>Shell Type</u>	<u>Collapse Load (%)</u>	<u><math> \psi_s </math> (degrees)</u>	<u><math> \epsilon_4 </math> (radians)</u>
8	12", NC	100.0	1.9	0.0008760
8	12", Cutout	98.3	6.5	0.0010020
8	20", NC	98.9	4.6	0.0005240
8	20", Cutout	99.9	8.4	0.0014810
16	20", NC	93.4	9.3	0.0006674
16	20", Cutout	96.7	8.8	0.0030680
24	20", NC	88.2	6.0	0.0011790
24	20", Cutout	96.4	8.9	0.0042070

Note: NC = No Cutout

Shells are either 12" X 12" or 12" X 20"

As expected, intuitively, the shells without cutouts displayed greater stiffness than those with large cutouts; requiring larger compressive loads to collapse the solid shell panels (see Figures 12, 13, 14). Note also how linear the curves are for the solid panels versus the panels with cutouts, where in this case the nonlinearity occurs throughout most

of the loading range. This indicates that a greater magnitude of bending is occurring in the panels with the large cutouts. The greatest degree of bending appears to be present in the 24-ply solid shell panels. The difference in panel axial length appeared to significantly affect the difference in collapse loads between shell panels with cutouts and those without. A collapse load increase of 139% between the 8-ply 12" X 12" panel with cutout and the solid one of the same dimensions was observed; whereas an increase of only 79% was observed for the 12" X 20", 8-ply solid shells. An increase in collapse load of 79% was observed for the 16-ply case. However, the greatest increase in collapse load between panels with cutouts and those without was seen in the 24-ply case, where an increase of 154% was observed. In addition, as seen in Table 5, as the thickness of the shells increased so did the amount of top edge displacement required to collapse the panels.

When comparing the axial load ( $N_x$ ) versus top edge displacement ( $u$ ) curves for the three thicknesses of shells with no cutouts, it can be seen that the 16 and 24 ply curves exhibit a nonlinear behavior which the 8-ply curve does not. This is related to the fact that greater magnitudes of radial displacement ( $w$ ) occur in the 16 and 24 ply panels (see Table 6), which causes a greater coupling between  $u$  and  $w$ . Apparently at radial displacement values greater than that which occurs in the 8-ply case, the nonlinear  $w$  terms present in the  $\epsilon_1^o$  and  $\epsilon_2^o$  (in-plane normal strains) expressions [20: 44 - 45], used in SHELL's formulation, become more pronounced and cause the  $N_x$  versus  $u$  curves to go nonlinear. Note that  $\epsilon_6^o$  (in-plane shear strain) does not affect the  $N_x$  values for either the quasi-isotropic or cross-ply laminated shells since  $A_{16}$  is zero for both layups. For a more convenient reference, these in-plane strain expressions are presented below, where  $c = 1/R$ :

$$\epsilon_1^o = u_{,1} + (1/2)[(u_{,1})^2 + (v_{,1})^2 + (w_{,1})^2] \quad (28)$$

$$\begin{aligned} \epsilon_2^o = & v_{,2} - wc + (1/2)[(v_{,2})^2 + (w_{,2})^2 + (u_{,2})^2 + v^2c^2 + w^2c^2] + v(w_{,2})c \\ & - (v_{,2})wc \end{aligned} \quad (29)$$

$$\epsilon_6^o = u_{,2} + v_{,1} + (u_{,1})u_{,2} + (v_{,1})v_{,2} + (w_{,1})w_{,2} + c[ v(w_{,1}) - (v_{,1})w ] \quad (30)$$

As the shell thickness increased so did the overall stiffness of the panels for all cases including those with cutouts (see Figures 15 and 16). Figures 17 and 18 show that when comparing all panels with the common dimension of 12" X 20", the loads required to collapse the shells increased exponentially with a linear increase in thickness. Note that the slope of the curve is steeper for the case comparing collapse loads versus thickness of the shells without cutouts, than it is for the case comparing shells with cutouts. This effect is probably due to the significant increase in the magnitudes of transverse shear strain present in the shells with cutouts versus those without cutouts (see Table 7).

When comparing the 12" X 12" shells to the 12" X 20" shells it can be seen that significantly greater magnitudes of transverse shear strain occur in the panels which are longer in axial length. By referring to Table 7, it can be seen that about a 60% difference in transverse shear strain exists between the two lengths of 8-ply shells, for both with and without cutouts. It should be noted that the maximum transverse shear strain values represent shear strain distributions of similar orders of magnitude, which symmetrically exist around the four corners of a cutout and along a panel's unsupported vertical edges. Also, the greater bending rotations associated with the longer panels would indicate that these panels respond less stiffly than the shorter panels to compressive loading. In addition, the panels with the smaller aspect ratios collapsed at higher loads, up to 72% higher for the solid panel cases. Therefore, it can be concluded that increasing a shell's aspect ratio will reduce the load levels required to collapse the panel.

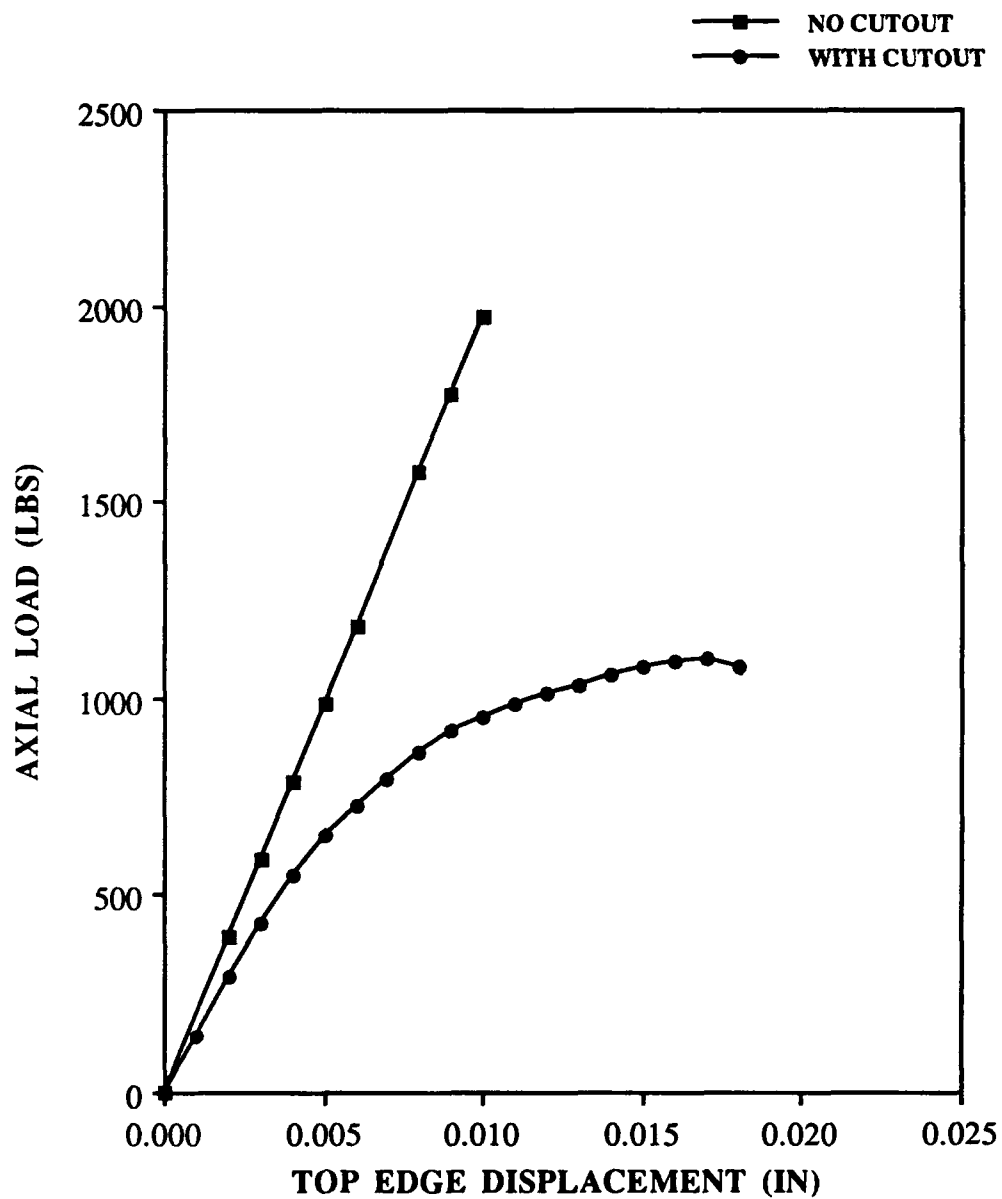


Fig. 12: Comparison of Collapse Response  
For 8-Ply Quasi-Isotropic Shells,  
With and Without Cutouts (12"X20")



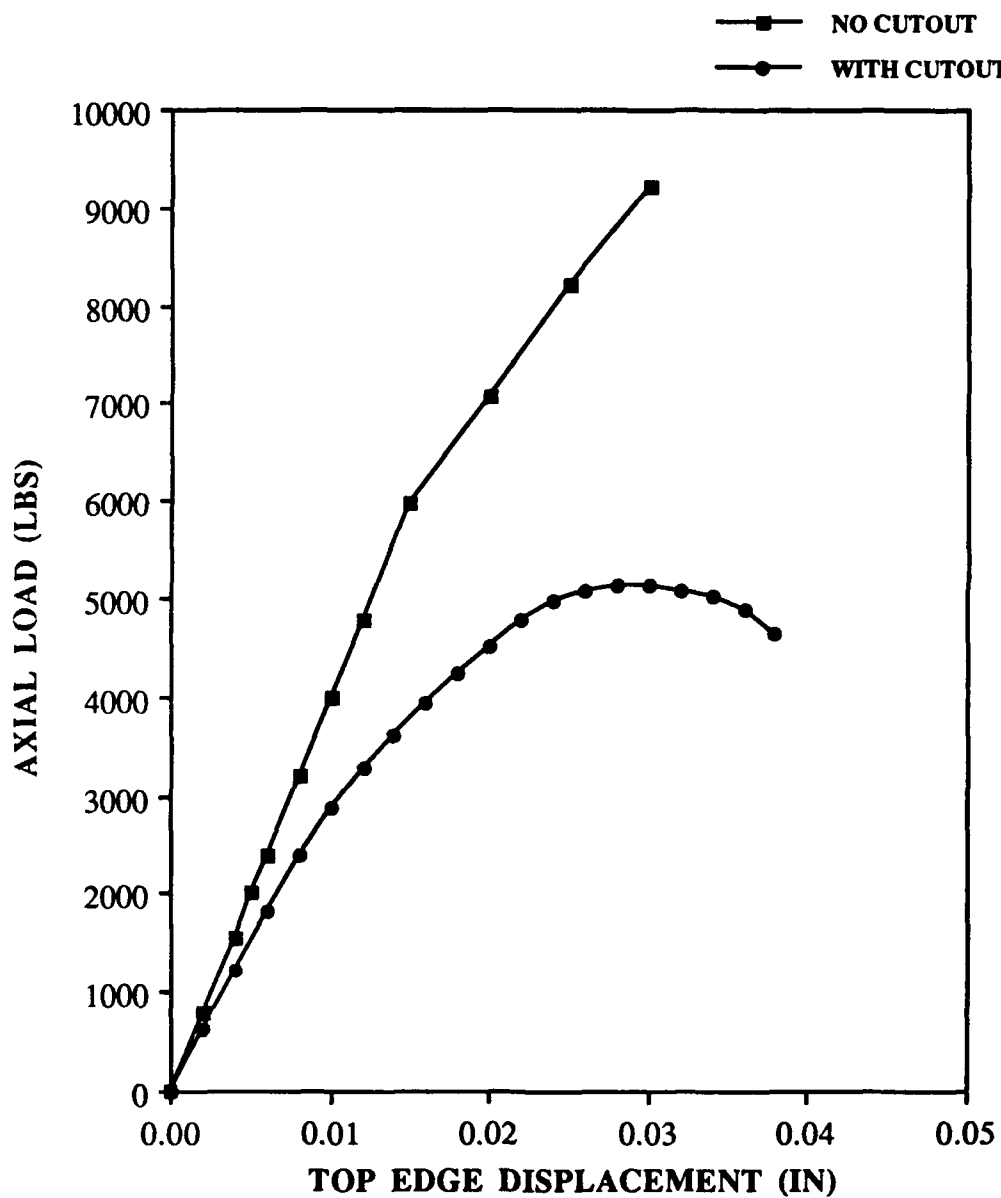


Fig.13: Comparison of Collapse Response  
For 16-Ply Quasi-Isotropic Shells,  
With and Without Cutouts (12" X 20")

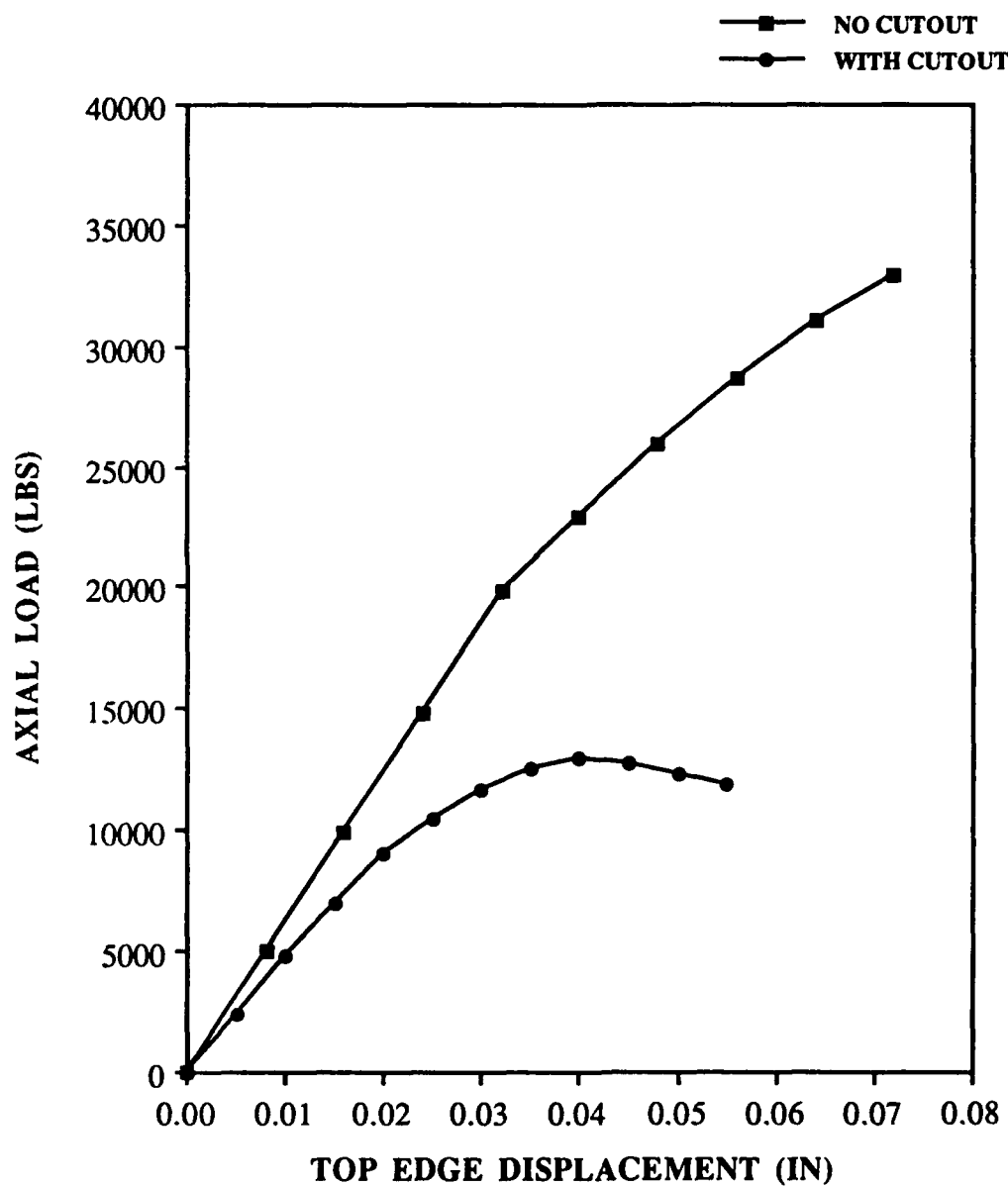


Fig.14: Comparison of Collapse Response  
For 24-Ply Quasi-Isotropic Shells,  
With and Without Cutouts (12" X 20")

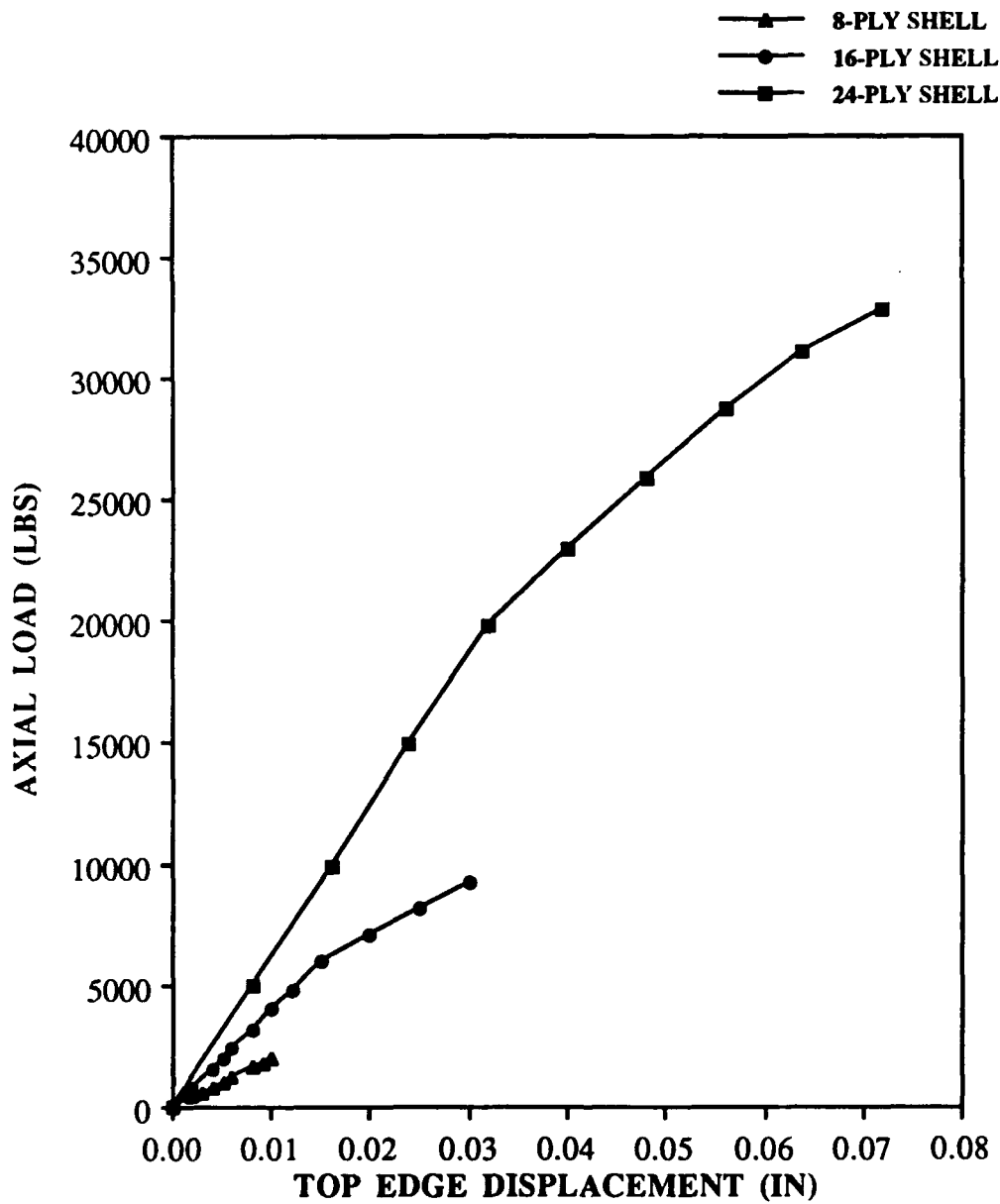


Fig.15: Comparison of Load vs. Top Edge Displacement Curves, For Quasi-Isotropic Shells with No Cutouts(20")

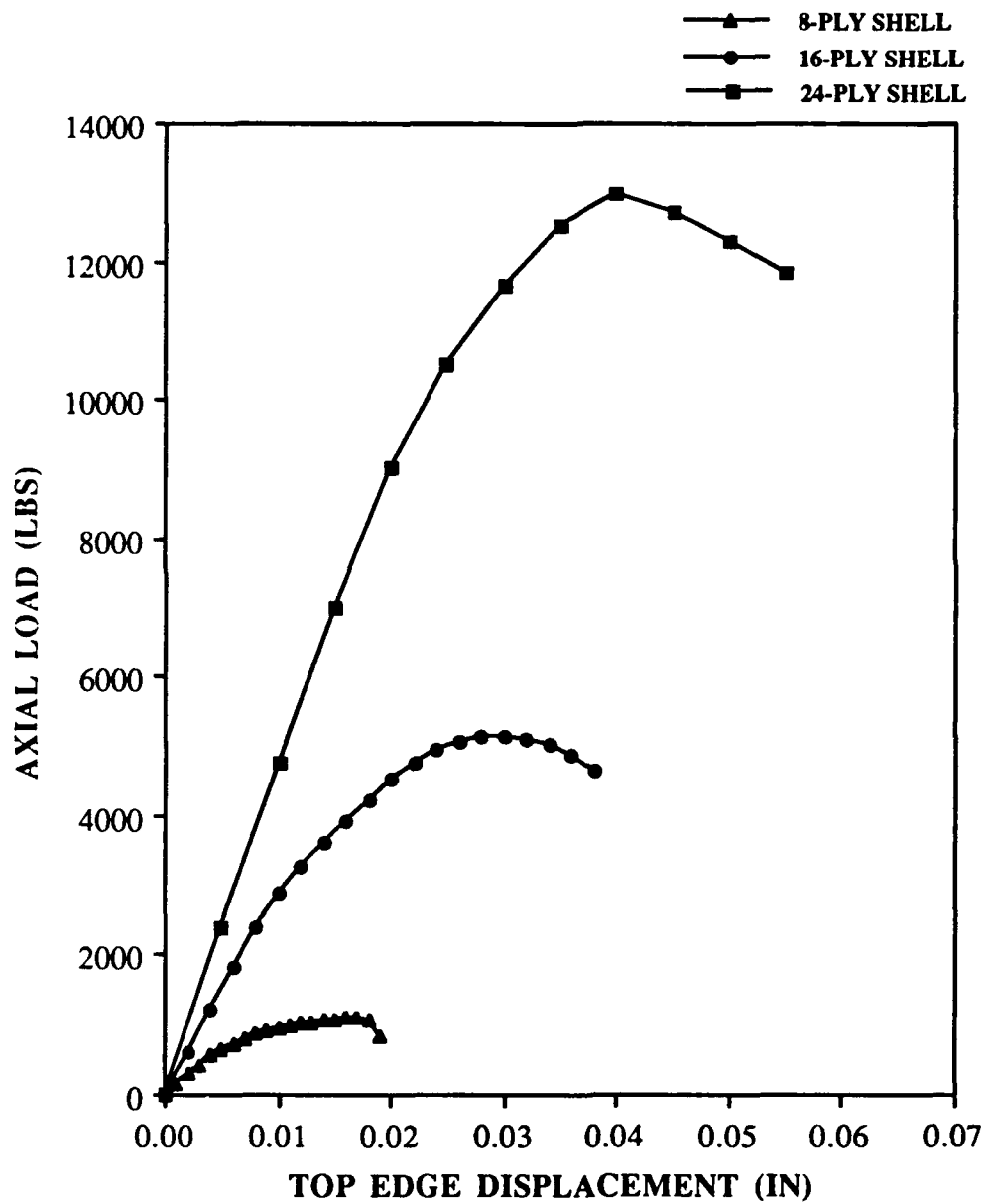
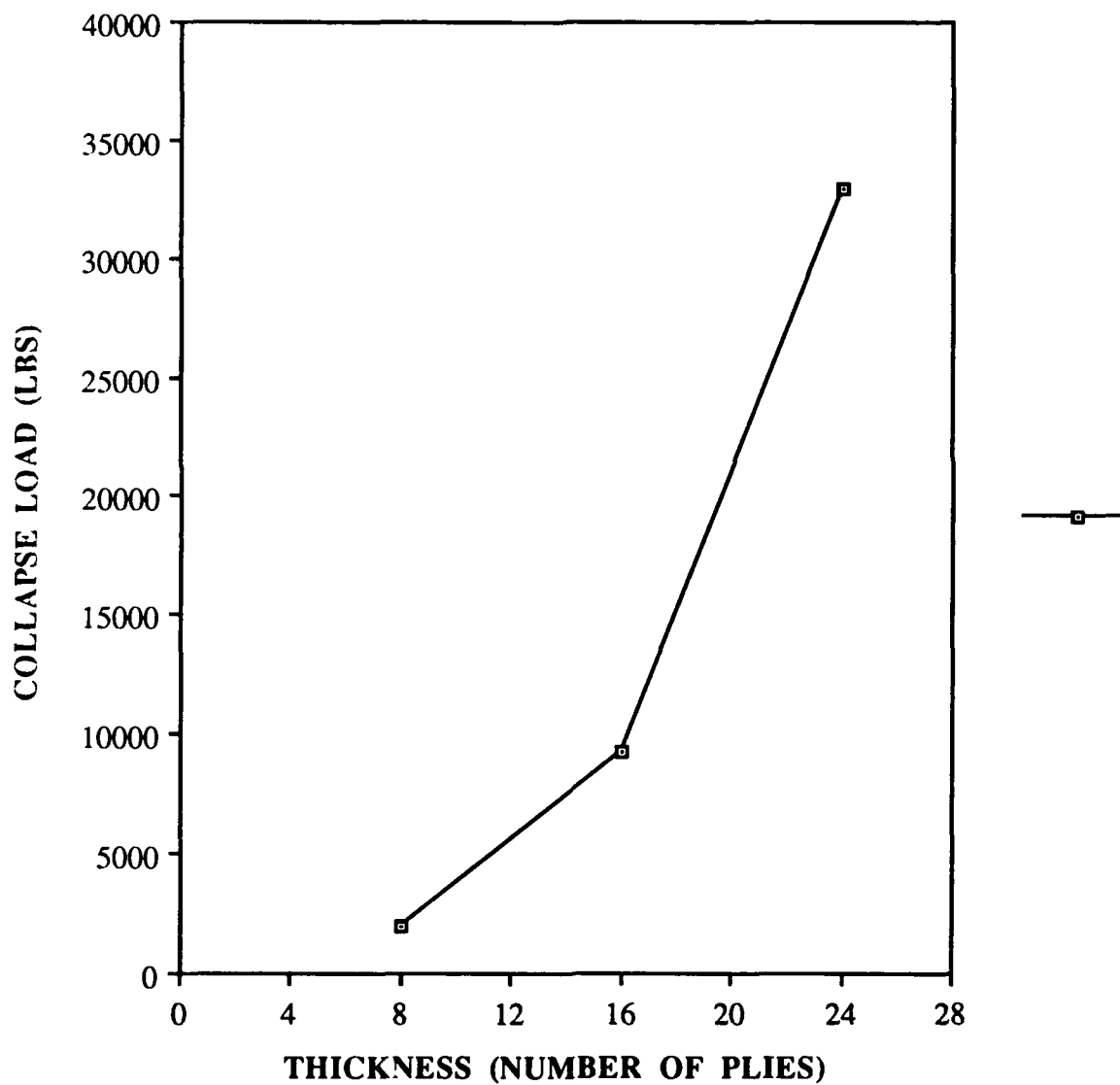
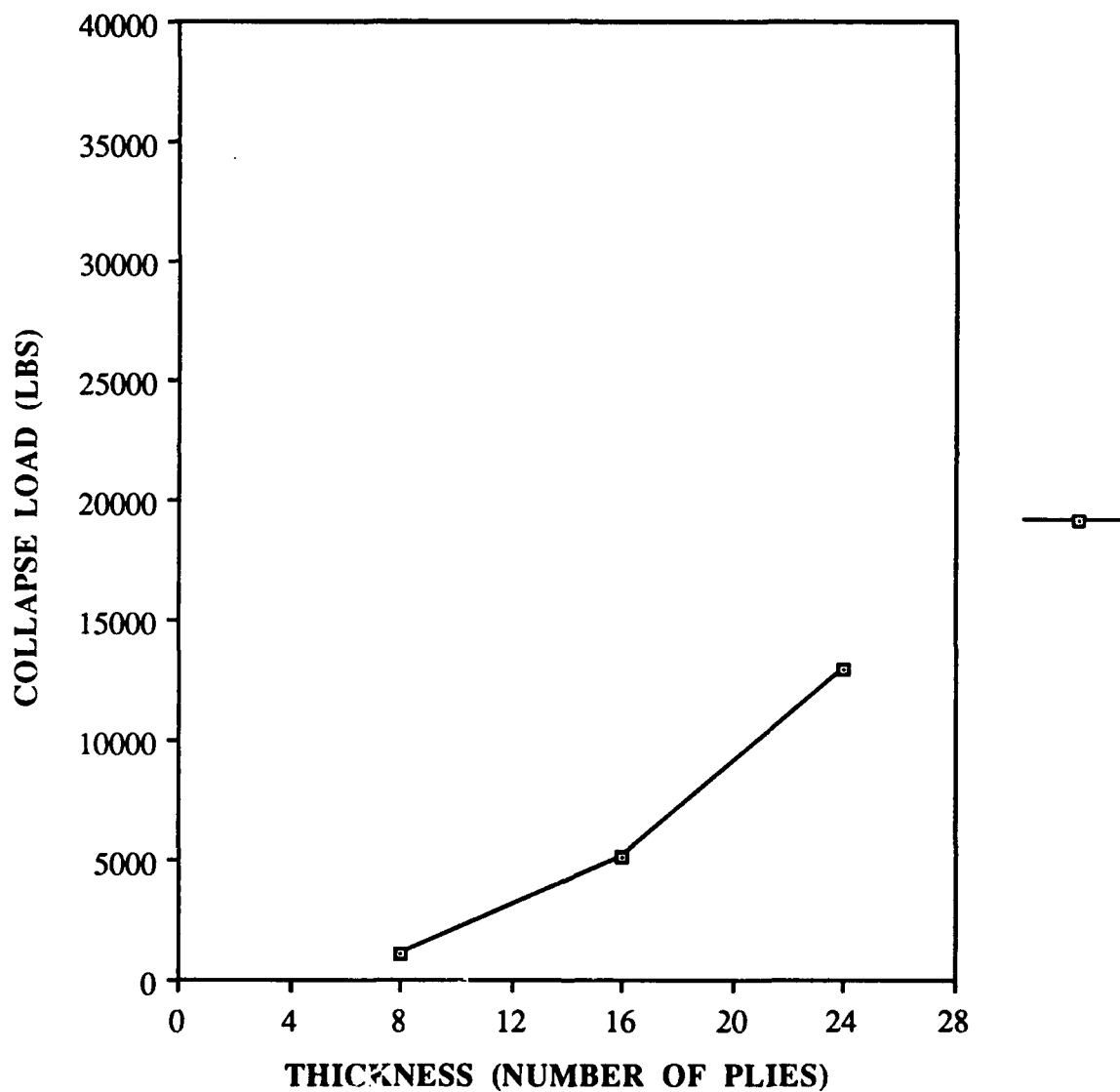


Fig.16: Comparison of Load vs. Top Edge Displacement Curves, For Quasi-Isotropic Shells with Cutouts(12 X 20)



**Fig. 17: Collapse Load vs. Shell Thickness**  
(Quasi-Isotropic, No Cutouts)  
(12" X 20")



**Fig. 18: Collapse Load vs. Shell Thickness**  
(Quasi-Isotropic, 4" Cutouts)  
(12" X 20")

The magnitudes of transverse shear strain increased with increasing panel thickness. The change in the magnitudes of transverse shear strain present in the collapsed panels is fairly insignificant in a comparison between the 8 and 16 ply shells; but becomes significant when comparing the 16-ply shells to the 24-ply shells, where the magnitudes increase by a factor of two. This result was consistent for the shell panels with cutouts as well as those without cutouts. It should also be noted that the presence of a large cutout dramatically increased the magnitudes of transverse shear strain found in the shells when compared to the solid shells. It was consistently observed that the largest transverse shear strains for panels with cutouts occurred near the four corners of the square cutouts. For the 8-ply and 16-ply solid shells, the greatest transverse shear strain distributions occurred along the vertical unsupported edges near the panel center. However, for the stiffest panel (24-ply solid shell) these transverse shear distributions migrated towards the clamped edges at the top and bottom of the panel, forming four small pockets of intense transverse shear strain about 2-3 inches from the clamped edges. As expected, the magnitudes of transverse shear strain for all the solid panels gradually decreased as the nodal locations moved towards the panel's vertical centerline, with zero shear strain resulting along the centerline. In particular, for the stiffer 16-ply and 24-ply solid panels, extremely small bending rotations were observed along the vertical centerlines at collapse.

#### 5.2.2 *Cross-Ply Shell Panels*

The numerical analysis performed on the cross-ply shell panels indicates that the largest radial displacements generally occurred along the vertical free edges and near the panel's horizontal centerline. However, in one case ( $[0/90]_{2s}$ , 12" X 12" solid shell) it was noticed that in addition to this phenomena, even larger magnitudes of radial displacement occurred along the vertical edges, about 2" away from the clamped nodes. This indicates that this particular panel behaved more stiffly with respect to its planform area than the other panels investigated. In fact, there was a 251% increase in collapse load for this panel

when the large cutout configuration was compared to the no cutout configuration. This percentage increase was the largest of all the panels studied, including the thicker quasi-isotropic shell panels. In addition, at the points near the clamps where large radial displacements were noticed, the largest transverse shear strains in the shell occurred. The transverse shear strain locally reduces the stiffness of the panel, which enhances the effect of the bending in this area and increases the radial displacements. With respect to the 12" X 20" cross-ply configurations, a 38% increase in collapse load was observed for the 8-ply solid shell versus shell with a cutout; a 72% increase was observed for the 16-ply solid shells and a more significant increase of 142% in collapse load was seen for the 24-ply solid shell.

Figures 19, 20, and 21 indicate that, as with the quasi-isotropic shells, the shells with cutouts are more flexible than the shells without cutouts. As with the quasi-isotropic shells, greater nonlinearity exists in the load versus top edge displacement curves for the cross-ply shells with cutouts, indicating that a greater degree of bending is occurring in the shells with cutouts. In addition, when comparing the curves for shells with no cutouts, nonlinear behavior enters into the collapse of only the 16-ply shells at around 5500 lbs. Table 7 shows that for these shells under discussion, the solid 16-ply shell has significantly larger bending rotations (around  $9^\circ$ ) than the 8 and 24 ply cases, at  $5^\circ$  and  $6^\circ$  respectively. Table 6 shows that the radial displacements near the panel center are greater for this 16-ply case than the 8 and 24 ply cases with no cutouts. It is also interesting to note that the maximum radial displacement for the 24-ply panel under discussion is very close in magnitude to the maximum radial displacement for the 8-ply (no cutout) case cited in Figure 12, where the curve was also linear. Therefore, as noted in the 16 and 24 ply quasi-isotropic cases with no cutouts, the nonlinear terms involving radial displacement ( $w$ ) in the SHELL in-plane strain expressions are becoming more important in accurately capturing the collapse response of the 16-ply shell without cutouts. When comparing the cross-ply



responses to the quasi-isotropic responses (Figures 12, 13, 14), the only significant difference in curve trends involves the 24-ply, no cutout cases. The 24-ply cross-ply curve is a straight line all the way up to panel collapse, while the curve for the 24-ply quasi-isotropic case begins as a straight line but bends over at around 20,000 lbs and becomes increasingly more nonlinear. This phenomena implies that for 24-ply cross-ply solid shells a lesser degree of bending exists (along with smaller radial displacements) than in 24-ply quasi-isotropic solid shells. It makes sense that greater bending is occurring in the quasi-isotropic shells because of the much greater rotations in the 24-ply quasi-isotropic case ( $12^\circ$ ) than the 24-ply cross-ply case ( $6^\circ$ ). This 6 degree difference in magnitude of maximum bending rotations results in an 83% increase in magnitudes of radial displacements in the 24-ply quasi-isotropic shell with no cutout versus a similar 24-ply cross-ply shell. These larger radial displacements in the quasi-isotropic case cause the nonlinear terms (with respect to  $w$ ) in the strain-displacement relations to become more pronounced. In addition the bending and twisting, with respect to the circumferential degree-of-freedom, becomes more important because the bending rotations in the curvature expressions are squared [20:44 - 45].

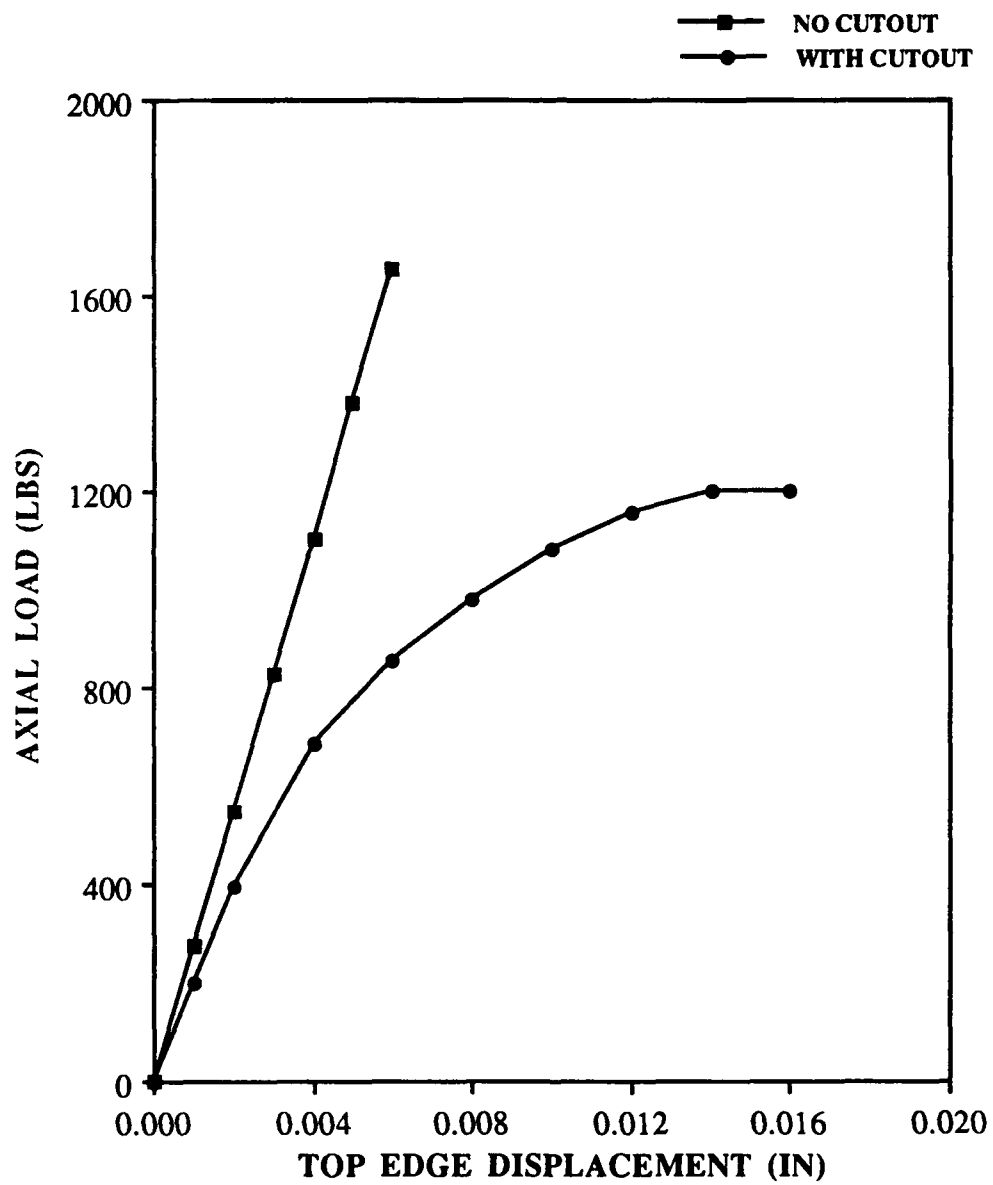


Fig.19: Comparison of Collapse Response  
For 8-Ply Cross-Ply Shells,  
With and Without Cutouts (12" X 20")

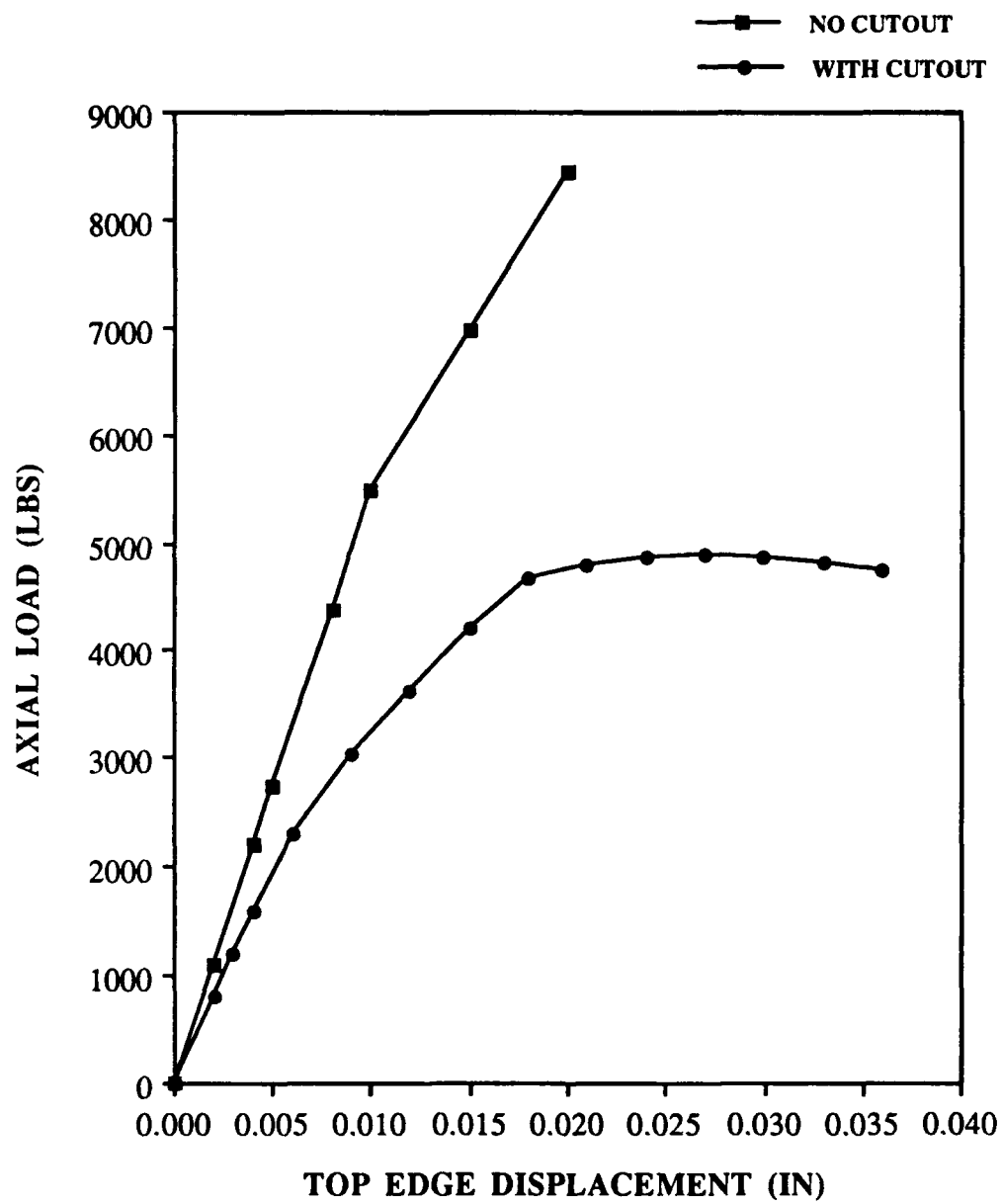


Fig.20: Comparison of Collapse Response  
For 16-Ply Cross-Ply Shells,  
With and Without Cutouts (12" X 20")

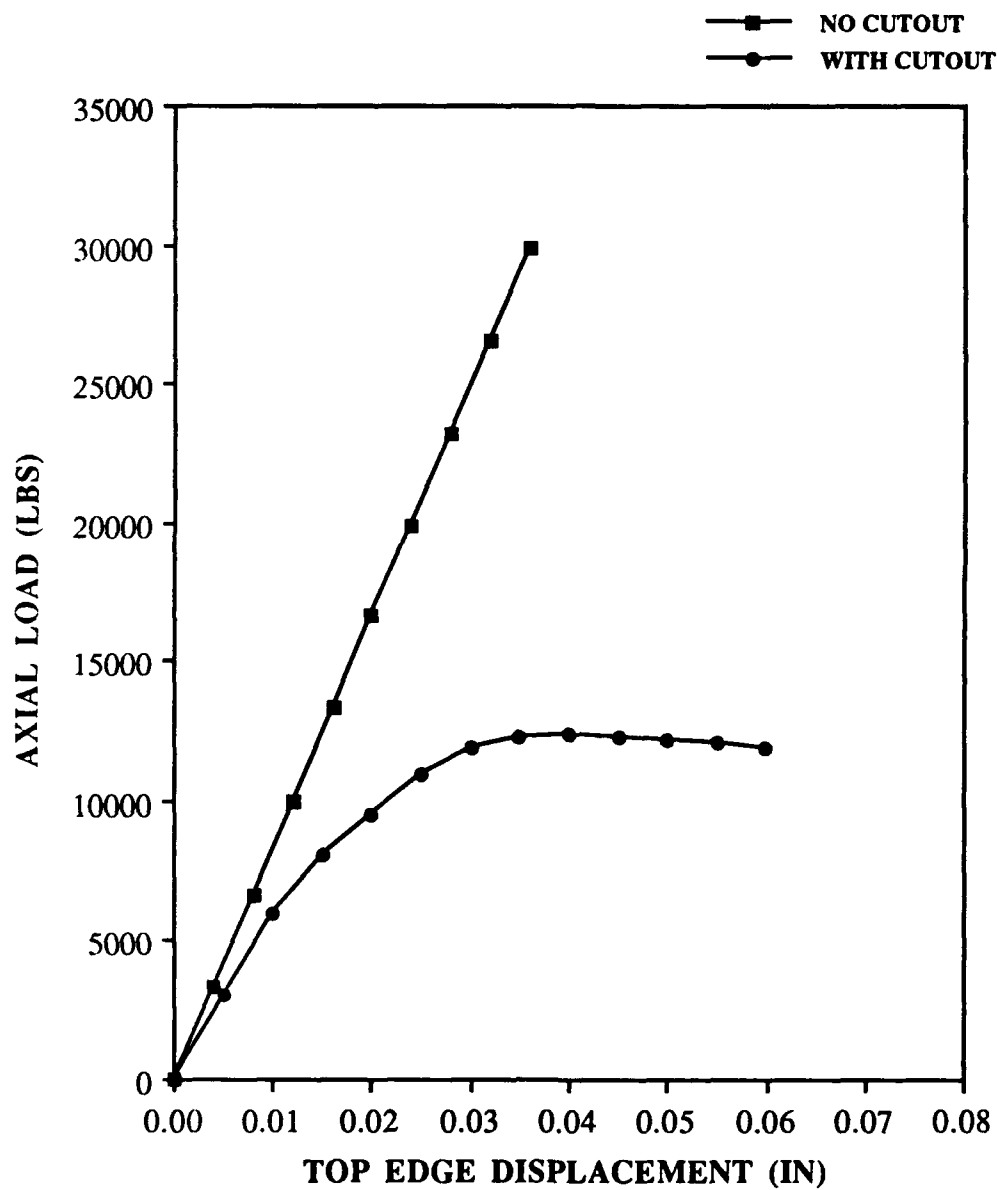


Fig.21: Comparison of Collapse Response  
For 24-Ply Cross-Ply Shells,  
With and Without Cutouts (12" X 20")

Next a comparison was made between Figures 22 and 23 for the various thicknesses of 12" X 20" cross-ply shells with the 12" X 20" quasi-isotropic cases in Figures 15 and 16. No significant difference in the curves was noticed for the 8-ply cases. However, with respect to both the 16-ply and 24-ply cases with cutouts, the cross-ply curves appear to bend over at a faster rate than the quasi-isotropic curves. In addition, another difference noticed was that for the cross-ply shells, the curves tend to flatten out near the top of the curve around the collapse load. This implies that for a unit increase in top edge displacement, the cross-ply shells are less stiff and thus support a lesser unit load increase than the quasi-isotropic shells as the load levels approach the collapse load. Figures 24 and 25 display how the collapse loads vary with thickness for panels with and without cutouts. These curves show an excellent correlation with the similar trends found in the quasi-isotropic cases.

Intuitively, one would think since the cross-ply shell laminates have a greater percentage of  $0^\circ$  fibers than the quasi-isotropic shell laminates that the cross-ply shells would always be more stiff and collapse at higher loads than the quasi-isotropic panels. In fact, axially the cross-ply panels have a higher stiffness ( $A_{11}$ ) than the quasi-isotropic panels. However, there are other phenomena present during axial compression that contribute to making the cross-ply panels more flexible than the quasi-isotropic panels as the compressive loads are increased. As Table 7 (page 47) shows, transverse shear strain magnitudes increase with increasing panel thickness and are greatest in shells with cutouts. Note also that the transverse shear strain levels are very similar in magnitude for both the cross-ply and quasi-isotropic cases with respect to the 16-ply cases. However, significant differences in transverse shear strain magnitudes occur within the 8-ply cases and to a lesser extent with the 24-ply shells with cutouts. The greatest difference in transverse shear strain occurs with the solid 12" X 12" 8-ply shell, where the strain is 62% greater in the cross-ply case than in the quasi-isotropic case. A much more similar transverse shear strain

level is noted (within 17%) when large cutouts are placed in these panels. The other cases where a significant difference (about 40%) in the transverse shear strain occurs involves the 12" X 20" 8-ply shell panels, where the cross-ply panels (with and without cutouts) display a greater magnitude of transverse shear than the quasi-isotropic panels. Increases in transverse shear strain make a shell panel more flexible and thus enhance the bending and twisting present. In addition, it has already been noted that due to a greater  $D_{66}$  and the existence of  $D_{16}$  and  $D_{26}$  in the quasi-isotropic bending stiffness matrix that greater twisting resistance will occur in these types of laminates than in cross-ply laminates for a similar increase in compressive load. Since the out-of-plane normal strains are zero and the transverse shear strains are of similar orders of magnitude for both the cross-ply and quasi-isotropic shell cases, the phenomena which is significantly enhancing the bending in the 16 and 24 ply (and possibly the stiffer 8-ply cases) must be related to the in-plane strains/stresses. Furthermore, for a given shell thickness, cross-ply laminates are inherently more resistant to in-plane normal stresses (due to larger  $A_{11}$  and  $A_{22}$  stiffnesses) than quasi-isotropic laminates because of a greater percentage of  $0^\circ$  and  $90^\circ$  fibers. However, the area where cross-ply laminates are definitely weaker than the quasi-isotropic laminates is in dealing with in-plane shear stresses and twisting moments, due to a lack of  $\pm 45^\circ$  fibers. Therefore, in-plane effects can become more important when bending rotations and radial displacements are fairly large.

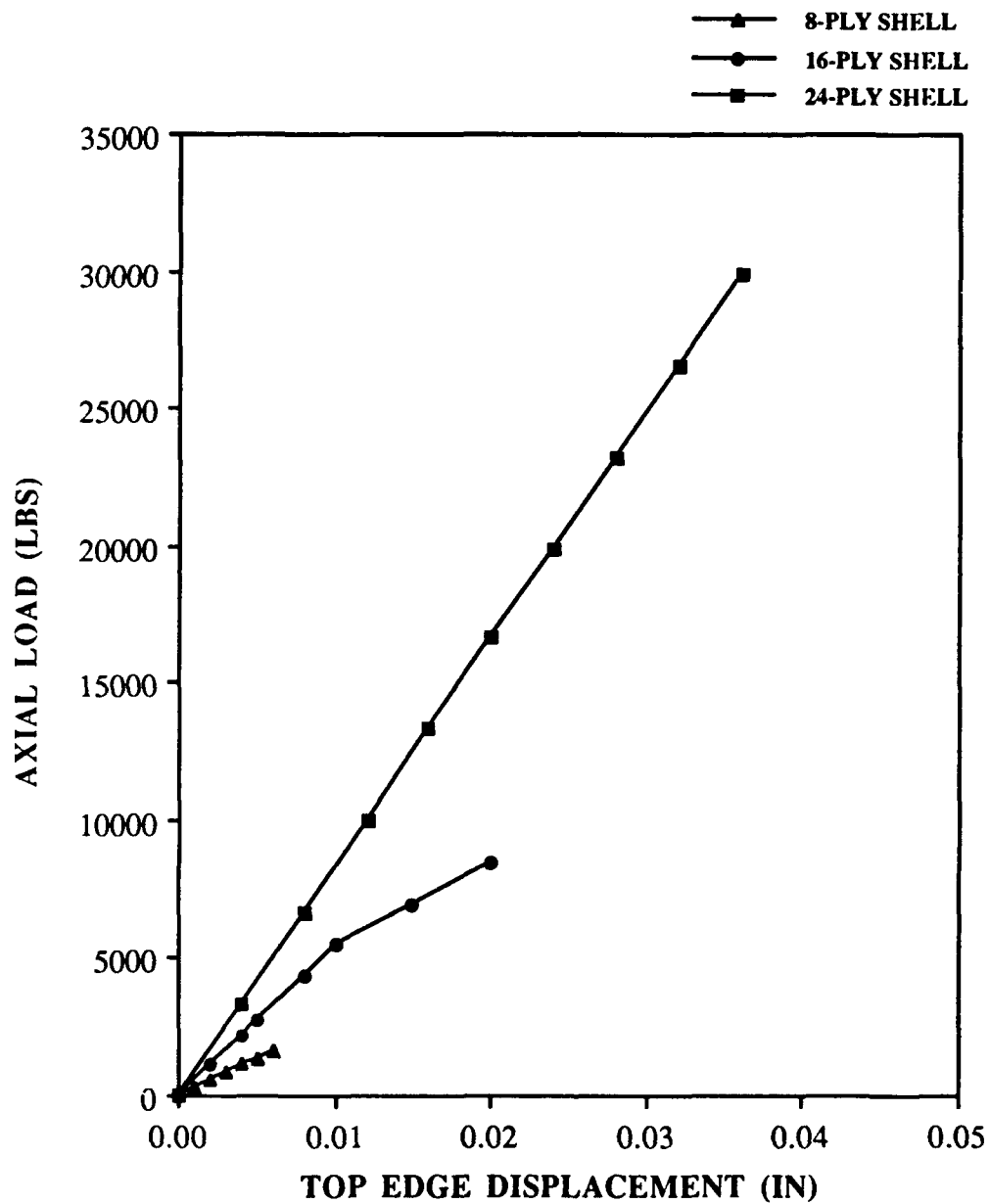


Fig.22: Comparison of Load vs. Top Edge Displacement Curves, For Cross-Ply Shells with No Cutouts (12" X 20")

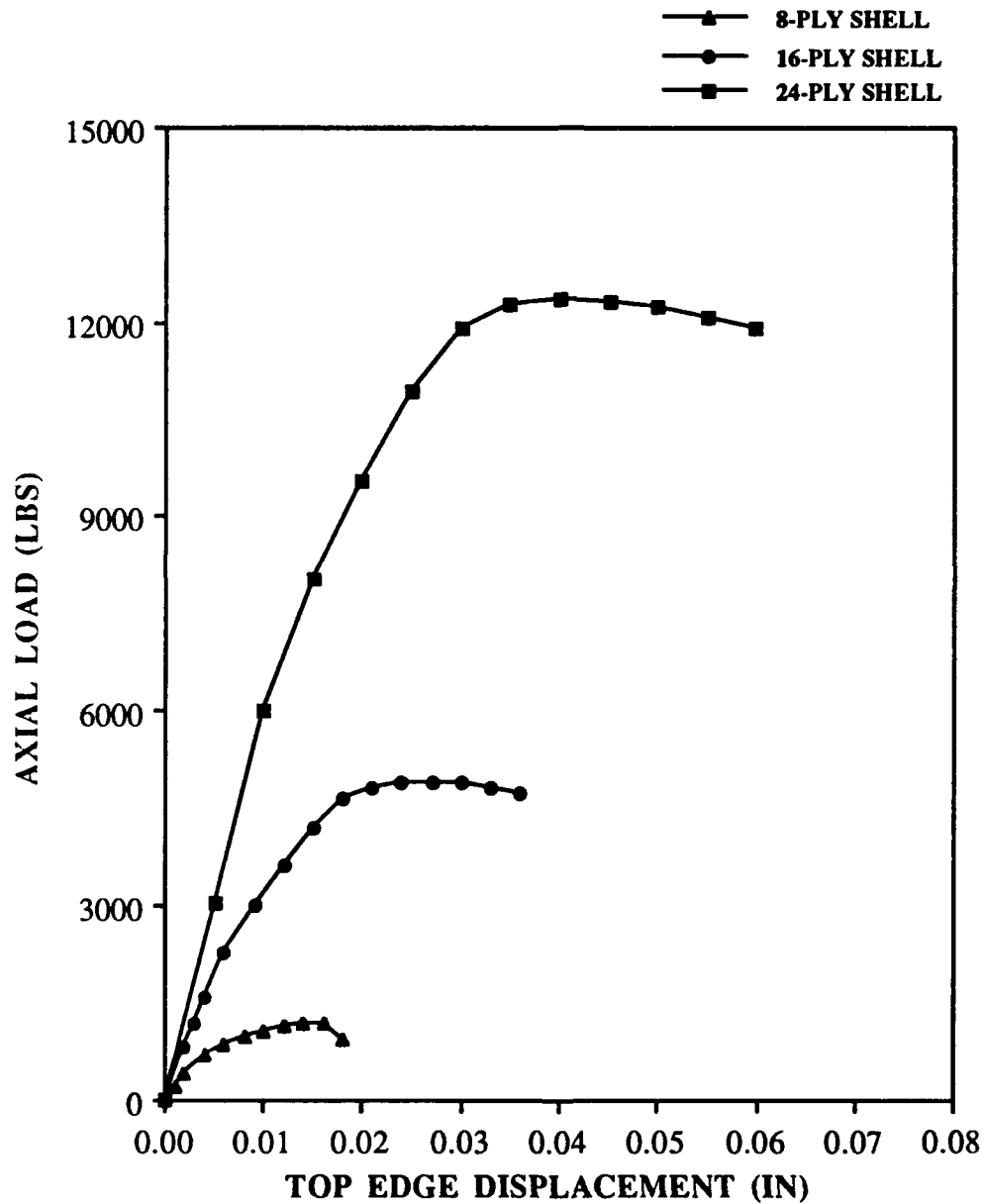


Fig. 23: Comparison of Load vs. Top Edge Displacement Curves, For Cross-Ply Shells with Cutouts (12" X 20")



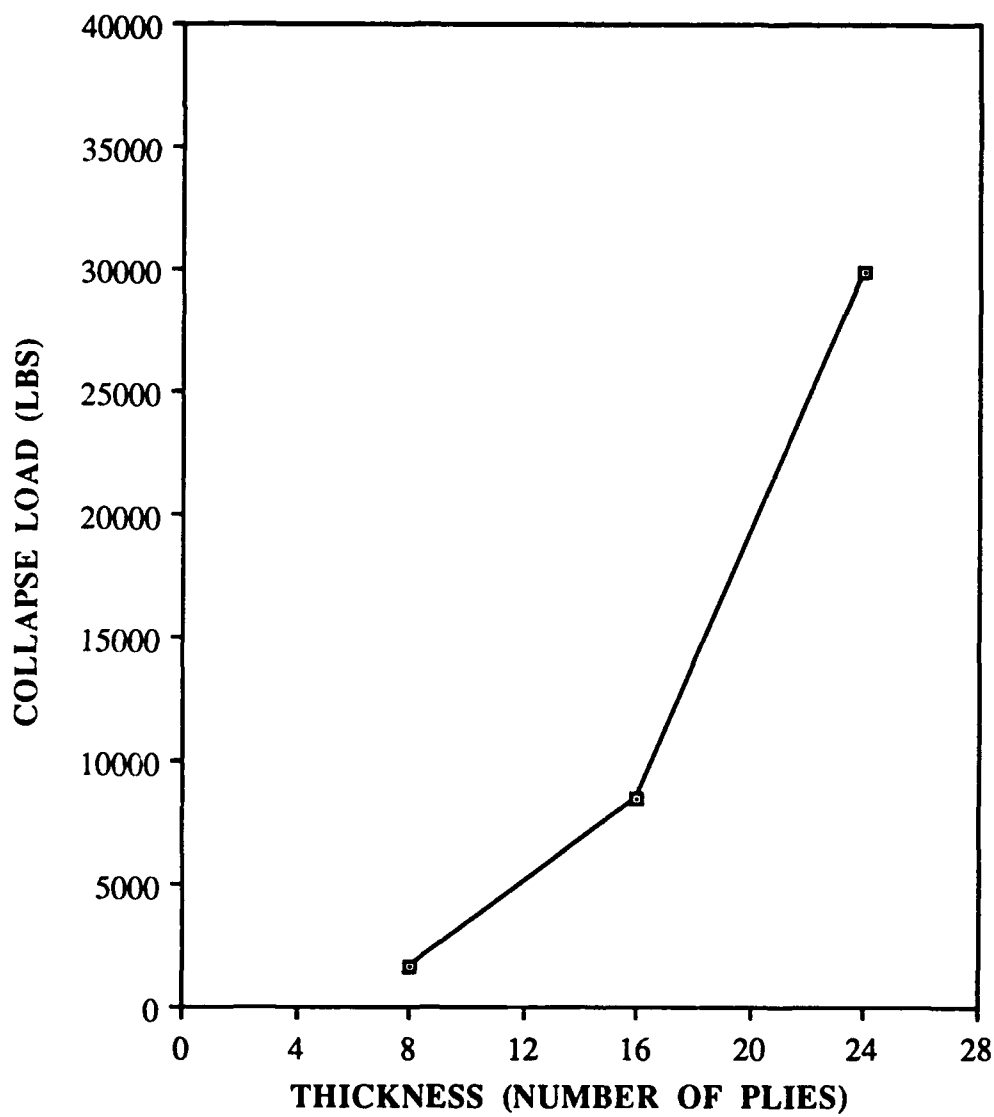


Fig. 24: Collapse Load vs. Shell Thickness  
(Cross-Ply, No Cutouts)  
(12" X 20")

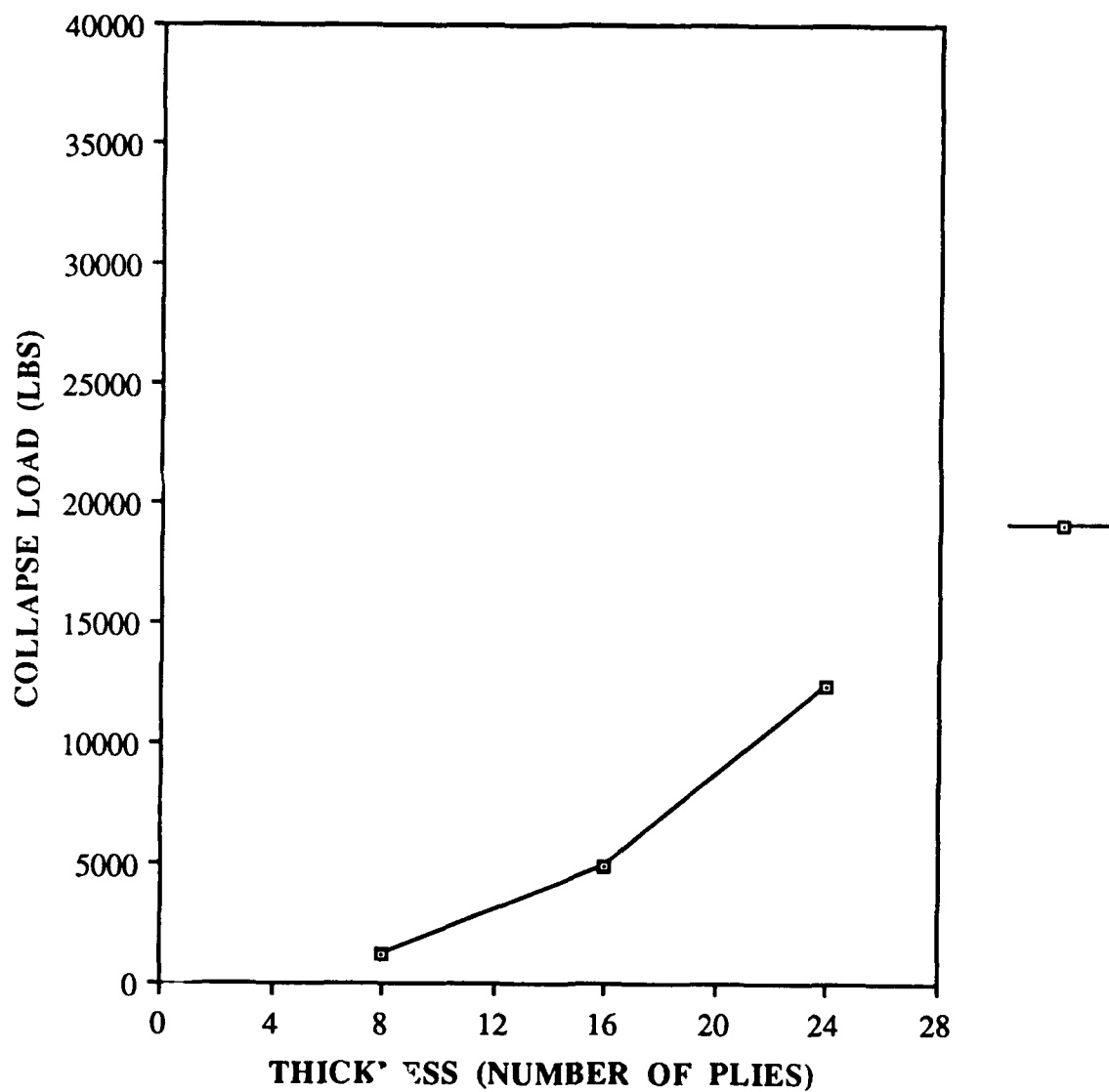


Fig. 25: Collapse Load vs. Shell Thickness  
(Cross-Ply, 4" Cutouts)  
(12" X 20")

Another hypothesis involving interlaminar behavior may also explain the difference in stiffness behavior between the cross-ply and quasi-isotropic shell laminates as panel thickness increases. There is a more gradual change in strength properties and stress behavior going from ply to ply with quasi-isotropic laminates versus cross-ply laminates. This is due to a greater difference in ply orientation angles for the cross-ply laminates as one moves from ply to ply. This ply-to-ply difference in the stress behavior, becomes more pronounced as the magnitude of bending becomes greater. This increase in bending is greatly enhanced by the significant increase in transverse shear strain which occurs as the thickness of the shell panel increases.

### 5.3 *Experimental Results*

The test plan (see Appendix A) was executed and all 32 panels that were manufactured for this research effort were tested. Some interesting results, both quantitatively and qualitatively were obtained. In all cases, the experimental shell panels responded more flexibly to loading than predicted by the stiffer analytical models. A comparison between experimental and numerical results for the global collapse load response is presented in Table 8. Three tests were run for each panel configuration and in most cases the collapse load presented in Table 8 is an average value. However, in some of the thicker panels, obtaining even loading throughout the test became a problem; in these cases an average was taken only of the tests that had fairly even loading. Many of the 16 and 24 ply panels with cutouts suffered fiber crimping/breakage and delamination (near the cutout) during collapse and could not be retested. Only the stiffest panel  $[(0/+45/-45/90)_{3s}]$  with no cutout) when retested was capable of reaching collapse loads of equal or greater value to the first three runs. Therefore, the other panels must have had some type of failure mechanism present that was not apparent to the naked eye. In addition to Table 8, experimental versus numerical panel response is graphically displayed throughout this section and in Appendix B in the form of load versus top edge displacement curves and

load versus radial displacement curves. The experimental and numerical radial displacement curves compare data obtained at discrete points, which correspond to the node numbers displayed in Figures 9 and 10.

The general trend depicted in Table 8 is that there is a greater difference between the experimental and the numerically-derived collapse loads for the shells with no cutouts. There are numerous reasons why this is the case, but keep in mind that the response of the shells without cutouts is largely a factor of the degree of precision in the panel manufacturing process. With any composite material there will be fiber/matrix material property imperfections, imperfect adhesion between laminae, as well as stress discontinuities between lamina boundaries which develop when the laminate is loaded. The greater the difference between the stress response from lamina to lamina, the greater the probability that these stress discontinuities will contribute to decreasing the overall panel stiffness. Table 7 showed that the magnitudes of transverse shear strain present in the collapsed 8-ply shell panels was fairly small for those panels without cutouts. This indicates that transverse shear strain for 8-ply shell panels without cutouts is negligible and does not significantly contribute to the panel collapse. Note that the transverse shear strain (see Table 7) becomes significantly more pronounced in the 24-ply solid panels than it is in the 8 and 16 ply shells.

The SHELL algorithm assumes the material properties are constant throughout each ply, neglects interlaminar slipping, and assumes each ply is of the same thickness. In actuality, these factors vary from lamina to lamina and the fiber/matrix properties may vary even within each ply. Variation in ply thickness can affect how each lamina and overall laminate responds to loading. If this variation in thickness induces off-axis loading, with respect to the fibers, then unaccounted for shear stresses could develop and reduce the stiffness of the shells used in the experiments.

*Table 8. Comparison Between Experimental and Numerical Collapse Loads*

**8-Ply Shell Panels**

<u>Configuration</u>	<u>Experimental Load (lbs)</u>	<u>Numerical Load (lbs)</u>	<u>Difference (%)</u>
CP, NC, 12"	2128	4683	54.6
CP, NC, 20"	1460	1654	11.7
CP, C, 12"	1163	1333	12.8
CP, C, 20"	928	1200	22.7
QI, NC, 12"	2075	3387	38.7
QI, NC, 20"	1459	1971	26.0
QI, C, 12"	997	1418	29.7
QI, C, 20"	751	1100	31.7

**16-Ply Shell Panels**

<u>Configuration</u>	<u>Experimental Load (lbs)</u>	<u>Numerical Load (lbs)</u>	<u>Difference (%)</u>
CP, NC, 20"	7767	8439	8.0
CP, C, 20"	4928	4896	+ 0.65 *
QI, NC, 20"	8363	9218	9.3
QI, C, 20"	4286	5131	16.5

**24-Ply Shell Panels**

<u>Configuration</u>	<u>Experimental Load (lbs)</u>	<u>Numerical Load (lbs)</u>	<u>Difference (%)</u>
CP, NC, 20"	14,007	29,838	53.1
CP, C, 20"	9032	12,346	26.8
QI, NC, 20"	16,409	32,874	50.1
QI, C, 20"	10,088	12,959	22.2

CP = Cross-Ply Laminate

QI = Quasi-Isotropic Laminate

C = 4" X 4" Cutout

NC = No Cutout

\* See Section 5.4: Experimental Difficulties

Another factor contributing to the sometimes large differences (up to 53%) between the theoretically-derived numerical results and the experimental results has to do with imperfections in the shell's curvature. First, the radius of curvature of the datum surface can vary within the manufactured shell panel and therefore two panels of the same "prescribed" curvature may in fact respond differently, all else being equal. In fact, the shell's curvature affects the geometric stability of the panel from the start. The panels were layed up before curing for a 12" radius of curvature. However, a visual inspection of the panels after curing revealed that this curvature was not entirely constant (geometric imperfection existed) in the panels' relaxed state, especially near the panels' center. During experimentation, when the shell is clamped into the 12" radius of curvature loading fixture, residual stresses may be induced into the panel (in addition to the residual stresses that may already be present from the curing process). These stresses would become increasingly larger towards a panel's center due to the greater amount of stiff material surrounding the center, which acts to constrain its movement. When a large cutout is placed in the center of the shell panel, these stresses are relieved. Similar trends with respect to curvature imperfection were also documented in a technical report by Leissa [16].

In most experimental cases, it was noted that the percent difference between the results and the numerical data was decreased for the shells with large cutouts. The presence of a cutout increases the surface bending rotations and significantly increases the magnitude of transverse shear strain. Therefore, the affect of a cutout on the collapse greatly overrides many of the geometric or material imperfections that may be present.

One final factor that could partly explain the differences between analytical and experimental results concerns the evenness of the applied distributed load. The effect of uneven loading was investigated during the experimentation done for this research effort and will be discussed later in the section on experimental difficulties.

Figures 26 - 43 represent the global responses (applied load versus top edge displacement curves) and the local responses (applied load versus radial displacement curves) near the panel center along the unsupported vertical edges and around the cutouts, for those configurations where the most even loading distribution was experimentally obtained. Cases where uneven loading was a significant factor are discussed in the next section. It should also be noted that in these graphs the numbers in parentheses indicate the node numbers where the data was collected and can be cross-referenced to Figure 10.

Experimental radial displacement data was collected at locations which corresponded as close as possible to similar locations in Figures 9 and 10, which depict the analytical models. Note that due to a limitation in the apparatus which held the LVDTs in place, it was not possible to collect data at points near nodes 921 and 897 (which are the same relative points for the two different models). Overall, the experimental panels responded more flexibly to the compressive loads with a greater degree of bending. The reasons for the differences between the experimental and numerical global responses of the panels were discussed earlier in this section. Despite the differences in panel stiffness, the SHELL algorithm was able to predict fairly accurately the local response behavior trends. Even though the increased flexibility of the experimental shell panels, as expected, resulted in larger magnitudes of displacements, the experimental curves followed closely the general movement of the curves in terms of direction and slope.

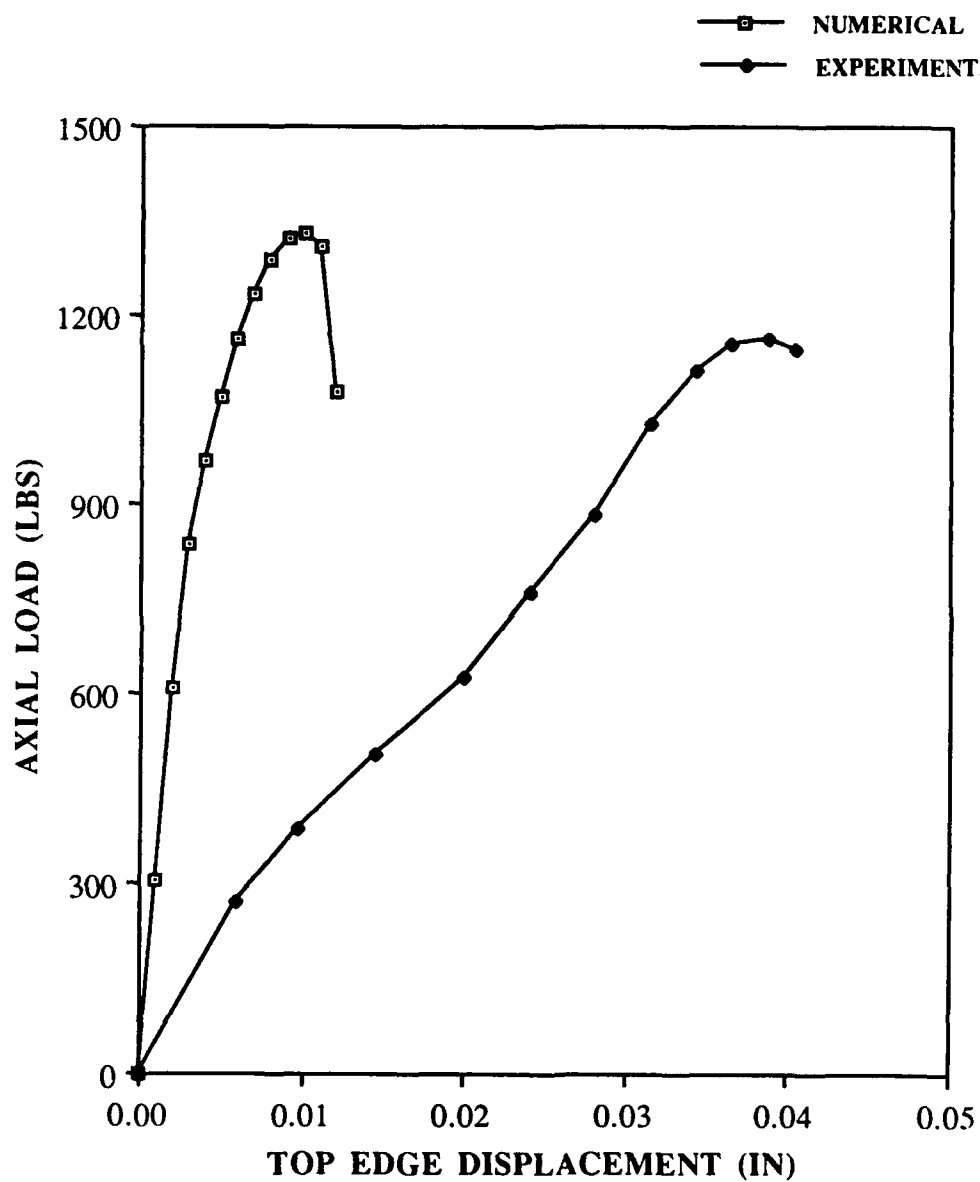


Fig. 26: Load vs. Top Edge Displacement,  
[0/90]2s, 4" Cutout  
(12" X 12")



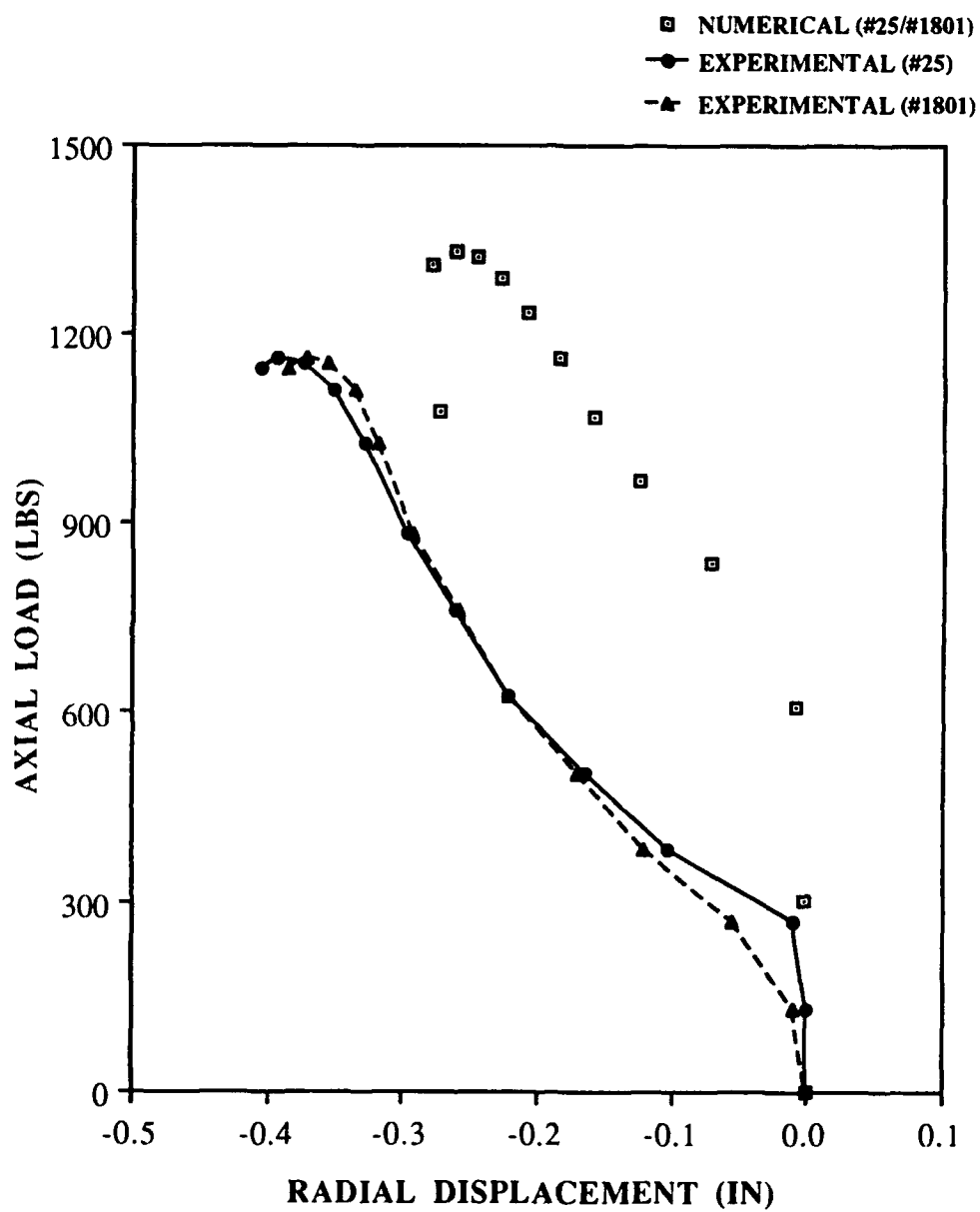


Fig. 27: Load vs. Radial Displacement,  
[0/90]<sub>2s</sub>, 4" Cutout  
(12" X 12")

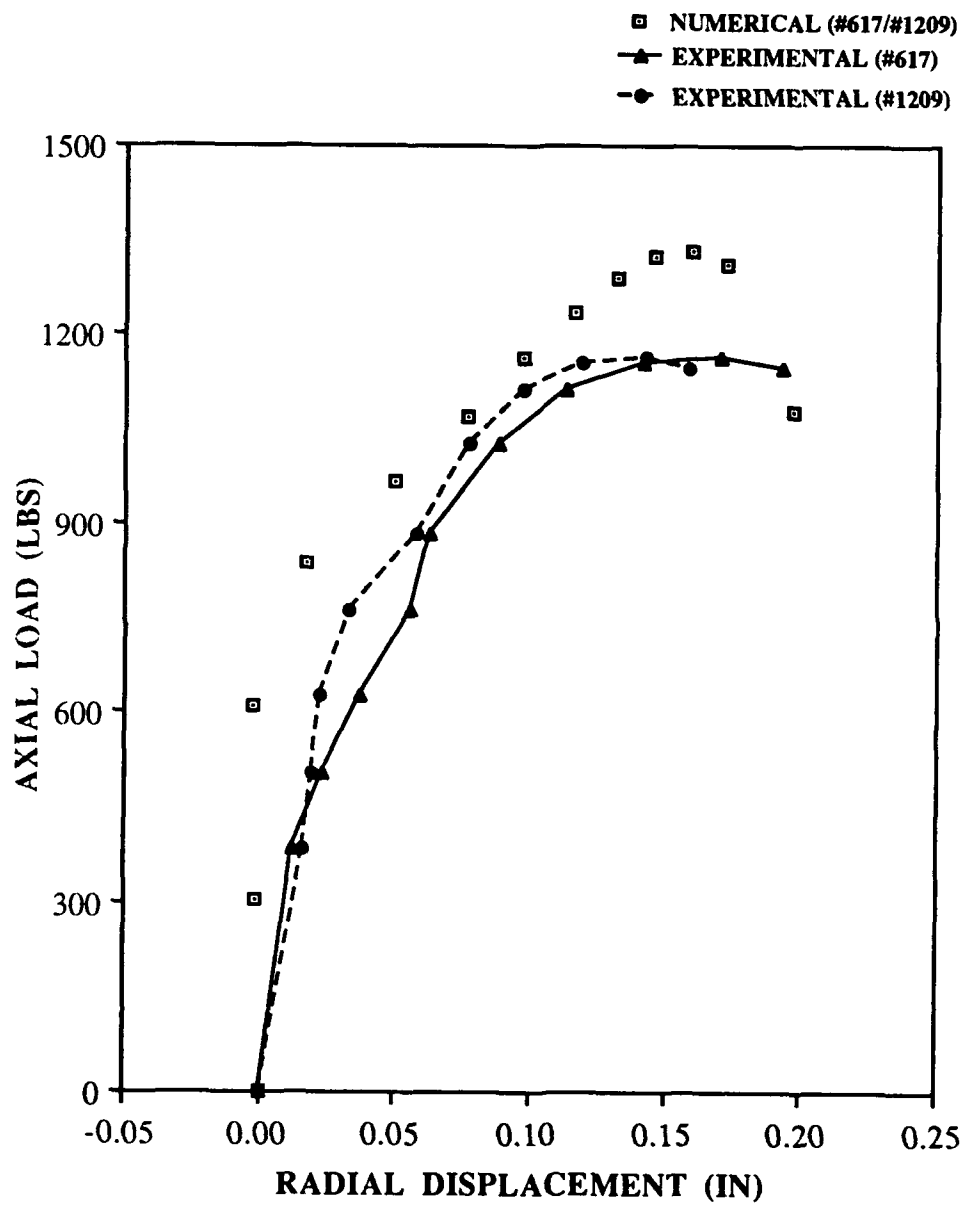


Fig. 28: Load vs. Radial Displacement,  
[0/90]<sub>2s</sub>, 4" Cutout  
(12" X 12")

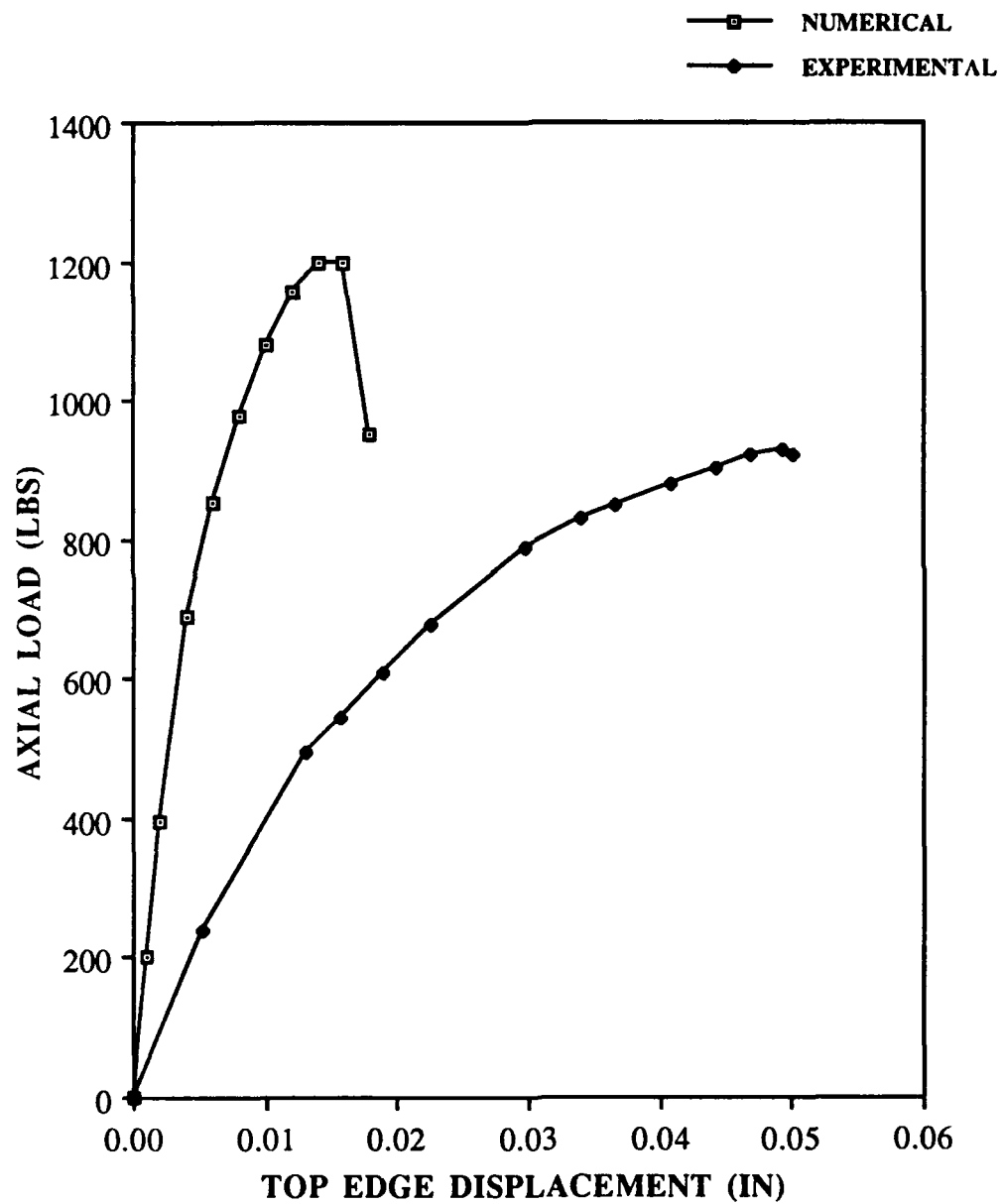


Fig. 29: Load vs. Top Edge Displacement,  
[0/90]2s, 4" Cutout  
(12" X 20")

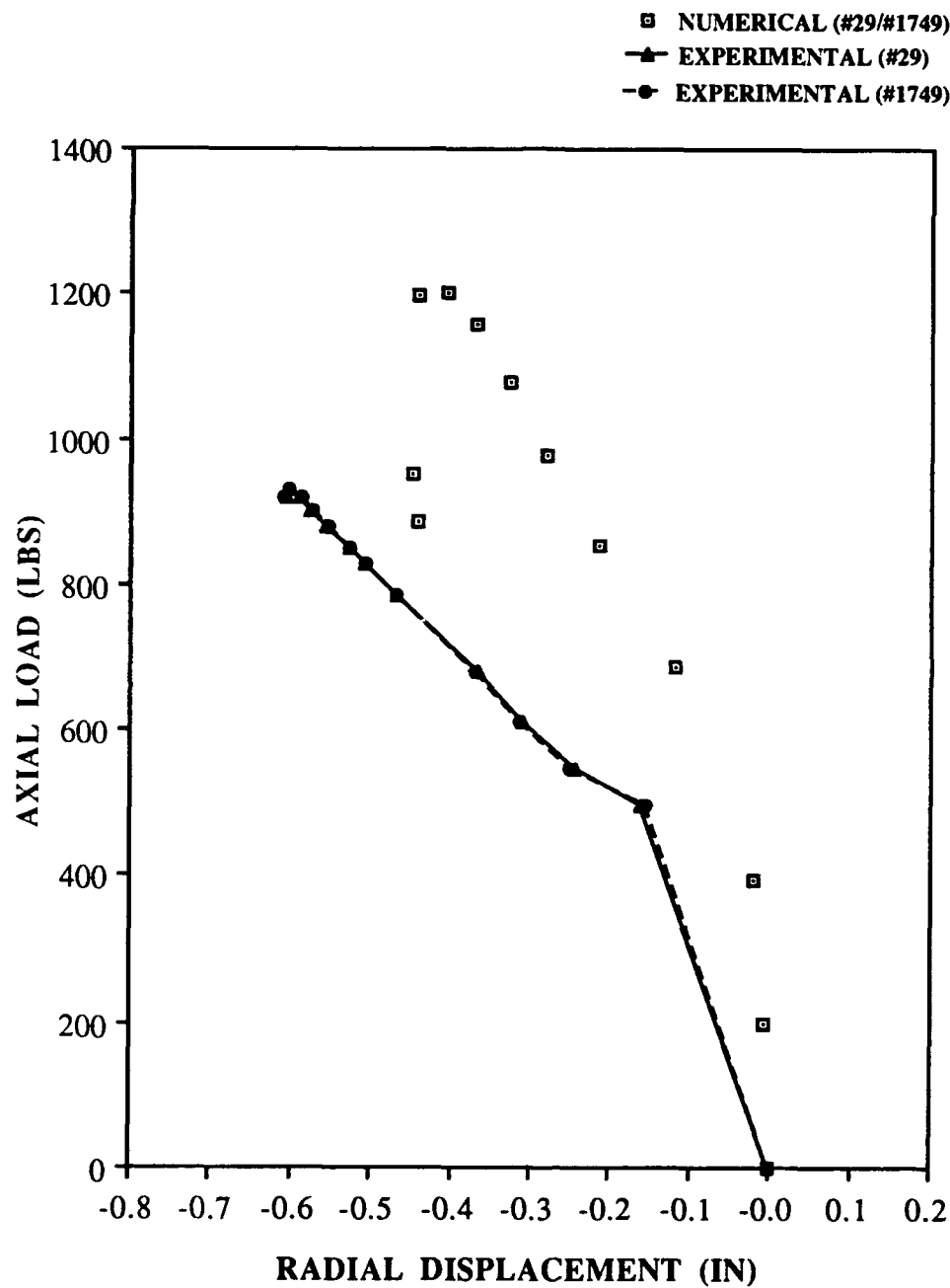


Fig. 30: Load vs. Radial Displacement,  
[0/90]<sub>2s</sub>, 4" Cutout  
(12" X 20")

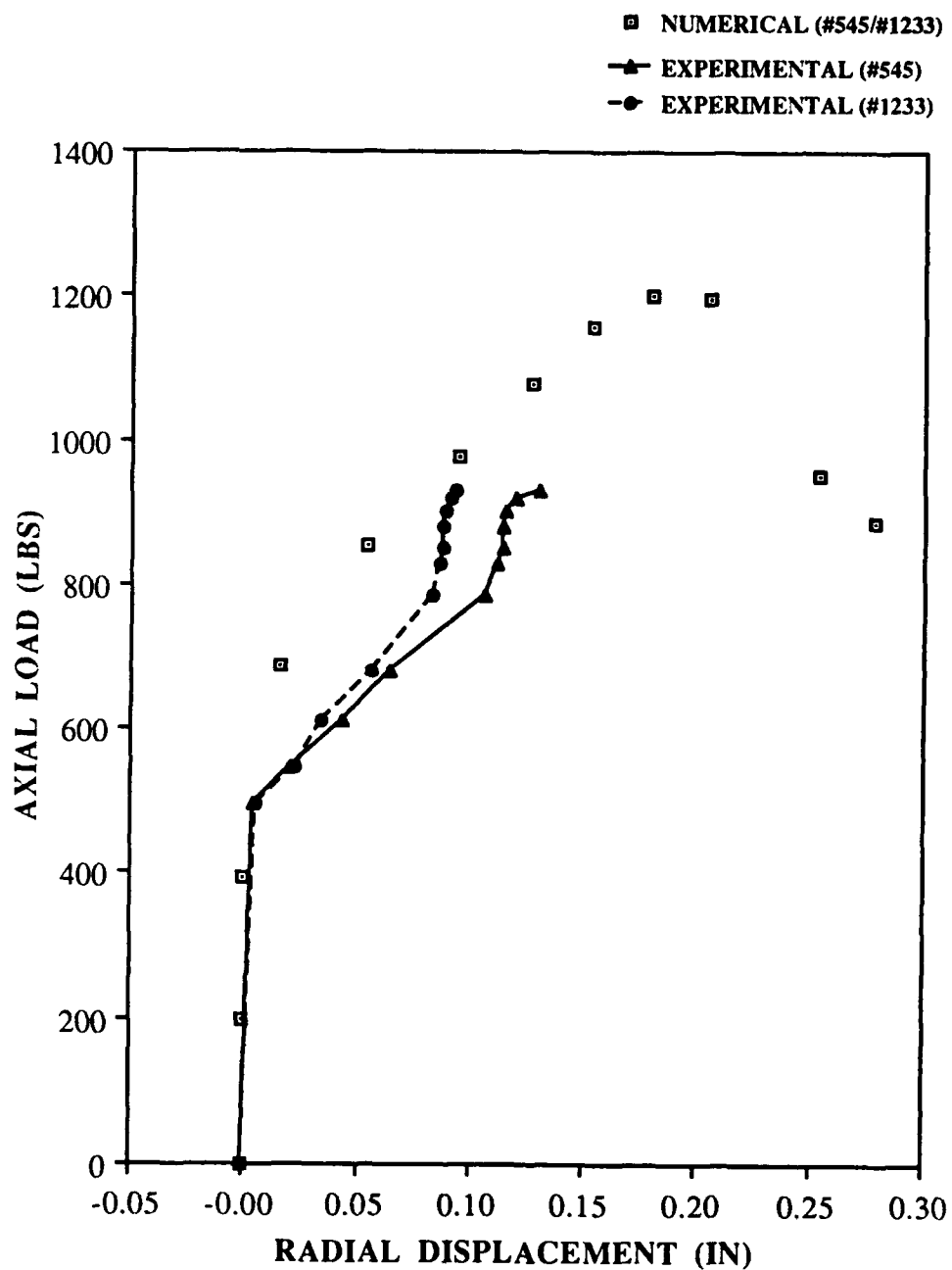


Fig. 31: Load vs. Radial Displacement,  
[0/90]<sub>2s</sub>, 4" Cutout  
(12" X 20")

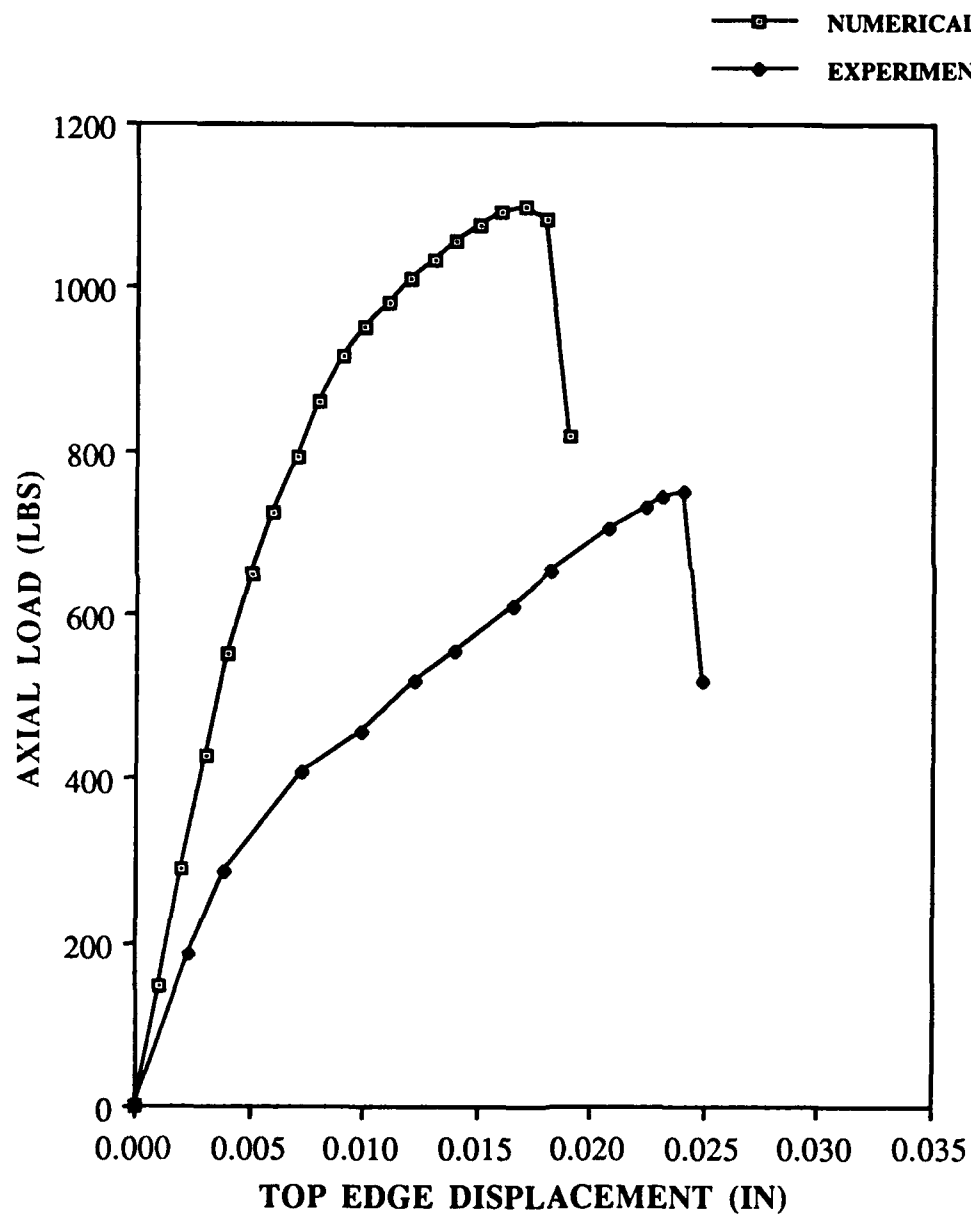


Fig. 32: Load vs. Top Edge Displacement,  
[0/+45/-45/90]<sub>s</sub>, 4" Cutout  
(12" X 20")

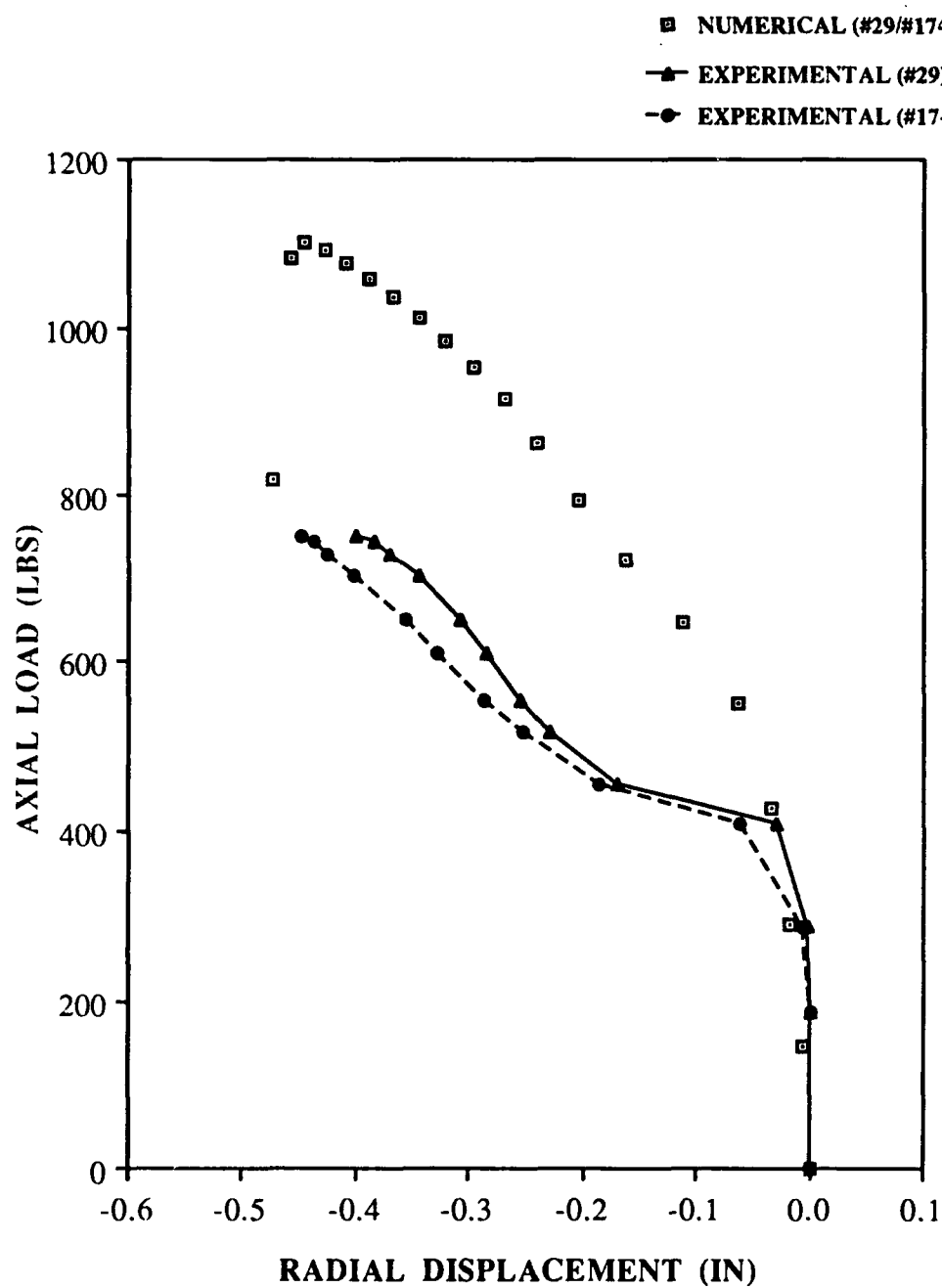


Fig. 33: Load vs. Radial Displacement,  
[0/+45/-45/90]<sub>s</sub>, 4" Cutout  
(12" X 20")

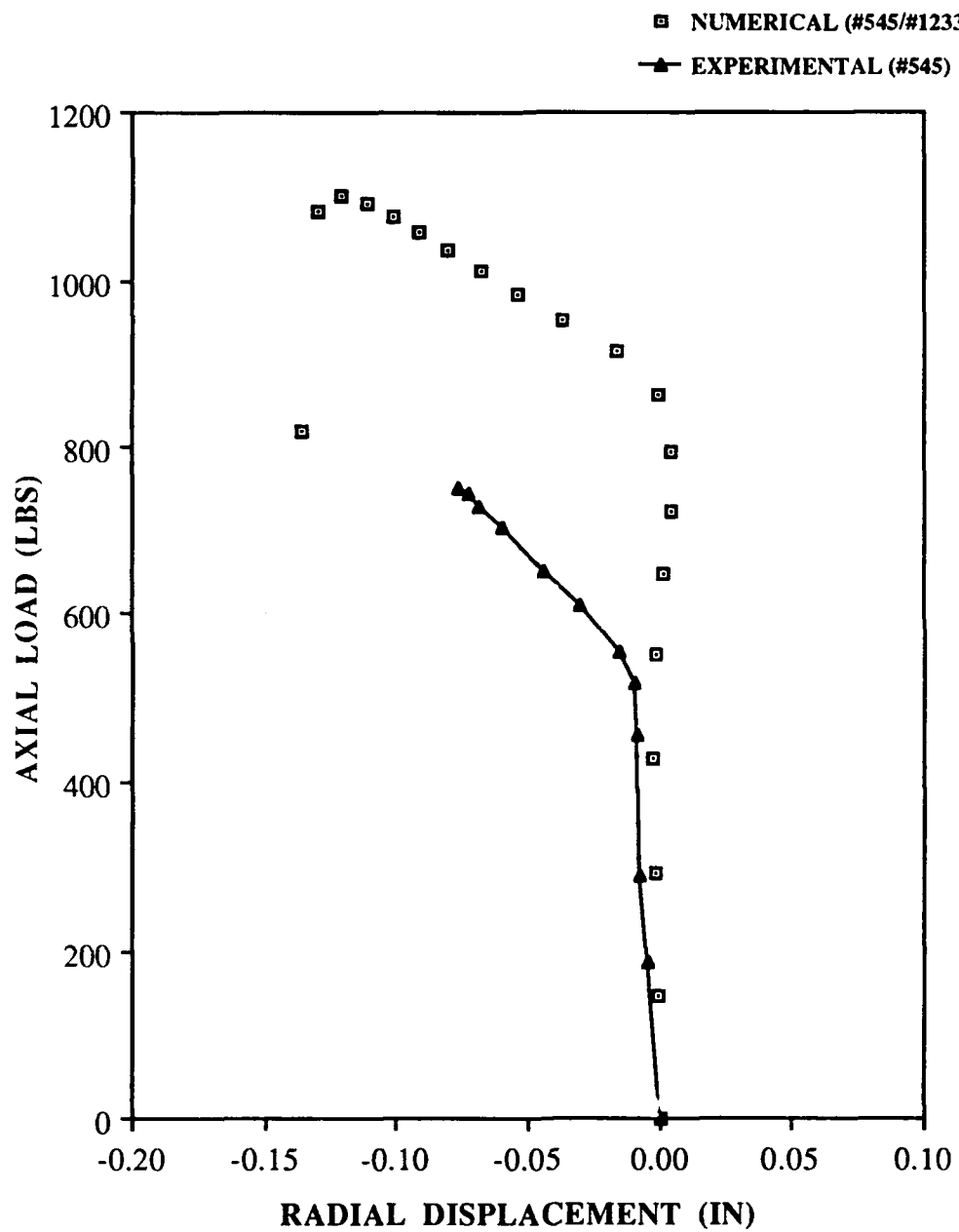


Fig. 34: Load vs. Radial Displacement,  
[0/+45/-45/90]s, 4" Cutout  
(12" X 20")



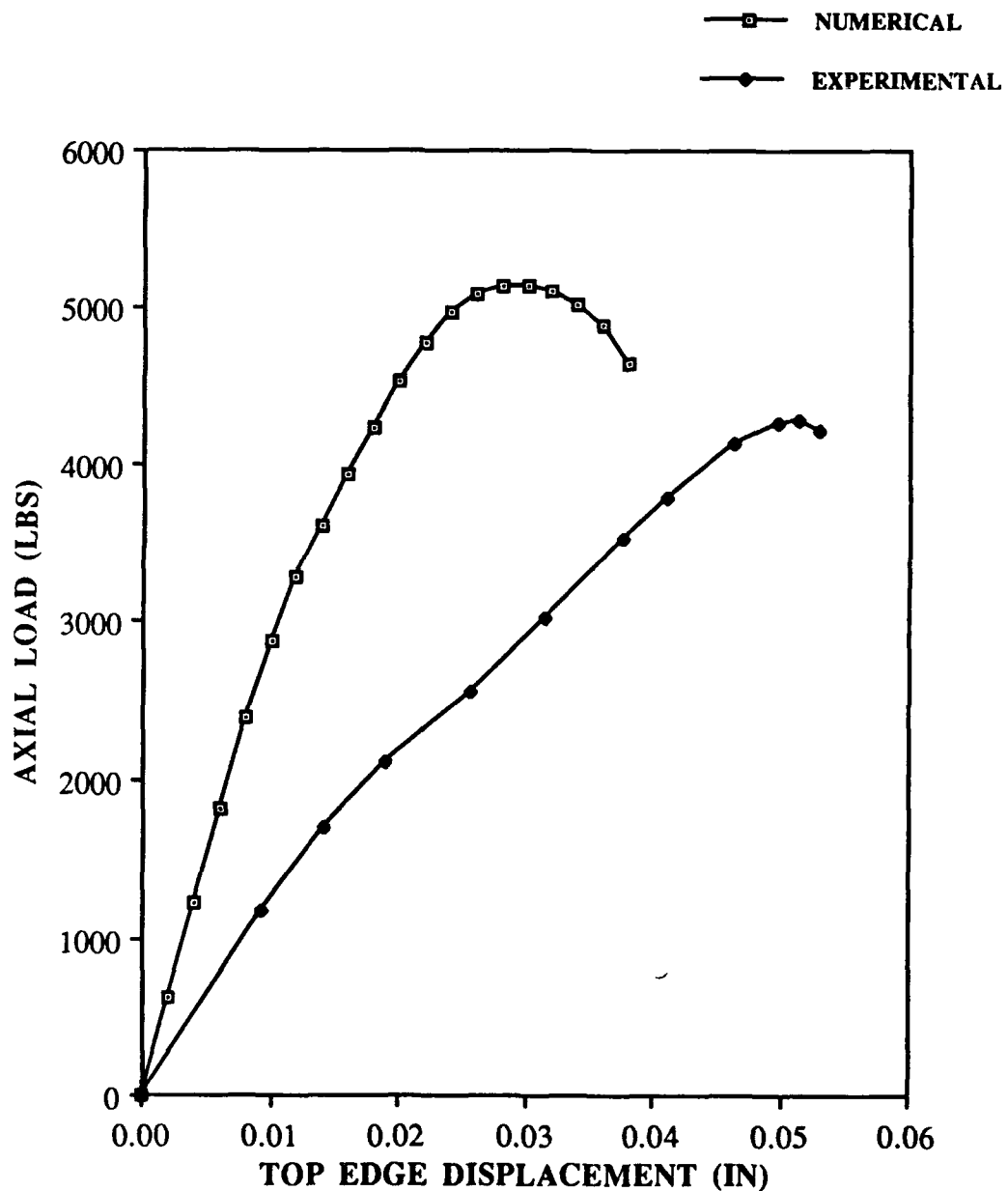


Fig. 35: Load vs. Top Edge Displacement,  
[0/+45/-45/90]2s, 4" Cutout  
(12" X 20")

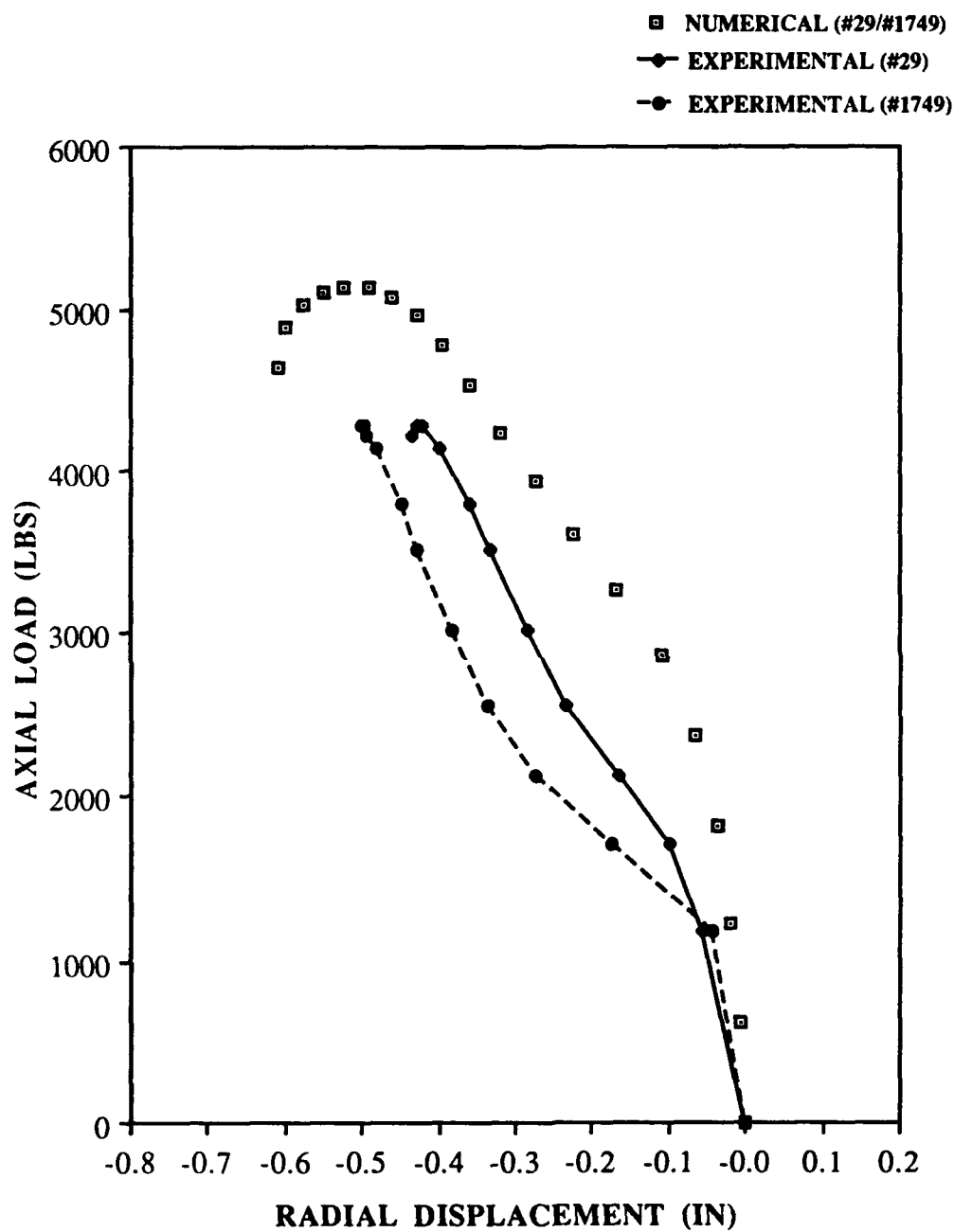


Fig. 36: Load vs. Radial Displacement,  
[0/+45/-45/90]<sub>2s</sub>, 4" Cutout  
(12" X 20")

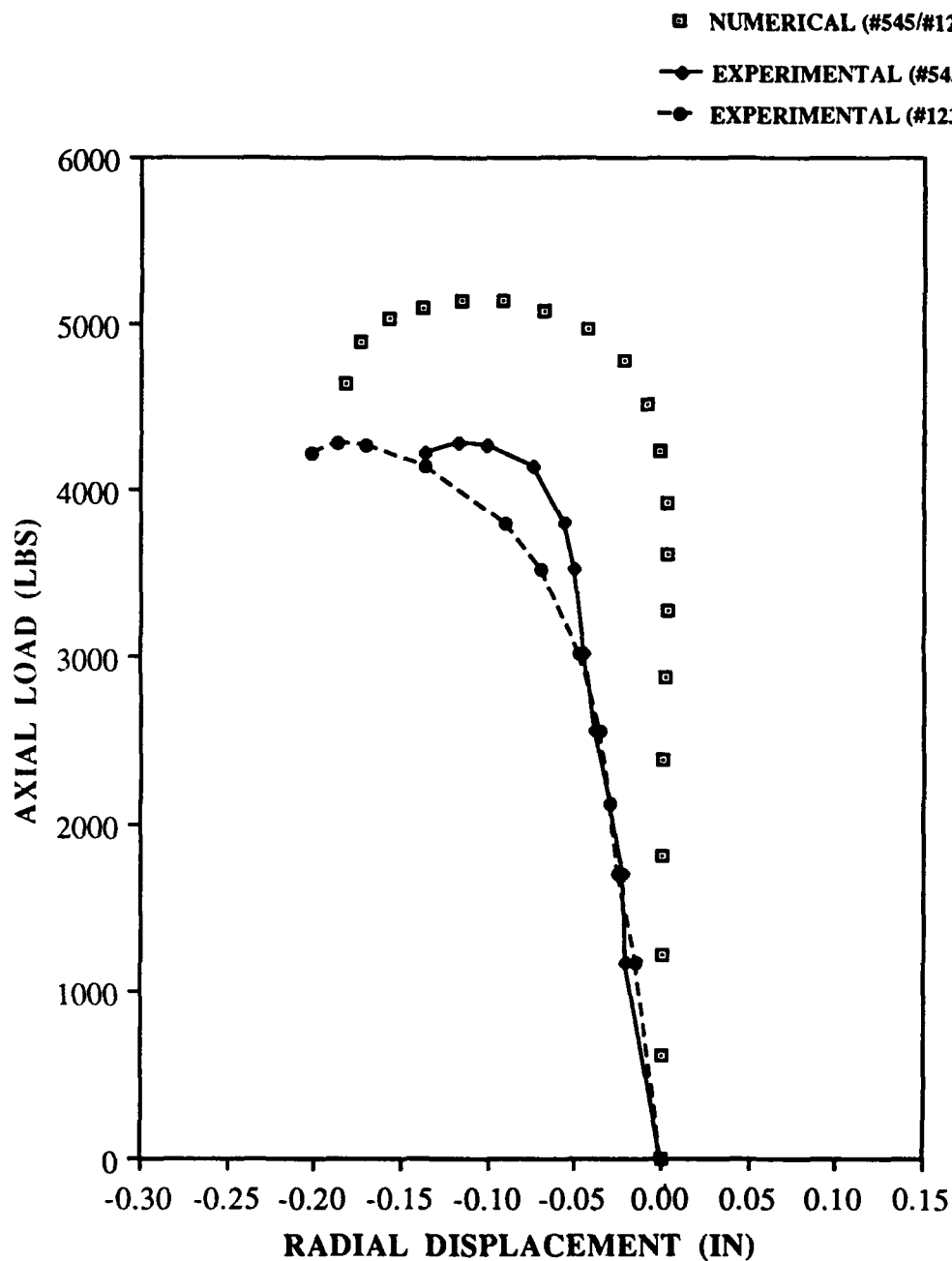


Fig. 37: Load vs. Radial Displacement,  
[0/+45/-45/90]<sub>2s</sub>, 4" Cutout  
(12" X 20")

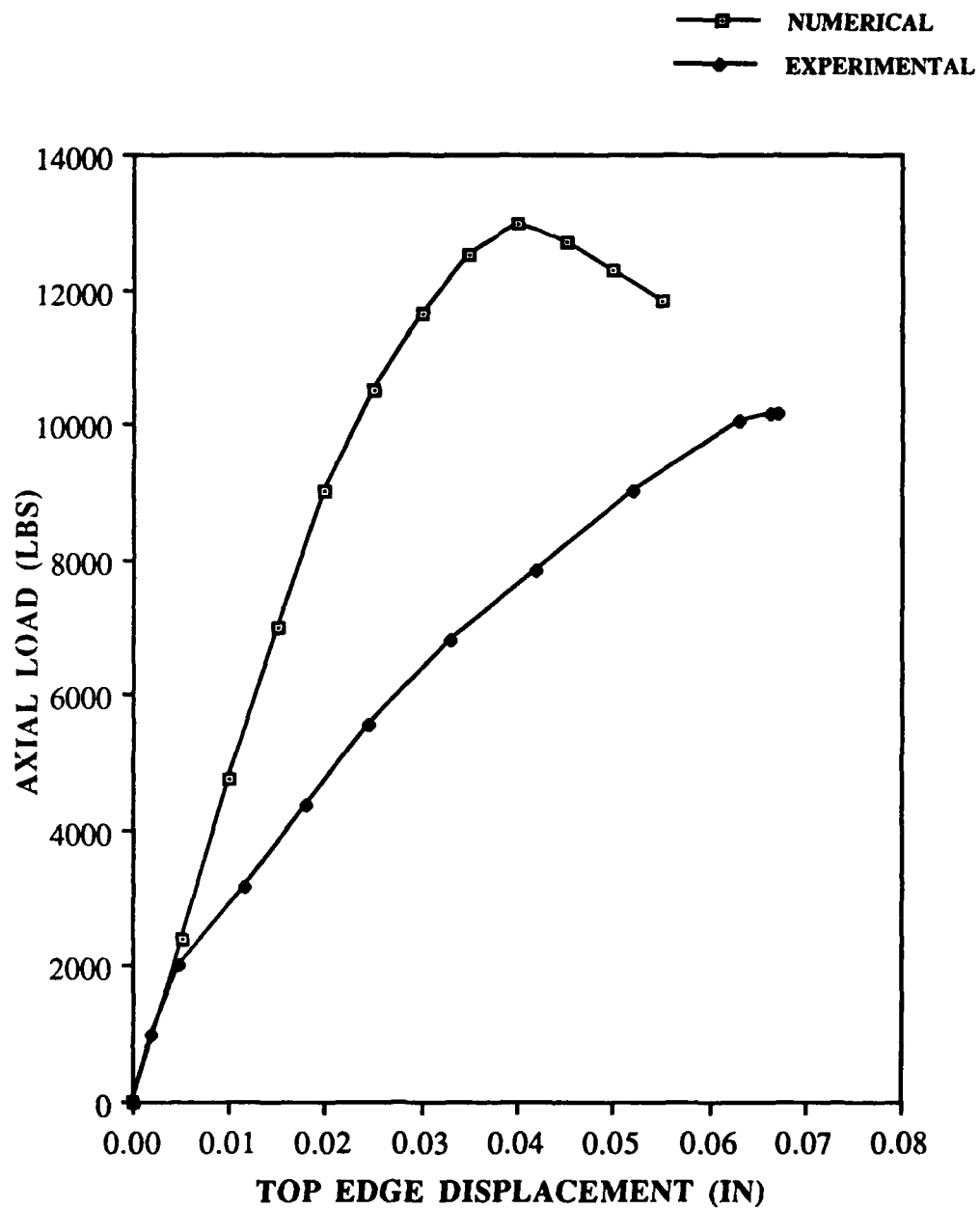


Fig. 38: Load vs. Top Edge Displacement,  
[0/+45/-45/90]3s, 4" Cutout  
(12" X 20")

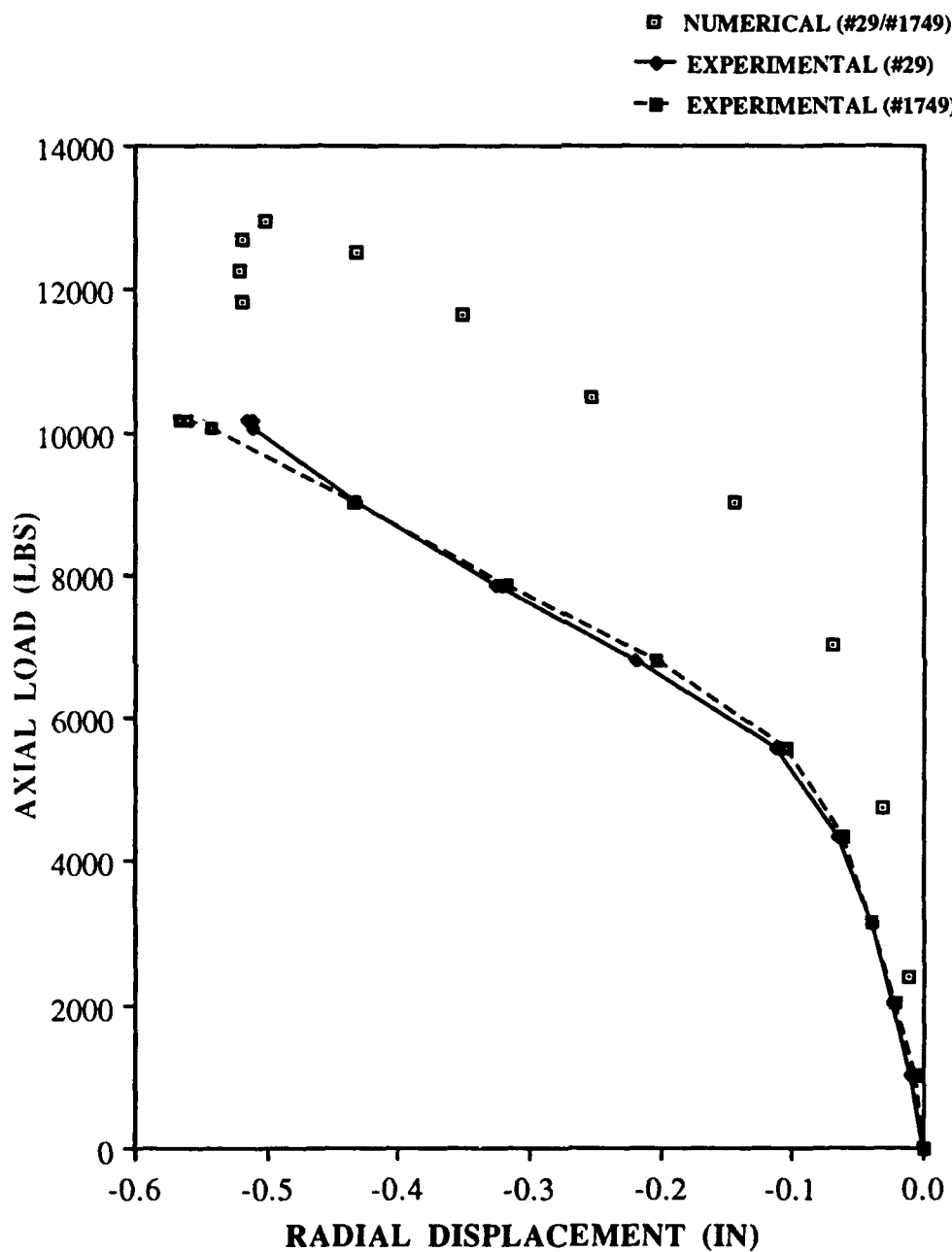


Fig. 39: Load vs. Radial Displacement,  
[0/+45/-45/90]3s, 4" Cutout  
(12" X 20")

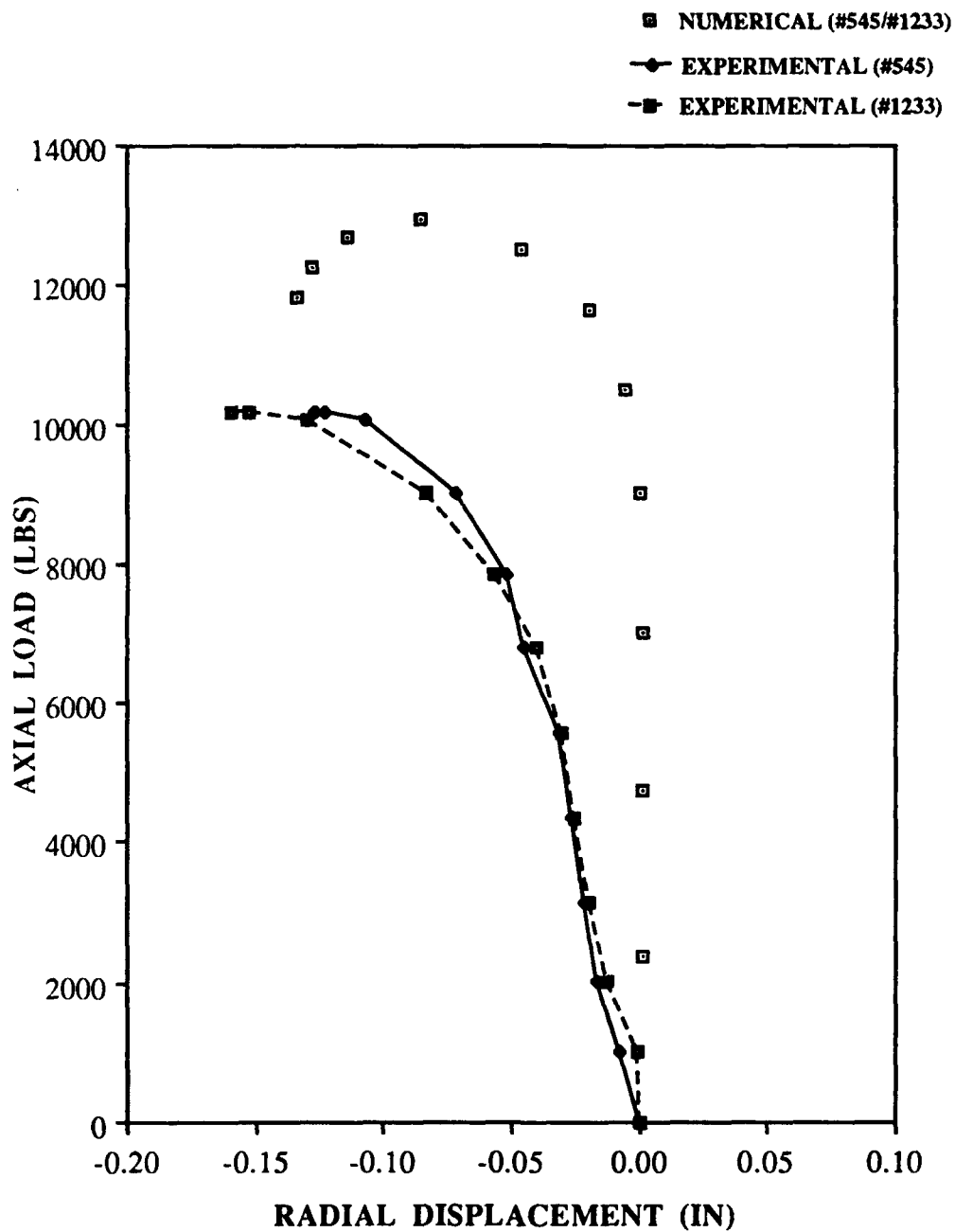


Fig. 40: Load vs. Radial Displacement,  
[0/+45/-45/90]<sub>3s</sub>, 4" Cutout  
(12" X 20")

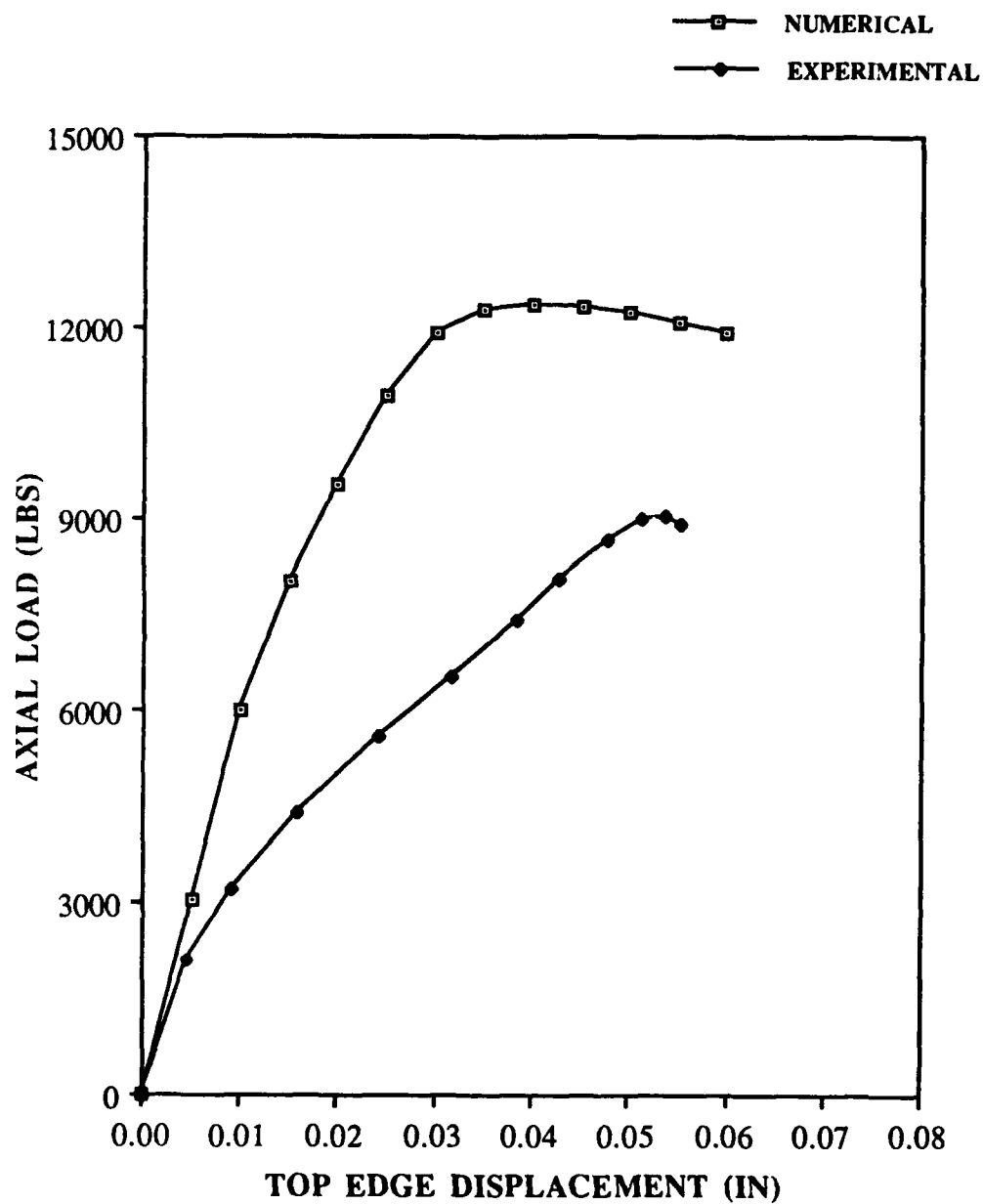


Fig. 41: Load vs. Top Edge Displacement,  
[0/90]6s, 4" Cutout  
(12" X 20")

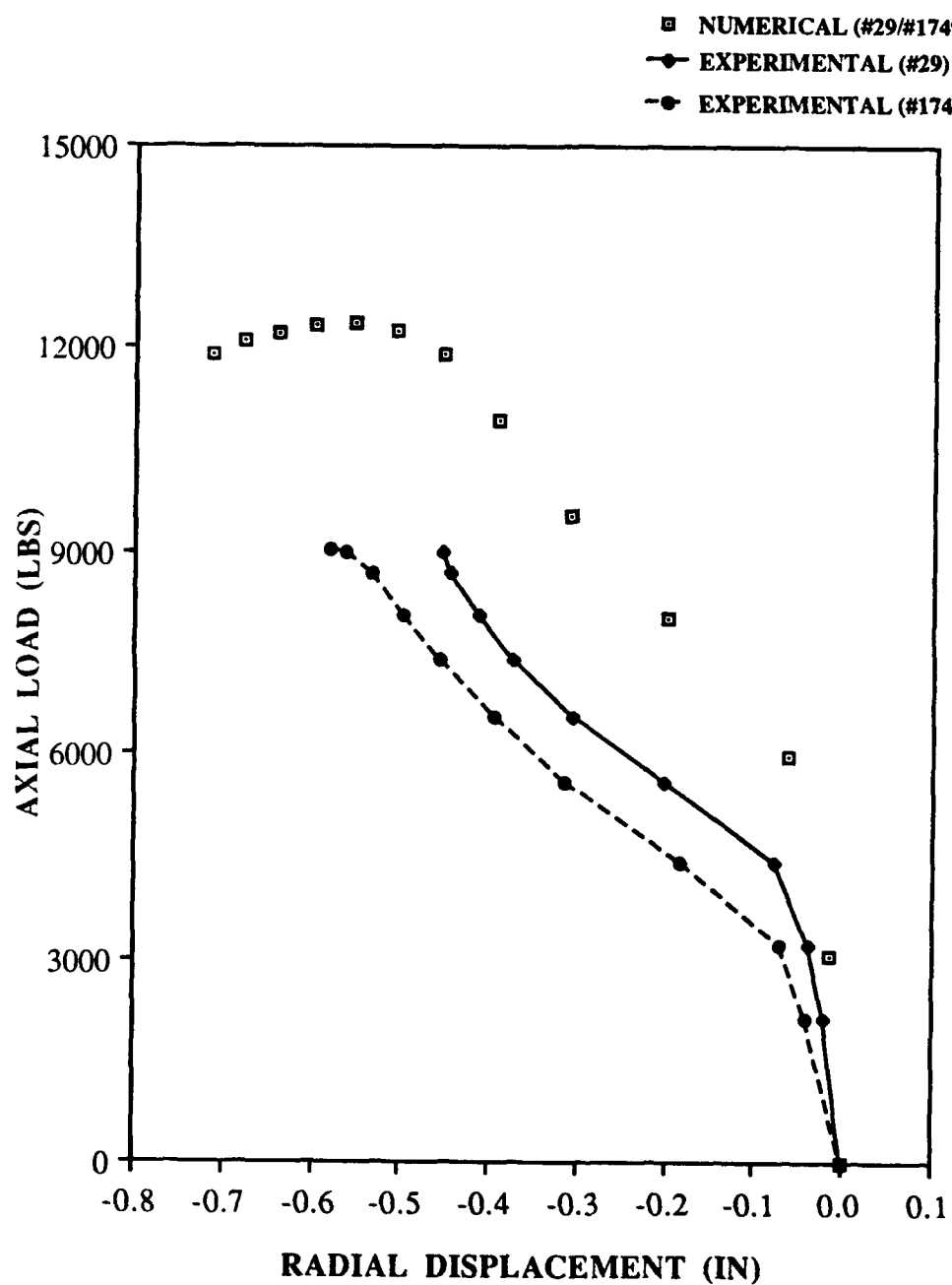


Fig. 42: Load vs. Radial Displacement,  
[0/90]<sub>6s</sub>, 4" Cutout  
(12" X 20")



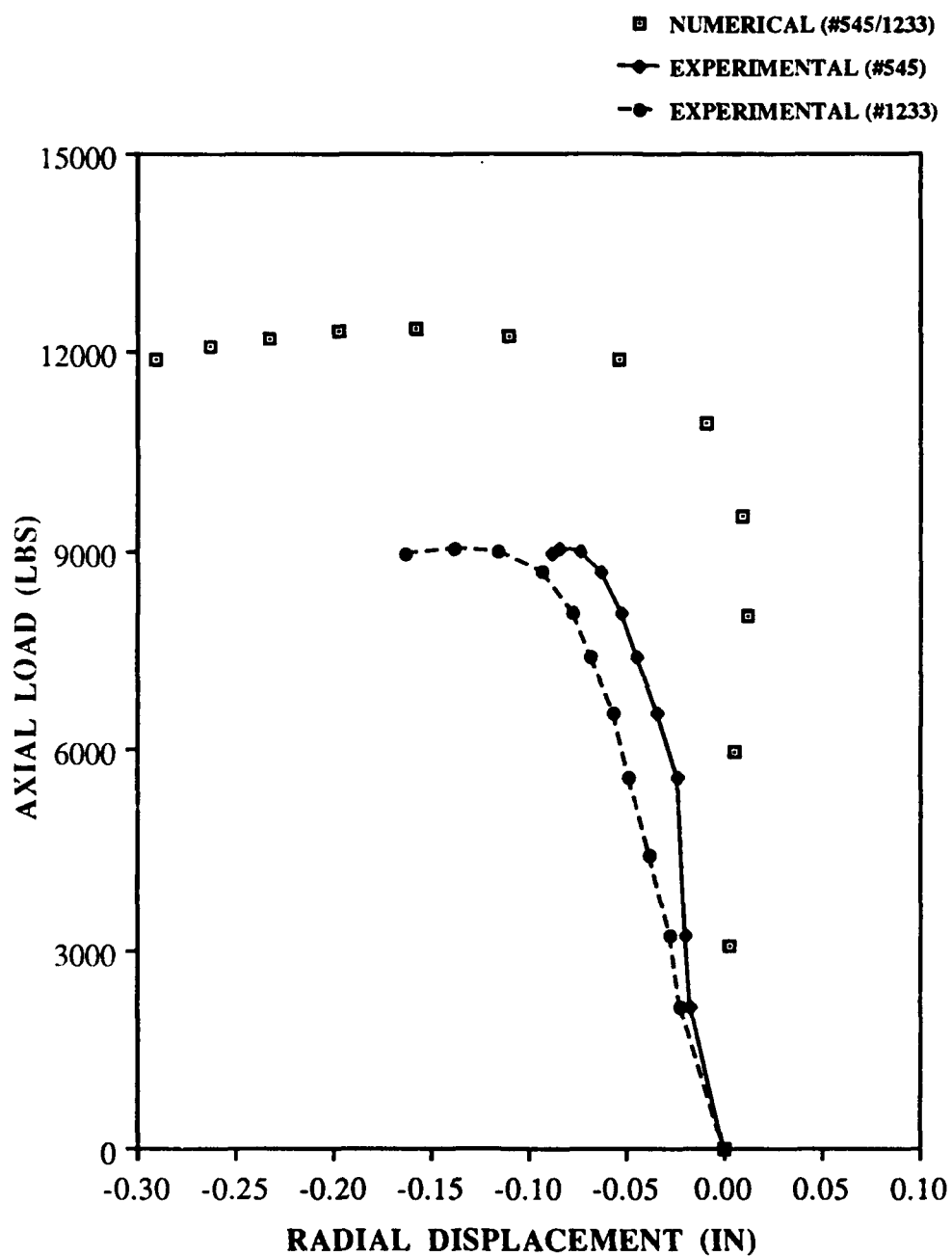


Fig. 43: Load vs. Radial Displacement,  
[0/90]6s, 4" Cutout  
(12" X 20")

In order for a comparison between the experimental data and the numerical data obtained from SHELL to be valid, the boundary conditions and loading distributions have to be similar. Experimentally, when the applied loading was the most evenly distributed across the panel's top edge, a very symmetrical radial displacement response was obtained, with respect to the vertical centerline. At the panel nodal points chosen to investigate, the SHELL finite-element program predicts exact symmetry (with respect to the panel's horizontal and vertical centerlines) for the radial displacements. Since the test panels responded more flexibly than the numerical models, lower experimental collapse loads and greater radial and top edge displacements were obtained.

Table 8 indicated that the best correlation between the experimental and numerical global collapse response of the shell panels occurred with the 16-ply shell configurations and the 8-ply cross-ply shells (except for the 12" X 12", no cutout panel). In addition, fairly good correlation was obtained for the 24-ply panels with cutouts, especially when compared to these same configurations without cutouts.

In terms of local collapse responses, the radial displacement curves related to shell panels with the 4" X 4" cutouts displayed a greater degree of symmetry than the curves related to shells with no cutouts. Again this shows how much a large cutout dominates the local collapse characteristics of a shell within proximity of the cutout, despite other influences that may result from boundary condition problems, slight unparallel loading edges, and ply layup. Curves relating to the shell panels without cutouts are displayed in Appendix B.

#### 5.4 *Experimental Difficulties*

The SHELL computer code analytically applies a distributed load across the shell panel's top edge by incrementing uniform displacements at each top-edge node. This ensures that the top edge will displace parallel to the panel's bottom edge, which is fully clamped. To experimentally check for uniform applied loading, two sets of back-to-back strain gages located near the top edge recorded strain up through the collapse load. If the strain readings were similar between the gage on the left edge and the gage on the right edge, then it was concluded that even loading was occurring.

In the analytical model used in SHELL, the top and bottom horizontal edges of the panels are clamped, while the vertical edges are unsupported. Circumferential displacement ( $v$ ) of the panel sides within the clamps is not allowed to occur. However, it was noticed during the testing that the clamps designed for the curved panel loading fixture relied upon curved metal blocks tightened up against the panels with bolts to restrain movement in the X and Z coordinate axis directions (see Figure 44), but only friction was available to keep the panel from sliding left or right in the circumferential direction within these clamps. Apparently, under certain conditions a shearing force is large enough to overcome the Coulomb friction, causing the panel to slip within the clamps. As the axial loading increases, so does the intensity of the shear force which further enhances the unevenness in loading. Once panel slipping is allowed to occur, the in-plane shear stresses and uneven axial loads act to continually intensify each other. Under conditions where this in-plane shear is likely to significantly affect the collapse response of a shell panel, either physical restraints need to be used or quasi-isotropic laminates must be used in order to hinder this shearing process.

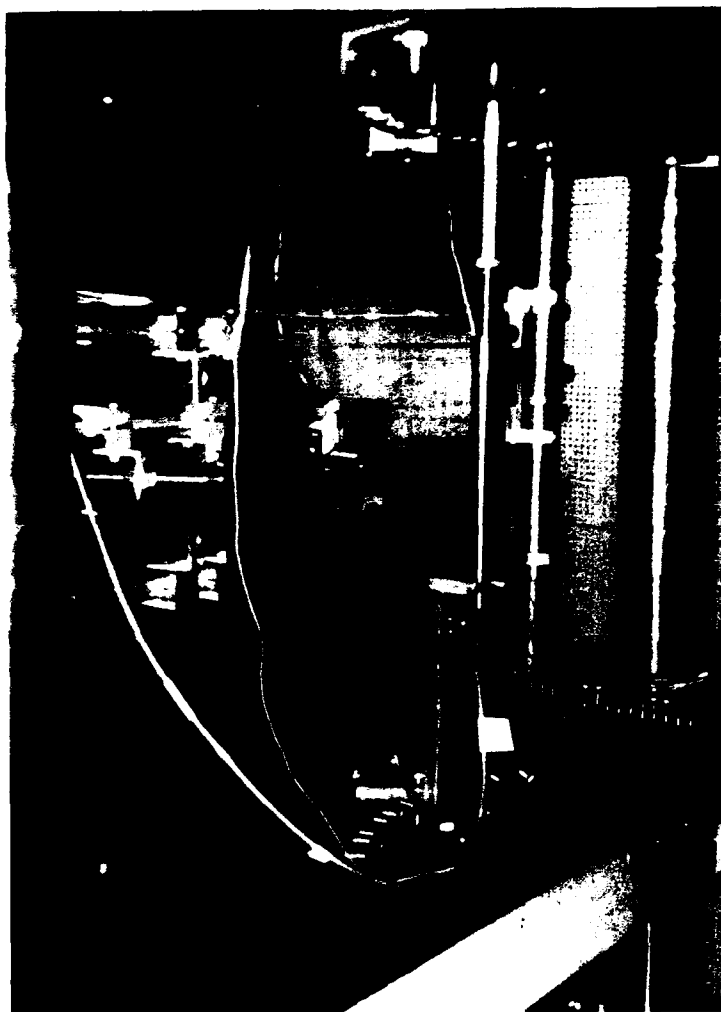


Figure 44. Photograph Showing Method Used for Clamping the Horizontal Panel Edges

The numerical results from SHELL indicate that in all cases, the shells' displacements in the radial direction are fairly symmetric throughout the entire loading range. In the cross-ply shell panels, the magnitudes and directions of the radial displacements are exactly symmetric with respect to the horizontal and vertical centerlines, thus quarter-panel symmetry exists. However, for the quasi-isotropic panels the only exact symmetry with respect to radial displacements occurs along the horizontal and vertical centerlines of the panels. The general radial displacement asymmetry which exists in the quasi-isotropic shells becomes increasingly more important as the shell thickness increases, due to the larger radial displacements encountered and the greater effect of transverse shear strain on panel collapse. During the experiments, this asymmetry was the least noticeable for the 8-ply shells with cutouts, when the radial displacements were fairly small. These thin shells maintained a very symmetrical looking response up to and through the collapse load. However, it is also important to note that when the thicker 16 and 24 ply panels were evenly loaded, the panels with and without cutouts, also appeared visually to respond in a manner that was close to symmetrical. Therefore, it is concluded that an uneven loading distribution adversely affects the symmetrical response of a shell panel to axial compression, and it appears that the cross-ply shells are more affected by this type of loading discrepancy. The reason for this is that cross-ply shells have less resistance to in-plane shear forces and twisting moments than quasi-isotropic shells. As the panel bending rotations ( $\psi$ ) and radial displacements ( $w$ ) become larger, then in-plane stresses and moments become more pronounced due to higher order  $w$  and  $\psi$  terms, which nonlinearly increase the strains and shell curvatures. As the load levels increase, the cross-ply panels begin to twist more than the quasi-isotropic panels because of a much lower  $D_{66}$  stiffness (related directly to twisting) and a lack of  $D_{16}$  and  $D_{26}$  stiffness terms which also resist  $M_{xy}$ . This twisting may cause the shell panel to shift within the clamps, which produces

uneven loading and the onset of in-plane shear effects. This in turn leads to increased uneven loading and asymmetrical local panel collapse responses.

Figure 45 shows the collapse of a 24-ply cross-ply shell panel with a large cutout. Prior to collapse, this panel responded fairly symmetrically to the compressive loads. However, just after the collapse load was reached the right side of the panel near the cutout (outlined in white chalk) suddenly and loudly snapped forward towards the center of curvature. Since the theoretical response of this cross-ply panel has been verified (via the SHELL program) to be symmetric up to and past the collapse load, it can be concluded that uneven loading caused by the influence of an in-plane shearing force or twisting moment caused the unsymmetrical snapping. Initially, the strain gage data showed a very even loading, which was expected because axial length measurements showed that the top and bottom edges of the panel were exactly parallel (up to three decimal places). However, as the load on the panel increased, the loading distribution became more uneven, and strain gage data indicated a more compressive reading on the side that snapped out. The loading cell was rechecked to ensure it was displacing evenly and it was found to be very parallel. Therefore, it was concluded that some degree of in-plane twisting caused the panel to shift within the clamps as it was being loaded, which led to a shearing of the panel under uneven load, causing the symmetrical radial displacement responses to skew. This resulting asymmetrical radial displacement response, along the unsupported vertical edges, was shown previously in Figure 42.

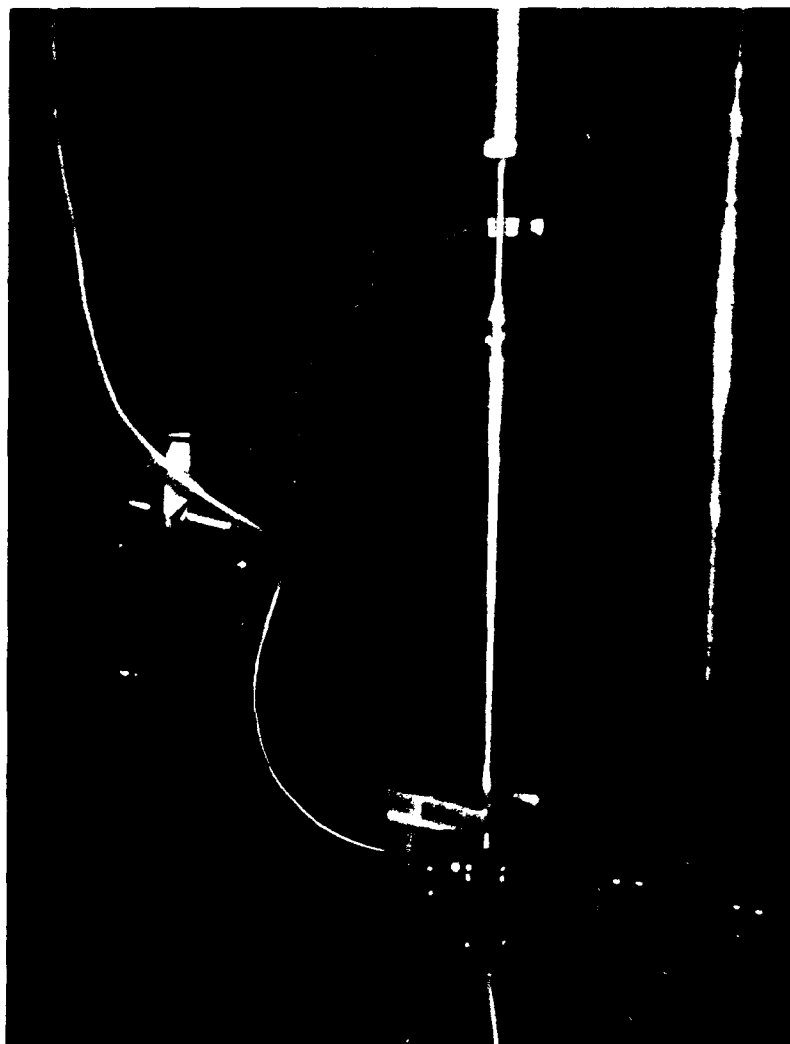


Figure 45. Photograph of  $[0/90]_{6s}$  with a 4" X 4" Cutout, Just After Collapse

Experimentally, it was observed that the tests with the most even application of loads resulted in more symmetrical radial displacement responses with respect to the vertical centerline of the panels (see Figures 46 and 47). The tests in which the most uneven loading occurred involved cross-ply shells: a 24-ply panel with no cutout and a 12" X 12" 8-ply panel with no cutout (see Figures 48 - 51). The measurable quantities involved in the cause of this uneven loading appear to include the stiffness of the panel, ply-layup of the shell laminate, and the horizontal parallelism of the top and bottom edges of the panel. Numerically, this 8-ply panel ( $[0/90]_{2s}$ ) under discussion had the highest collapse load of all the 8-ply shell panels and this was confirmed during the experiments. And, the 24-ply panels in general (both cross-ply and quasi-isotropic) behaved significantly stiffer than the 16-ply panels, which can be seen by examining the collapse loads in Table 5. However, it should be noted that within the 24-ply class of shells the stiffness difference between quasi-isotropic and cross-ply solid panels, as related to collapse loads, was only 9% and similarly under 5% for these panels with cutouts.

The parallel-edge tolerance specified when the panels were manufactured was the standard used in compressive composite flat panel tests. This tolerance dictated that the largest difference in panel length, from one side to the next, should be no greater than 0.010". However, it was determined that although this tolerance appeared to be low enough for most of the shell panels tested, a greater degree of parallelism is required for the stiffest cross-ply panels to ensure as even a loading as possible across the top edge. This was evidenced by the fact that the 24-ply quasi-isotropic shell panel in Figures 46 and 47, with horizontal edge parallelism within 0.003" resulted in very even loading and symmetrical radial displacement response; while the 24-ply cross-ply shell panel in Figures 48 and 49 (with horizontal parallelism within 0.005") resulted in loading that became increasingly more uneven as the loads increased. Note in this case how the radial displacement responses have diverged.



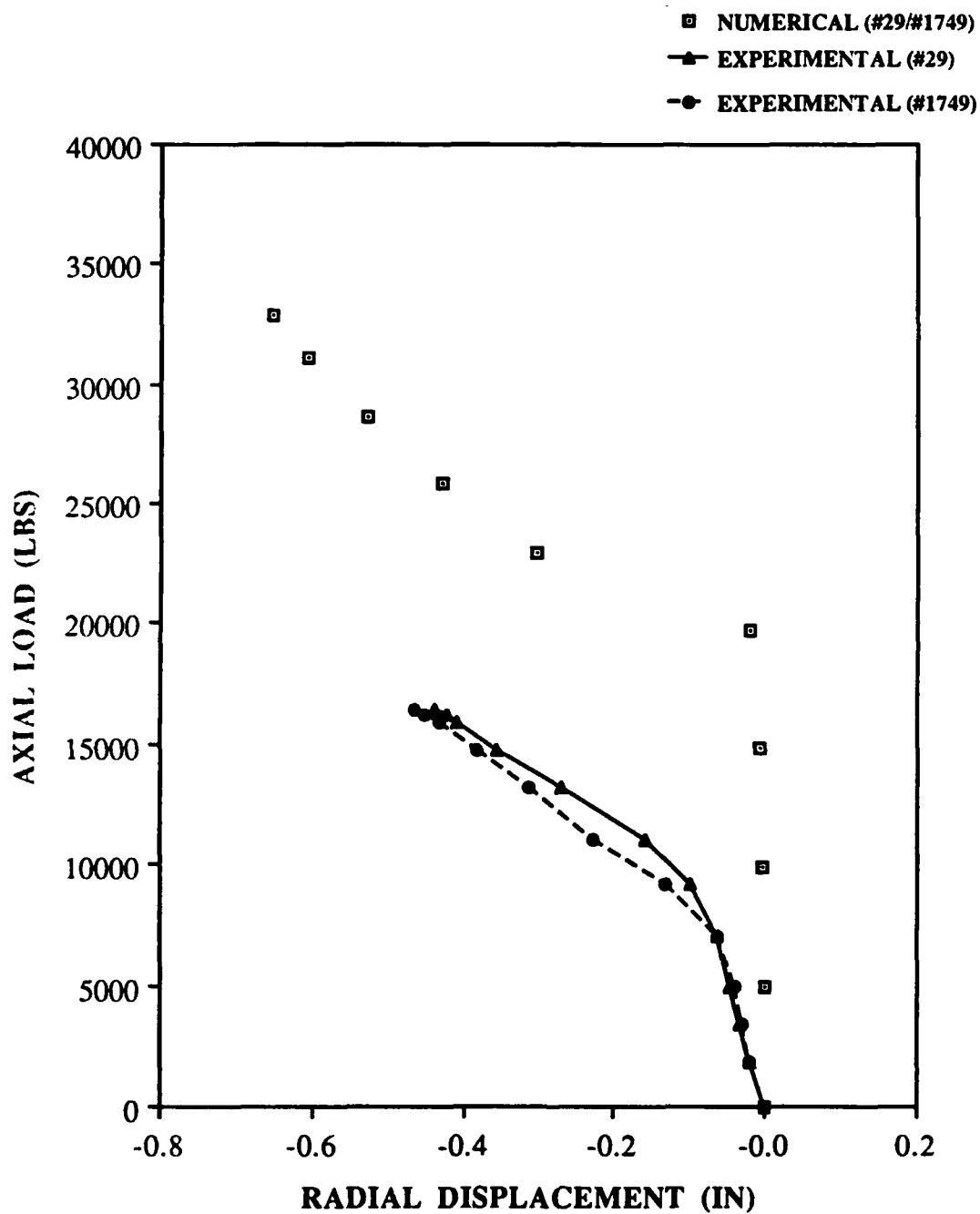


Fig. 46: Load vs. Radial Displacement,  
[0/+45/-45/90]3s, No Cutout  
(12" X 20")

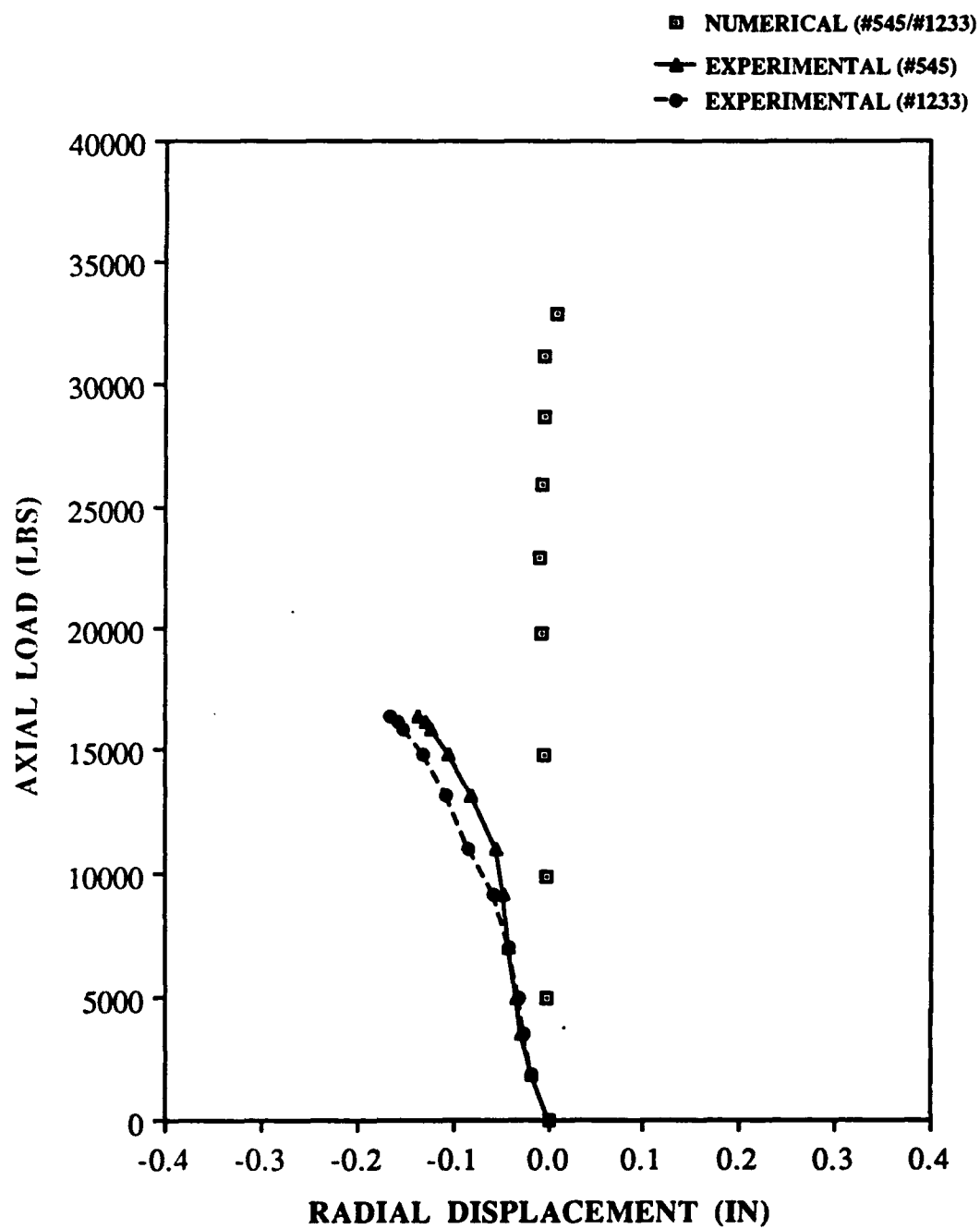


Fig. 47: Load vs. Radial Displacement,  
[0/+45/-45/90]3s, No Cutout  
(12" X 20")

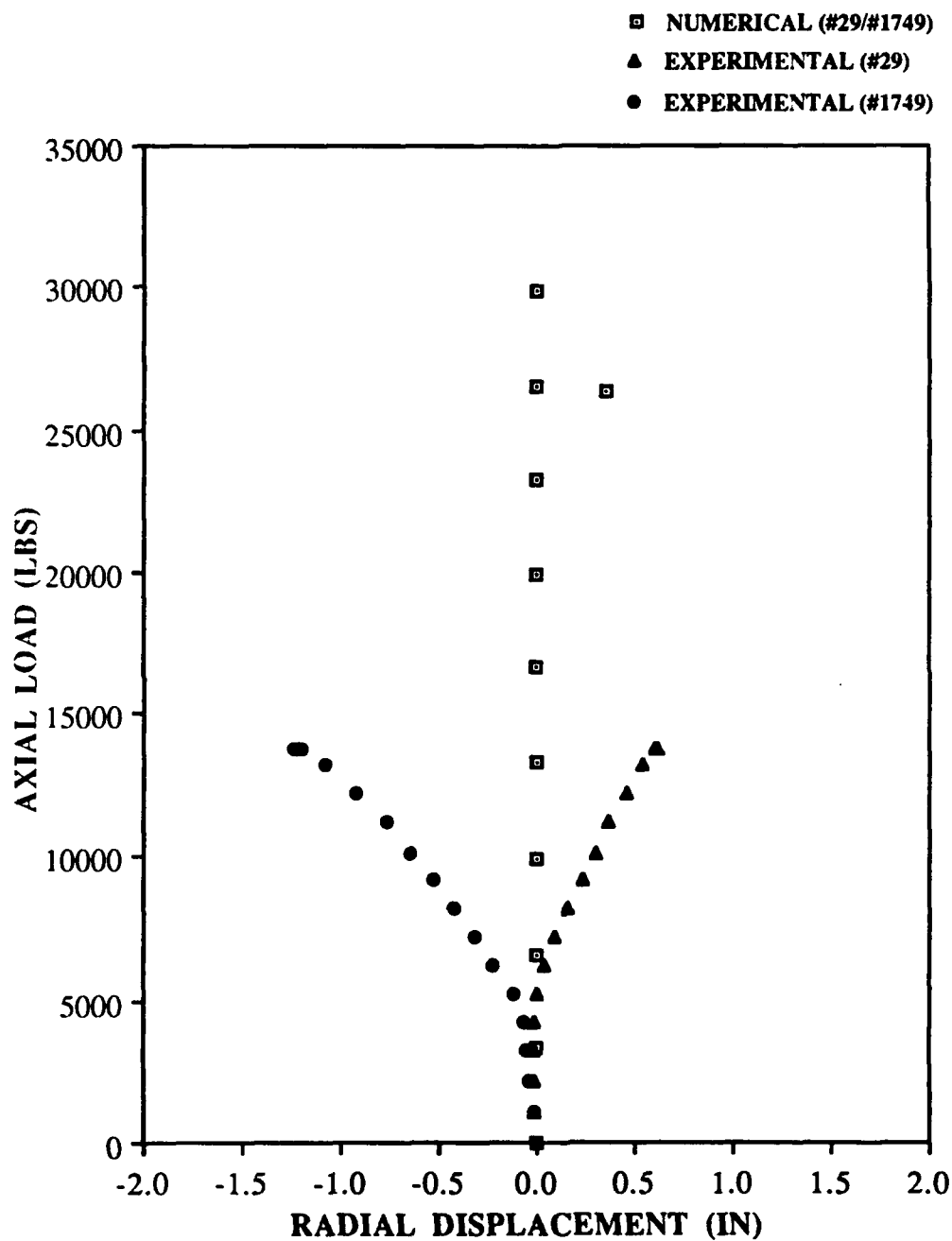


Fig. 48: Load vs. Radial Displacement,  
[0/90]6s, No Cutout  
(12" X 20")

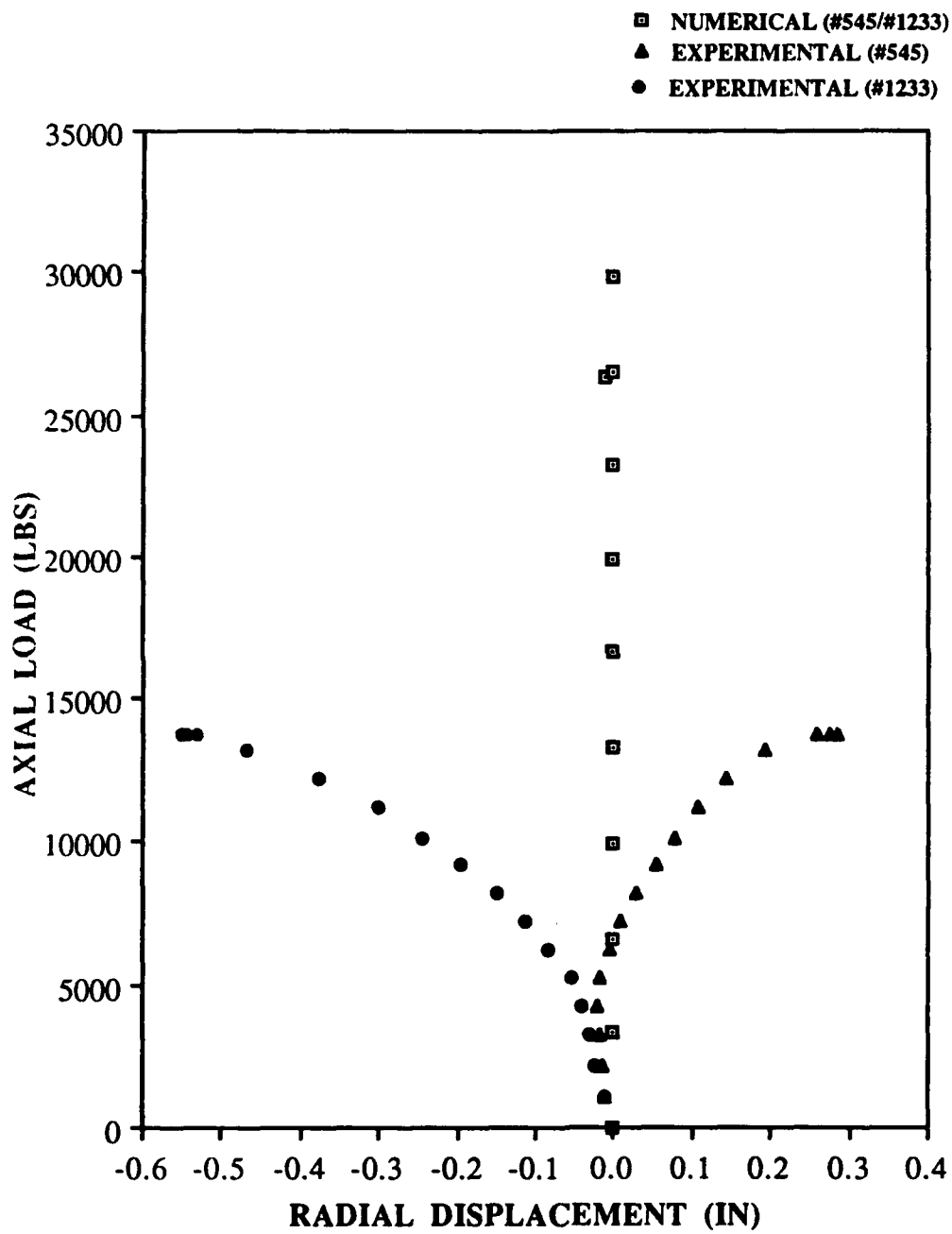


Fig. 49: Load vs. Radial Displacement,  
[0/90]6s, No Cutout  
(12" X 20")

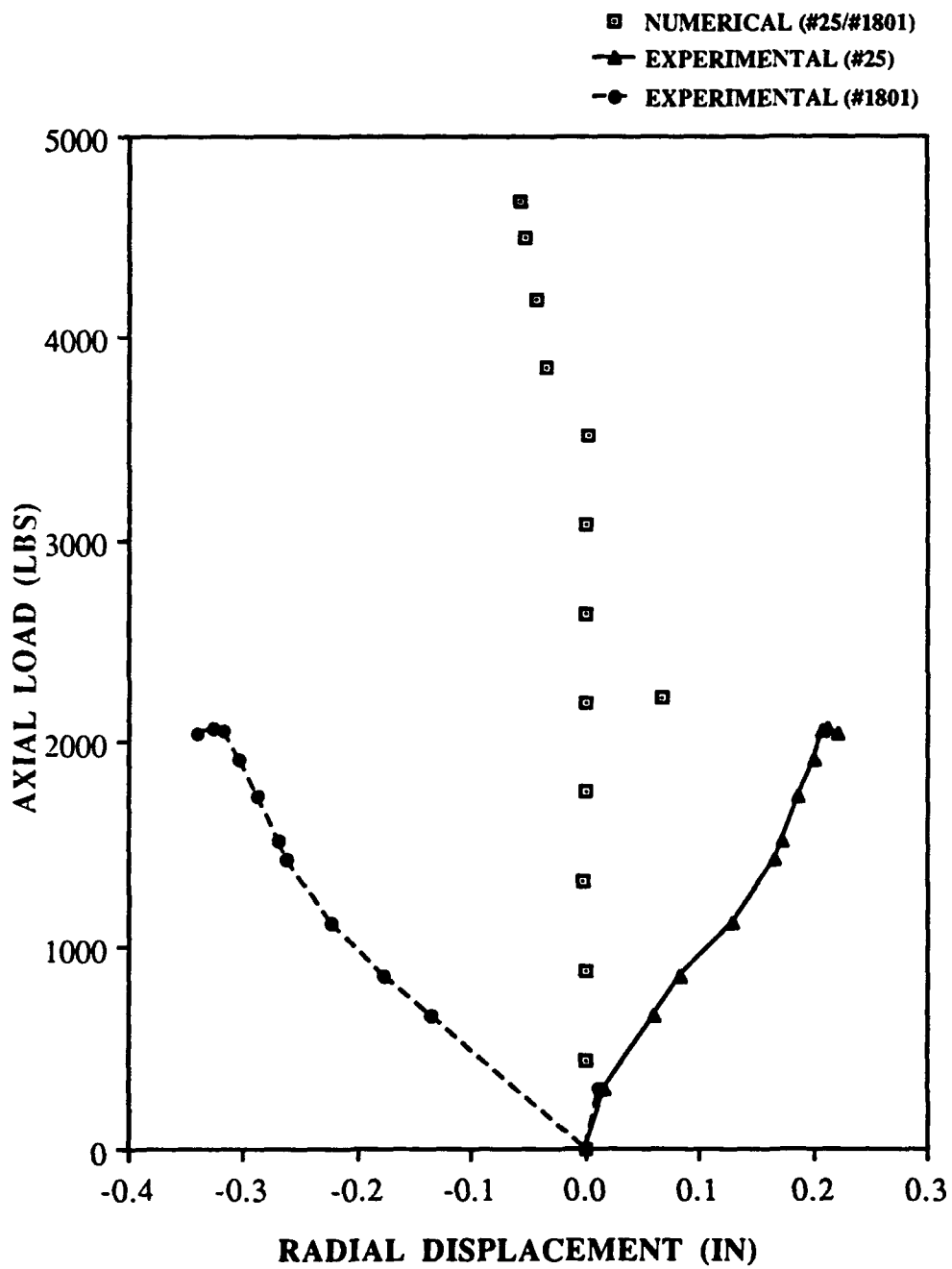
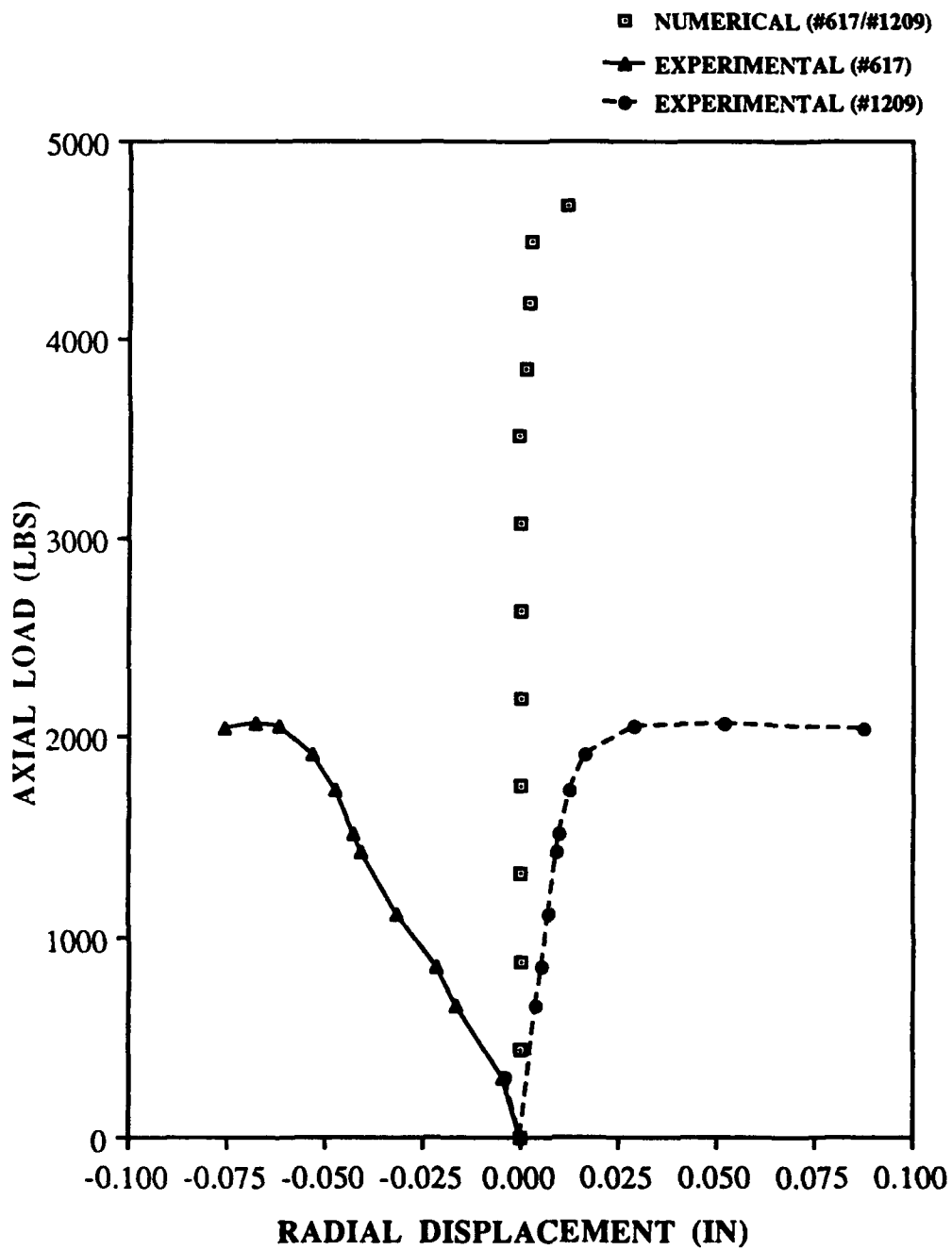


Fig. 50: Load vs. Radial Displacement,  
[0/90]2s, No Cutout  
(12" X 12")



Based upon these observations, it was concluded that in order to achieve panel response trends more similar to the analytical predictions from SHELL it is critical, especially for thicker panels when the load levels are extremely high, that the horizontal edges be almost exactly parallel to within three decimal places. This strict tolerance is more critical for the composite shells than it was for flat plates, because the shell is inherently more unstable due to its curved geometry. Bending and twisting moments occur as soon as compressive loading is applied, causing the shell to displace in the transverse direction, although for the thicker panels the initial displacements are less noticeable. At this time, unparallel loading edges and in-plane twisting moments ( $M_{xy}$ ) may cause the panels to shift within the clamps in the circumferential direction if this degree-of-freedom is not securely fixed during the testing. Then uneven loading across the panel's top edge will occur and cause an in-plane shearing action to begin. Once the shearing has begun, and unless the panel's laminate construction hinders this action, this shearing force becomes progressively more intense as the applied loads continue to escalate. Due to the fact that the quasi-isotropic shell laminates have a greater resistance to in-plane shear than do the cross-ply laminates, the parallelism tolerance for quasi-isotropic shells can be a little higher, on the order of 0.003".

Based upon experimental observation of the 24-ply cross-ply solid shell, the result of this unconstrained in-plane shear stress is a severely unsymmetrical panel collapse response, where at loads over 5,000 lbs, the radial displacement curves significantly diverge (see Figures 48 and 49) and the panel twisting becomes more dramatic. Figure 52 shows the collapse of a 24-ply cross-ply shell with no cutout. This photograph displays how diverse the radial displacements of the vertical free edges become, not only in magnitude but in direction. The side of the panel in the forefront of the picture radially displaced 1.216 inches away from the center of curvature, while the other side of the panel radially displaced 0.614 inches towards the center of curvature. In fact, as the load levels

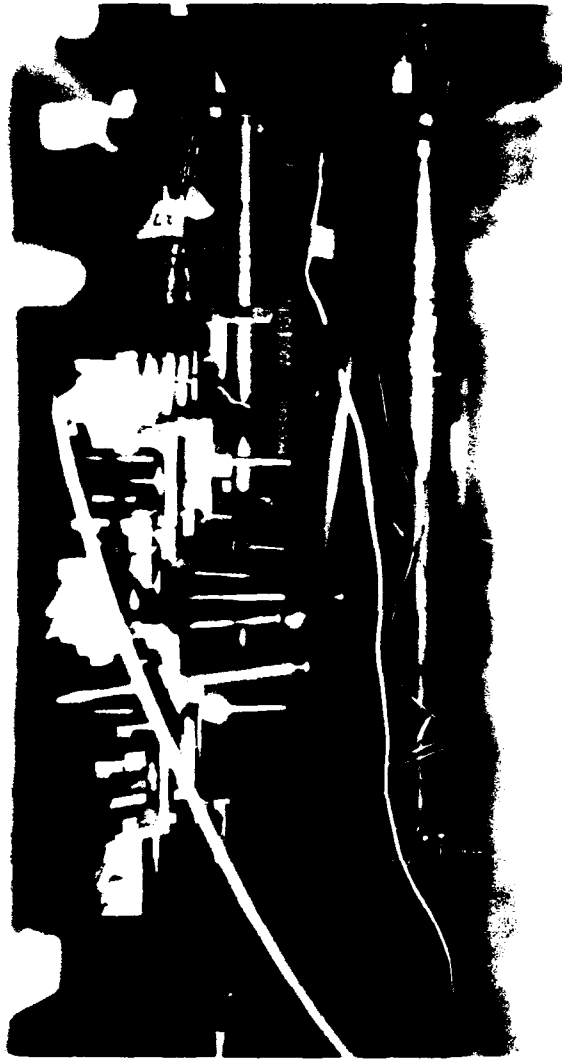


Figure 52. Side View of  $[0/90]_{6s}$  Solid Shell Panel, Depicting Asymmetrical Collapse



approached the collapse load, the strain gages read that the side of the panel which was more greatly displaced was in compression, while the other side was in tension. Based upon observation and radial displacement data collected it appears that the 24-ply quasi-isotropic solid shell panel, which had the highest collapse load of all the panels tested, was able to resist this in-plane shearing force and twisting moment because of the presence of  $\pm 45^\circ$  fibers in its laminate. The presence of these fibers provides the quasi-isotropic laminates with a much larger in-plane shear stiffness ( $A_{66}$ ) and a much greater resistance to in-plane twisting ( $D_{66}$ ,  $D_{16}$  and  $D_{26}$ ) than the cross-ply laminates. Similar in-plane twisting and shearing probably occurs to some lesser degree in the thinner shells but becomes increasingly more pronounced as the panel aspect ratio approaches unity.

Several tests were conducted in order to confirm these hypotheses. A 24-ply quasi-isotropic shell panel with no cutouts (the stiffest panel tested), for which even loading was previously achieved was shimmed up 0.004" on one side of the panel to simulate a panel with an unparallel loading edge. The test results revealed uneven loading and an asymmetrical panel response in terms of radial displacements. This confirmed how critical parallelism is to achieving response trends similar to the analytical model. Another test was conducted that attempted to fix any circumferential movement (which was undetectable to the naked eye) and see the affect this would have on the overall collapse load. The same 24-ply quasi-isotropic solid panel was used for this test and thin steel blocks were securely wedged in next to the four panel sides within the clamps. This test resulted in increasing the overall collapse load of the panel over all the previously run tests. However, these crude devices only increased the collapse load by about 5.5%. Also, collapse of the thicker quasi-isotropic panels (where transverse shear strains are the greatest) is more affected by transverse shear strain than in-plane shear strain, because the quasi-isotropic panels are much stiffer in the in-plane ( $A_{66}$ ) than in the transverse directions ( $A_{44}$  and  $A_{55}$ ). Therefore, it was concluded that shell panels with slightly unparallel horizontal edges

(within standard tolerances) can lead to uneven loading distributions, which may result in significant changes to the local response of the shell to axial compression. Even though the radial displacement patterns may be dramatically altered under these conditions, the change in the global resistance of the shell panel to collapse and thus its point of geometric instability (collapse load) is relatively small.

One final example of how uneven loading affected the collapse response of a 16-ply cross-ply shell panel with a large cutout is shown in Figure 53. Figure 54 shows that at about 20% of the collapse load the experimental radial displacement curves deviate significantly, indicating uneven loading is occurring across the panel's top edge. Even though for this case the experimental collapse load is 32 lbs higher than the numerical collapse load, this difference is not significant enough to make an assertion that there is a problem with the finite-element model used, especially in light of the fact that uneven loading is present. In fact, Figure 54 shows that the experimental radial displacement curve for the vertical free edge (node #29) very closely matches the numerical curve at lower load levels (up to about 40% of the collapse load) but then the two curves deviate, with the experimental shell responding more flexibly than the numerical shell model. The fact that the experimental load/displacement curves peak just slightly above the numerical curves, despite the panel's greater flexibility, could be explained by the inaccuracies involved with using a displacement-control finite-element method. With this type of solution method, the displacements are prescribed and incremented and the corresponding load components become the unknowns. In fact, there are as many load versus displacement curves as there are degrees of freedom [20: 133 - 134]. Therefore, for each increment of displacement, the solution converges on a load value based upon a user prescribed global convergence tolerance. In this research effort, a convergence tolerance of 0.1% was used, which according to Palazotto and Dennis [20] is the value typically used. Numerical test runs were also performed using 0.01% and no change in solution was found.

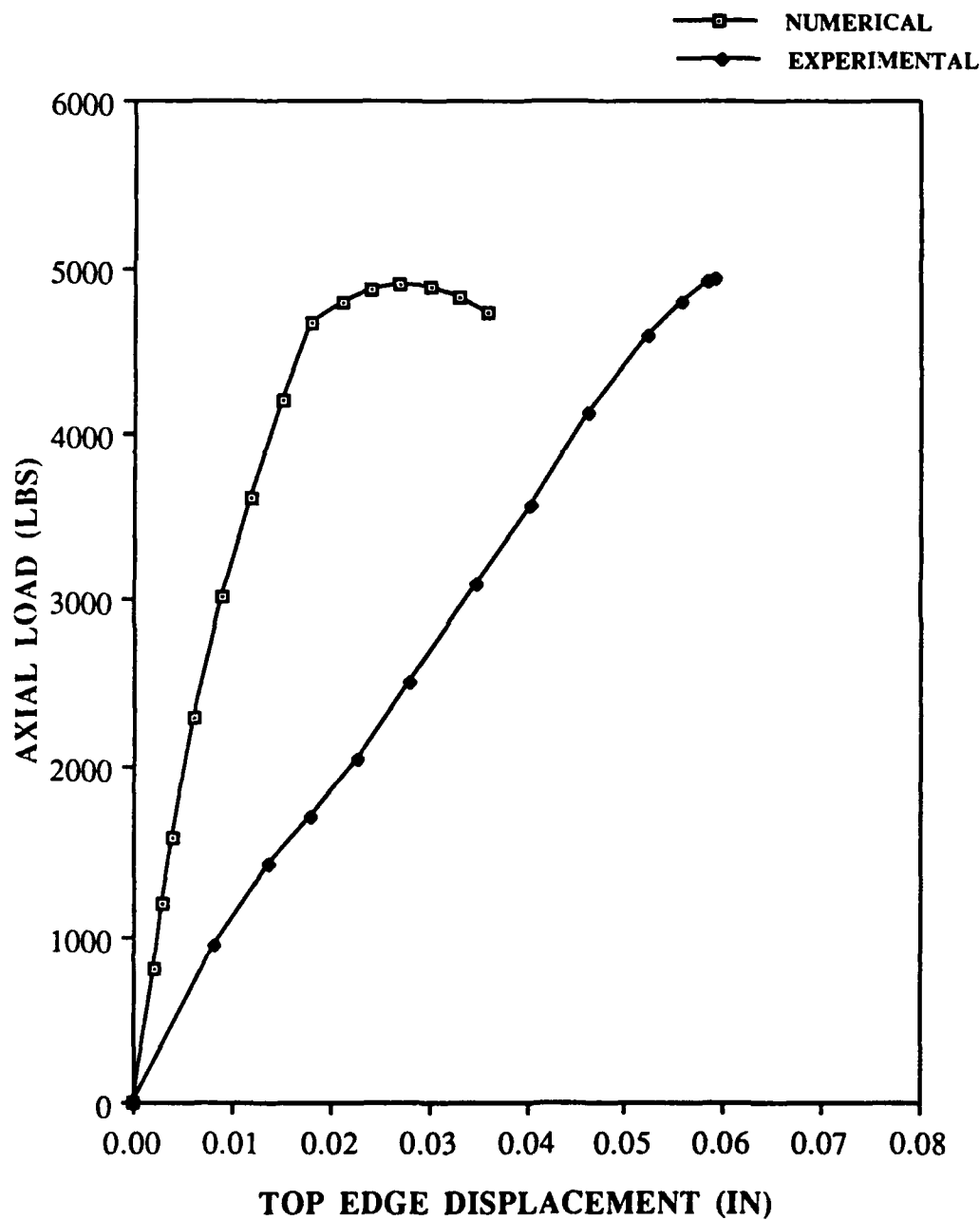


Fig. 53: Load vs. Top Edge Displacement,  
[0/90]4s, 4" Cutout  
(12" X 20")

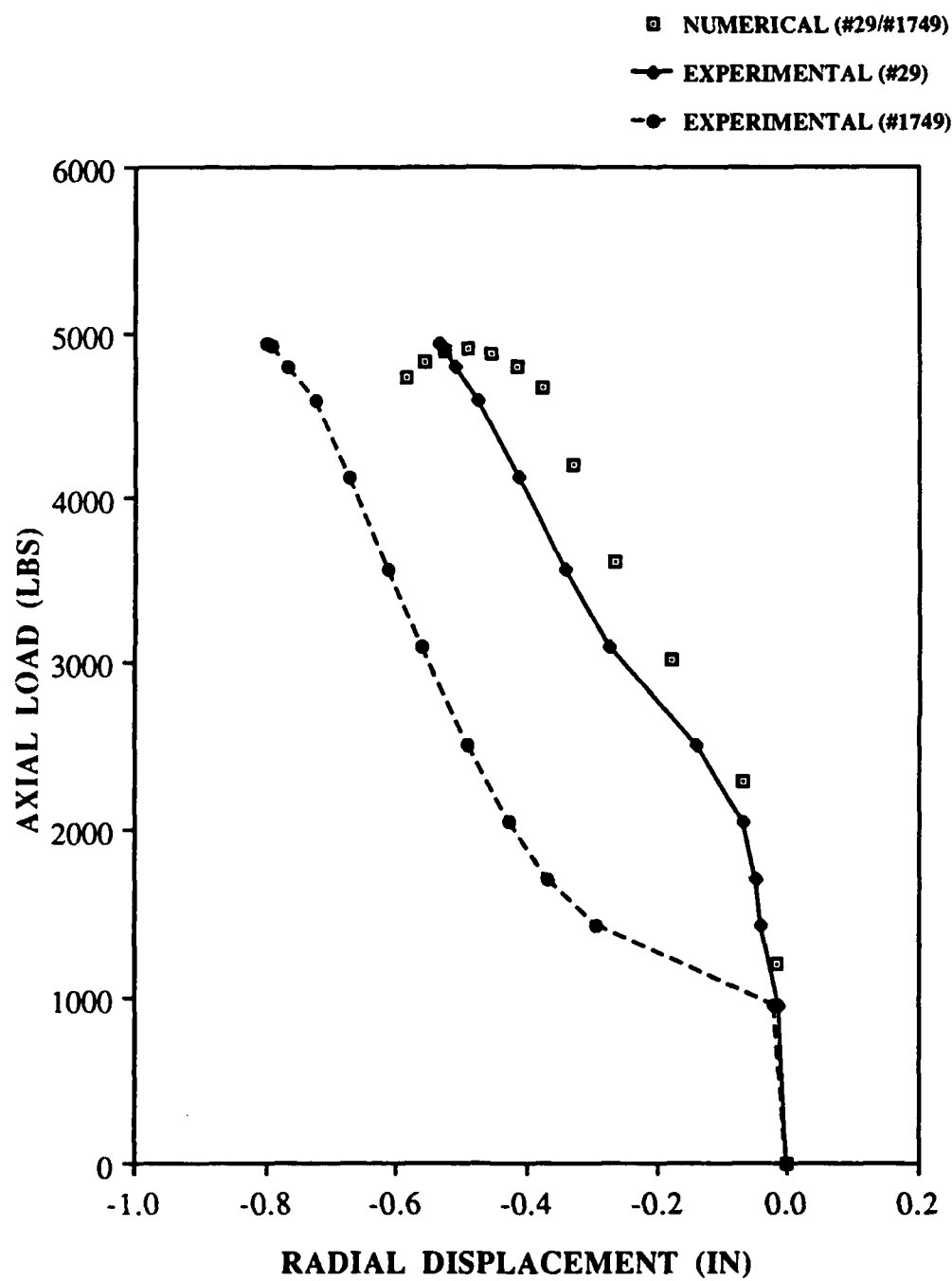


Fig. 54: Load vs. Radial Displacement  
[0/90]4s, 4" Cutout  
(12" X 20")

## **6. CONCLUSIONS**

1. Taking into consideration geometric (curvature, parallelism of edges) and material imperfections that occur in the experimental test panels, the numerical data from SHELL is a good predictor of the collapse characteristics of cylindrical shell panels. Correlation between experimental and numerical data is the best for shells with large cutouts, where the largest bending rotations and transverse shear strains occur. In these cases, a more true reading of the accuracy of SHELL is obtained since any panel imperfections are insignificant compared to the influence a large cutout has on panel collapse.
2. The magnitude of transverse shear strain increases with shell thickness and increases significantly when a large cutout is centrally placed in a shell. The presence of transverse shear strain decreases the global stiffness of the shell panel and thus enhances any bending or twisting in the panels. The ply layup also appears to affect the magnitudes of transverse shear strains present in the shells; the difference in magnitudes being the most significant in the 8-ply cases. It was also noted that the largest transverse shear strains occurred in the 24-ply quasi-isotropic shells with large cutouts; the magnitudes being 20% higher than a similar cross-ply configuration. Even though this occurred, the quasi-isotropic shell still collapsed at a higher load than the cross-ply shell. This indicates that under large displacement and moderately large rotation conditions, the cross-ply shells are more affected by thru-the-thickness transverse shear strain.

3. The greatest levels of surface bending rotations, radial displacements, and transverse shear strain occur, as the panel collapses, along unsupported vertical edges near the panel's horizontal center and at the four corners of a square cutout. In addition, for the very stiff panels, large displacements and transverse shear strain also occur along the vertical edges near the clamps.
4. It was found that the collapse characteristics of shell panels are sensitive to the parallelism of the shell's edges. In particular, parallelism is critical with respect to the horizontal edges when distributed axial loads are applied. The degree of parallelism affects the evenness of the load application. If the panel's horizontal edge is not parallel with the loading platen, then the resulting uneven loading leads to asymmetrical local collapse responses.
5. Due to the fact that quasi-isotropic laminates have a much greater stiffness than cross-ply laminates against in-plane shear forces and twisting moments, the cross-ply shell panels are more affected by any slippage within the clamps and uneven loading distributions. Unlike the quasi-isotropic shells which have  $\pm 45^\circ$  fibers, the cross-ply shells have little resistance to the inertial movement of the panel caused by in-plane shearing as the load levels increase.

6. The quasi-isotropic shell panels globally responded in a stiffer manner than the cross-ply panels, except for the 8-ply cross-ply case where the aspect ratio was unity. Therefore, aspect ratio is an important factor in the collapse of shells and its contribution may vary with different ply layups. In addition, it was interesting to note that in all cases, when a large cutout was present in the shell panel, the cross-ply panels per configuration responded more flexibly during collapse than the quasi-isotropic panels. This was even true for the 8-ply panel discussed above.
7. The presence of a large cutout in a shell panel significantly reduces the stiffness of the panel, which results in much lower loads required to collapse the shells with cutouts. In addition, the stiffer the solid version of a shell configuration is due to either a greater thickness or smaller aspect ratio, the more dramatic the drop in collapse load when a cutout is placed in the shell.
8. The best correlation between the numerically-derived collapse loads and the experimental collapse loads consistently occurred with the 16-ply cross-ply and quasi-isotropic shell panels. The possible reasoning behind this finding is probably due more to panel manufacturing than to any theoretical differences between the different shell thicknesses. The manufactured 8-ply panels appeared to have the greatest curvature imperfections of all the panels studied, due to their significantly greater flexibility compared to the 16 and 24 ply shells. In addition, the greater thickness of the 24-ply panels may have contributed to more imperfections resulting from the curing process. In particular, greater residual stresses and greater thickness variation within and between laminae may be more prevalent in the 24-ply cases than in the 8 and 16 ply cases.

## BIBLIOGRAPHY

1. Agarwal, B. D. and Broutman, L. J. Analysis and Performance of Fiber Composites. (Second Edition). New York: John Wiley and Sons, Inc., 1990.
2. Almroth, B. O. and Brogran, F. A. Numerical Procedures for Analysis of Structural Shells. AFWAL-TR-80-3128, Air Force Flight Dynamics Laboratory, Wright-Patterson AFB OH, March 1981.
3. Bathe, K. J. and Ho, L. W. "Some Results in the Analysis of Thin Shell Structures," Nonlinear Finite Element Analysis in Structural Mechanics. 125-150. Heidelberg, NY: Springer-Verlag Berlin, 1981.
4. Bergan, P. G., "Automated Incremental-Iterative Solution Methods in Structural Mechanics," Recent Advances in Nonlinear Computational Mechanics, Pineridge Press, 1982.
5. Cook, R. D., Malkus, D.S. and Plesha, M.E. Concepts and Applications of Finite Element Analysis. (Third Edition). New York: John Wiley and Sons, 1989.
6. Dennis, Scott T. Large Displacement and Rotational Formulation for Laminated Cylindrical Shells Including Parabolic Transverse Shear. Ph.D. Dissertation, AFIT/DS/AA/88-1. School of Engineering, Air Force Institute of Technology (AU), Wright-Patterson AFB Oh, May 1988 (AD-A194871).
7. Dennis, S. T. and Palazotto, A. N., "Static Response of a Cylindrical Composite Panel with Cutouts Using a Geometrically Nonlinear Theory," AIAA Journal, Vol. 28, No. 6: 1082-1088 (June 1990).
8. Dennis, S. T. and Palazotto, A. N., "Large Displacement and Rotational Formulation for Laminated Shells Including Parabolic Transverse Shear," International Journal of Nonlinear Mechanics, Vol. 25, No. 1: 67-85 (1990).
9. Dennis, S. T. and Palazotto, A. N., "Laminated Shell in Cylindrical Bending, Two-Dimensional Approach vs Exact," AIAA Journal, Vol. 29, No. 4: 647-650 (April 1991).
10. Horban, B. A. The Effects of Through-the-Thickness Delaminations on Curved Composite Panels. MS Thesis, AFIT/GAE/AA/85D-8. School of Engineering, Air Force Institute of Technology (AU), Wright-Patterson AFB OH, December 1985.
11. Janisse, T. C. A Parametric Study of Surface Imperfections and Small Cutouts in a Composite Panel. MS Thesis, AFIT/GAE/AA/82D-15. School of Engineering, Air Force Institute of Technology (AU), Wright-Patterson AFB OH, December 1982.
12. Jones, R. M. Mechanics of Composite Materials. New York: Hemisphere Publishing Corporation, 1975.



13. Knight, N. F., Jr. and Starnes, J. H., Jr. "Postbuckling Behavior of Axially Compressed Graphite-Epoxy Cylindrical Panels With Circular Holes," Proceedings of the 1984 Pressure Vessel and Piping Conference and Exhibition. 153-167. New York: The American Society of Mechanical Engineers, 1984.
14. Knight, N. F., Jr. and Starnes, J. H., Jr. "Postbuckling Behavior of Selected Graphite-Epoxy Cylindrical Panels Loaded in Axial Compression," Proceedings of the 27th Structures, Structural Dynamics, and Materials Conference, San Antonio TX, May 1986 (AIAA 86-0881).
15. Lee, Catherine E. Numerical Determination of the Effects of Boundary Conditions on the Instability of Composite Panels with Cutouts. MS Thesis, AFIT/GAE/AA/83D-4. School of Engineering, Air Force Institute of Technology (AU), Wright-Patterson AFB OH, December 1983.
16. Leissa, A. W. Buckling of Laminated Composite Plates and Shell Panels. AFWAL-TR-85-3069. Air Force Flight Dynamics Laboratory, Wright-Patterson AFB OH, June 1985.
17. Librescu, L., "Refined Geometrically Nonlinear Theories of Anisotropic Laminated Shells," Quarterly of Applied Mathematics, Vol. 45:1-22 (April 1987).
18. Noor, A. K. and Burton, W. S., "Assessment of Shear Deformation Theories," Applied Mechanics Reviews, Vol. 42, No. 1: 1-13 (January 1989).
19. Noor, A. K., Starnes, J. H. Jr. and Waters, W. A. Jr., "Numerical and Experimental Simulations of the Postbuckling Response of Laminated Anisotropic Panels," AIAA Paper No. 90-0964-CP (April 1990).
20. Palazotto, A. N. and Dennis, S. T. Nonlinear Analysis of Shell Structures. Washington, DC: American Institute of Aeronautics and Astronautics, Inc., 1992.
21. Palazotto, A. N. and Tisler, T. W., "Considerations of Cutouts in Composite Cylindrical Panels," Computers and Structures, 29: 1101-1110 (1988).
22. Rhodes, M., Mikulas, M. and McGowan, P., "Effect of Orthotropic Properties and Panel Width on the Compression Strength of Graphite-Epoxy Laminates with Holes," AIAA Paper No. 82-0749 (1982).
23. Saada, A. S. Elasticity Theory and Application. (Reprint Edition) Malabar, FL: Krieger Publishing Co., Inc., 1989.
24. Sandhu, R. S., Sendekyj, G. P., Schoeppner, G. A. and Pappas, J. E., "Initiation and Prevention of Edge Delamination With and Without Residual Stresses," Presented at the 74th Meeting of Structure and Materials Panel of AGARD, Patras, Greece (May 1992).

25. Schimmels, Scott A. Investigation of Collapse Characteristics of Cylindrical Composite Panels with Large Cutouts. MS Thesis, AFIT/GAE/ENY/89D-33. School of Engineering, Air Force Institute of Technology (AU), Wright-Patterson AFB OH, December 1989.
26. Schimmels, S. A. and Palazotto, A. N., "Collapse Characteristics of Cylindrical Composite Panels Under Axial Loads," AIAA Journal, Vol. 30, No. 5: 1447-1449 (May 1992).
27. Silva, Kevin J. Finite Element Investigation of a Composite Cylindrical Shell Under Transverse Load With Through Thickness Shear and Snapping. MS Thesis, AFIT/GAE/ENY/89D-35. School of Engineering, Air Force Institute of Technology (AU), Wright-Patterson AFB OH, December 1989.
28. Tisler, Thomas W. Collapse Analysis of Cylindrical Composite Panels with Large Cutouts Under an Axial Load. MS Thesis, AFIT/GAE/AA/86D-1. School of Engineering, Air Force Institute of Technology (AU), Wright-Patterson AFB OH, December 1986.
29. Tsai, S. W. Composites Design. Dayton, OH: Think Composites, 1987.
30. Wilder, B. L. A Study of Damage Tolerance in Curved Composite Panels. MS Thesis, AFIT/GAE/AA/88D-2. School of Engineering, Air Force Institute of Technology (AU), Wright-Patterson AFB OH, December 1988.

**APPENDIX A**  
**EXPERIMENTAL TEST PLAN**

## TEST PLAN

### *Geometric Instability Studies*

#### 1. Program Information

a. Organization	WL/FIBCA
b. Project Number	24010366
c. Security Classification	Unclassified
d. Project Engineer	Capt James C. Hatfield, AFIT/ENY
e. Project Advisor	Dr. Anthony Palazotto, AFIT/ENY
f. Project Sponsor	Dr. R.S. Sandhu, WL/FIBCA
g. Fabrication Engineer	Mr. Jack Smith, WL/FIBCA
h. Instrumentation Engineer	Assigned by FIBT
i. Test Engineer	Assigned by FIBE
j. Test Location	WL/FIBEC, Bldg. 65, Area B

#### 2. Program Objective

The objective of this project is to study the geometric instability (collapse load/displacement) of composite panels under axial compressive load. The test specimens will be of cylindrical cross-section and be fabricated using AS4/3501-6 material.

#### 3. Fabrication

The following paragraphs provide technical details to fabricate specimens required to conduct the collapse studies.

##### 3.1 Material

The specimens required for this research will be fabricated using a graphite/epoxy (AS4/3501-6) material system.

##### 3.2 Stacking Sequence and Thickness of Panels

Curved specimens (sizes specified in paragraph 3.3) will be fabricated using the material system of paragraph 3.1, and will conform to the following sequences:

*Table 1*

<u>Panel Configuration</u>	<u>Stacking Sequence</u>	<u>Total Number of Plies</u>
A	[0/90]2s	8
B	[0/+45/-45/90]s	8
C	[0/90]4s	16
D	[0/+45/-45/90]2s	16
E	[0/90]6s	24
F	[0/+45/-45/90]3s	24

The panels will be uniform in thickness , having an average ply thickness after cure of  $0.00525" \pm 0.0003"$ .

### 3.3 Specimens

#### 3.3.1 Size

For the material system specified in paragraph 3.1, the size and the number of specimens will be in accordance with Table 2. The first number of the specimen size indicates the circumferential length of the curved panel, while the second number indicates the axial length. All panels have a radius of curvature of 12", as shown in Figures A1 - A4. In addition, some of the specimens will have centrally located square cutouts. Refer to Figures A1 thru A4 for details.

*Table 2*

<u>Specimen Designator</u>	<u>Panel Configuration</u>	<u>Specimen Size</u>	<u>Cutout Size *</u>	<u>Ref. Figure</u>
JH-1-0	A	12" X 13"	No Cutout	1
JH-3-4	A	12" X 13"	4" Square	3
JH-4-0	A	12" X 21"	No Cutout	2
JH-6-4	A	12" X 21"	4" Square	4
JH-7-0	B	12" X 13"	No Cutout	1
JH-9-4	B	12" X 13"	4" Square	3
JH-10-0	B	12" X 21"	No Cutout	2
JH-12-4	B	12" X 21"	4" Square	4
JH-13-0	C	12" X 21"	No Cutout	2
JH-14-0				
JH-15-0				
JH-19-4	C	12" X 21"	4" Square	4
JH-20-4				
JH-21-4				
JH-22-0	D	12" X 21"	No Cutout	2
JH-23-0				
JH-24-0				
JH-28-4	D	12" X 21"	4" Square	4
JH-29-4				
JH-30-4				

<u>Specimen Designator</u>	<u>Panel Configuration</u>	<u>Specimen Size</u>	<u>Cutout Size*</u>	<u>Ref. Figure</u>
JH-31-0 JH-32-0 JH-33-0	E	12" X 21"	No Cutout	2
JH-37-4 JH-38-4 JH-39-4	E	12" X 21"	4" Square	4
JH-40-0 JH-41-0 JH-42-0	F	12" X 21"	No Cutout	2
JH-46-4 JH-47-4 JH-48-4	F	12" X 21"	4" Square	4

\* Cut holes of dimensions 4" X 4", as specified above, using a router with the method developed for cutting curved panels.

### 3.3.2 Curing Cycle

The curing cycle recommended by the manufacturer will be used.

### 3.3.3 Void Content

The void content will not be in excess of one percent, with variations of thickness specified in paragraph 3.2.

### 3.3.4 Determination of Flaws

All panels will be subjected to a C-scan to determine flaws before being cut. The final acceptance or rejection of panels will be made by the project engineer.

### 3.3.5 Resin Content

Samples will be taken at suitable locations to determine resin content, fiber volume, and void fractions for the panels being used.

## 3.4 Basic Material Properties

The elastic properties required will be extracted from "Initiation and Prevention of Edge Delamination With and Without Residual Stresses", Table 2 (May 1992).

## **4. Testing**

### **4.1 Test Procedure**

4.1.1 Specimens will be instrumented with back-to-back strain gages and linear variable differential transducers (LVDTs) as shown in Figures A5 thru A7. The purpose of the strain gages is to insure uniform loading across the top of the panels. The LVDTs will be measuring axial displacements (u) and radial displacements (w) during the compressive static loading.

4.1.2 The testing will be performed on the 30,000 lb hydraulic machine, with the curved-panel fixture which is currently in place. However, for these studies the vertical-edge supports will be removed. The compressive loads will be applied using a uniform displacement of 0.05" per minute. The panels will be compressed up to the collapse load and then the load will be released. A total of three tests will be performed on each different specimen configuration. The following data will be collected:

- a. Applied Load versus Radial Displacement
- b. Applied Load versus Axial Displacement

## **5. Report**

The results of this study will be compared to a finite element model. The final results and analysis will be incorporated into a master's degree thesis for the project engineer.

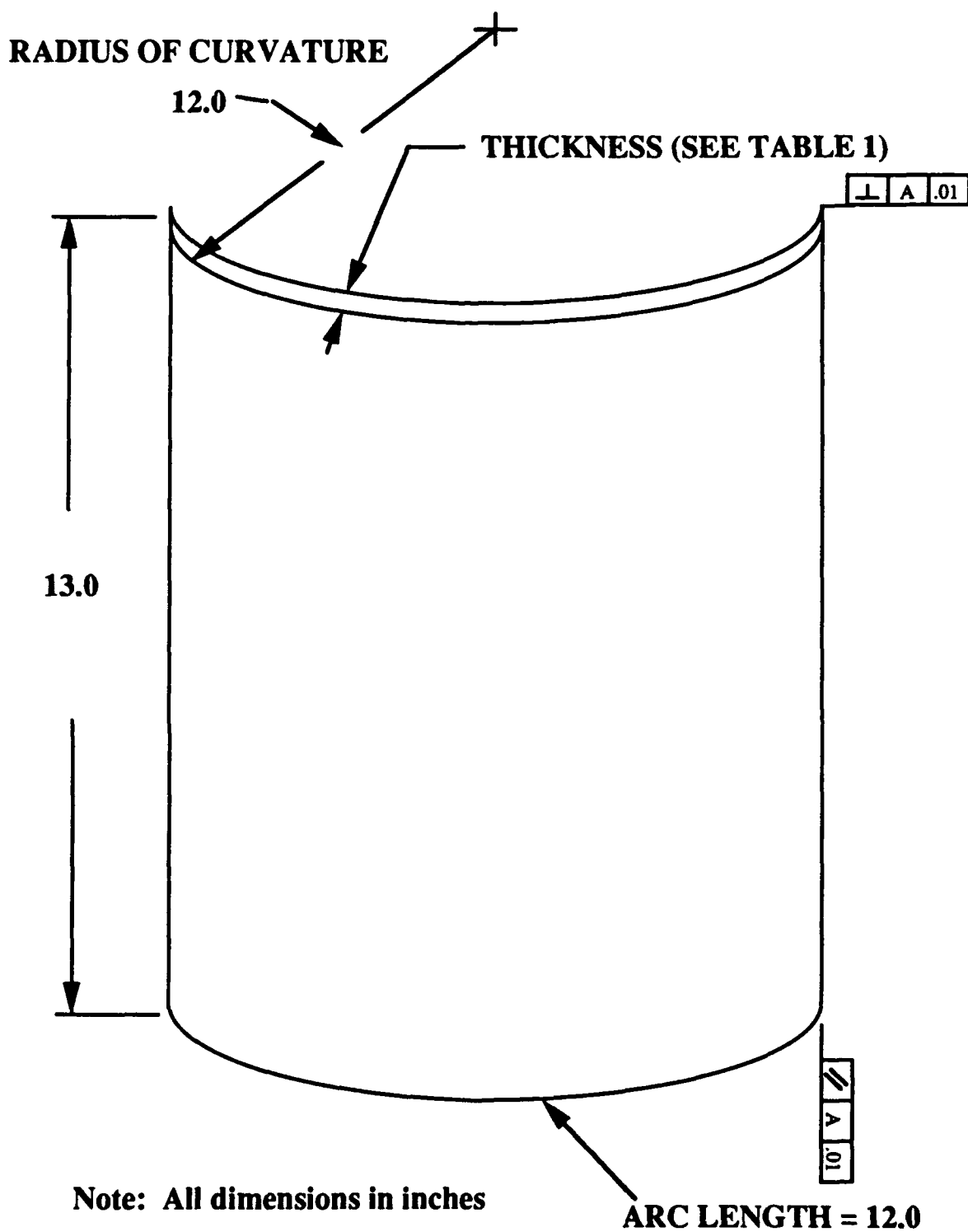


**Figure A1. Panel Size 12 X 13 Without Cutout**



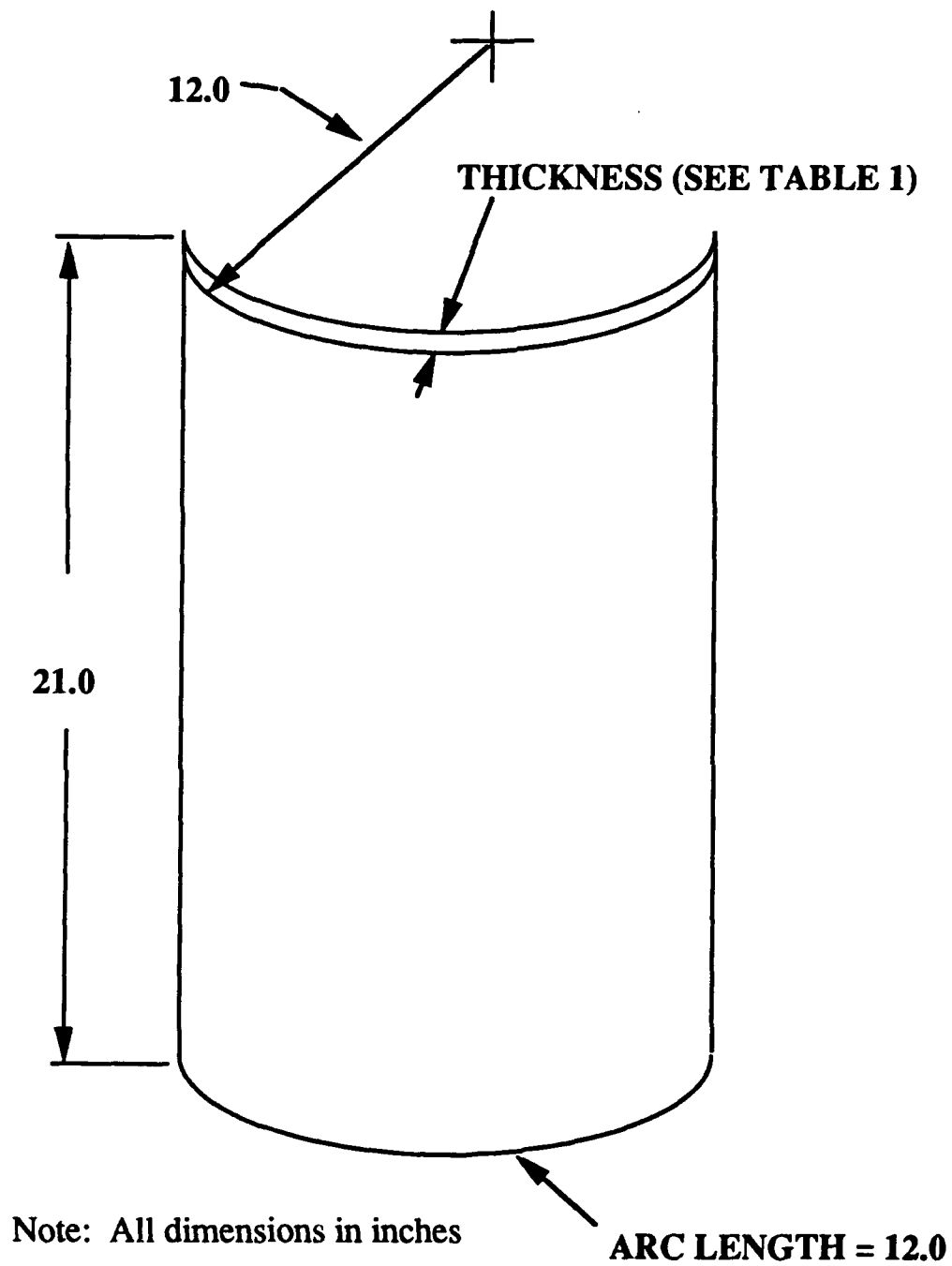
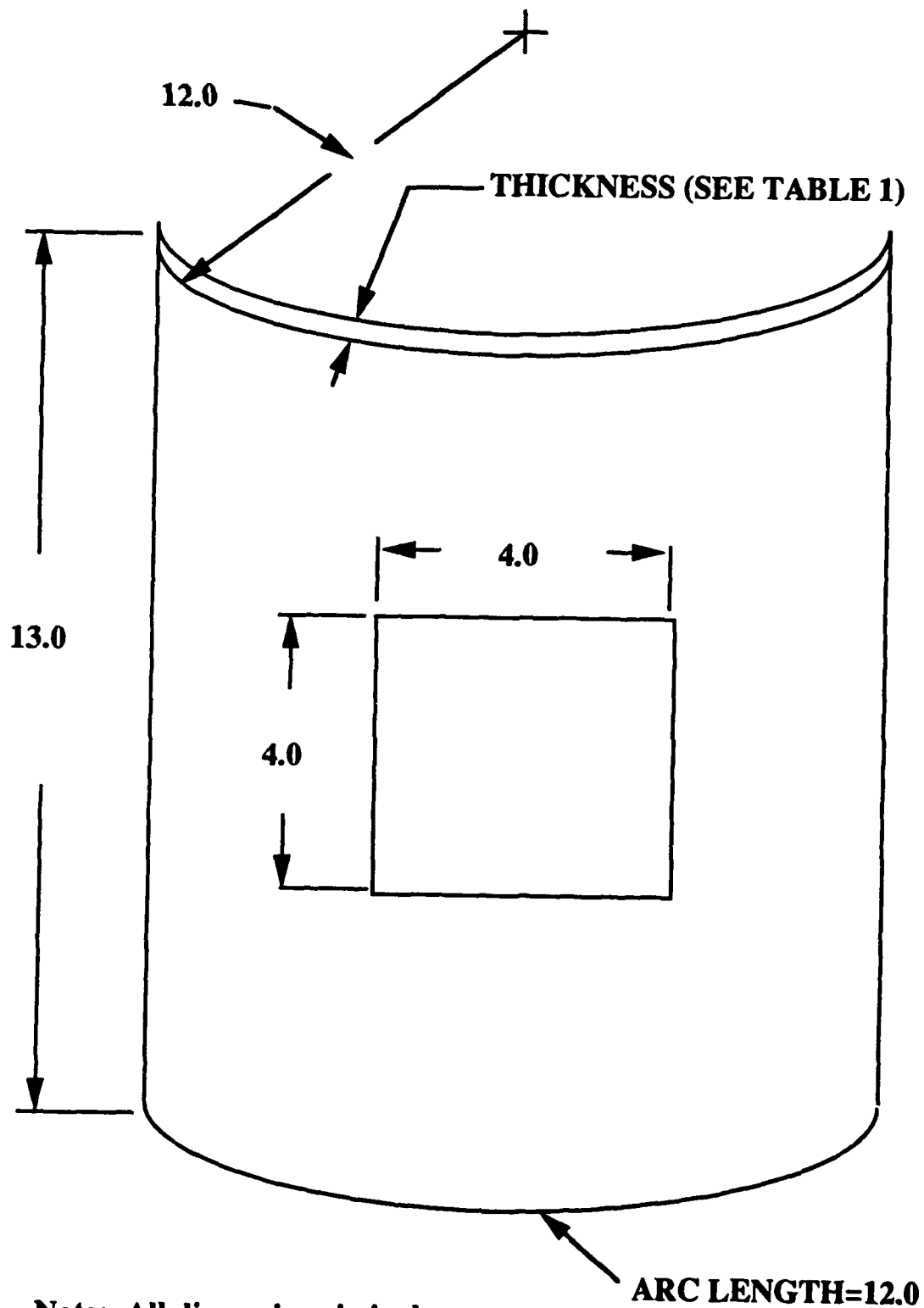


Figure A2. Panel Size 12 X 21 Without Cutout



**Note: All dimensions in inches**

**Figure A3. Panel Size 12 X 13 With 4 X 4 Central Cutout**

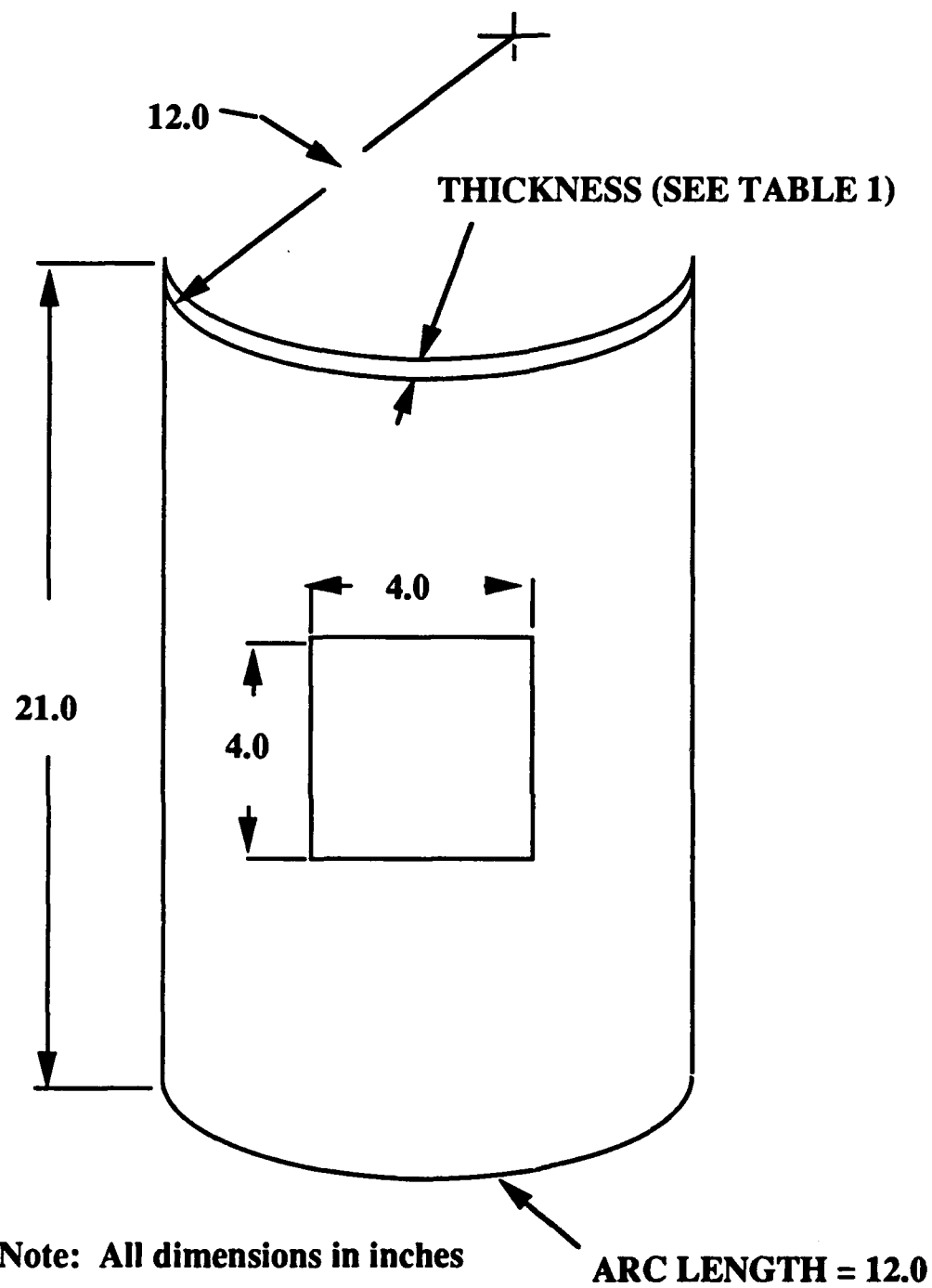


Figure A4. Panel Size 12 X 21 With 4 X 4 Central Cutout

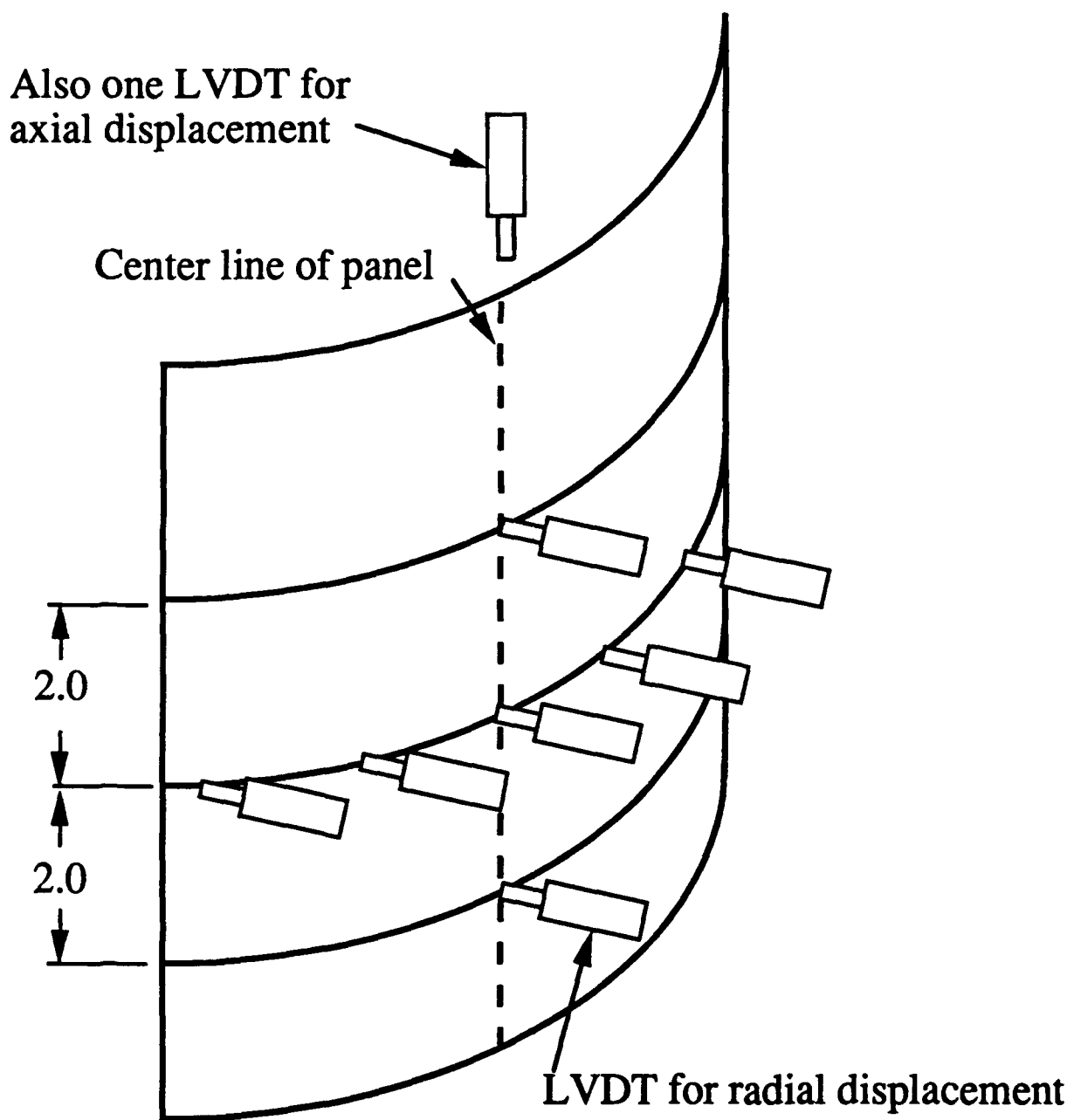


Figure A5. Displacement Measurements Using LVDTs

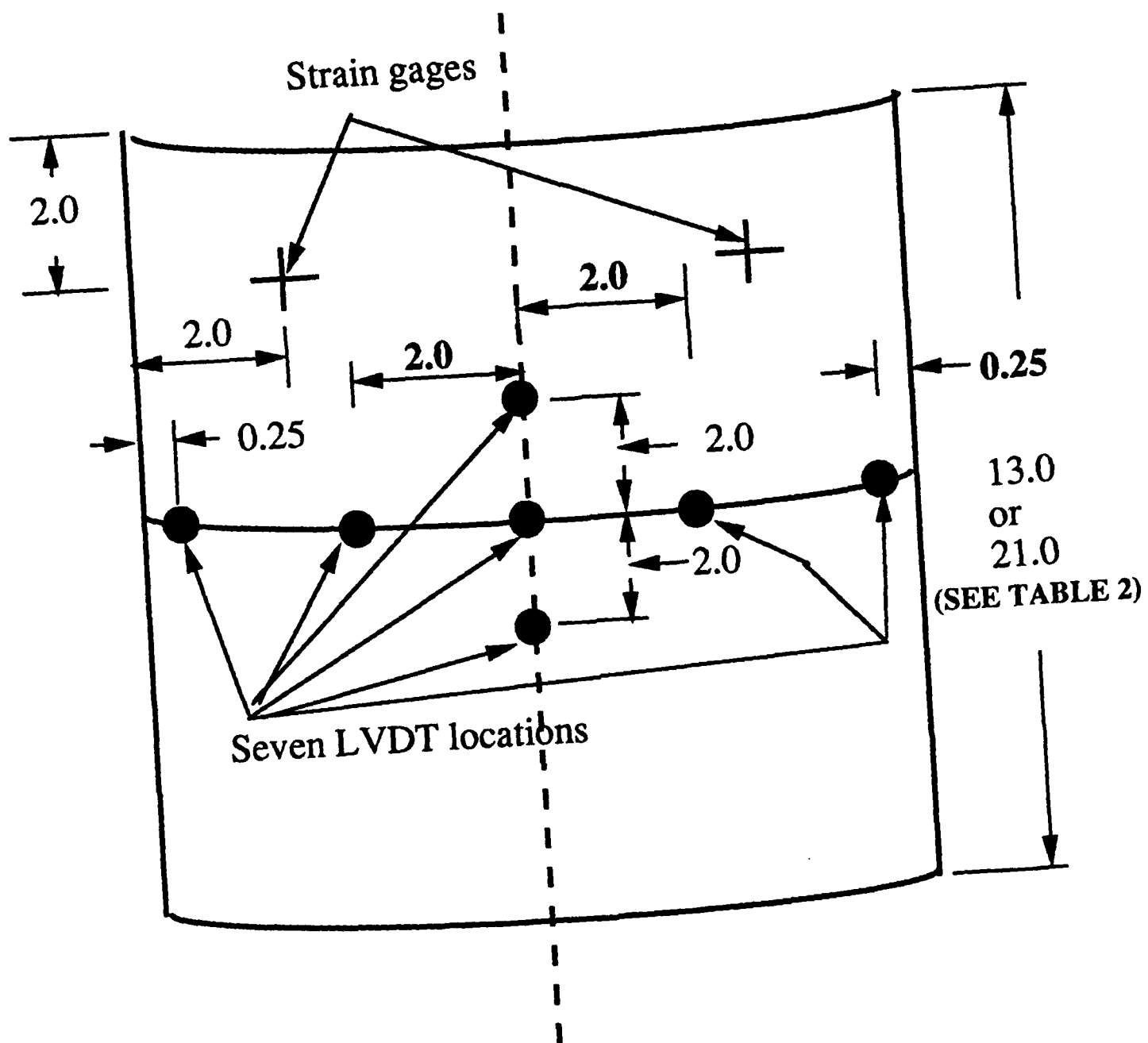


Figure A6. LVDT and Strain Gage Locations, Solid Panels

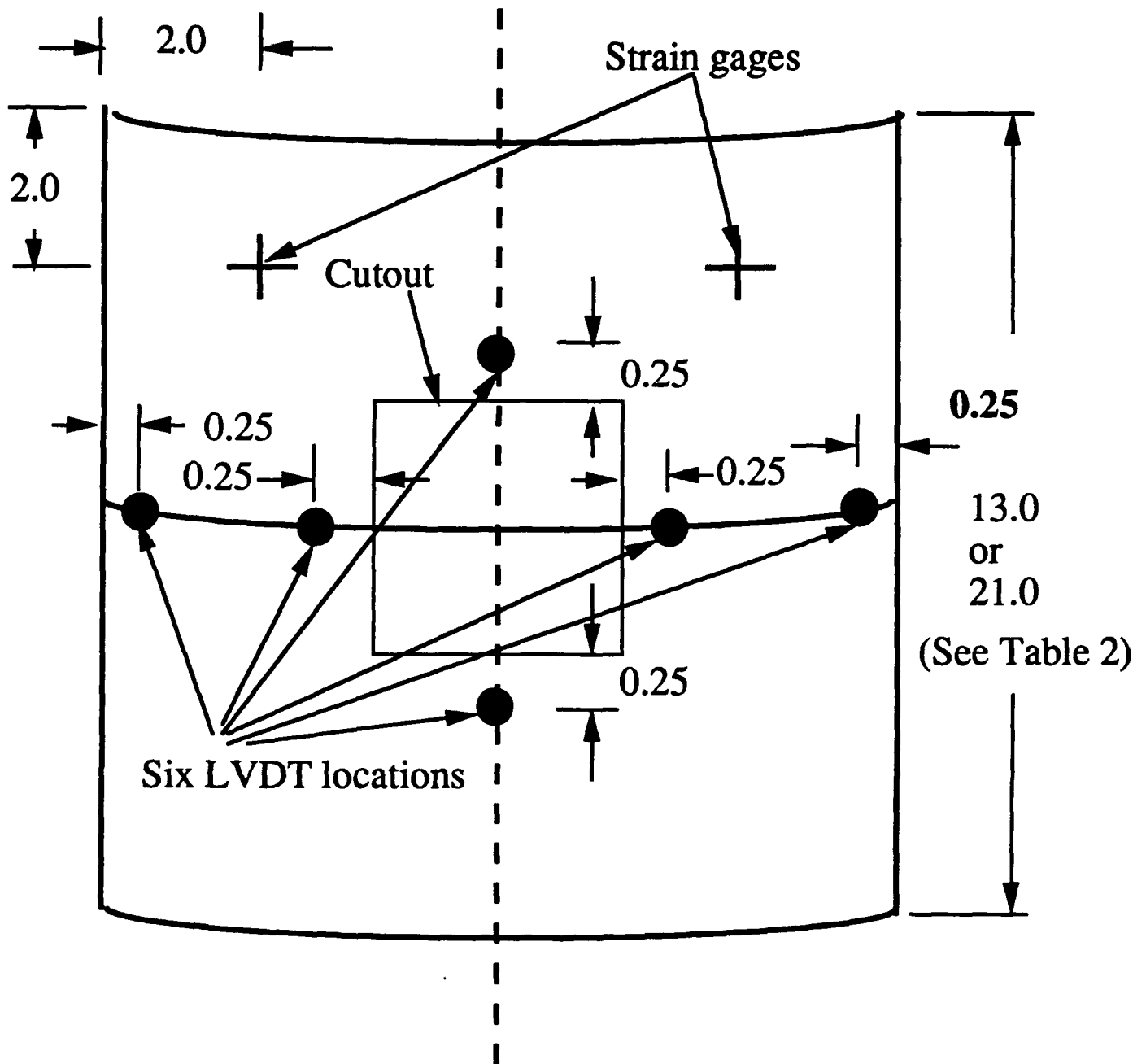


Figure A7. LVDT and Strain Gage Locations, Panels With Cutouts

**APPENDIX B**

**ADDITIONAL NUMERICAL / EXPERIMENTAL  
AXIAL LOAD VERSUS DISPLACEMENT CURVES**

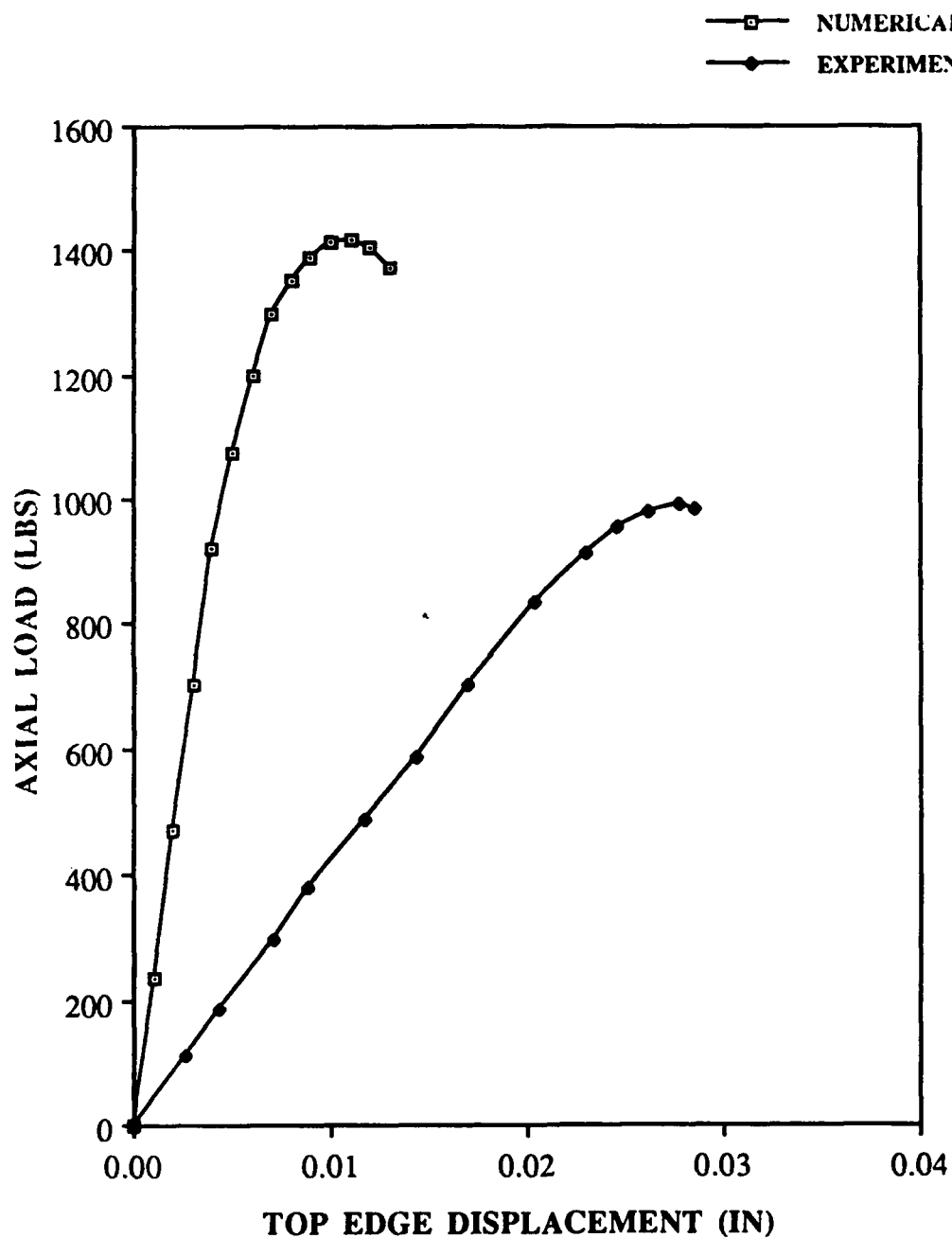


Fig. 55: Load vs. Top Edge Displacement,  
[0/+45/-45/90]s, 4" Cutout  
(12" X 12" )



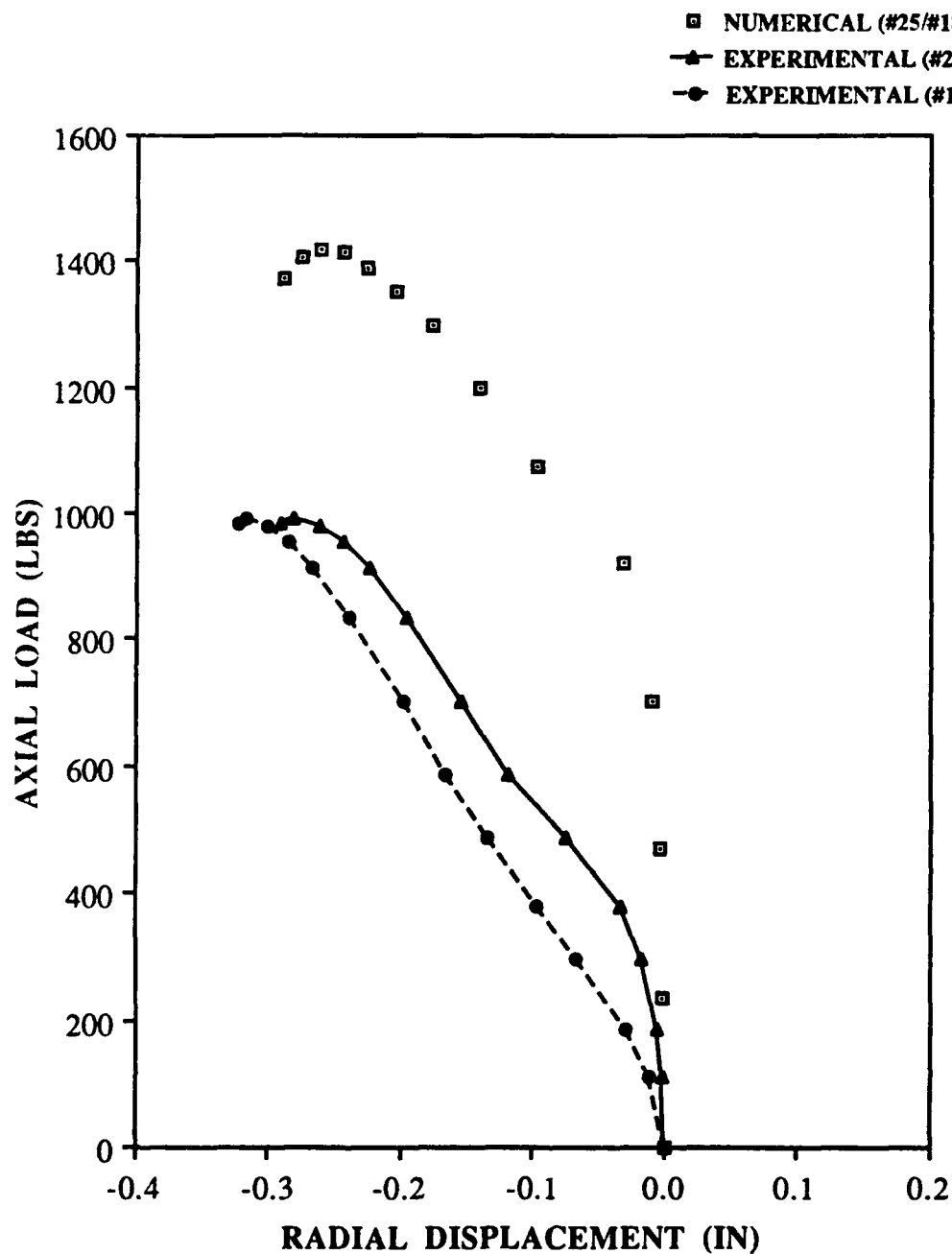


Fig. 56: Load vs. Radial Displacement,  
[0/+45/-45/90]<sub>s</sub>, 4" Cutout  
(12" X 12")

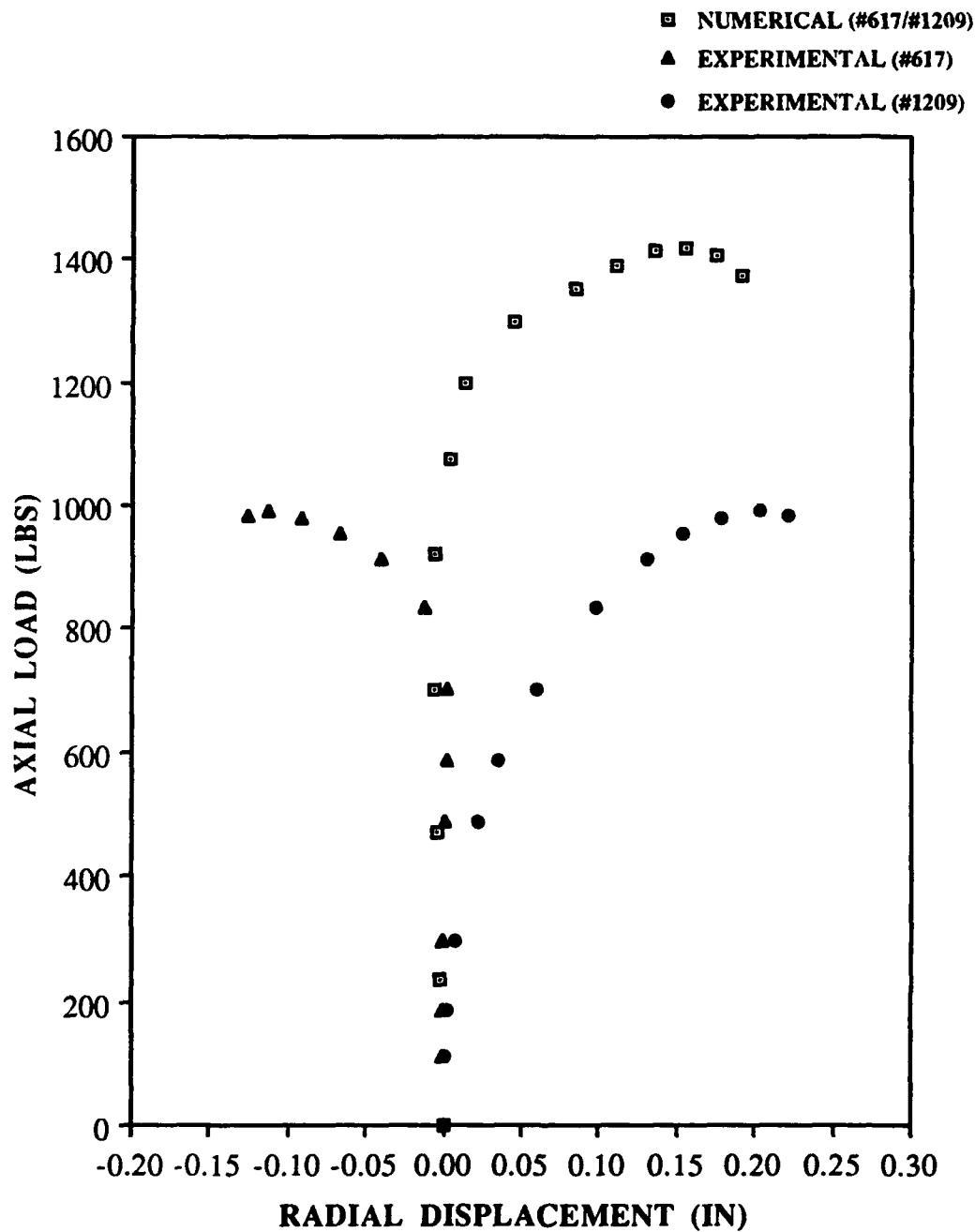


Fig. 57: Load vs. Radial Displacement,  
[0/+45/-45/90]<sub>s</sub>, 4" Cutout  
(12" X 12")

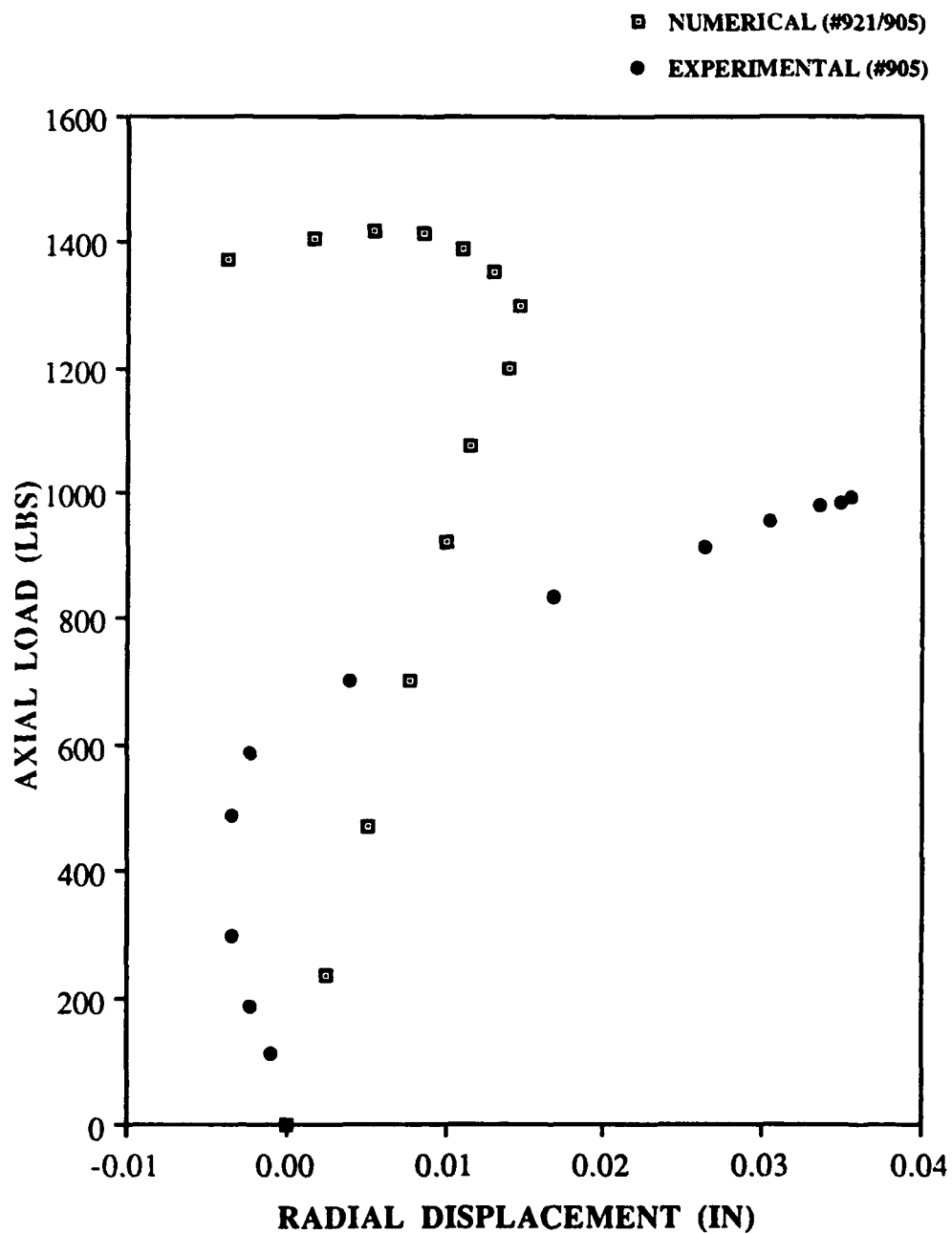


Fig. 58: Load vs. Radial Displacement,  
[0/+45/-45/90]s, 4" Cutout  
(12 " X 12")

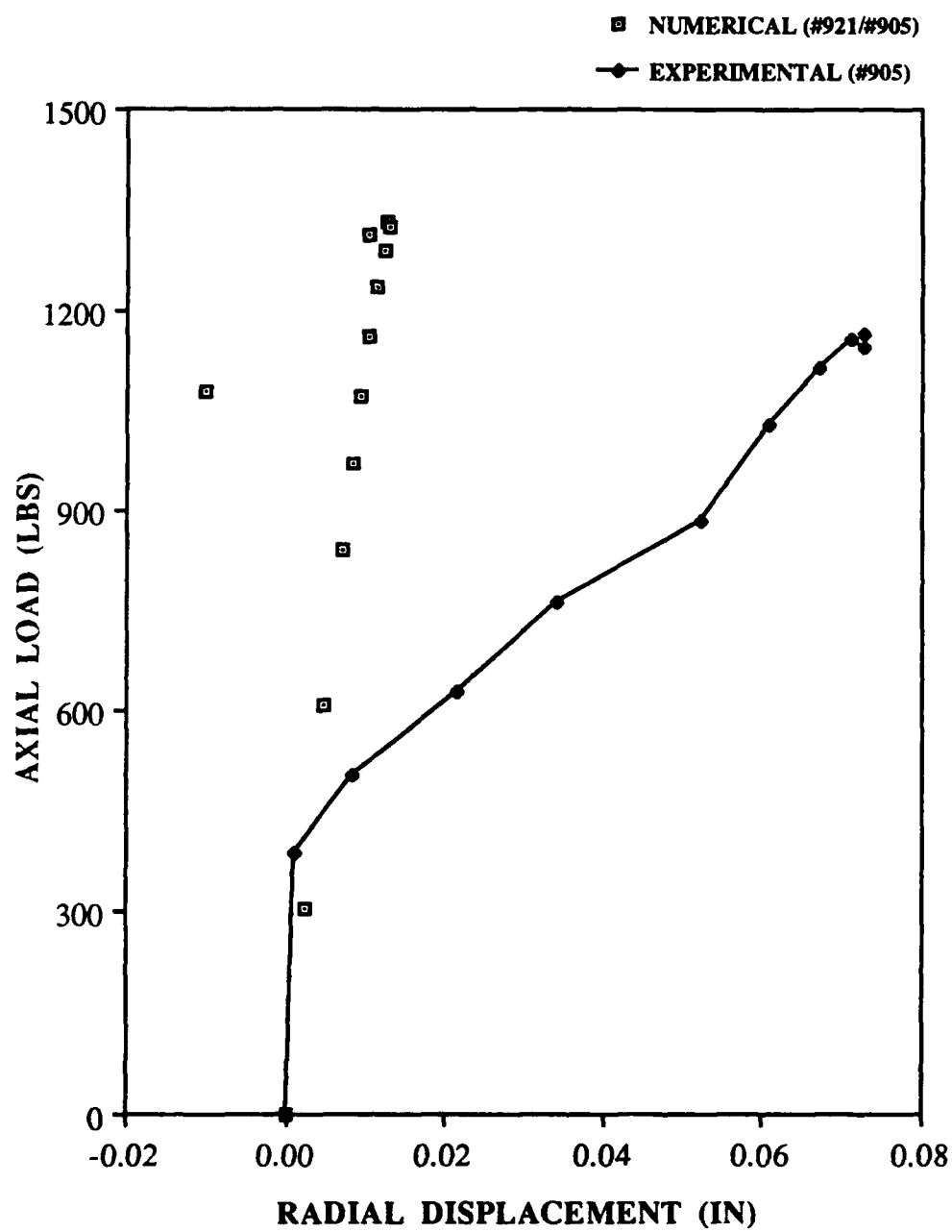


Fig. 59: Load vs. Radial Displacement,  
[0/90]2s, 4" Cutout  
(12" X 12")

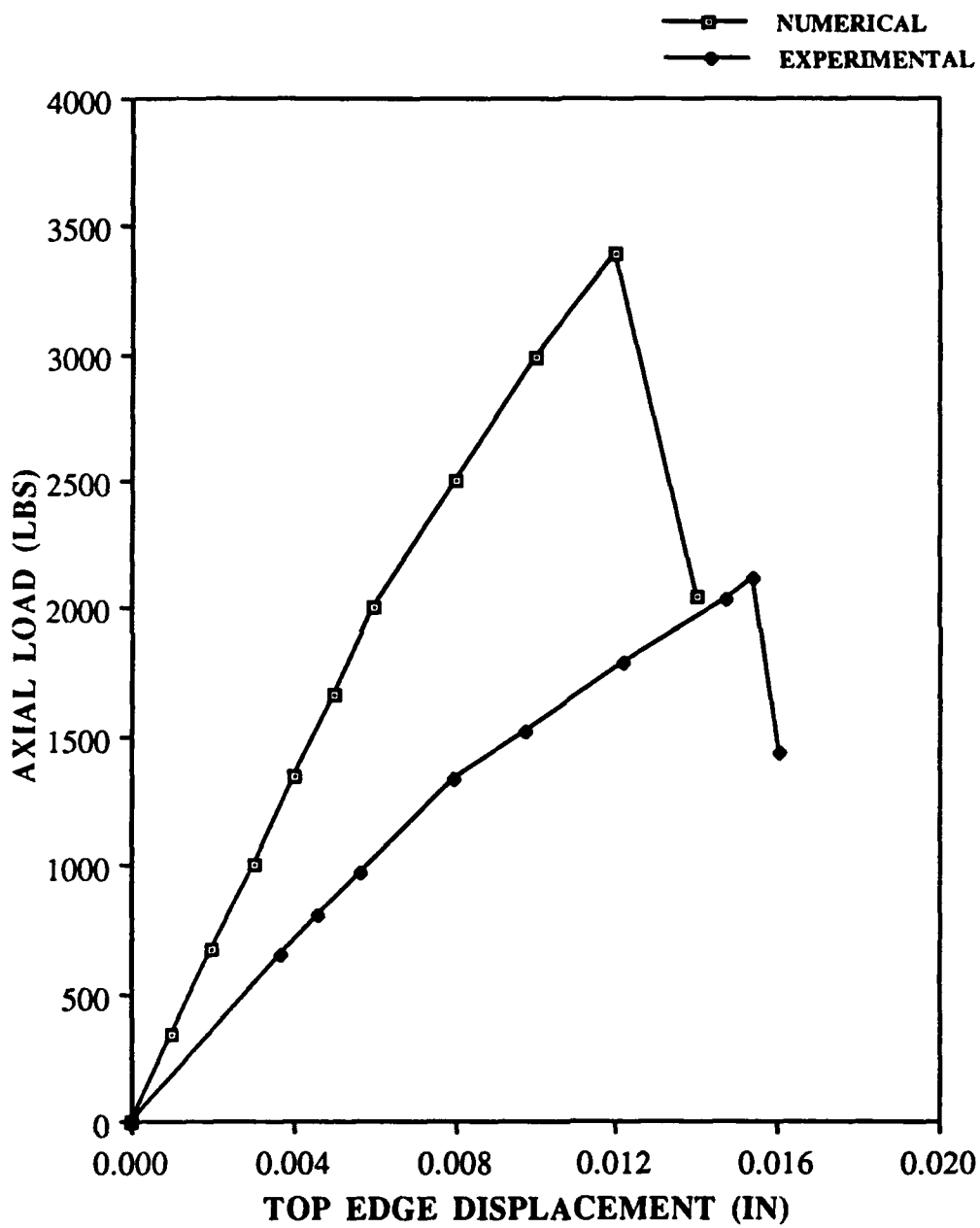


Fig. 60: Load vs. Top Edge Displacement,  
[0/+45/-45/90]<sub>s</sub>, No Cutout  
(12" X 12")

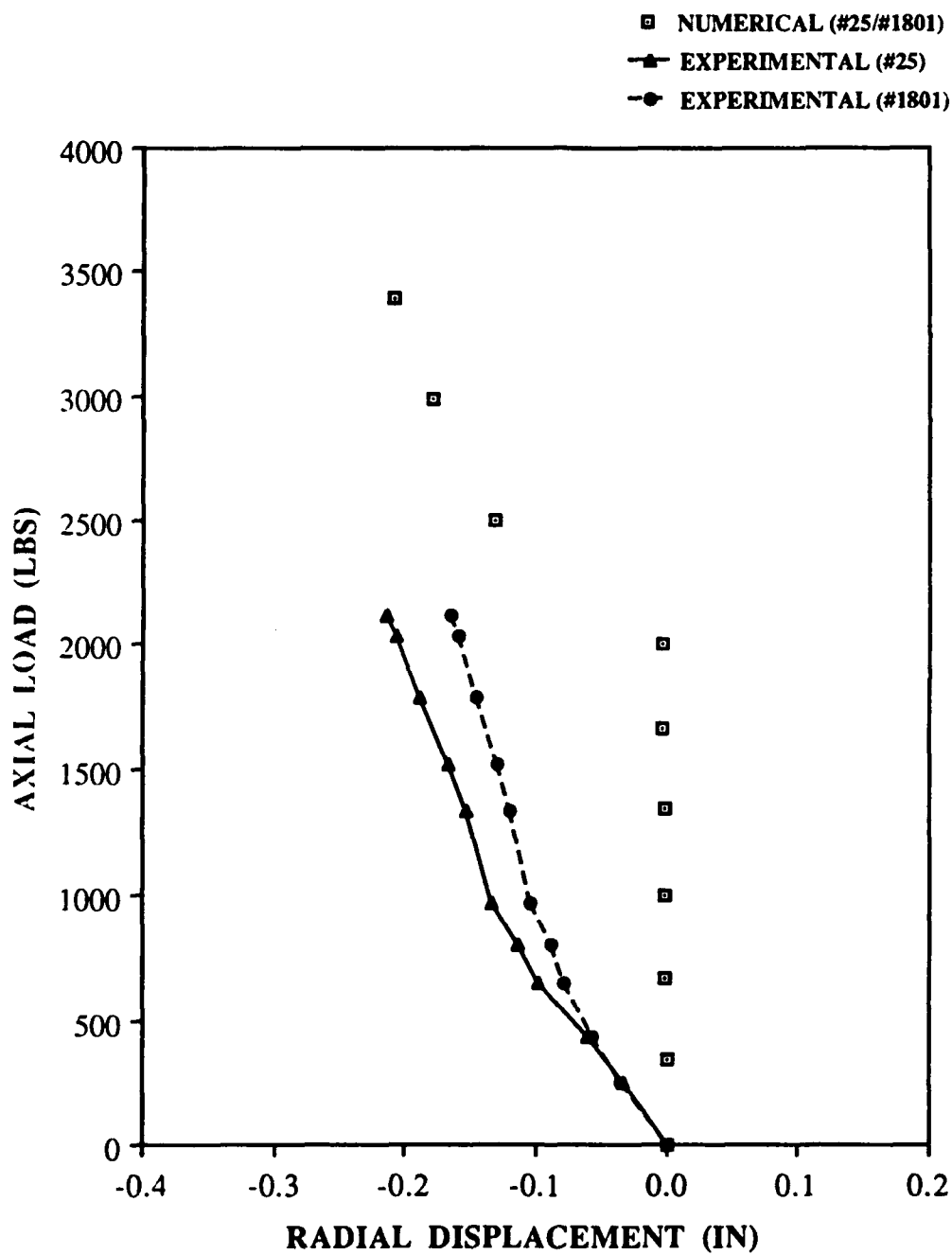


Fig. 61: Load vs. Radial Displacement,  
[0/+45/-45/90]s, No Cutout  
(12" X 12")

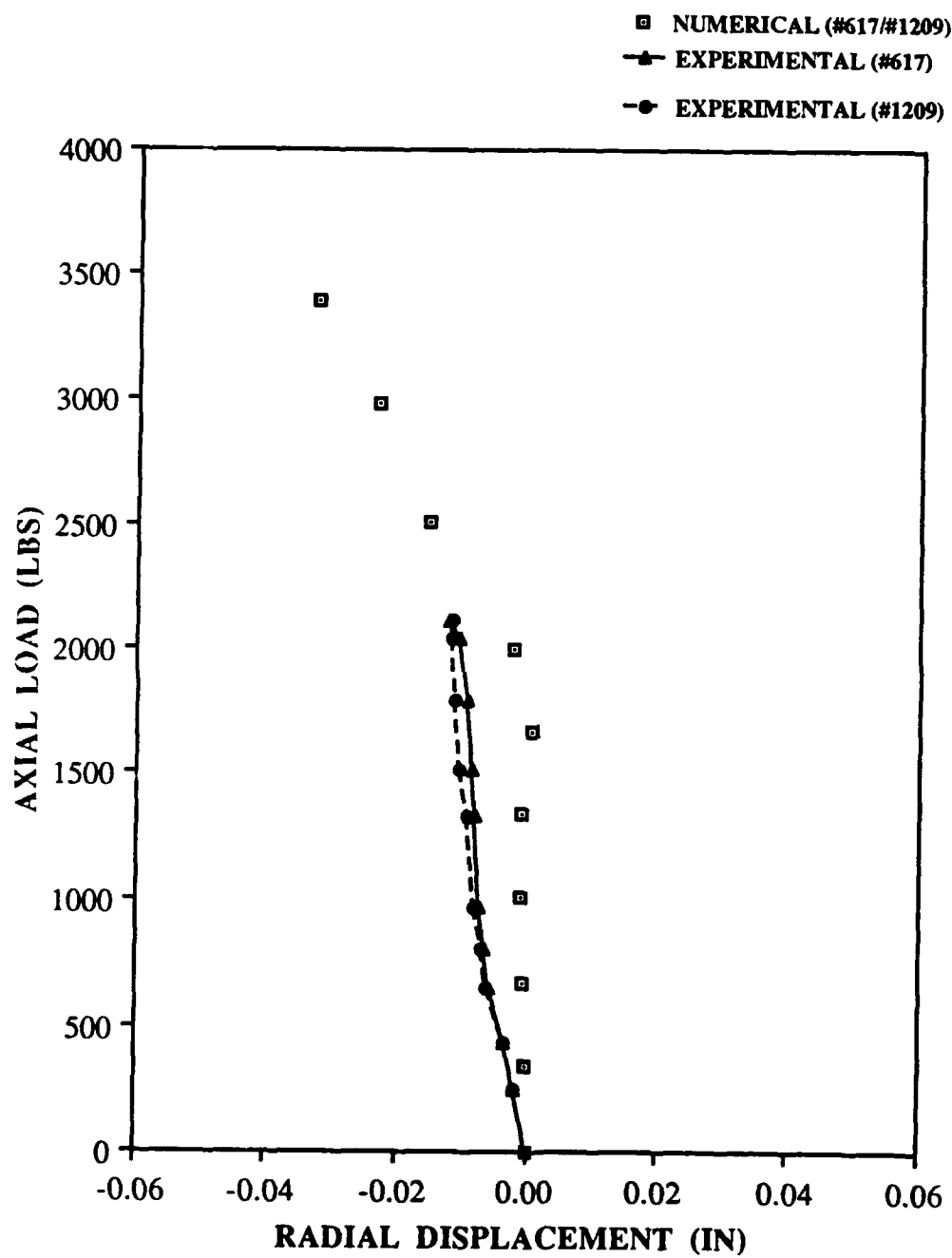


Fig. 62: Load vs. Radial Displacement,  
[0/+45/-45/90]s, No Cutout  
(12" X 12")

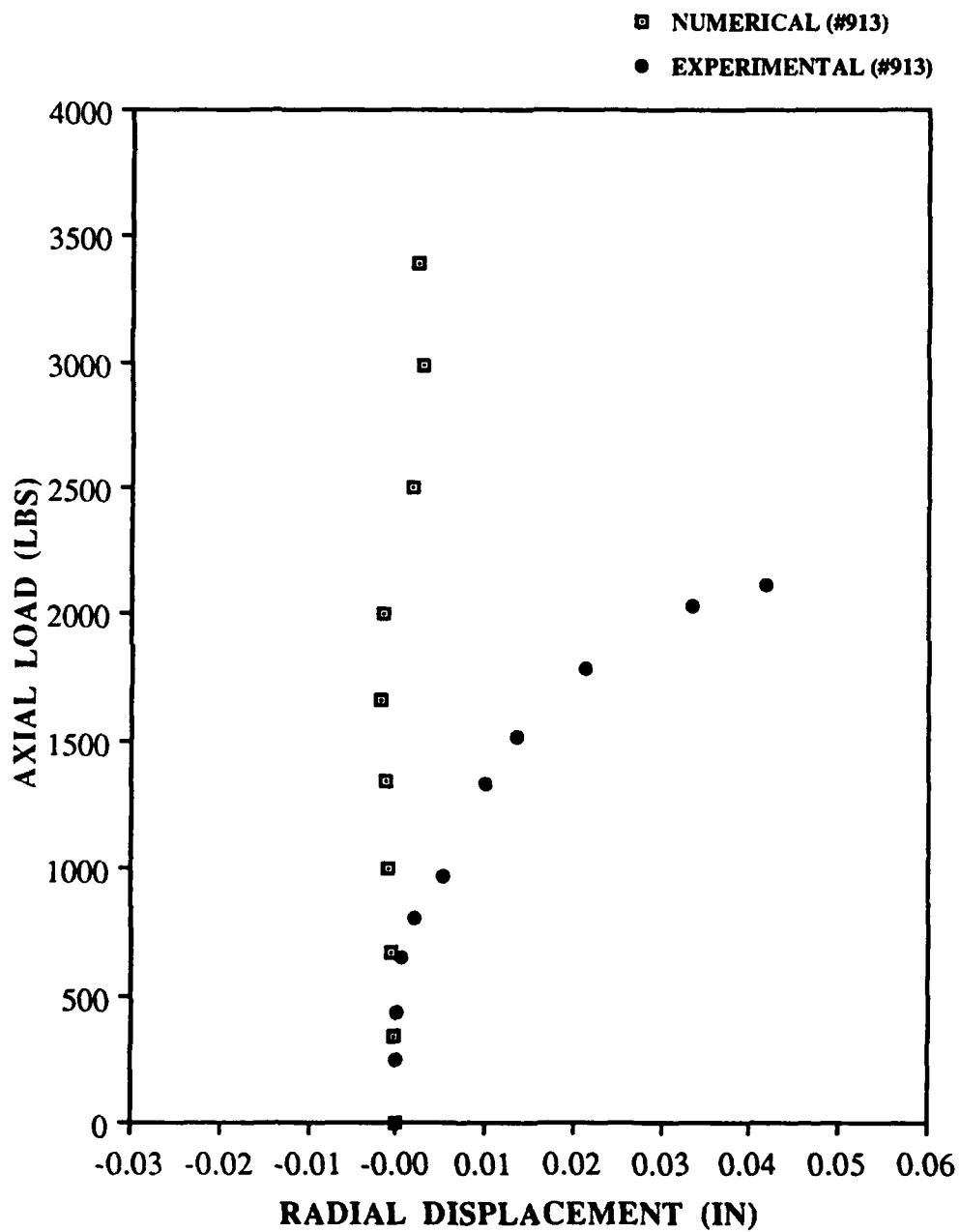


Fig. 63: Load vs. Radial Displacement,  
[0/+45/-45/90]s, No Cutout  
(12" X 12")



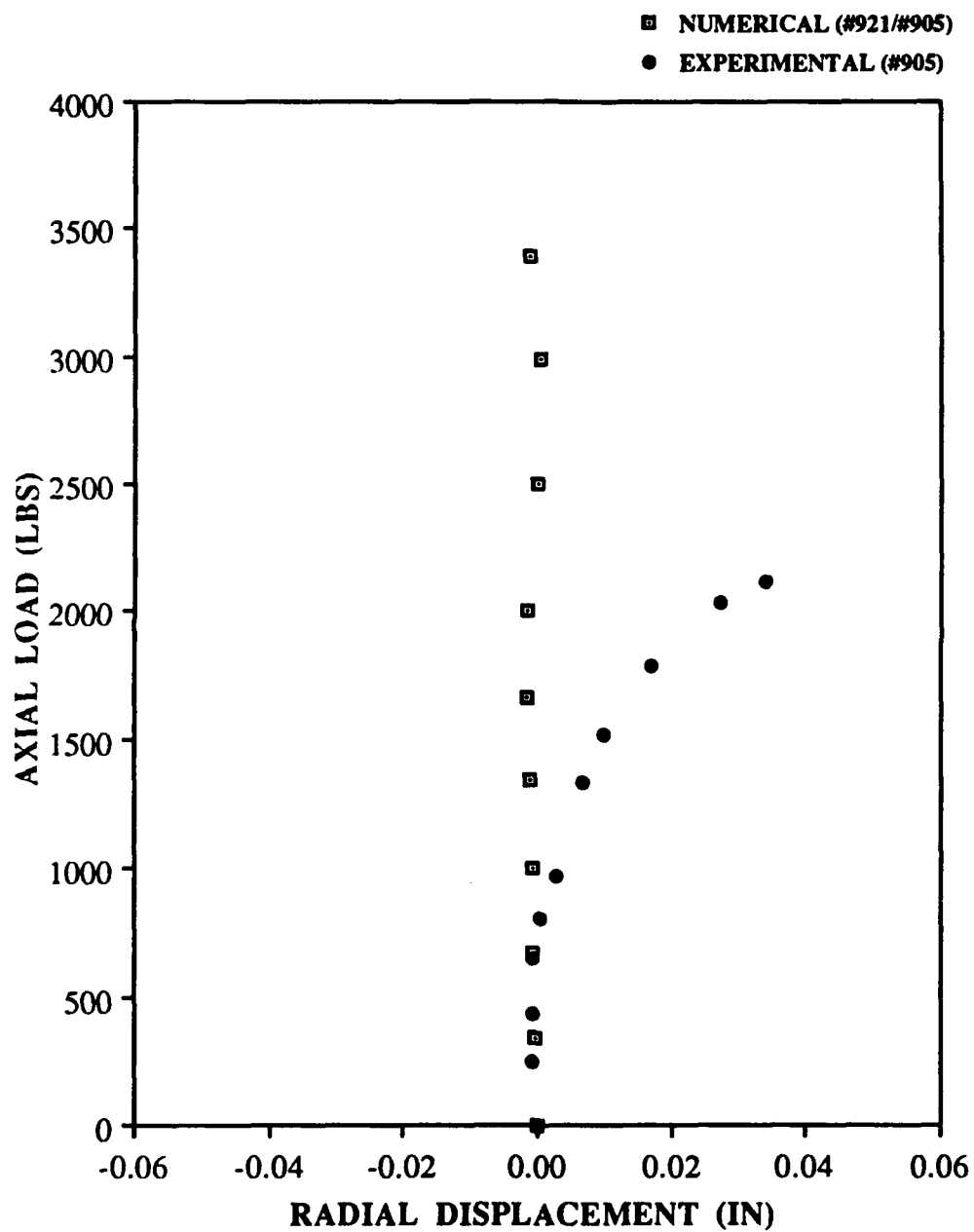


Fig. 64: Load vs. Radial Displacement,  
[0/+45/-45/90]s, No Cutout  
(12" X 12")

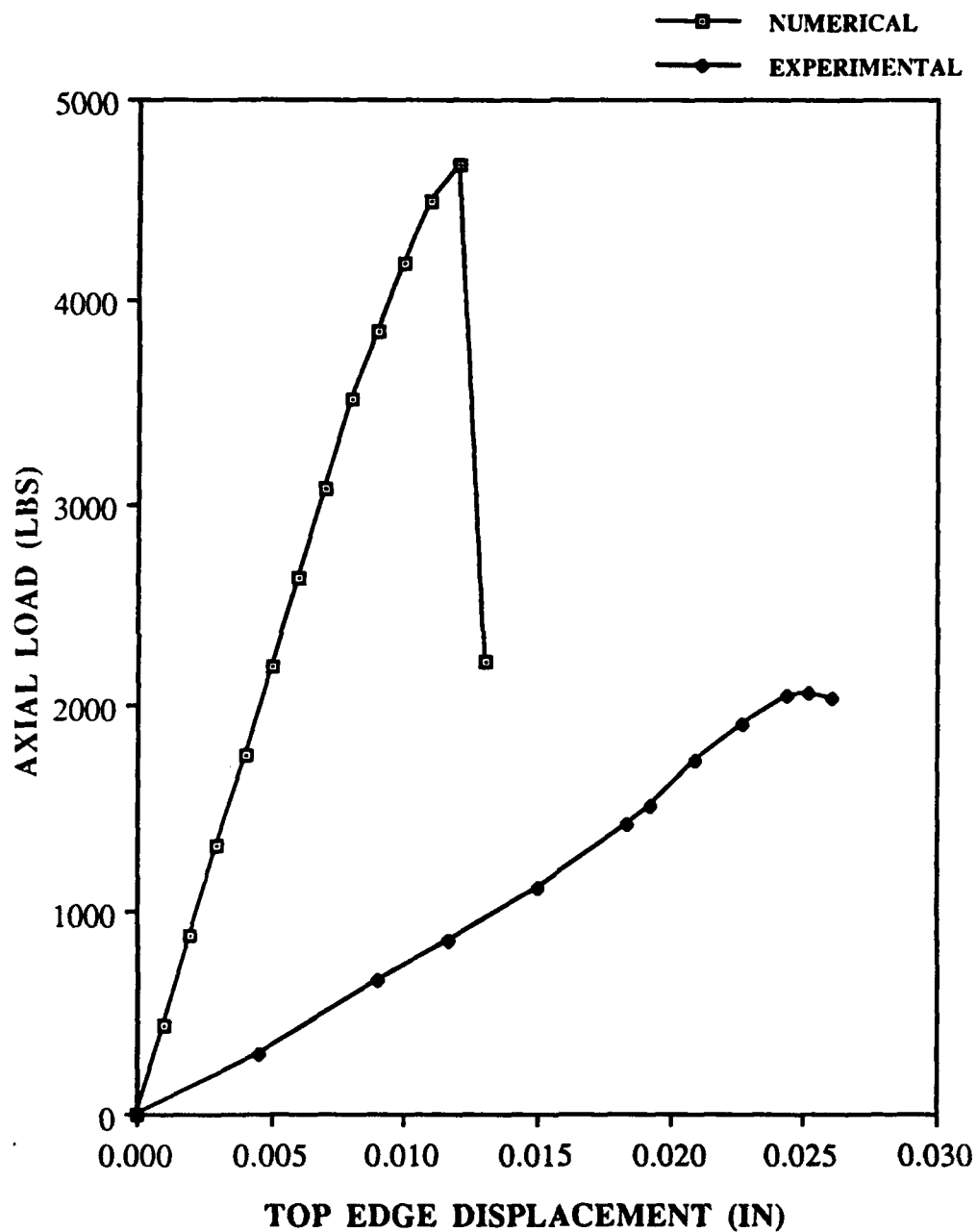


Fig. 65: Load vs. Top Edge Displacement,  
[0/90]2s, No Cutout  
(12" X 12")

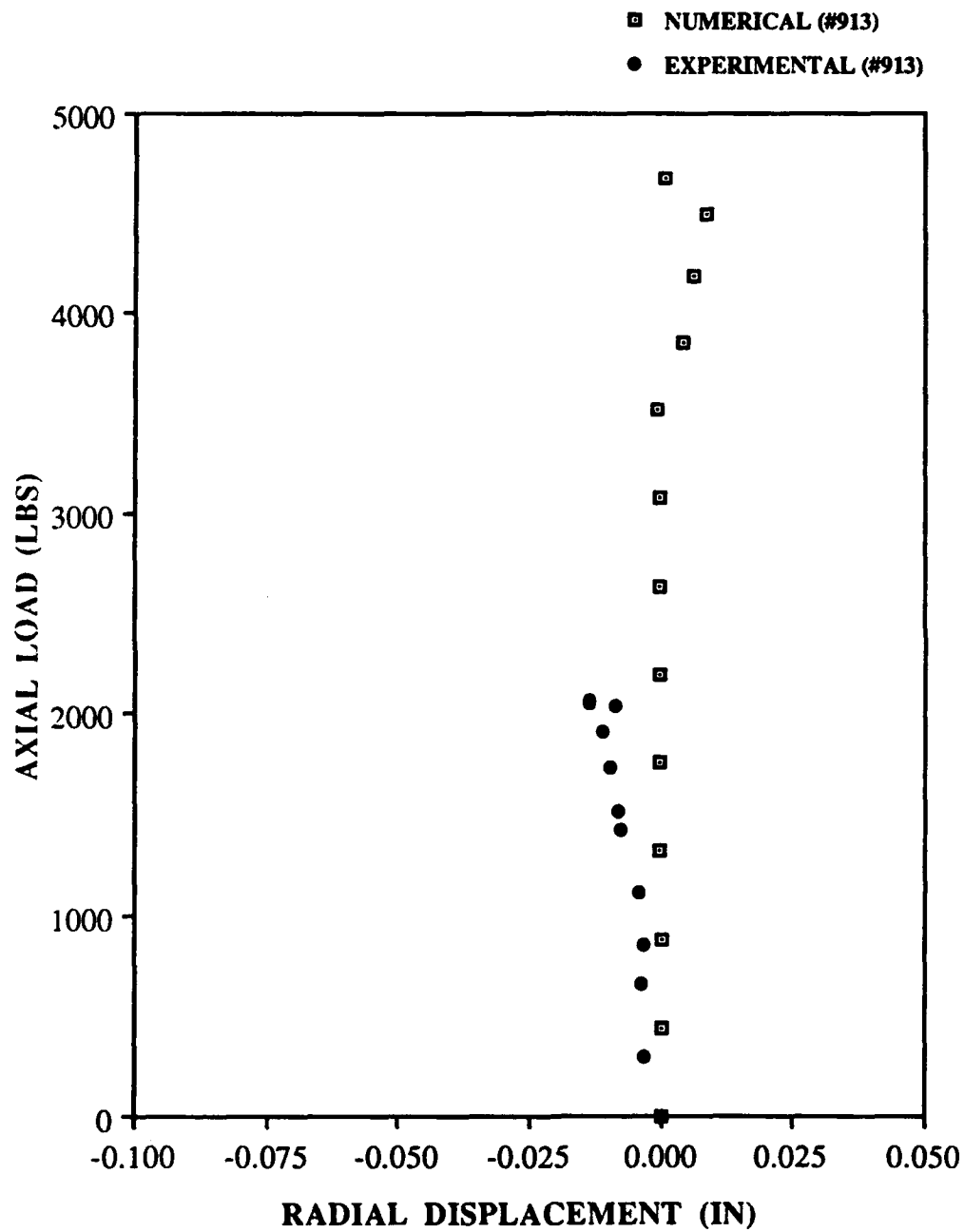


Fig. 66: Load vs. Radial Displacement,  
[0/90]<sub>2s</sub>, No Cutout  
(12" X 12")

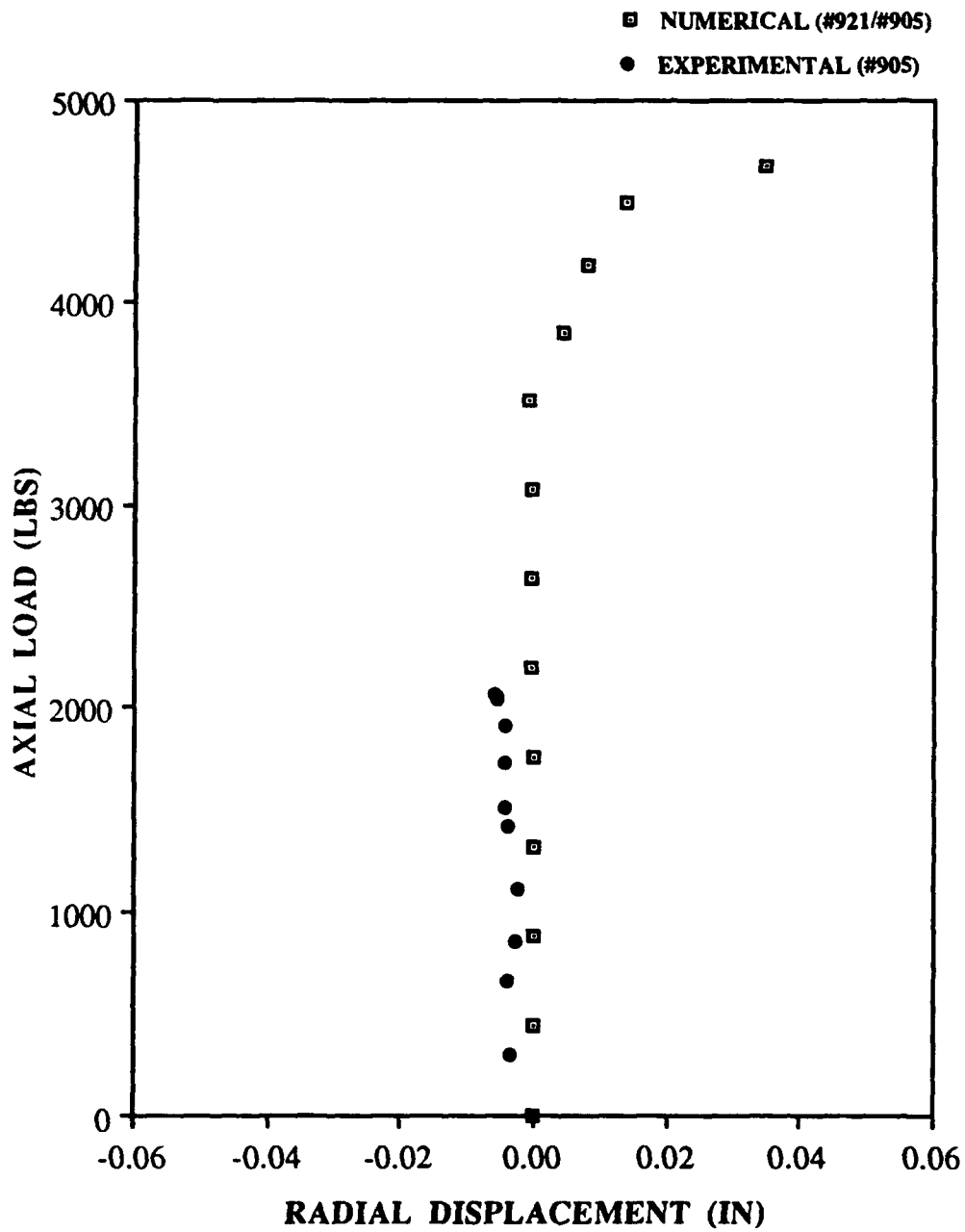


Fig. 67: Load vs. Radial Displacement,  
[0/90]<sub>2s</sub>, No Cutout  
(12" X 12")

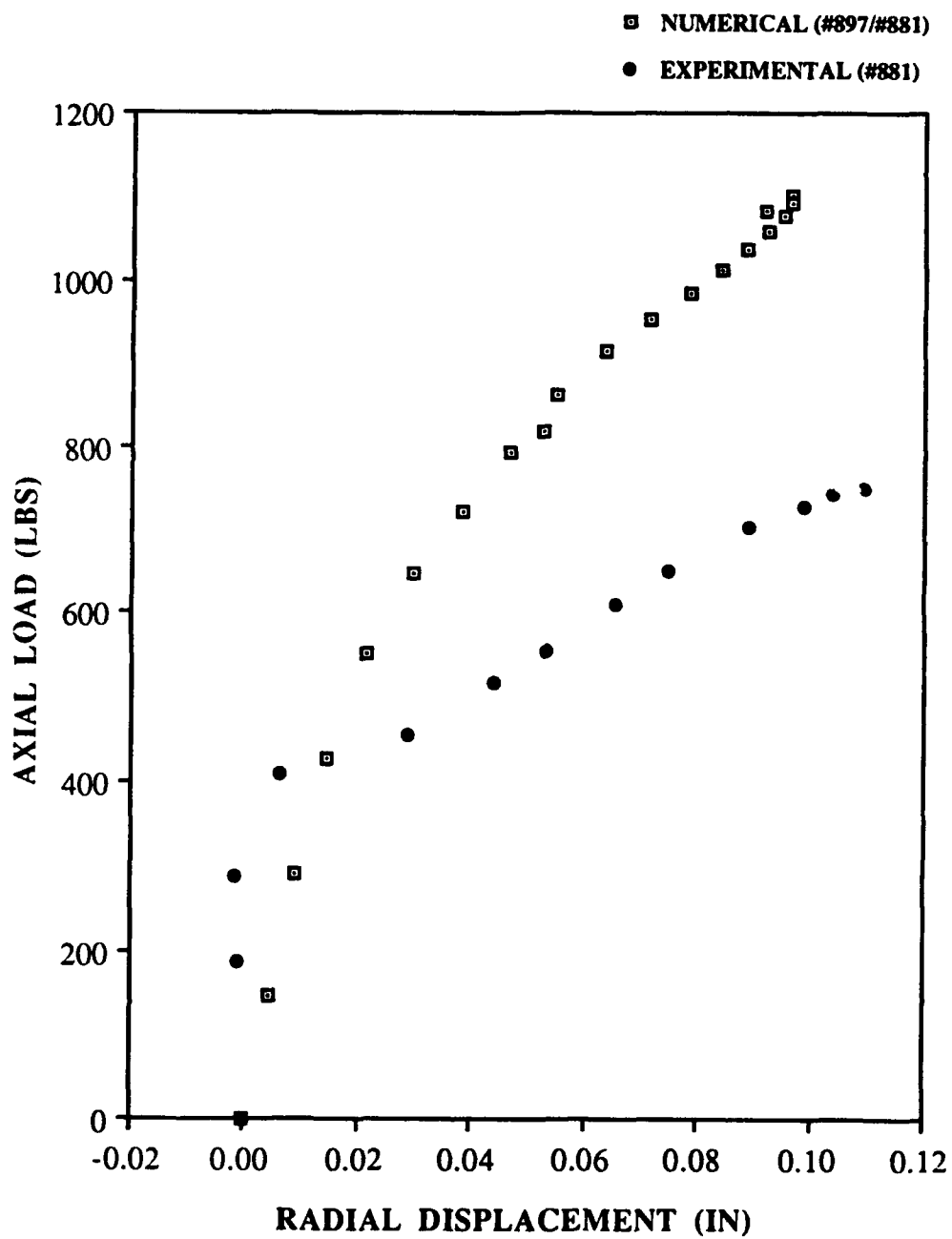


Fig. 68: Load vs. Radial Displacement,  
[0/+45/-45/90]s, 4" Cutout  
(12" X 20")

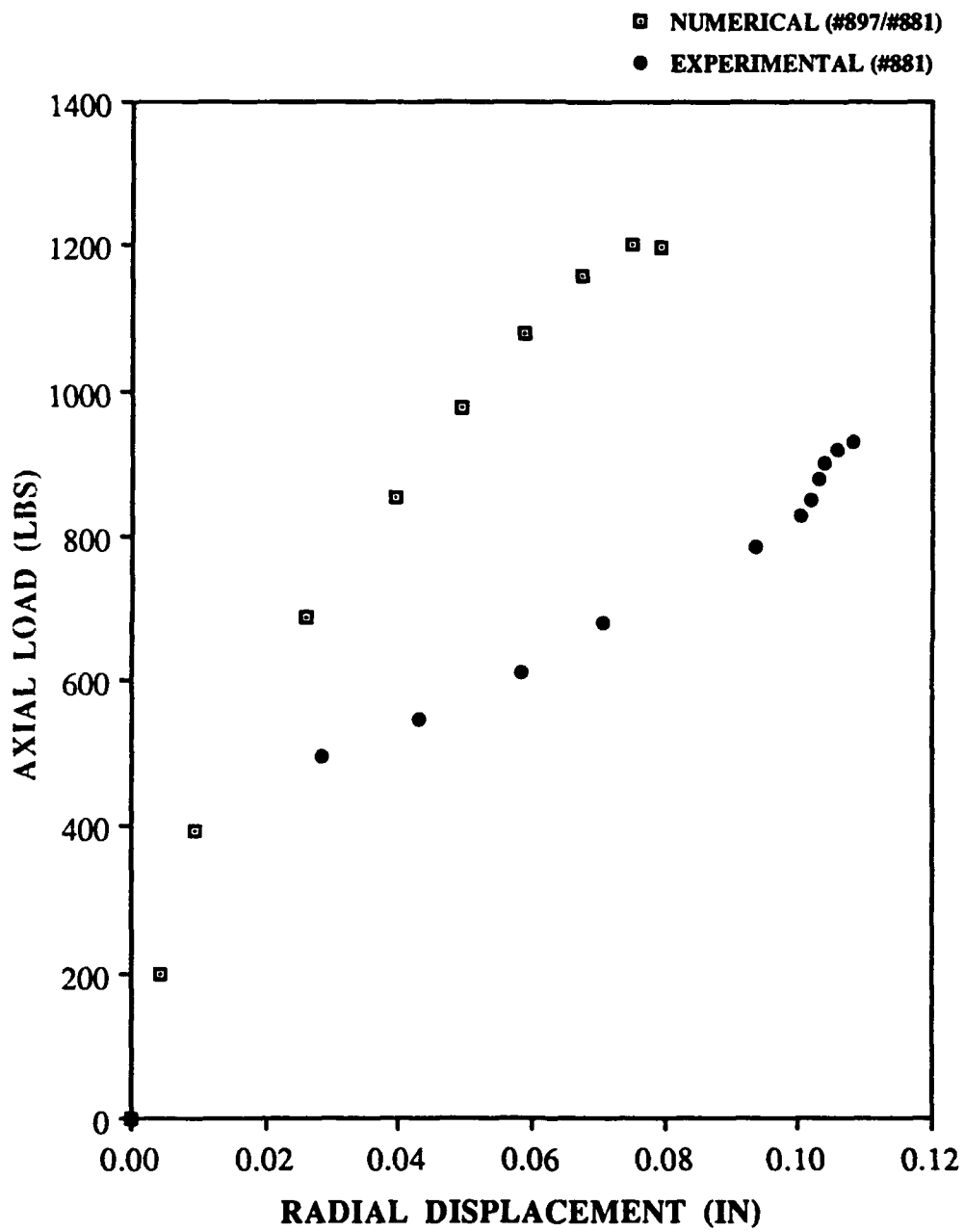


Fig. 69: Load vs. Radial Displacement,  
[0/90]<sub>2s</sub>, 4" Cutout  
(12" X 20")

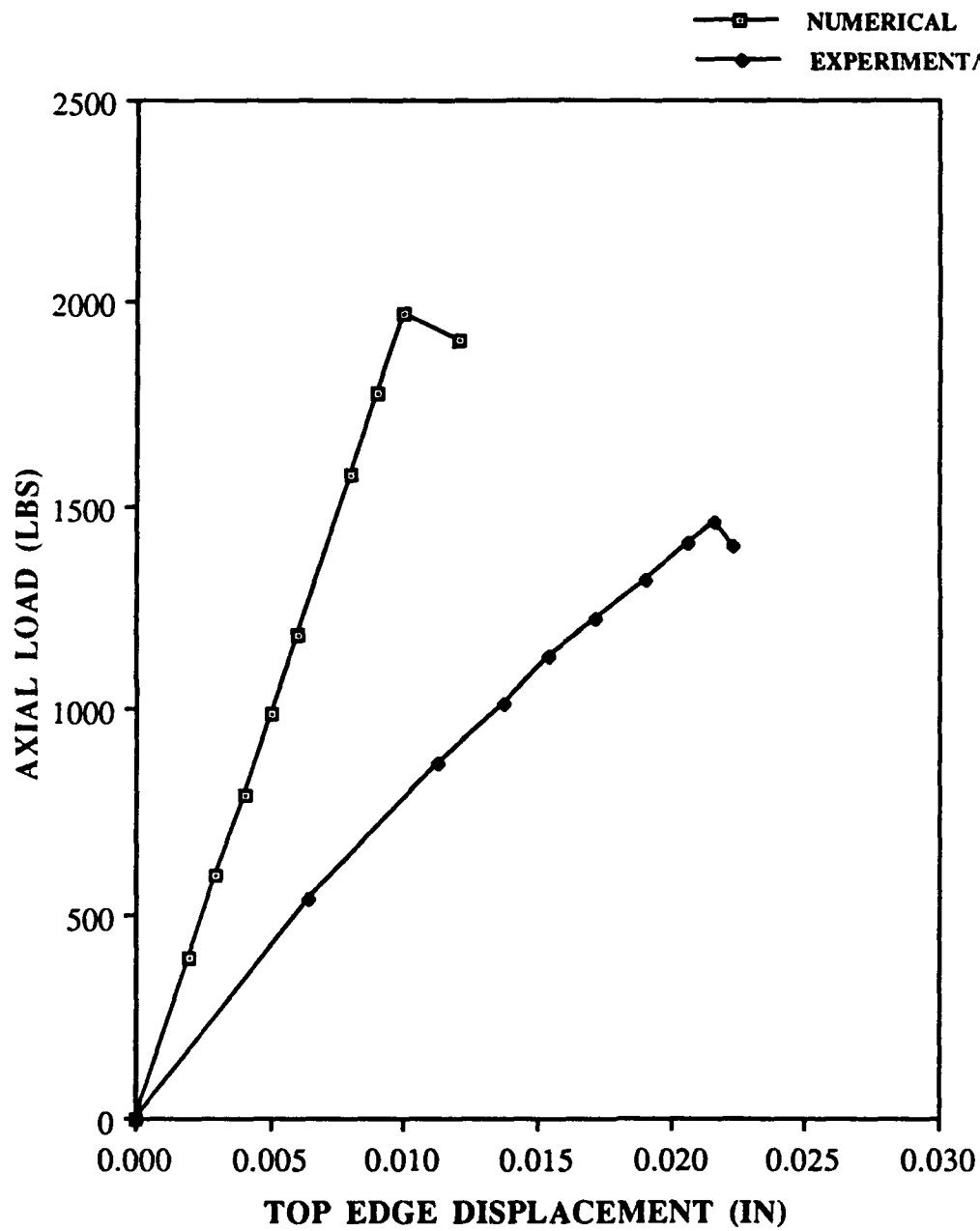


Fig. 70: Load vs. Top Edge Displacement,  
[0/+45/-45/90]s, No Cutout  
(12" X 20")

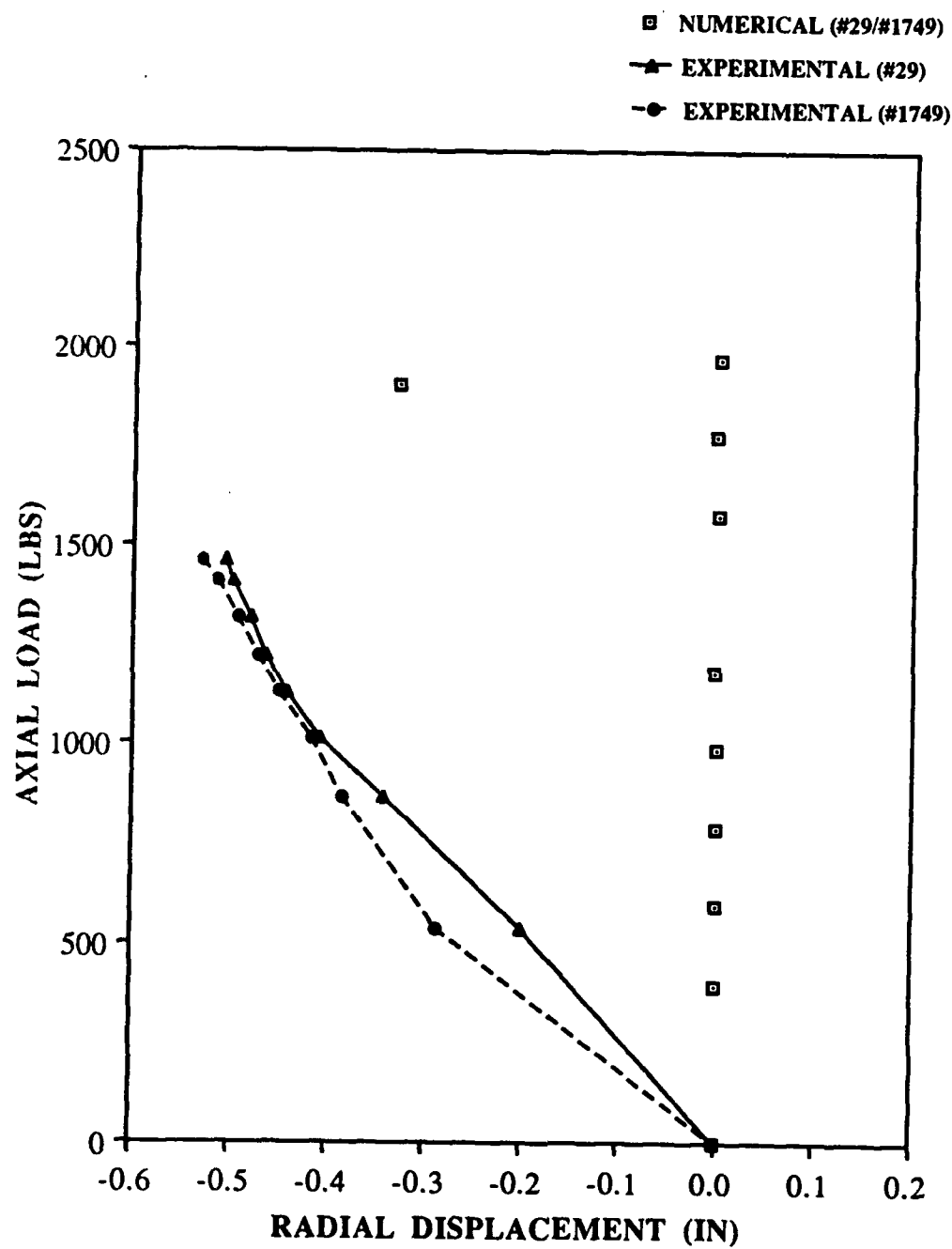


Fig. 71: Load vs. Radial Displacement,  
[0/+45/-45/90]<sub>s</sub>, No Cutout  
(12" X 20")



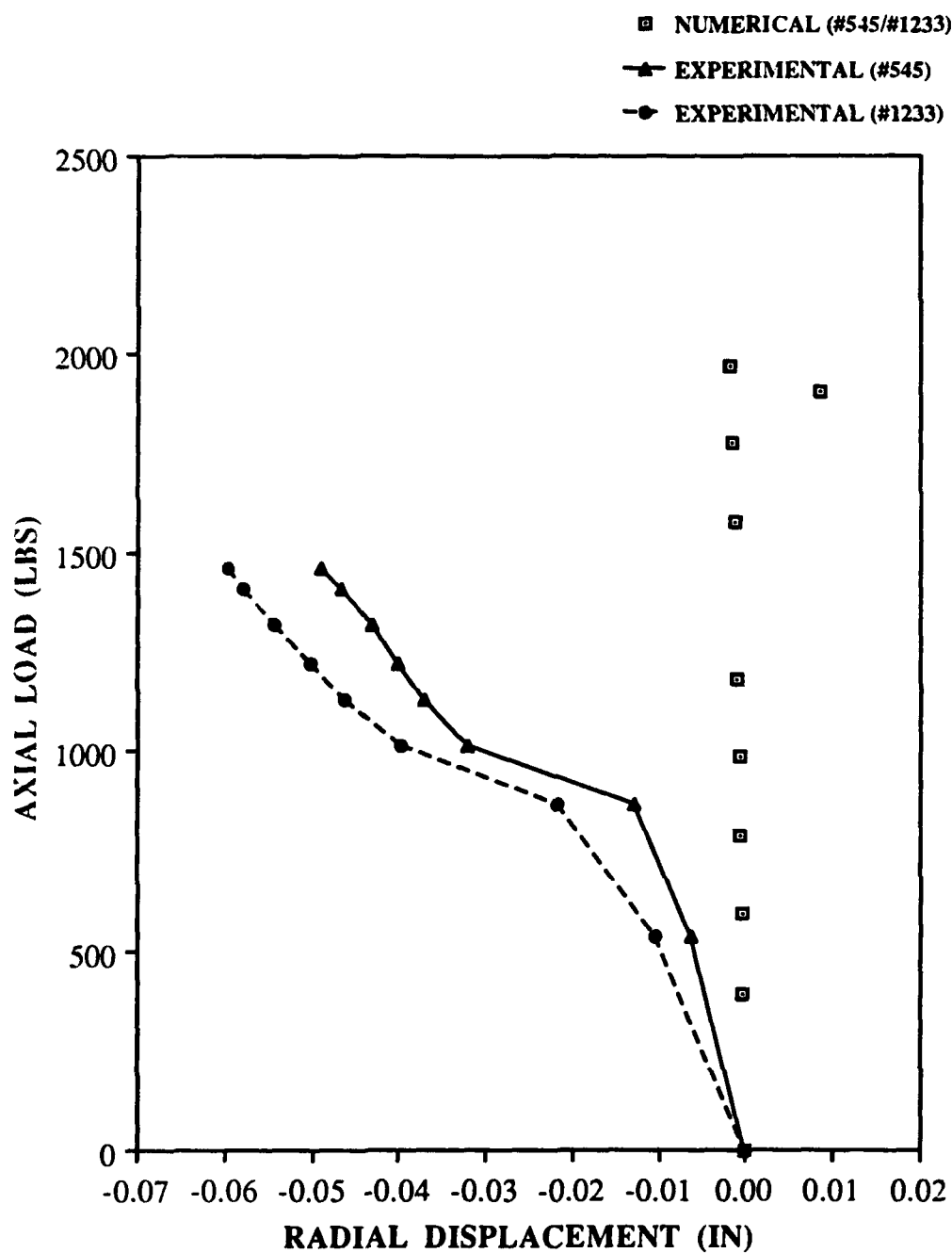


Fig. 72: Load vs. Radial Displacement,  
[0/+45/-45/90]s, No Cutout  
(12" X 20")

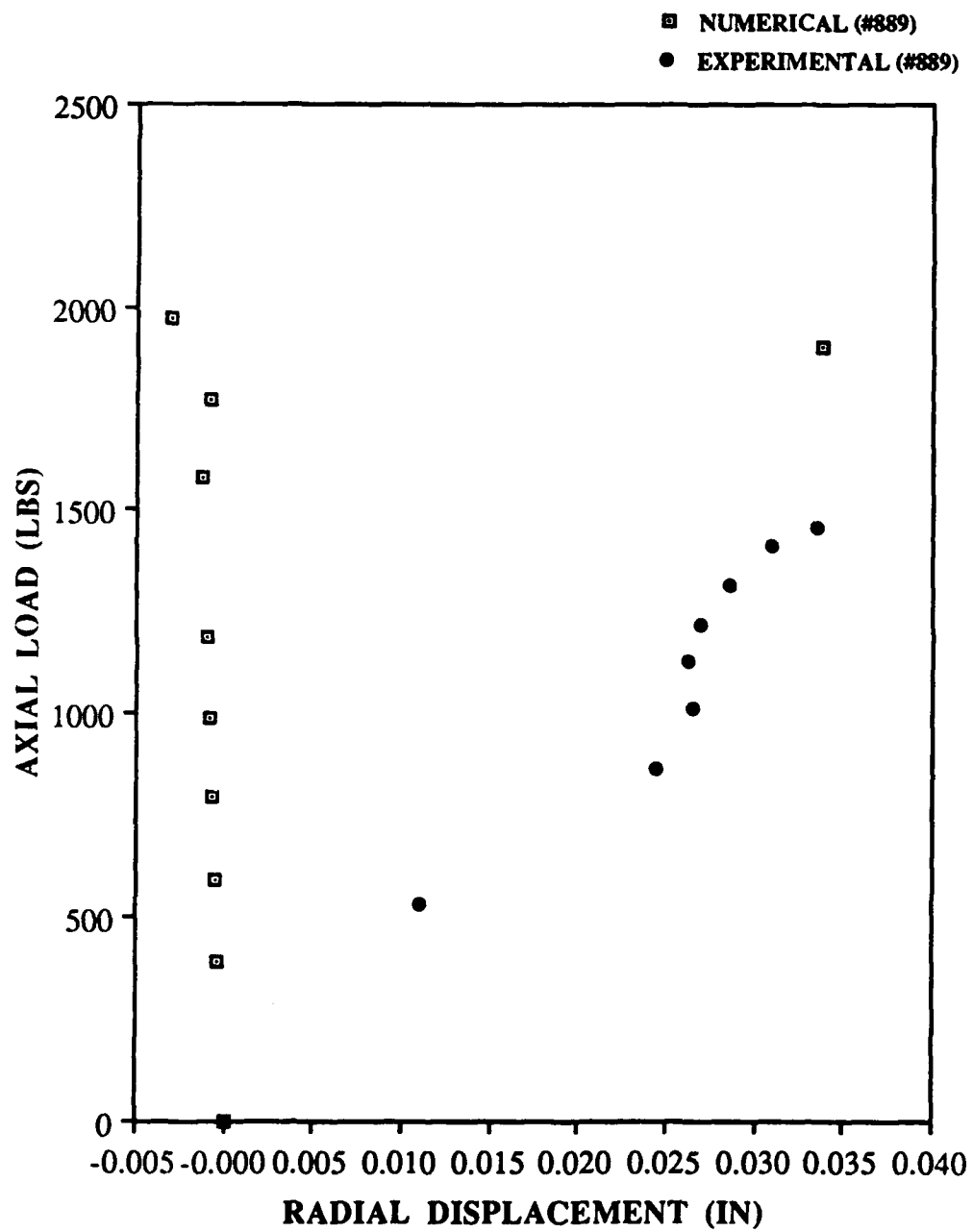


Fig. 73: Load vs. Radial Displacement,  
[0/+45/-45/90]<sub>s</sub>, No Cutout  
(12" X 20")

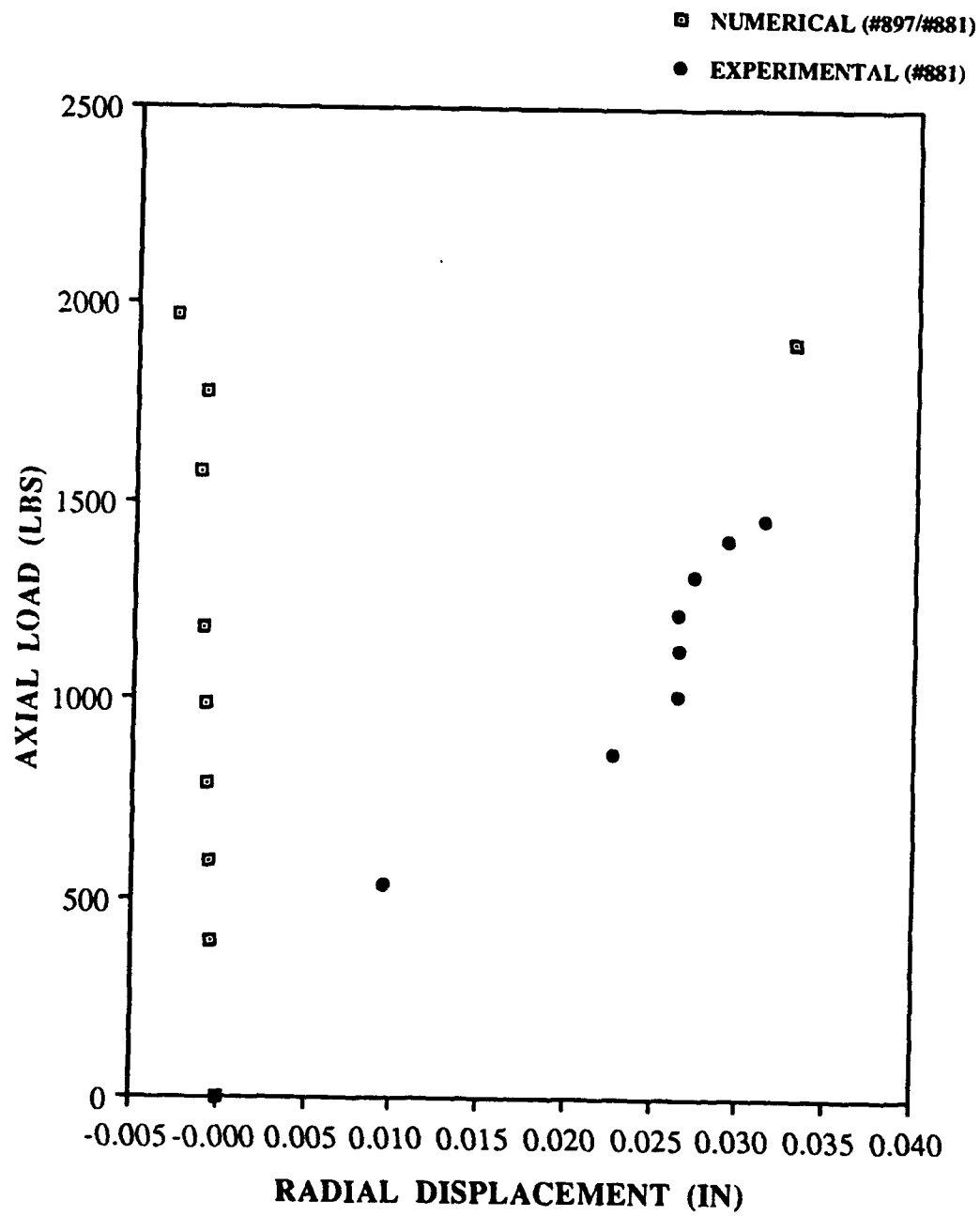


Fig. 74: Load vs. Radial Displacement,  
[0/+45/-45/90]<sub>s</sub>, No Cutout  
(12" X 20")

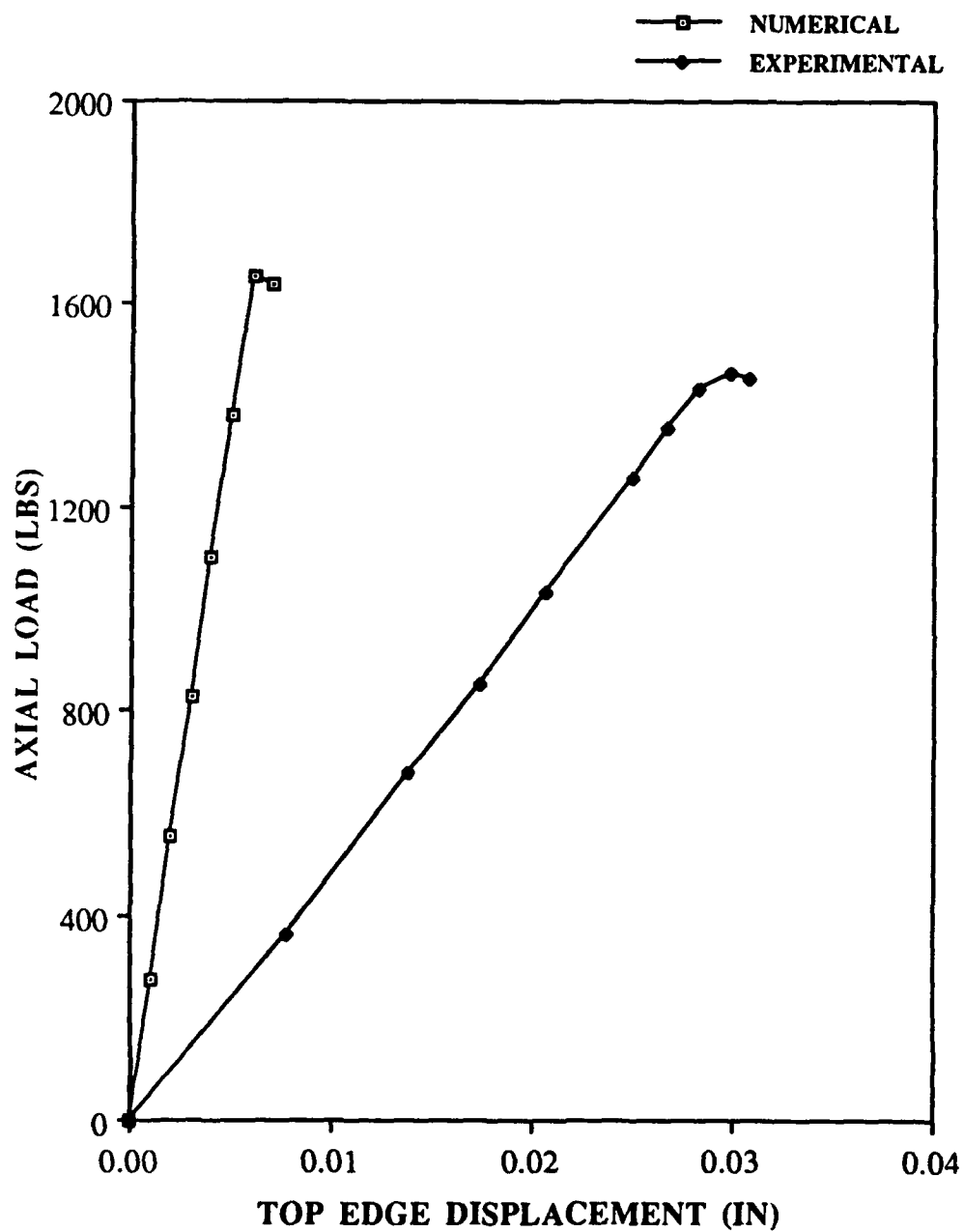


Fig. 75: Load vs. Top Edge Displacement,  
[0/90]<sub>2s</sub>, No Cutout  
(12" X 20")

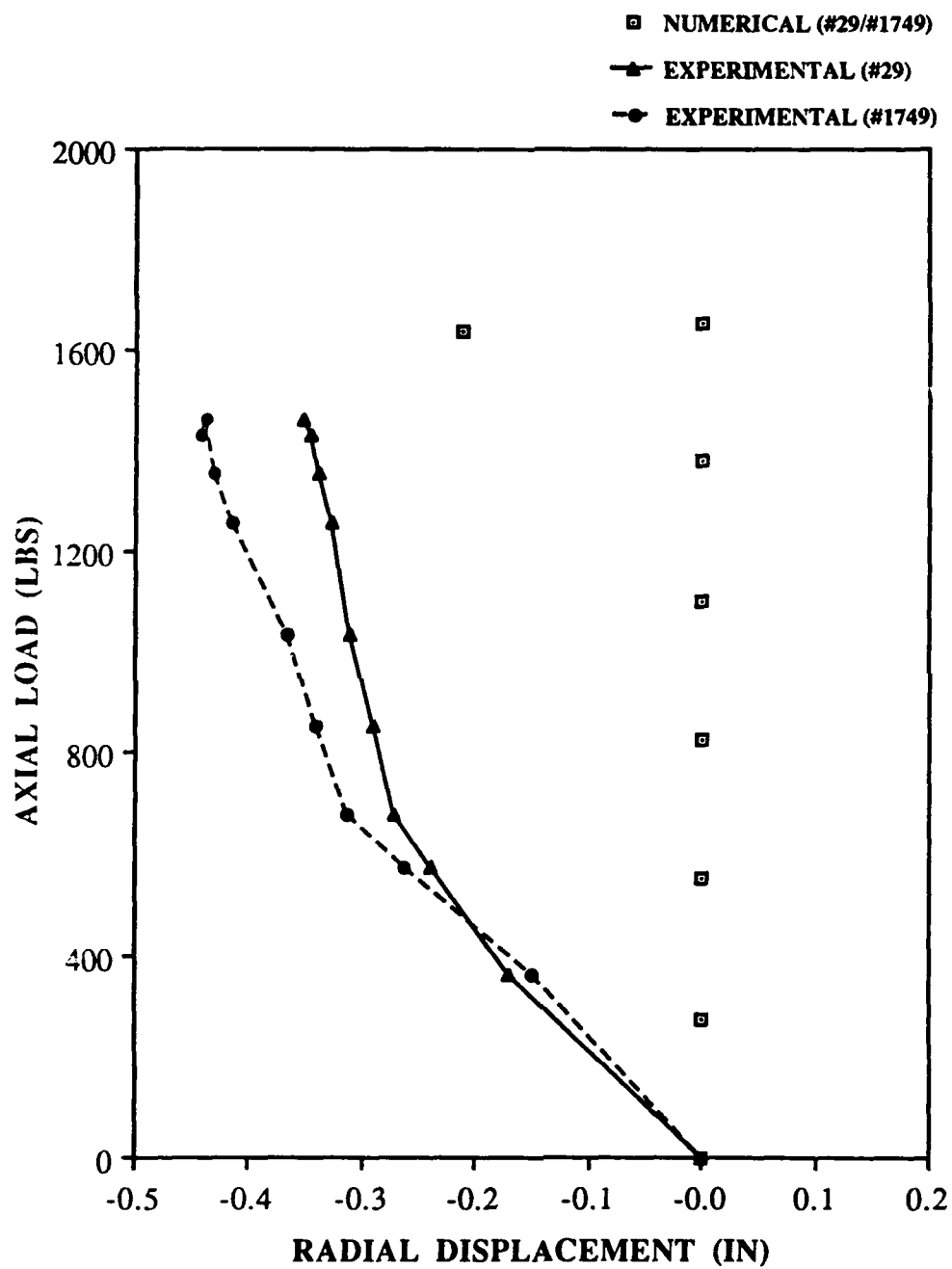


Fig. 76: Load vs. Radial Displacement,  
[0/90]<sub>2s</sub>, No Cutout  
(12" X 20")

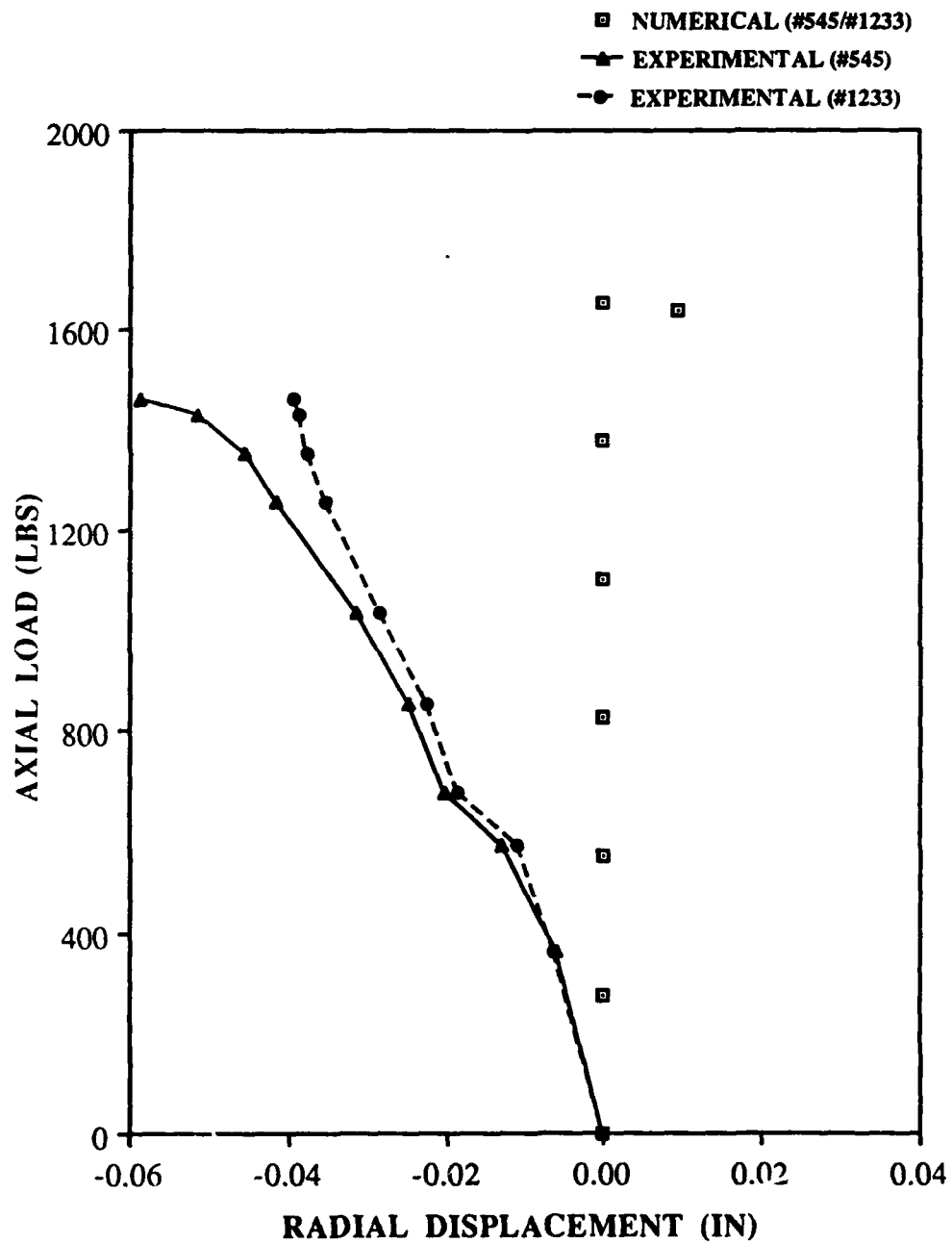


Fig. 77: Load vs. Radial Displacement,  
[0/90]<sub>2s</sub>, No Cutout  
(12" X 20")

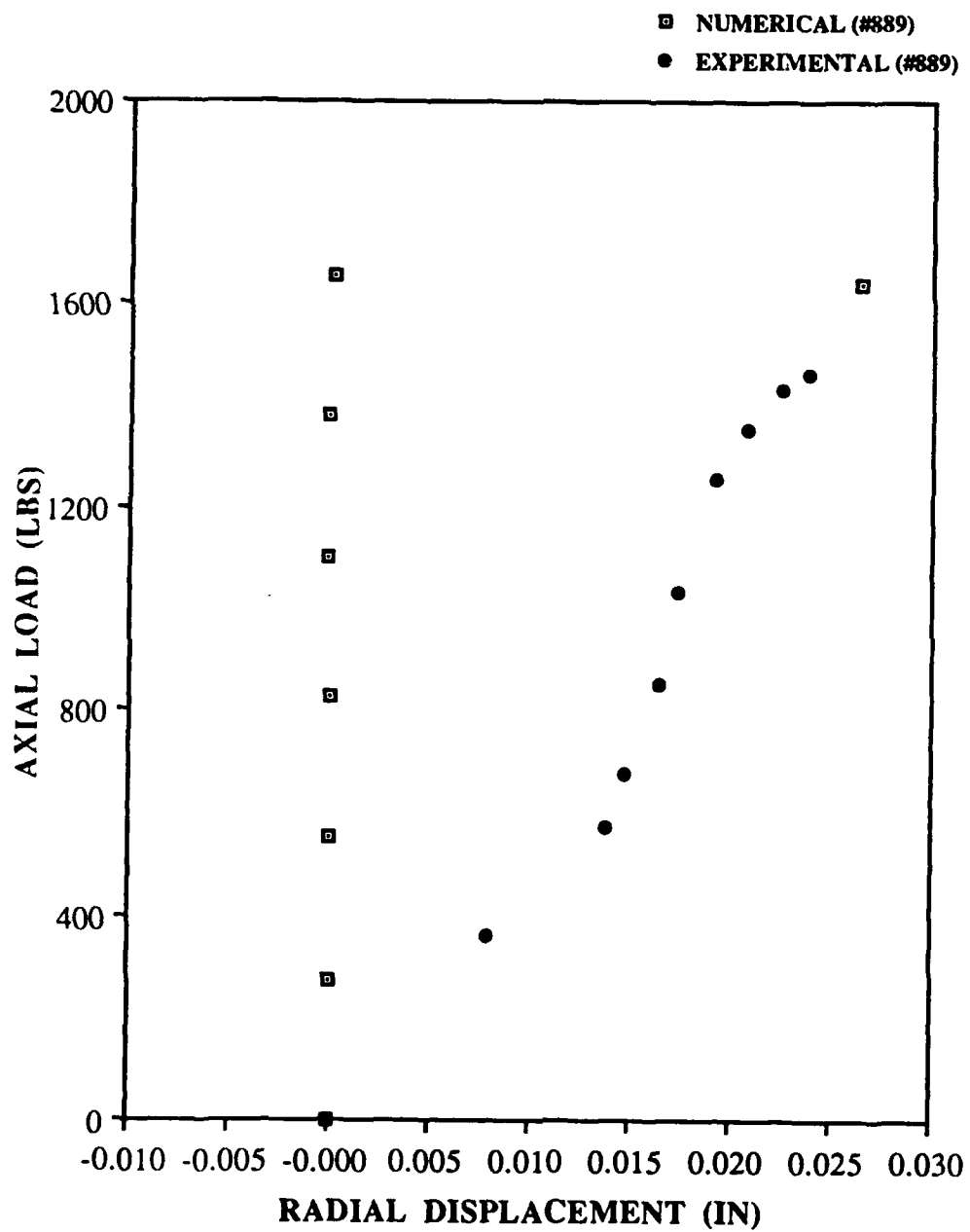


Fig. 78: Load vs. Radial Displacement,  
[0/90]<sub>2s</sub>, No Cutout  
(12" X 20")

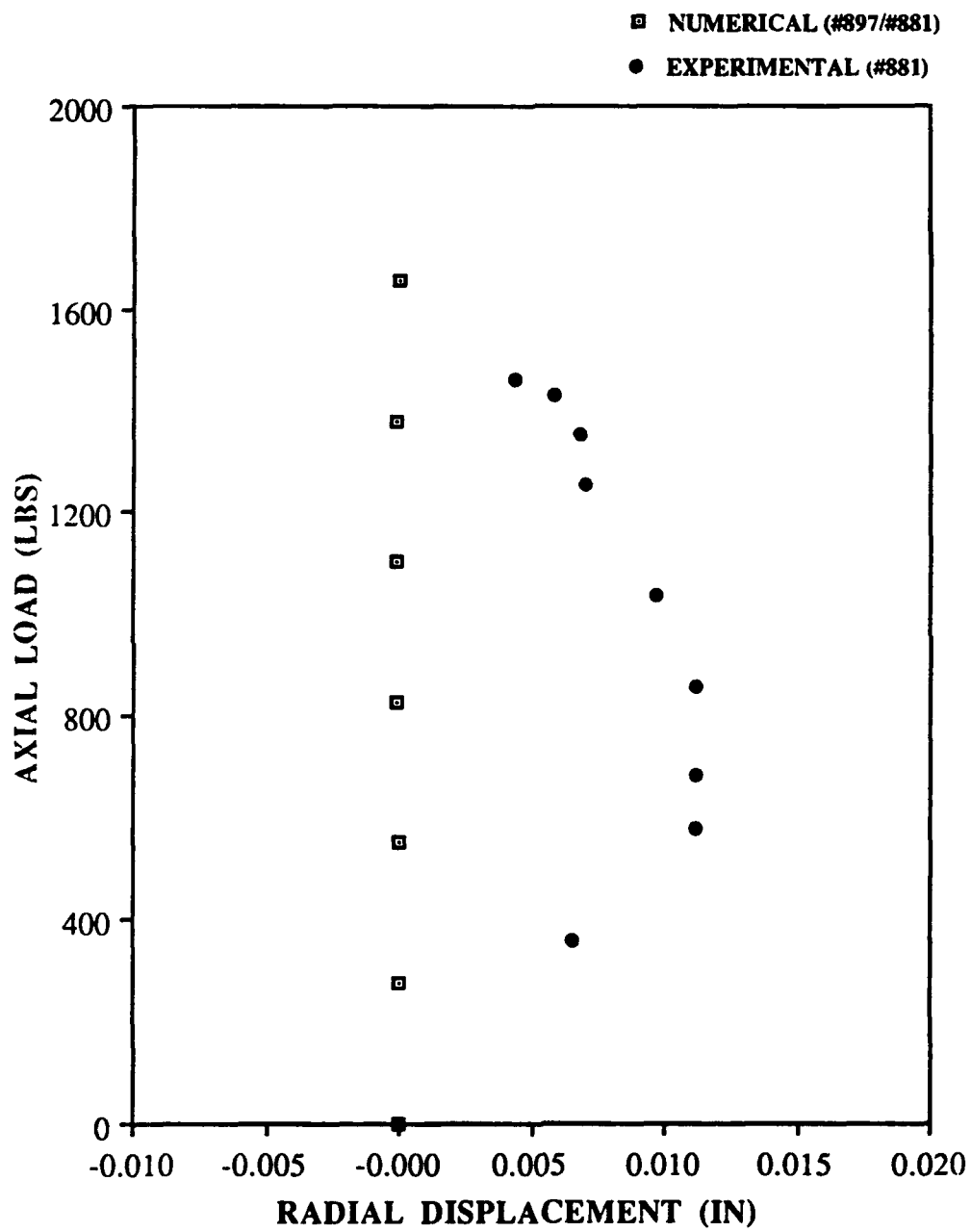


Fig. 79: Load vs. Radial Displacement,  
[0/90]<sub>2s</sub>, No Cutout  
(12" X 20")



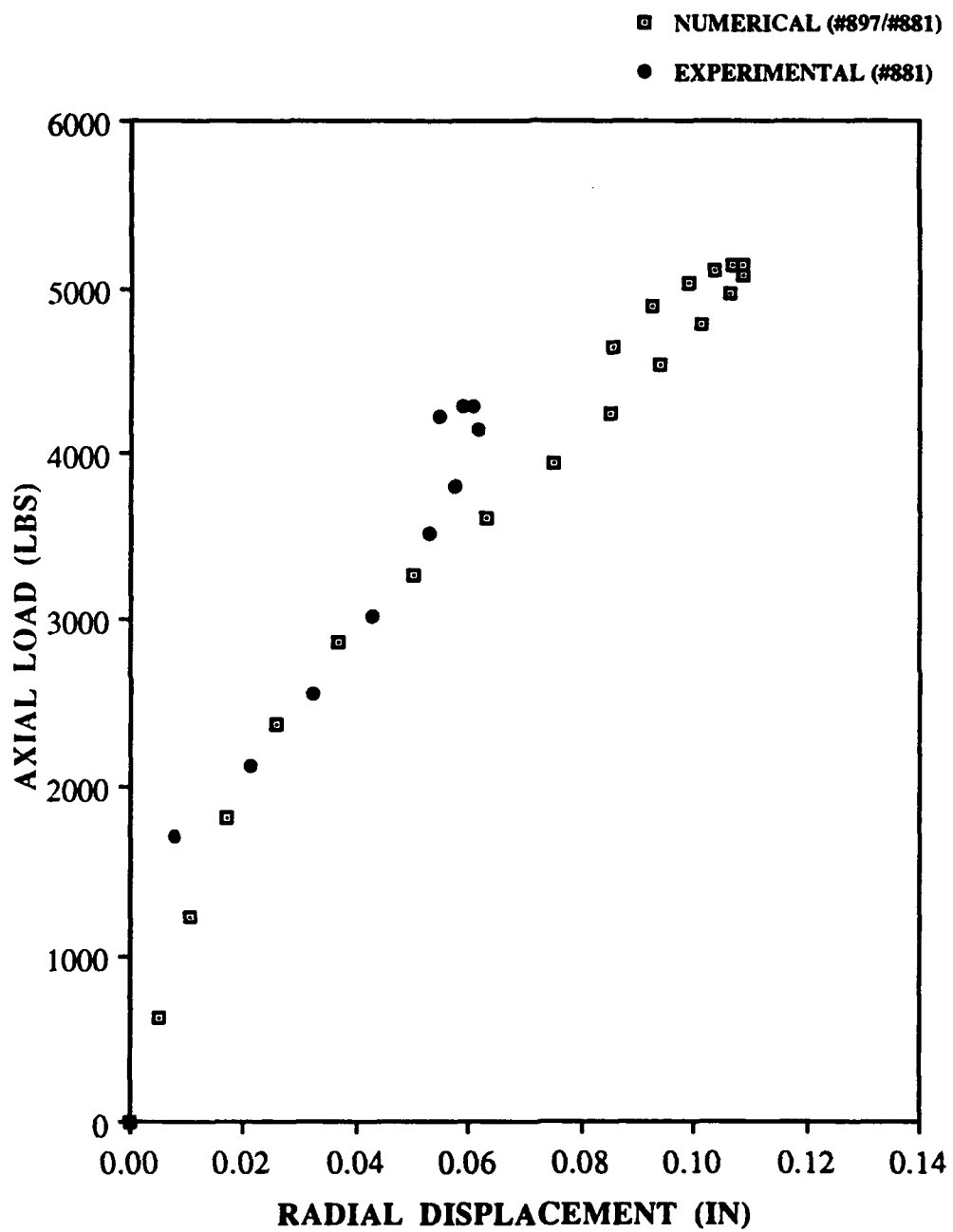


Fig. 80: Load vs. Radial Displacement,  
[0/+45/-45/90]2s, 4" Cutout  
(12" X 20")

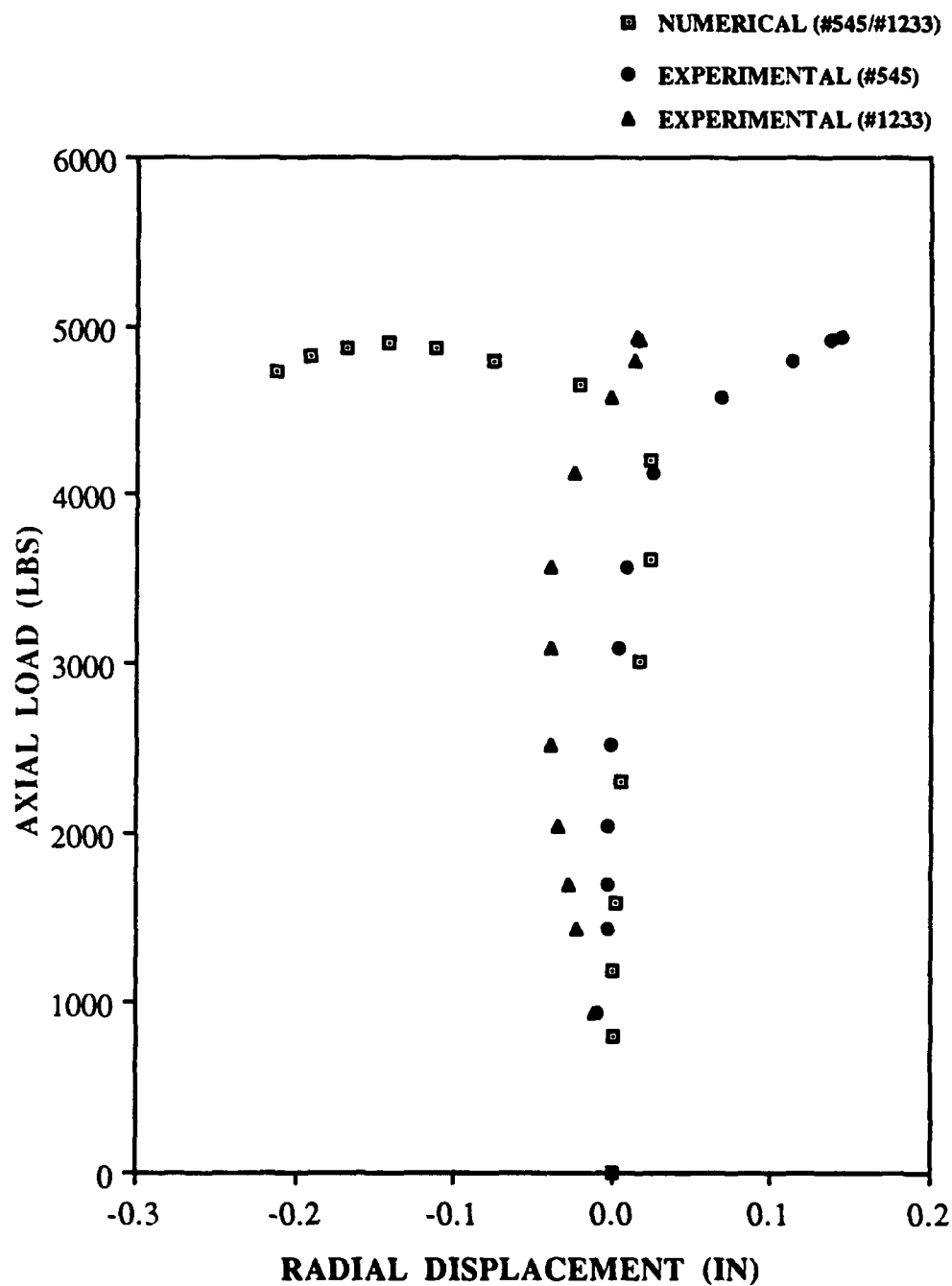


Fig. 81: Load vs. Radial Displacement,  
[0/90]4s, 4" Cutout  
(12" X 20")

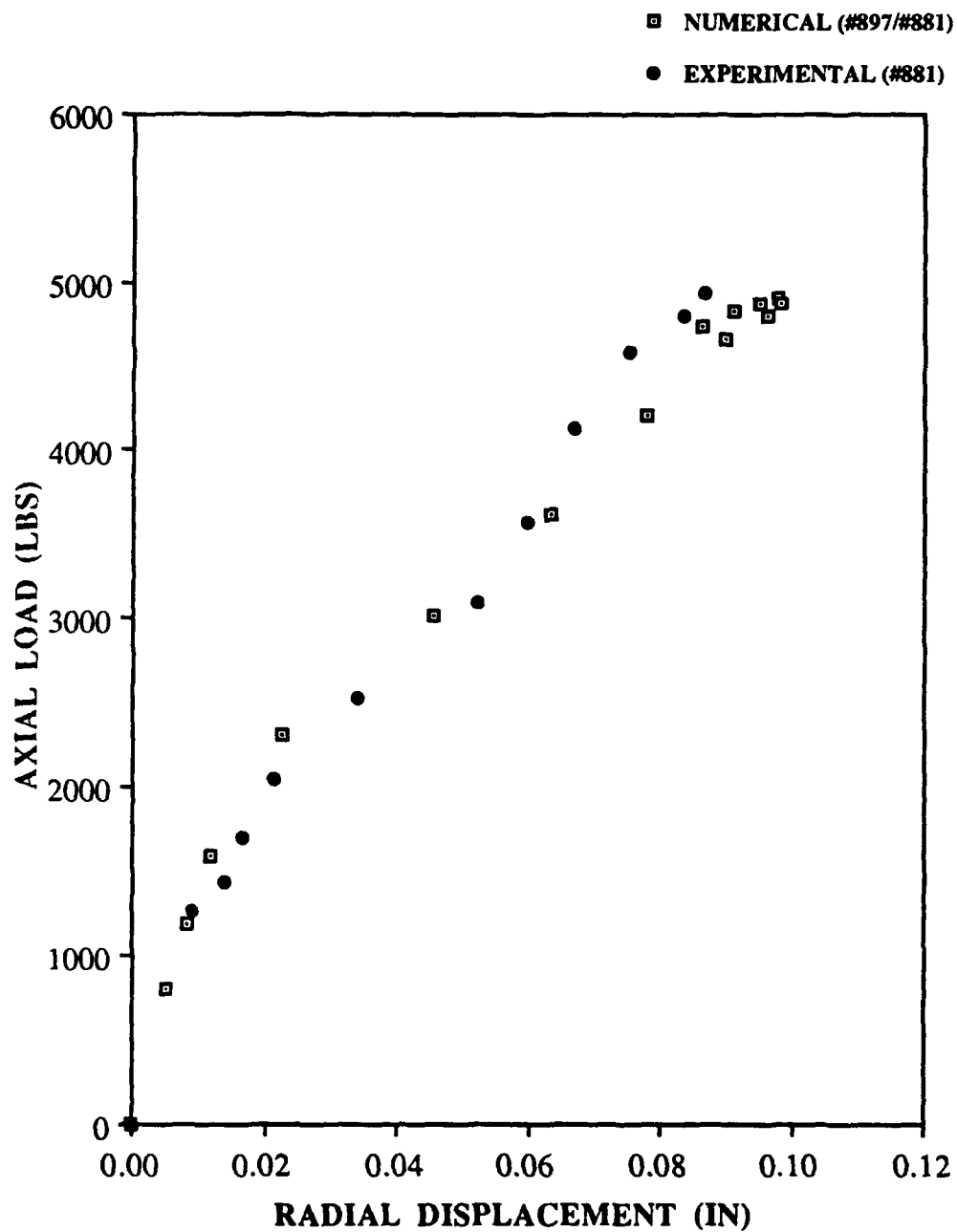


Fig. 82: Load vs. Radial Displacement,  
[0/90]<sub>4s</sub>, 4" Cutout  
(12" X 20")

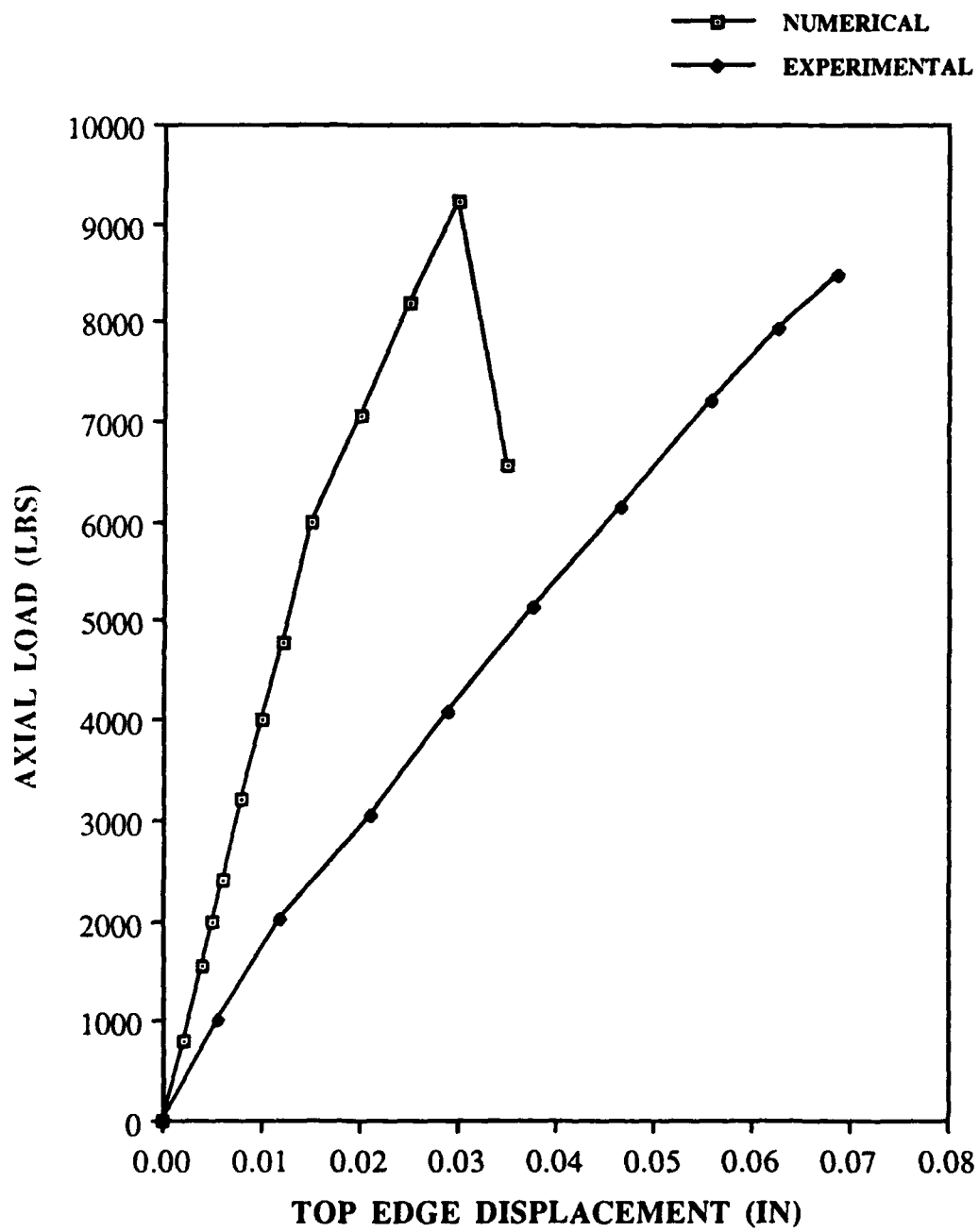


Fig. 83: Load vs. Top Edge Displacement,  
[0/+45/-45/90]2s, No Cutout  
(12" X 20")

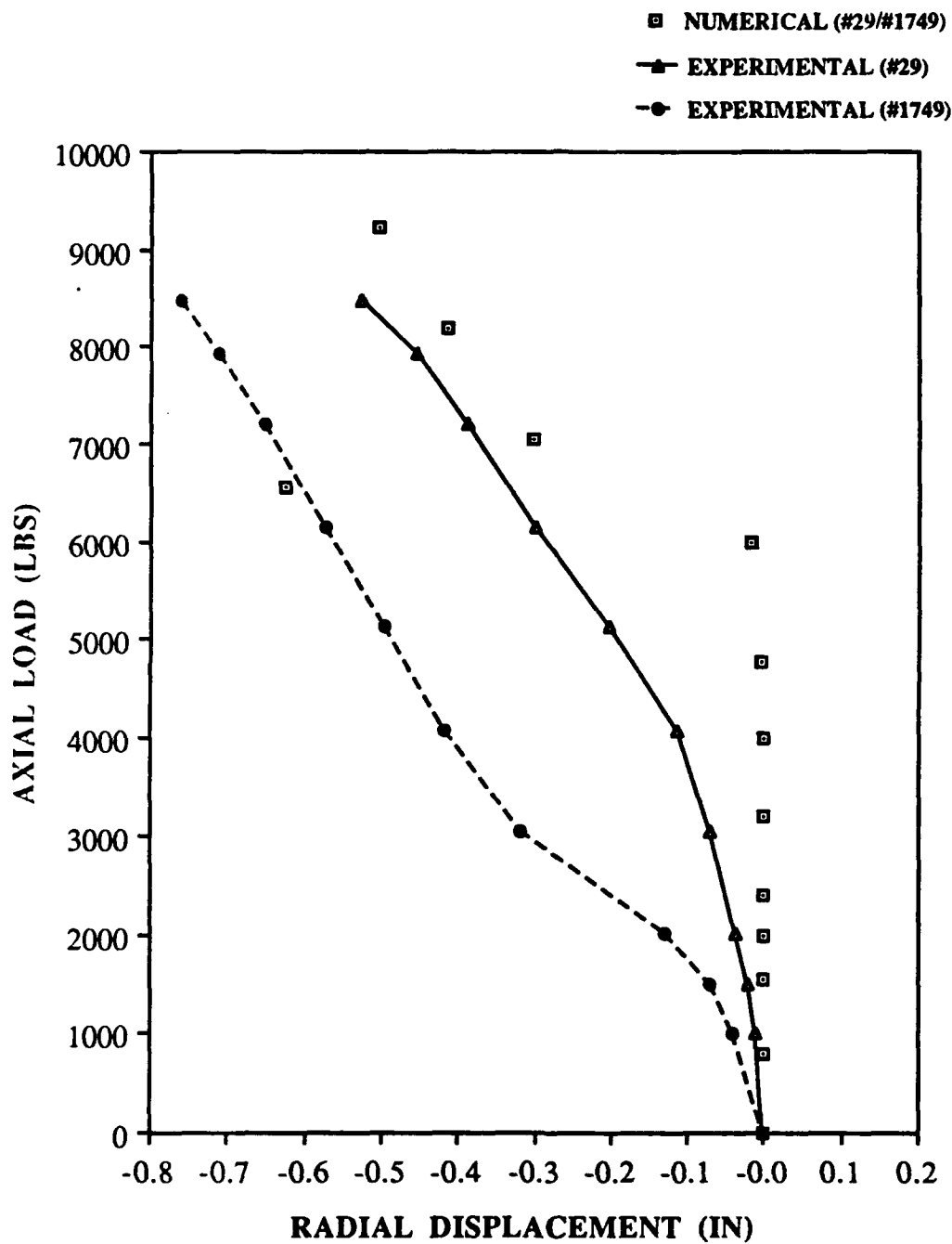


Fig. 84: Load vs. Radial Displacement,  
[0/+45/-45/90]<sub>2s</sub>, No Cutout  
(12" X 20")

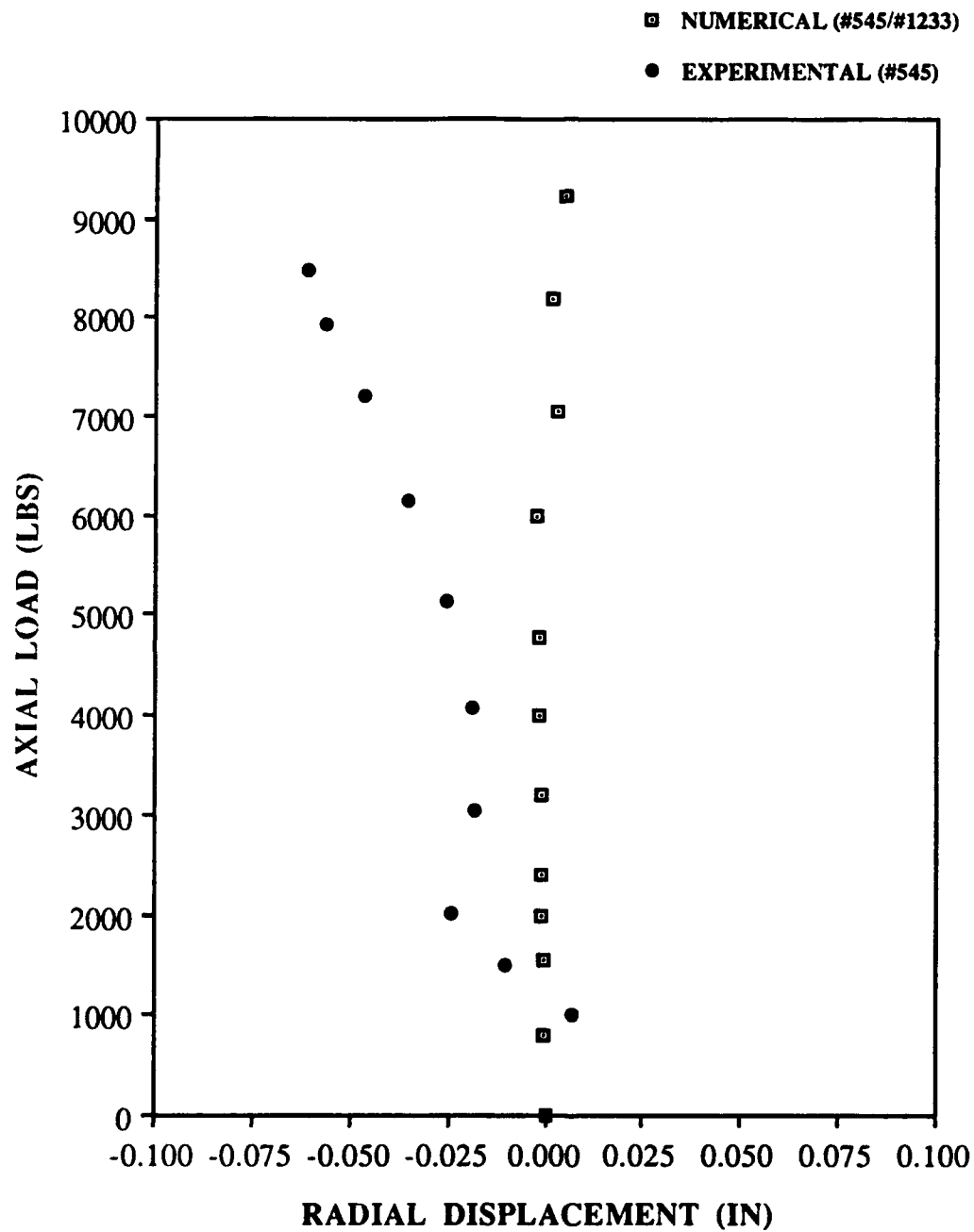


Fig. 85: Load vs. Radial Displacement,  
[0/+45/-45/90]2s, No Cutout  
(12" X 20")

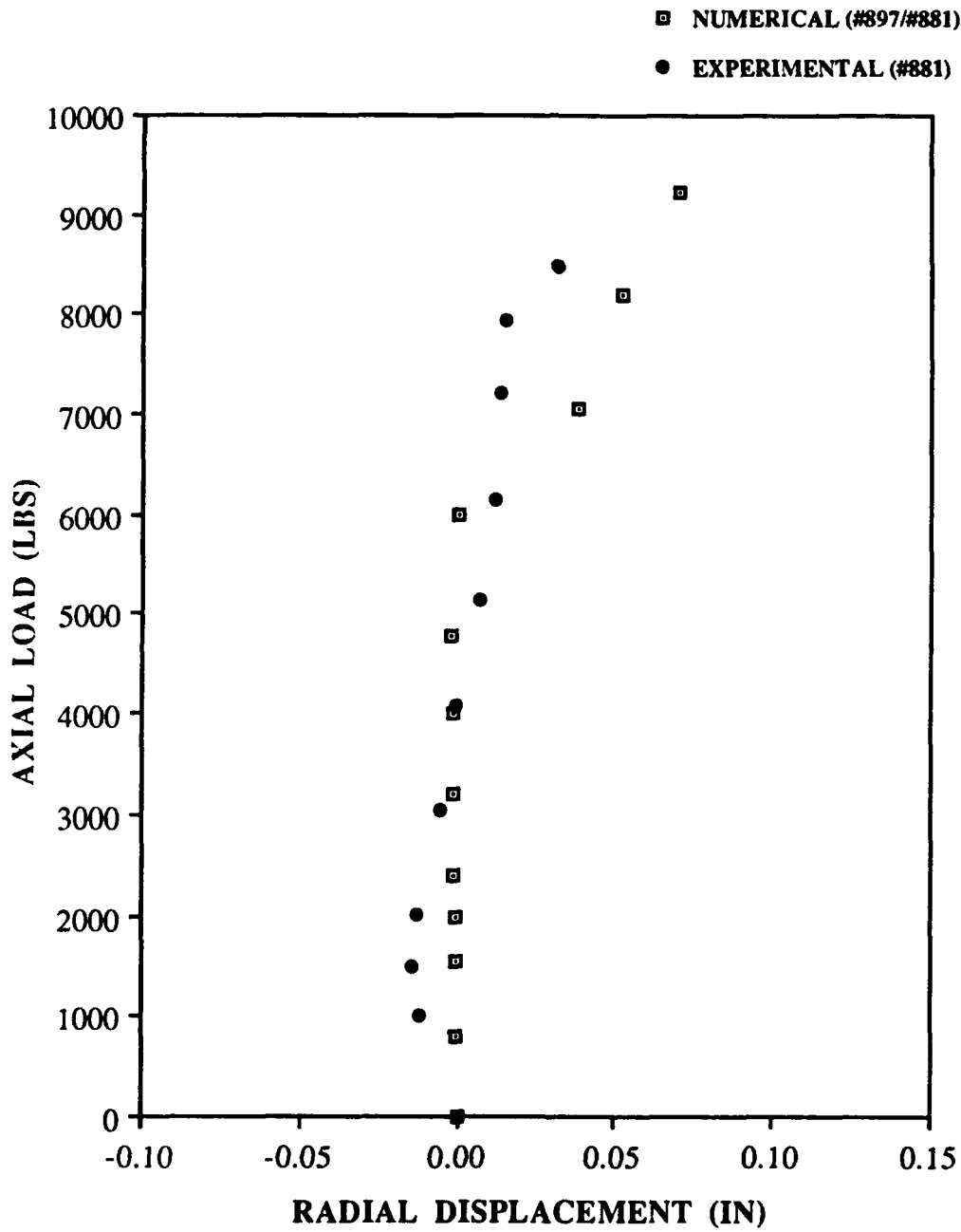


Fig. 86: Load vs. Radial Displacement,  
[0/+45/-45/90]2s, No Cutout  
(12" X 20")

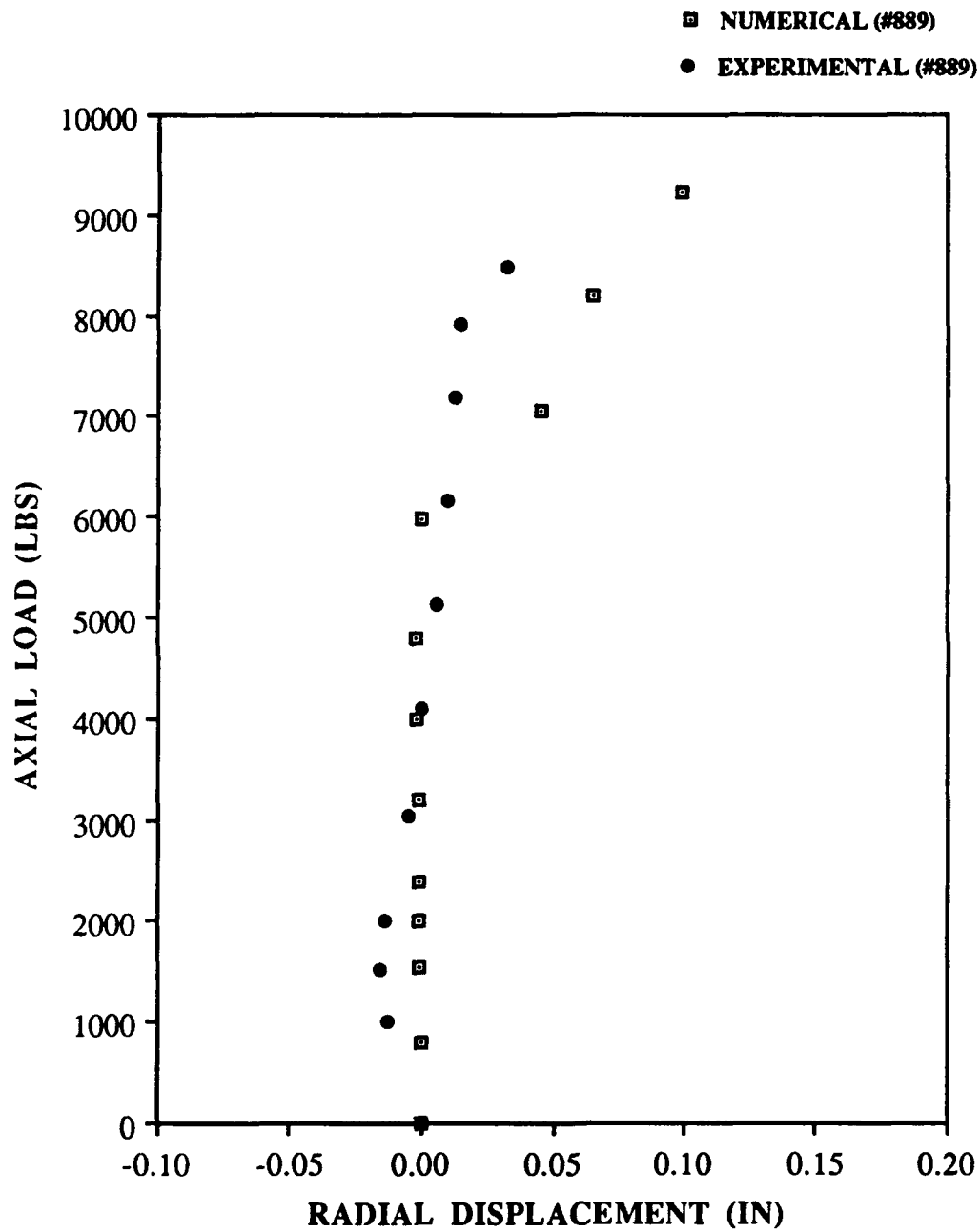


Fig. 87: Load vs. Radial Displacement,  
[0/+45/-45/90]2s, No Cutout  
(12" X 20")



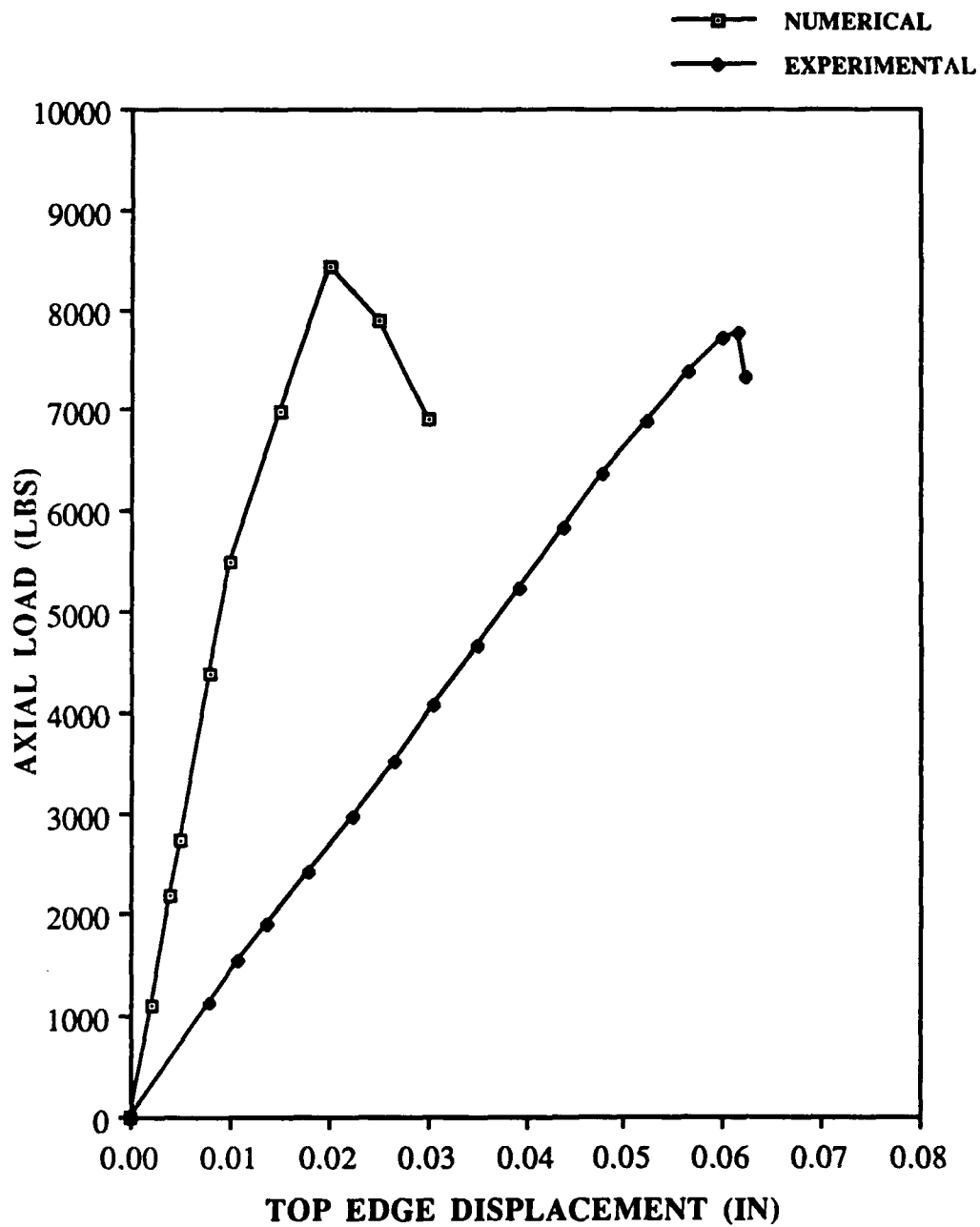


Fig. 88: Load vs. Top Edge Displacement,  
[0/90]4s, No Cutout  
(12" X 20")

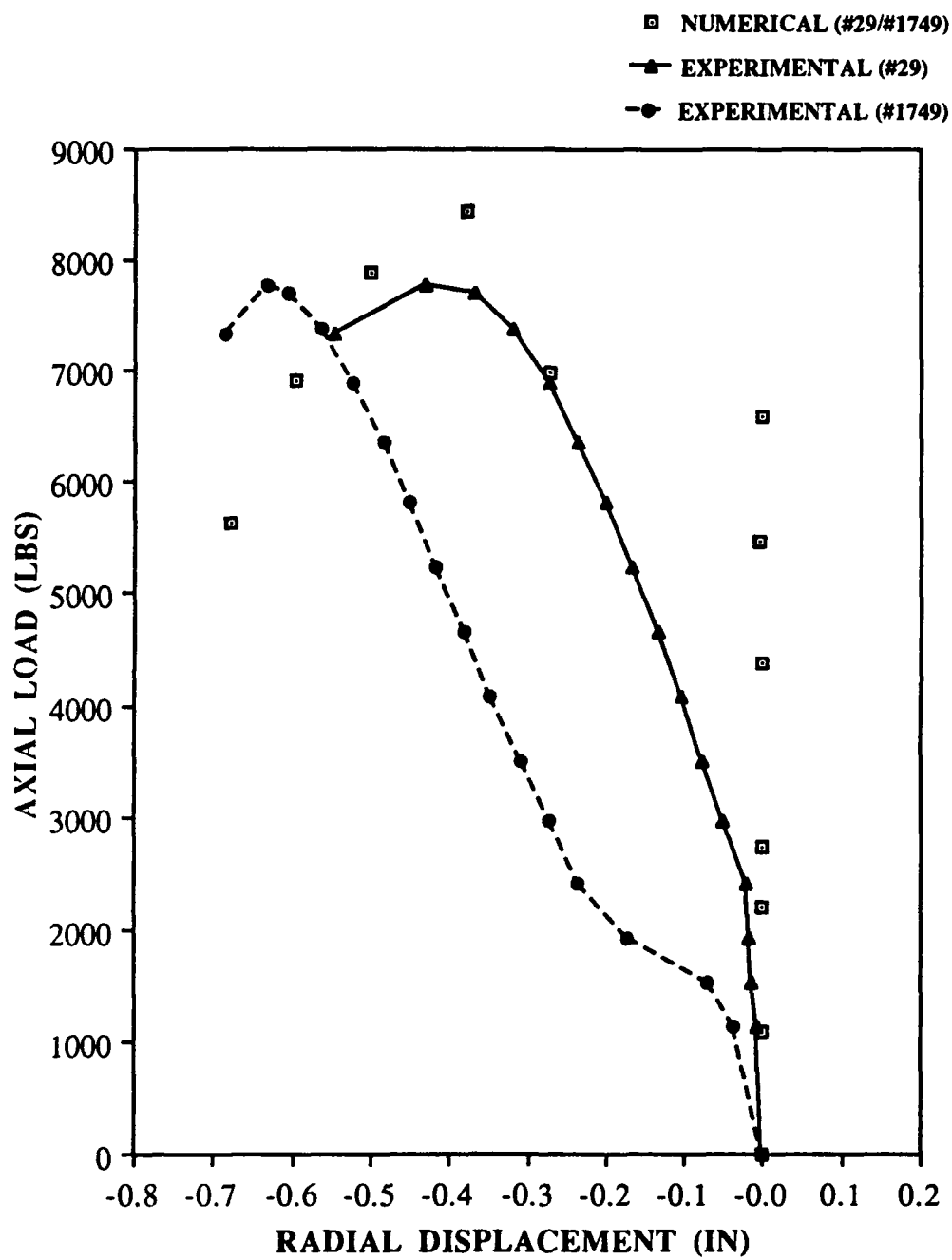
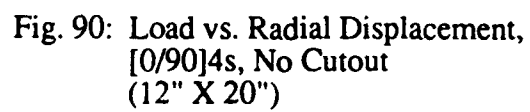


Fig. 89: Load vs. Radial Displacement,  
[0/90]<sub>4s</sub>, No Cutout  
(12" X 20")



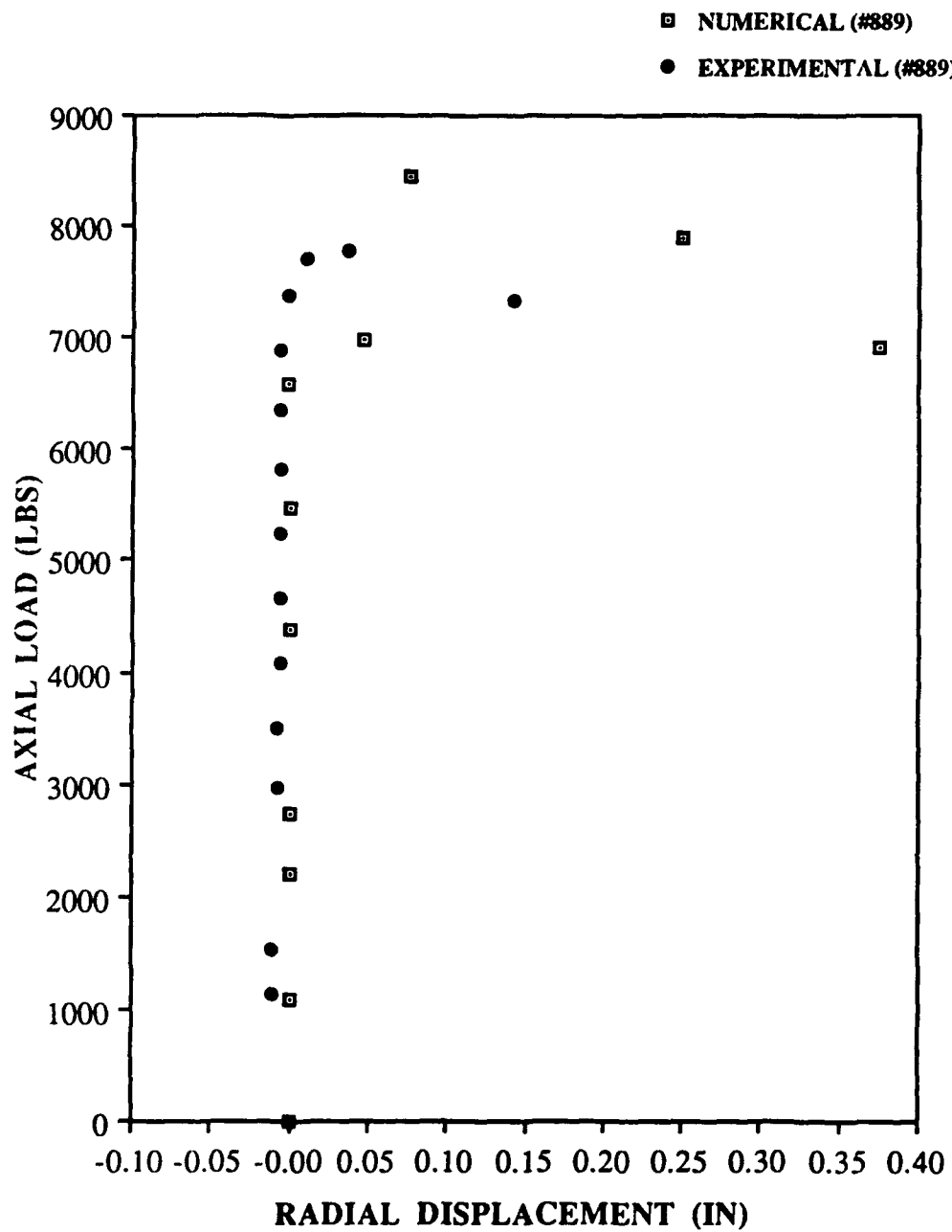


Fig. 91: Load vs. Radial Displacement,  
[0/90]4s, No Cutout  
(12" X 20")

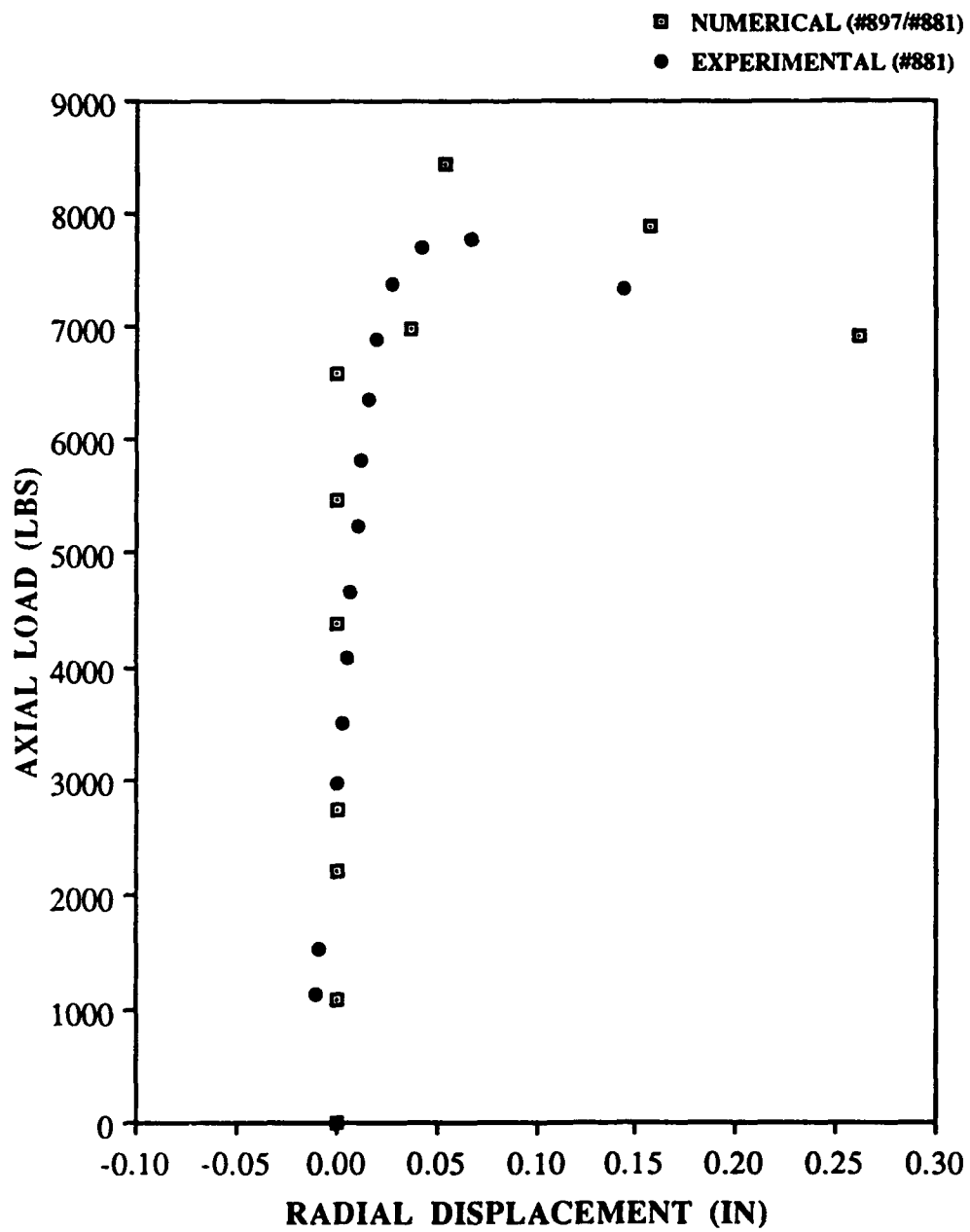


Fig. 92: Load vs. Radial Displacement,  
[0/90]<sub>4s</sub>, No Cutout  
(12" X 20")

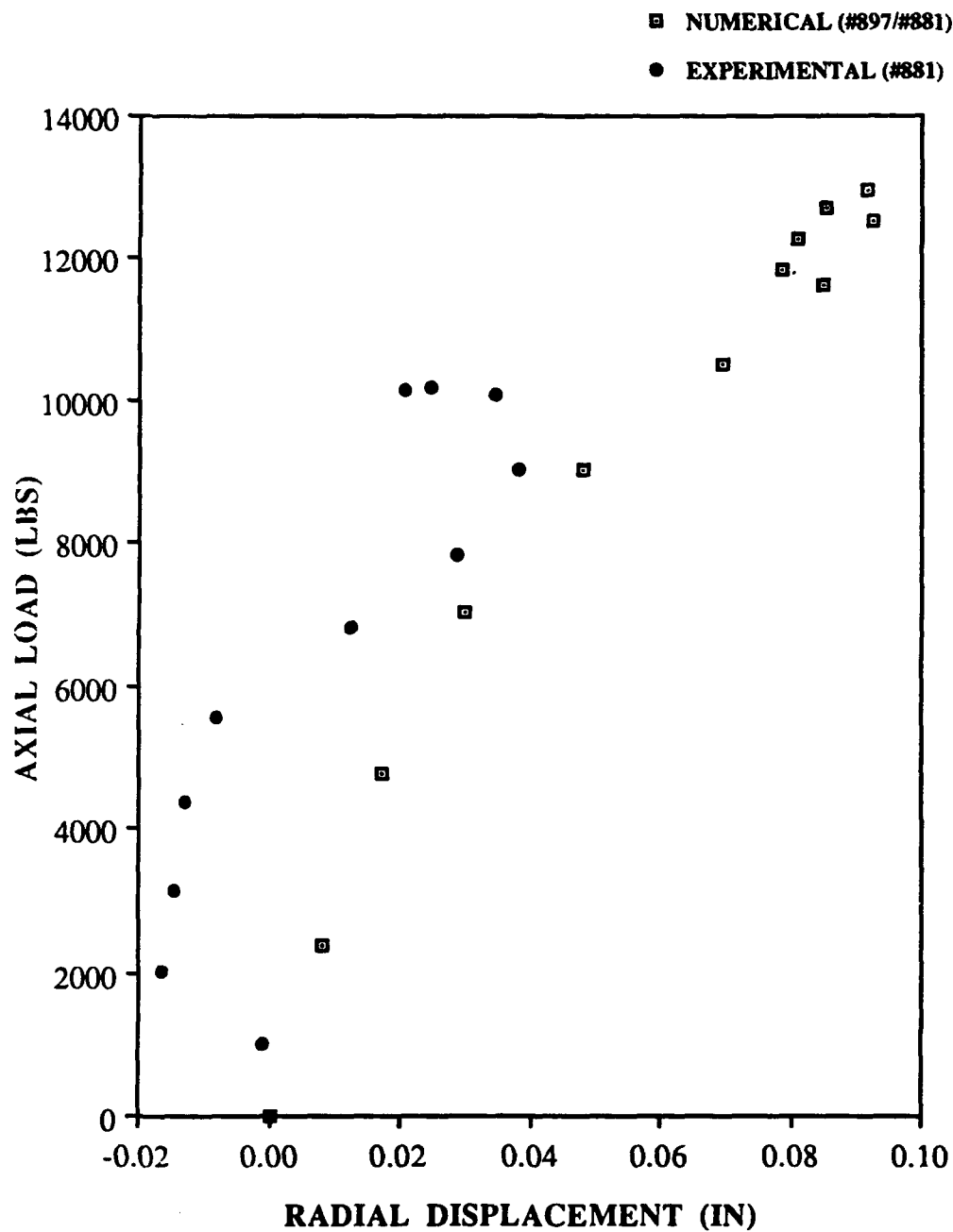


Fig. 93: Load vs. Radial Displacement,  
[0/+45/-45/90]3s, 4" Cutout  
(12" X 20")

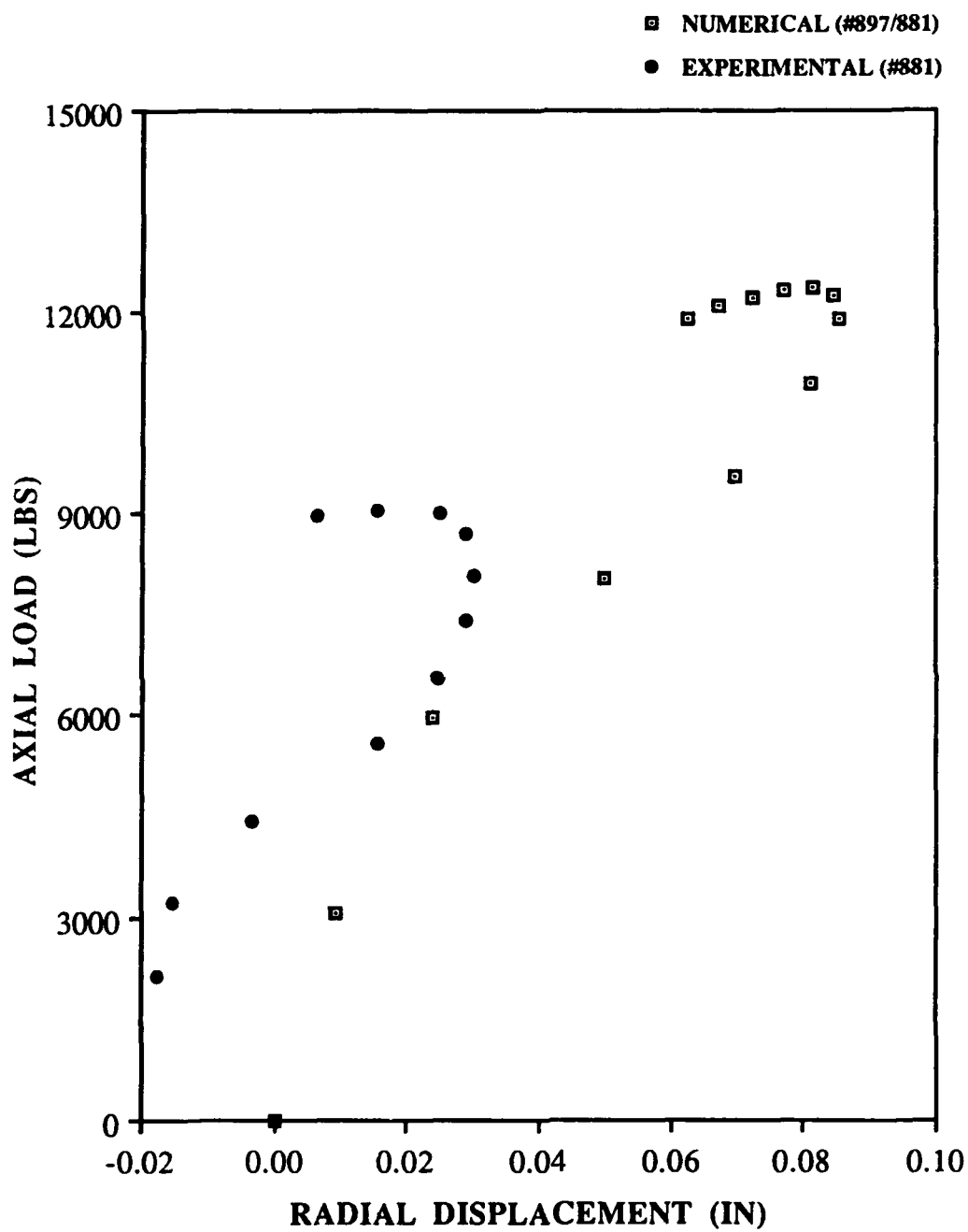


Fig. 94: Load vs. Radial Displacement,  
[0/90]6s, 4" Cutout  
(12" X 20")

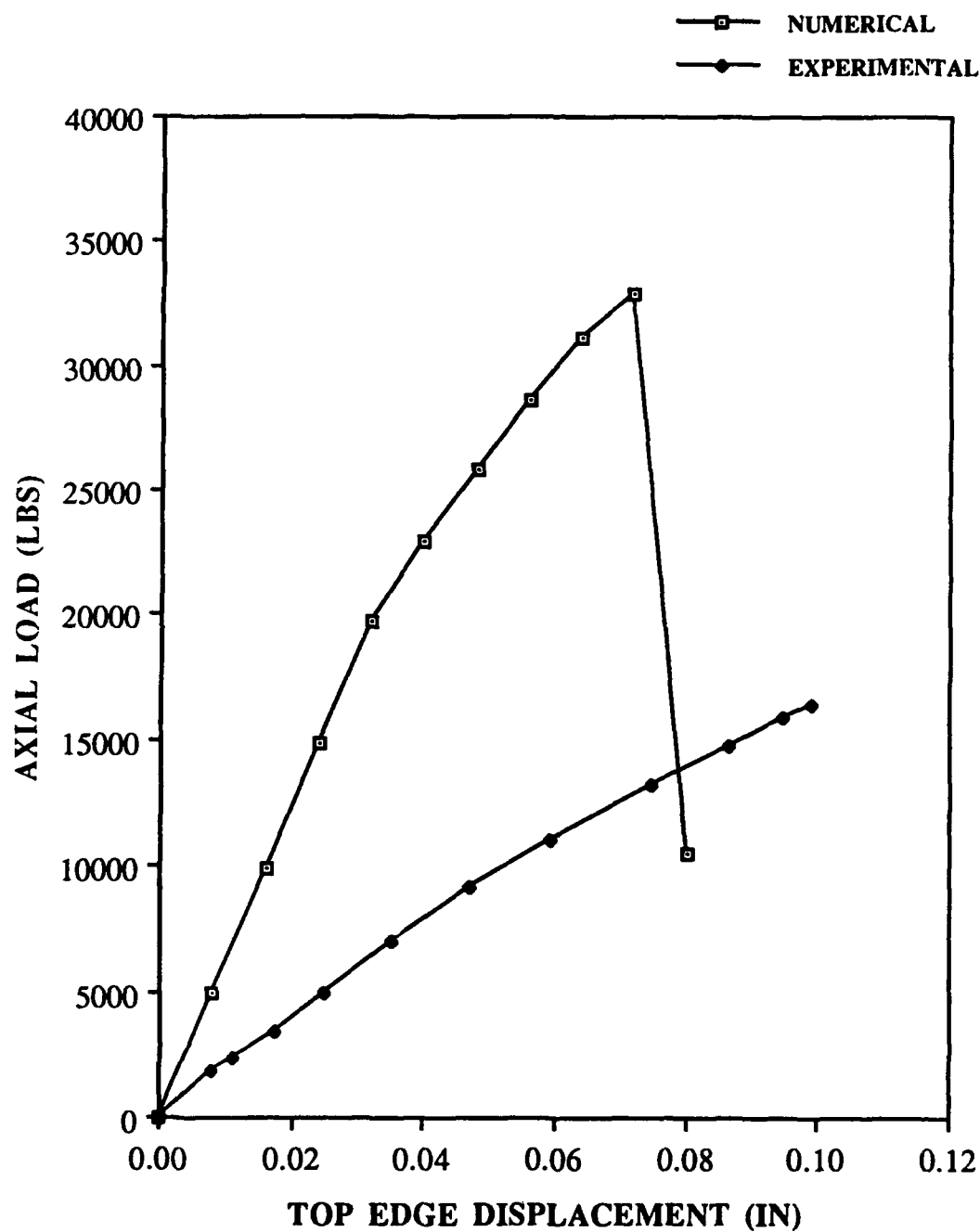


Fig. 95: Load vs. Top Edge Displacement,  
[0/+45/-45/90]3s, No Cutout  
(12" X 20")



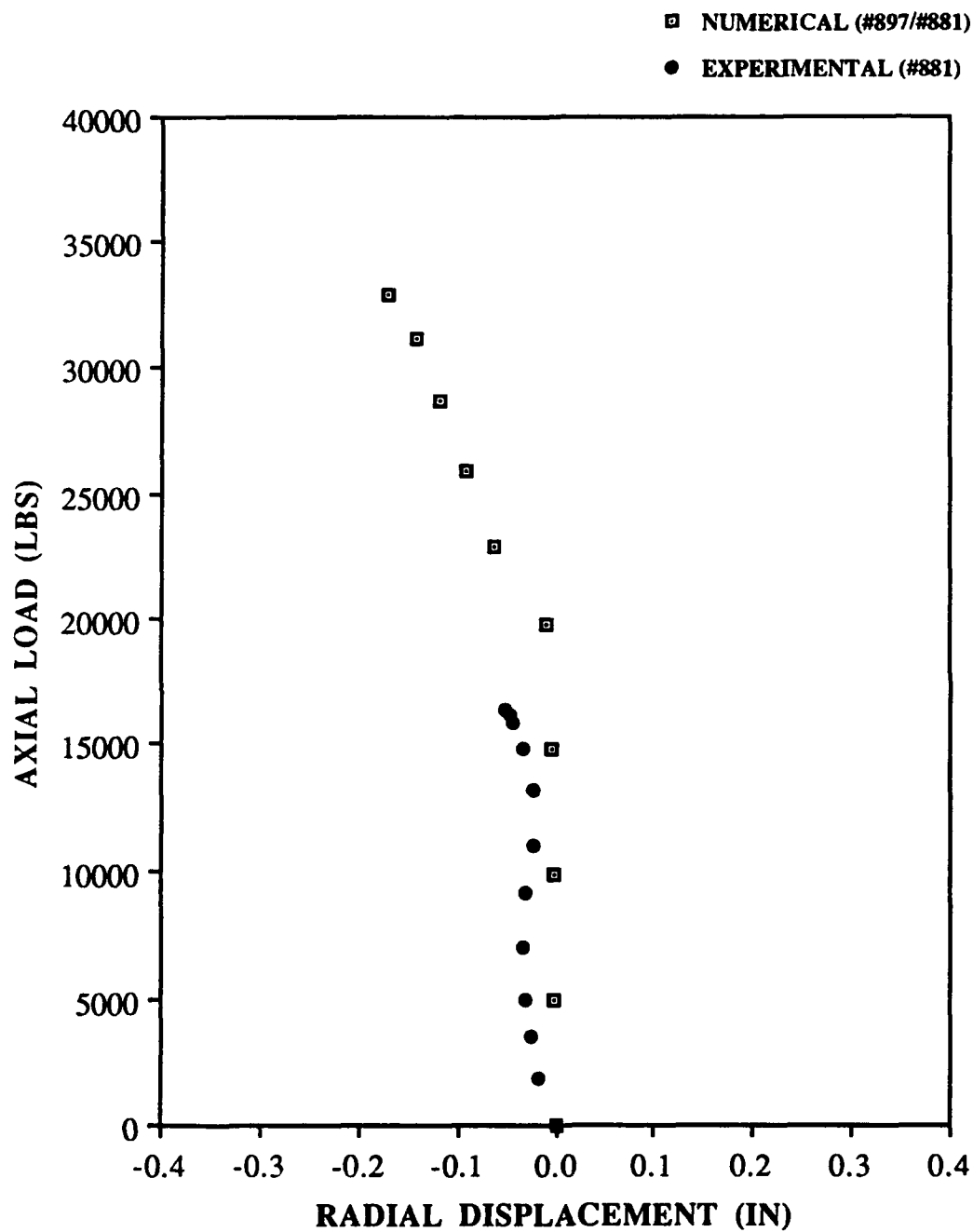


Fig. 96: Load vs. Radial Displacement,  
[0/+45/-45/90]3s, No Cutout  
(12" X 20")

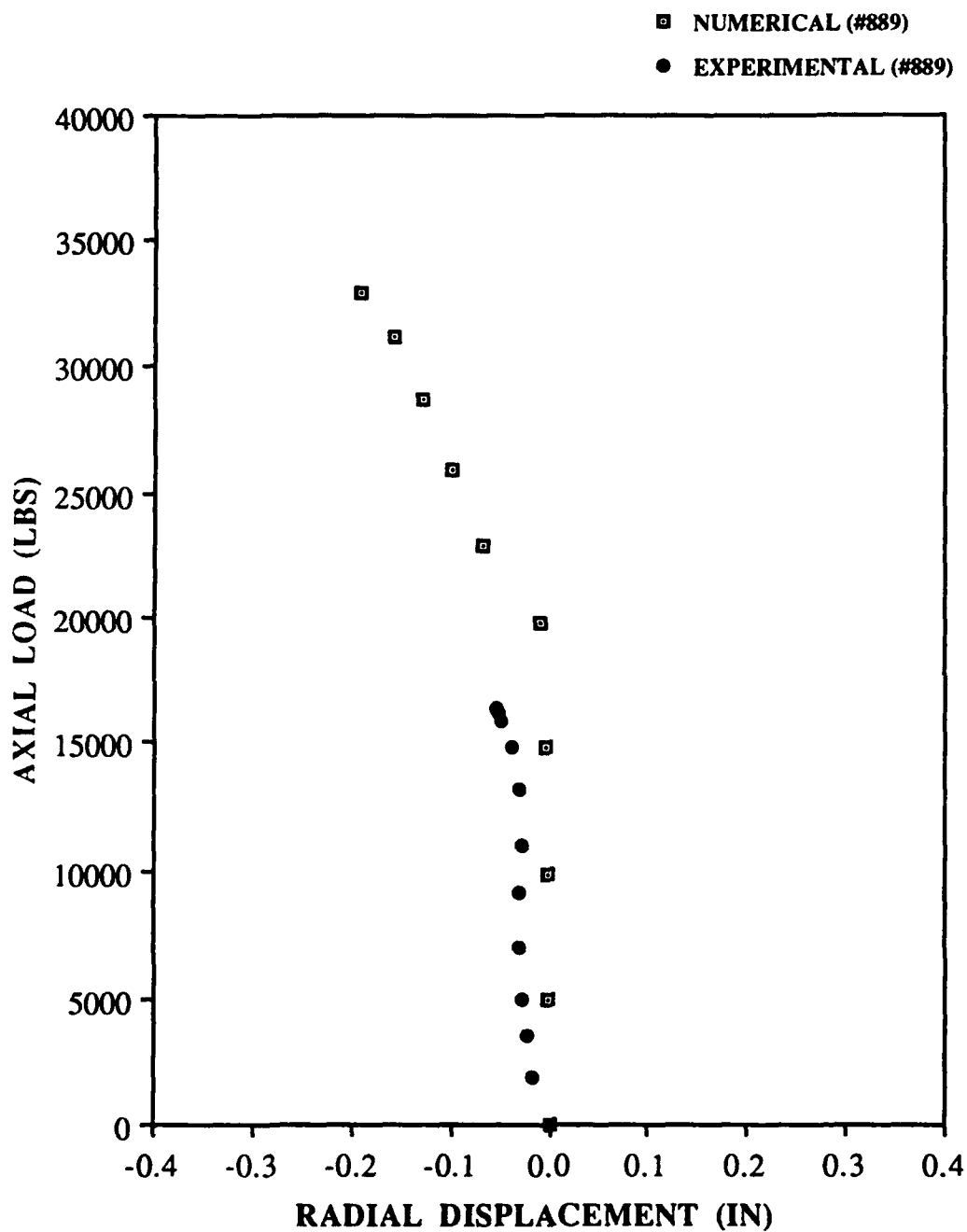


Fig. 97: Load vs. Radial Displacement,  
[0/+45/-45/90]3s, No Cutout  
(12" X 20")

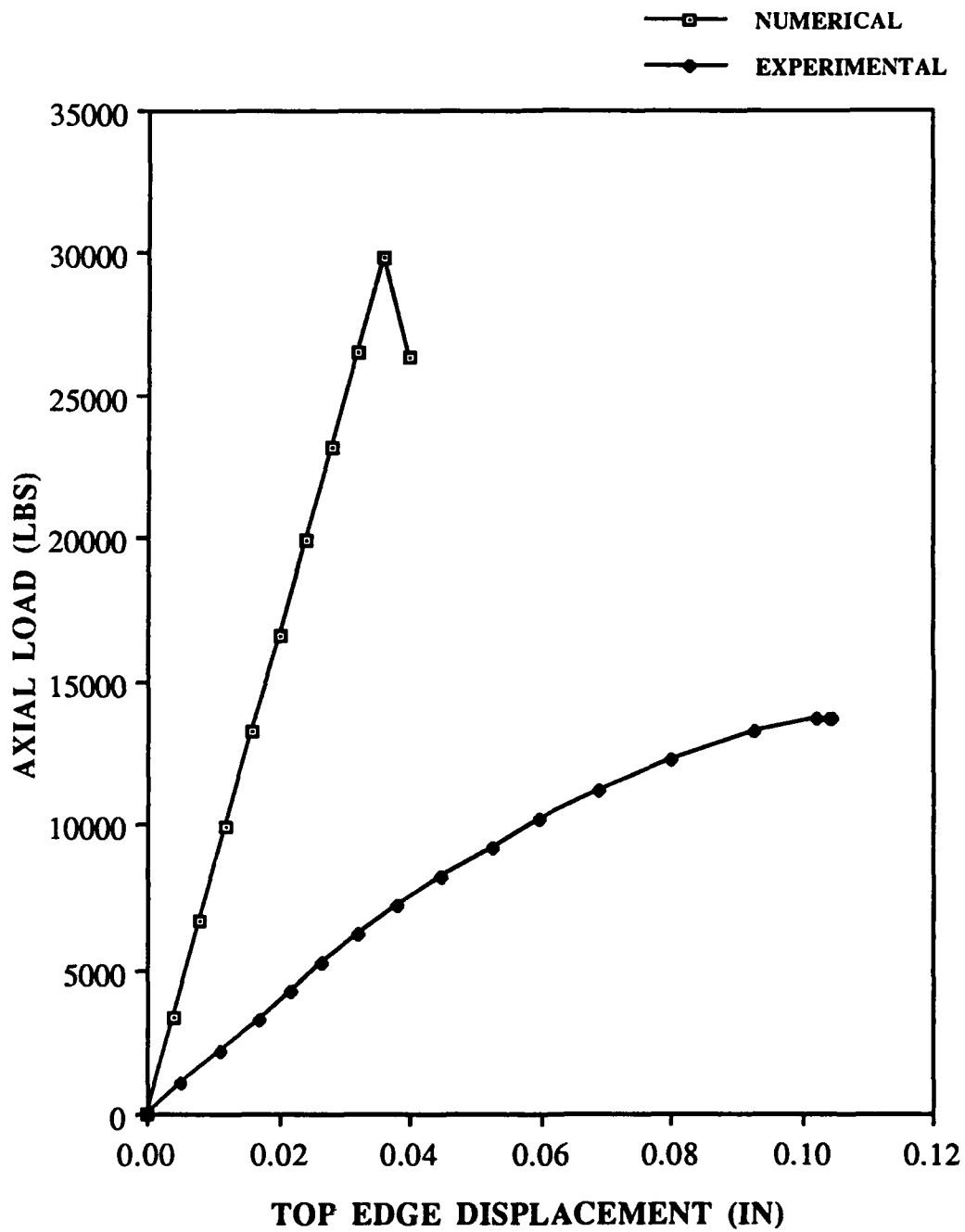


Fig. 98: Load vs. Top Edge Displacement,  
[0/90]6s, No Cutout  
(12" X 20")

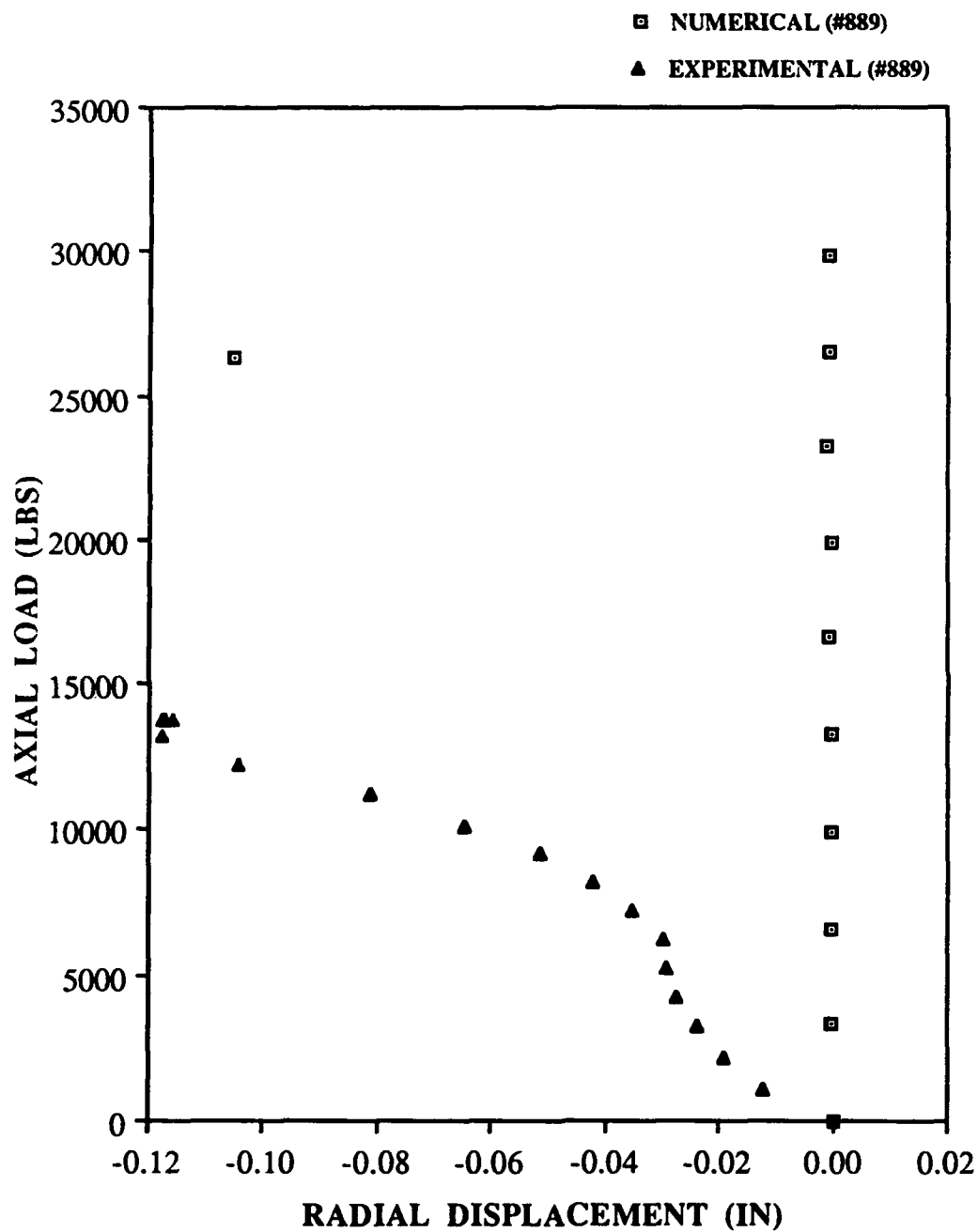


Fig. 99: Load vs. Radial Displacement,  
[0/90]6s, No Cutout  
(12" X 20")

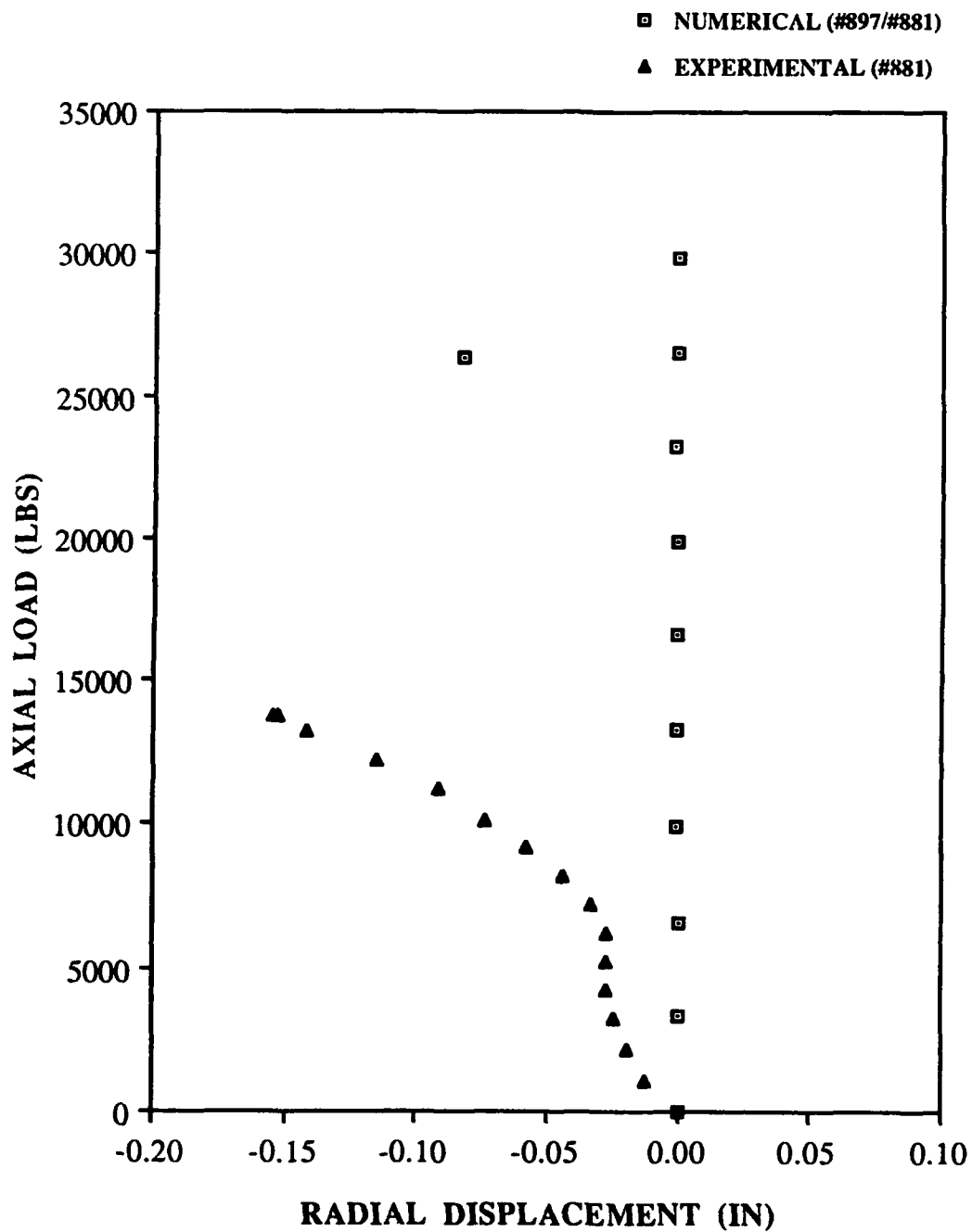


Fig. 100: Load vs. Radial Displacement,  
[0/90]6s, No Cutout  
(12" X 20")

## **APPENDIX C**

### **SAMPLE INPUT DECKS USED IN THE SHELL FINITE-ELEMENT PROGRAM**

## **SHELL INPUT DECK SEQUENCE**

- \* Title
- \* Cylindrical Shell Element, Nodes Per Element, Nonlinear Analysis, Symmetric Laminate, Large Rotation Shell, Mesh Generation Indicator, Indicator to Not Print Elasticity Matrices, Number of Elements in Cutout
- \* Load Displacement Increment, Number of Increments, Maximum Number of Iterations Per Increment, Indicator for Stiffness to Update Every Iteration, Percent Convergence Tolerance (Value is Percent Tolerance / 100)
- \* Real Number Multiplicative Factors of Prescribed Displacement
- \* Number of Elemental Subdivisions in the X and Y Directions
- \* Distance Between Nodes Along the X Direction (Values in Inches)
- \* Distance Between Nodes Along the Y Direction (Values in Inches)
- \* Assigned Element Numbers to Cut Out (Delete) From Shell Structure
- \* Load Type Parameter, Distributed Loading Intensity
- \* Number of Nodes With Specified Primary Degrees of Freedom
- \* Node Number and Seven Specified Degrees of Freedom (1 = "Prescribed" and 0 = "Free")  
Note: One Line Per Node; Nodes Within Cutout Elements Must be Prescribed With Zero Displacements
- \* Values of the Specified Degrees of Freedom (Either Zero or the Prescribed Displacement Increment in Inches)
- \* Number of Point Loads (Zero For This Research Effort)
- \* Material Properties for Composite Laminate:  $E_1$ ,  $E_2$ ,  $G_{12}$ ,  $\nu_{12}$ ,  $G_{13}$ ,  $G_{23}$  (Values in Psi)
- \* Number of Plies, Average Ply Thickness (Value in Inches)
- \* Ply Orientation Angles (Values in Degrees)
- \* Shell Radius of Curvature (Value in Inches)
- \* Number of Equivalent Nodal Forces to Calculate (Equals Number of Top-Edge Nodes Where Distributed Loading Occurs)
- \* Degree of Freedom Number, Associated With Loading Direction, For Each Top-Edge Node
- \* Number of Elements Where Stress Calculations Are Desired (Last Entry in Deck)

12X12 [0/90]2s No Cutout

2,8,0,2,0,1,0,0.

1,20,80,0,.001

1.,2.,3.,4.,5.,6.,7.,8.,9.,10.,11.,12.,

13.,14.,15.,16.,17.,18.,19.,20.

24,24

0.25,0.25,0.25,0.25,0.25,0.25,0.25,0.25,

0.25,0.25,0.25,0.25,0.25,0.25,0.25,0.25,

0.25,0.25,0.25,0.25,0.25,0.25,0.25,0.25,

0.25,0.25,0.25,0.25,0.25,0.25,0.25,0.25,

0.25,0.25,0.25,0.25,0.25,0.25,0.25,0.25,

0.25,0.25,0.25,0.25,0.25,0.25,0.25,0.25,

0.25,0.25,0.25,0.25,0.25,0.25,0.25,0.25,

0.25,0.25,0.25,0.25,0.25,0.25,0.25,0.25,

0.25,0.25,0.25,0.25,0.25,0.25,0.25,0.25,

0.25,0.25,0.25,0.25,0.25,0.25,0.25,0.25,

0.25,0.25,0.25,0.25,0.25,0.25,0.25,0.25,

0.25,0.25,0.25,0.25,0.25,0.25,0.25,0.25,

0,0.0

98

49,1,1,1,1,1,1,1

74,1,1,0,0,0,0,0

123,1,1,1,1,1,1,1

148,1,1,0,0,0,0,0

197,1,1,1,1,1,1,1

222,1,1,0,0,0,0,0

271,1,1,1,1,1,1,1

296,1,1,0,0,0,0,0

345,1,1,1,1,1,1,1

370,1,1,0,0,0,0,0

419,1,1,1,1,1,1,1

444,1,1,0,0,0,0,0

493,1,1,1,1,1,1,1

518,1,1,0,0,0,0,0

567,1,1,1,1,1,1,1

592,1,1,0,0,0,0,0

641,1,1,1,1,1,1,1

666,1,1,0,0,0,0,0

715,1,1,1,1,1,1,1

740,1,1,0,0,0,0,0

789,1,1,1,1,1,1,1

814,1,1,0,0,0,0,0

863,1,1,1,1,1,1,1

888,1,1,0,0,0,0,0

937,1,1,1,1,1,1,1

962,1,1,0,0,0,0,0

1011,1,1,1,1,1,1,1

1036,1,1,0,0,0,0,0

1085,1,1,1,1,1,1,1



1110,1,1,0,0,0,0,0  
 1159,1,1,1,1,1,1,1  
 1184,1,1,0,0,0,0,0  
 1233,1,1,1,1,1,1,1  
 1258,1,1,0,0,0,0,0  
 1307,1,1,1,1,1,1,1  
 1332,1,1,0,0,0,0,0  
 1381,1,1,1,1,1,1,1  
 1406,1,1,0,0,0,0,0  
 1455,1,1,1,1,1,1,1  
 1480,1,1,0,0,0,0,0  
 1529,1,1,1,1,1,1,1  
 1554,1,1,0,0,0,0,0  
 1603,1,1,1,1,1,1,1  
 1628,1,1,0,0,0,0,0  
 1677,1,1,1,1,1,1,1  
 1702,1,1,0,0,0,0,0  
 1751,1,1,1,1,1,1,1  
 1776,1,1,0,0,0,0,0  
 1825,1,1,1,1,1,1,1  
 1,1,1,1,1,1,1  
 50,1,1,0,0,0,0,0  
 75,1,1,1,1,1,1,1  
 124,1,1,0,0,0,0,0  
 149,1,1,1,1,1,1,1  
 198,1,1,0,0,0,0,0  
 223,1,1,1,1,1,1,1  
 272,1,1,0,0,0,0,0  
 297,1,1,1,1,1,1,1  
 346,1,1,0,0,0,0,0  
 371,1,1,1,1,1,1,1  
 420,1,1,0,0,0,0,0  
 445,1,1,1,1,1,1,1  
 494,1,1,0,0,0,0,0  
 519,1,1,1,1,1,1,1  
 568,1,1,0,0,0,0,0  
 593,1,1,1,1,1,1,1  
 642,1,1,0,0,0,0,0  
 667,1,1,1,1,1,1,1  
 716,1,1,0,0,0,0,0  
 741,1,1,1,1,1,1,1  
 790,1,1,0,0,0,0,0  
 815,1,1,1,1,1,1,1  
 864,1,1,0,0,0,0,0  
 889,1,1,1,1,1,1,1  
 938,1,1,0,0,0,0,0  
 963,1,1,1,1,1,1,1  
 1012,1,1,0,0,0,0,0  
 1037,1,1,1,1,1,1,1  
 1086,1,1,0,0,0,0,0  
 1111,1,1,1,1,1,1,1  
 1160,1,1,0,0,0,0,0

180

```
0
19.7e6,1.579e6,0.925e6,0.276,
0.925e6,0.462e6
8,0.00514
0.,90.,0.,90.,90.,0.,90.,0.
```

49

0

12X20 [0/45/-45/90]3s 4" Cutout  
 2,8,0,2,0,1,0,64  
 1,25,80,0,.001  
 1.,2.,3.,4.,5.,6.,7.,8.,9.,10.,11.,12.,  
 13.,14.,15.,16.,17.,18.,19.,20.,21.,22.,  
 23.,24.,25.  
 28,20  
 0.50,0.50,0.50,0.50,0.50,0.50,0.50,0.50,  
 0.50,0.50,0.50,0.50,0.25,0.25,0.25,0.25,  
 0.25,0.25,0.25,0.25,0.25,0.25,0.25,0.25,  
 0.25,0.25,0.25,0.25,0.25,0.25,0.25,0.25,  
 0.25,0.25,0.25,0.25,0.25,0.25,0.25,0.25,  
 0.25,0.25,0.25,0.25,0.50,0.50,0.50,0.50,  
 0.50,0.50,0.50,0.50,0.50,0.50,0.50,0.50,  
 0.50,0.50,0.50,0.50,0.25,0.25,0.25,0.25,  
 0.25,0.25,0.25,0.25,0.25,0.25,0.25,0.25,  
 0.25,0.25,0.25,0.25,0.25,0.25,0.25,0.25,  
 0.25,0.25,0.25,0.25,0.25,0.25,0.25,0.25,  
 0.25,0.25,0.25,0.25,0.50,0.50,0.50,0.50,  
 179,180,181,182,183,184,185,186,207,208,  
 209,210,211,212,213,214,235,236,237,238,  
 239,240,241,242,263,264,265,266,267,268,  
 269,270,291,292,293,294,295,296,297,298,  
 319,320,321,322,323,324,325,326,347,348,  
 349,350,351,352,353,354,375,376,377,378,  
 379,380,381,382  
 0,0.0  
 243  
 57,1,1,1,1,1,1,1  
 86,1,1,0,0,0,0,0  
 143,1,1,1,1,1,1,1  
 172,1,1,0,0,0,0,0  
 229,1,1,1,1,1,1,1  
 258,1,1,0,0,0,0,0  
 315,1,1,1,1,1,1,1  
 344,1,1,0,0,0,0,0  
 401,1,1,1,1,1,1,1  
 430,1,1,0,0,0,0,0  
 487,1,1,1,1,1,1,1  
 516,1,1,0,0,0,0,0  
 573,1,1,1,1,1,1,1  
 602,1,1,0,0,0,0,0  
 659,1,1,1,1,1,1,1  
 688,1,1,0,0,0,0,0  
 745,1,1,1,1,1,1,1  
 774,1,1,0,0,0,0,0  
 831,1,1,1,1,1,1,1  
 860,1,1,0,0,0,0,0  
 917,1,1,1,1,1,1,1  
 946,1,1,0,0,0,0,0

1003,1,1,1,1,1,1,1  
 1032,1,1,0,0,0,0,0  
 1089,1,1,1,1,1,1,1  
 1118,1,1,0,0,0,0,0  
 1175,1,1,1,1,1,1,1  
 1204,1,1,0,0,0,0,0  
 1261,1,1,1,1,1,1,1  
 1290,1,1,0,0,0,0,0  
 1347,1,1,1,1,1,1,1  
 1376,1,1,0,0,0,0,0  
 1433,1,1,1,1,1,1,1  
 1462,1,1,0,0,0,0,0  
 1519,1,1,1,1,1,1,1  
 1548,1,1,0,0,0,0,0  
 1605,1,1,1,1,1,1,1  
 1634,1,1,0,0,0,0,0  
 1691,1,1,1,1,1,1,1  
 1720,1,1,0,0,0,0,0  
 1777,1,1,1,1,1,1,1  
 1,1,1,1,1,1,1,1  
 58,1,1,0,0,0,0,0  
 87,1,1,1,1,1,1,1  
 144,1,1,0,0,0,0,0  
 173,1,1,1,1,1,1,1  
 230,1,1,0,0,0,0,0  
 259,1,1,1,1,1,1,1  
 316,1,1,0,0,0,0,0  
 345,1,1,1,1,1,1,1  
 402,1,1,0,0,0,0,0  
 431,1,1,1,1,1,1,1  
 488,1,1,0,0,0,0,0  
 517,1,1,1,1,1,1,1  
 574,1,1,0,0,0,0,0  
 603,1,1,1,1,1,1,1  
 660,1,1,0,0,0,0,0  
 689,1,1,1,1,1,1,1  
 746,1,1,0,0,0,0,0  
 775,1,1,1,1,1,1,1  
 832,1,1,0,0,0,0,0  
 861,1,1,1,1,1,1,1  
 918,1,1,0,0,0,0,0  
 947,1,1,1,1,1,1,1  
 1004,1,1,0,0,0,0,0  
 1033,1,1,1,1,1,1,1  
 1090,1,1,0,0,0,0,0  
 1119,1,1,1,1,1,1,1  
 1176,1,1,0,0,0,0,0  
 1205,1,1,1,1,1,1,1  
 1262,1,1,0,0,0,0,0  
 1291,1,1,1,1,1,1,1

1348,1,1,0,0,0,0,0  
1377,1,1,1,1,1,1,1  
1434,1,1,0,0,0,0,0  
1463,1,1,1,1,1,1,1  
1520,1,1,0,0,0,0,0  
1549,1,1,1,1,1,1,1  
1606,1,1,0,0,0,0,0  
1635,1,1,1,1,1,1,1  
1692,1,1,0,0,0,0,0  
1721,1,1,1,1,1,1,1  
585,1,1,0,0,0,0,0  
586,1,1,0,0,0,0,0  
587,1,1,0,0,0,0,0  
588,1,1,0,0,0,0,0  
589,1,1,0,0,0,0,0  
590,1,1,0,0,0,0,0  
591,1,1,0,0,0,0,0  
624,1,1,0,0,0,0,0  
625,1,1,1,1,1,1,1  
626,1,1,0,0,0,0,0  
627,1,1,1,1,1,1,1  
628,1,1,0,0,0,0,0  
629,1,1,1,1,1,1,1  
630,1,1,0,0,0,0,0  
631,1,1,1,1,1,1,1  
632,1,1,0,0,0,0,0  
633,1,1,1,1,1,1,1  
634,1,1,0,0,0,0,0  
635,1,1,1,1,1,1,1  
636,1,1,0,0,0,0,0  
637,1,1,1,1,1,1,1  
638,1,1,0,0,0,0,0  
671,1,1,0,0,0,0,0  
672,1,1,0,0,0,0,0  
673,1,1,0,0,0,0,0  
674,1,1,0,0,0,0,0  
675,1,1,0,0,0,0,0  
676,1,1,0,0,0,0,0  
677,1,1,0,0,0,0,0  
710,1,1,0,0,0,0,0  
711,1,1,1,1,1,1,1  
712,1,1,0,0,0,0,0  
713,1,1,1,1,1,1,1  
714,1,1,0,0,0,0,0  
715,1,1,1,1,1,1,1  
716,1,1,0,0,0,0,0  
717,1,1,1,1,1,1,1  
718,1,1,0,0,0,0,0  
719,1,1,1,1,1,1,1  
720,1,1,0,0,0,0,0  
721,1,1,1,1,1,1,1  
722,1,1,0,0,0,0,0

723,1,1,1,1,1,1,1  
724,1,1,0,0,0,0,0  
757,1,1,0,0,0,0,0  
758,1,1,0,0,0,0,0  
759,1,1,0,0,0,0,0  
760,1,1,0,0,0,0,0  
761,1,1,0,0,0,0,0  
762,1,1,0,0,0,0,0  
763,1,1,0,0,0,0,0  
796,1,1,0,0,0,0,0  
797,1,1,1,1,1,1,1  
798,1,1,0,0,0,0,0  
799,1,1,1,1,1,1,1  
800,1,1,0,0,0,0,0  
801,1,1,1,1,1,1,1  
802,1,1,0,0,0,0,0  
803,1,1,1,1,1,1,1  
804,1,1,0,0,0,0,0  
805,1,1,1,1,1,1,1  
806,1,1,0,0,0,0,0  
807,1,1,1,1,1,1,1  
808,1,1,0,0,0,0,0  
809,1,1,1,1,1,1,1  
810,1,1,0,0,0,0,0  
843,1,1,0,0,0,0,0  
844,1,1,0,0,0,0,0  
845,1,1,0,0,0,0,0  
846,1,1,0,0,0,0,0  
847,1,1,0,0,0,0,0  
848,1,1,0,0,0,0,0  
849,1,1,0,0,0,0,0  
882,1,1,0,0,0,0,0  
883,1,1,1,1,1,1,1  
884,1,1,0,0,0,0,0  
885,1,1,1,1,1,1,1  
886,1,1,0,0,0,0,0  
887,1,1,1,1,1,1,1  
888,1,1,0,0,0,0,0  
889,1,1,1,1,1,1,1  
890,1,1,0,0,0,0,0  
891,1,1,1,1,1,1,1  
892,1,1,0,0,0,0,0  
893,1,1,1,1,1,1,1  
894,1,1,0,0,0,0,0  
895,1,1,1,1,1,1,1  
896,1,1,0,0,0,0,0  
929,1,1,0,0,0,0,0  
930,1,1,0,0,0,0,0  
931,1,1,0,0,0,0,0  
932,1,1,0,0,0,0,0  
933,1,1,0,0,0,0,0  
934,1,1,0,0,0,0,0

935,1,1,0,0,0,0,0  
968,1,1,0,0,0,0,0  
969,1,1,1,1,1,1,1  
970,1,1,0,0,0,0,0  
971,1,1,1,1,1,1,1  
972,1,1,0,0,0,0,0  
973,1,1,1,1,1,1,1  
974,1,1,0,0,0,0,0  
975,1,1,1,1,1,1,1  
976,1,1,0,0,0,0,0  
977,1,1,1,1,1,1,1  
978,1,1,0,0,0,0,0  
979,1,1,1,1,1,1,1  
980,1,1,0,0,0,0,0  
981,1,1,1,1,1,1,1  
982,1,1,0,0,0,0,0  
1015,1,1,0,0,0,0,0  
1016,1,1,0,0,0,0,0  
1017,1,1,0,0,0,0,0  
1018,1,1,0,0,0,0,0  
1019,1,1,0,0,0,0,0  
1020,1,1,0,0,0,0,0  
1021,1,1,0,0,0,0,0  
1054,1,1,0,0,0,0,0  
1055,1,1,1,1,1,1,1  
1056,1,1,0,0,0,0,0  
1057,1,1,1,1,1,1,1  
1058,1,1,0,0,0,0,0  
1059,1,1,1,1,1,1,1  
1060,1,1,0,0,0,0,0  
1061,1,1,1,1,1,1,1  
1062,1,1,0,0,0,0,0  
1063,1,1,1,1,1,1,1  
1064,1,1,0,0,0,0,0  
1065,1,1,1,1,1,1,1  
1066,1,1,0,0,0,0,0  
1067,1,1,1,1,1,1,1  
1068,1,1,0,0,0,0,0  
1101,1,1,0,0,0,0,0  
1102,1,1,0,0,0,0,0  
1103,1,1,0,0,0,0,0  
1104,1,1,0,0,0,0,0  
1105,1,1,0,0,0,0,0  
1106,1,1,0,0,0,0,0  
1107,1,1,0,0,0,0,0  
1140,1,1,0,0,0,0,0  
1141,1,1,1,1,1,1,1  
1142,1,1,0,0,0,0,0  
1143,1,1,1,1,1,1,1  
1144,1,1,0,0,0,0,0  
1145,1,1,1,1,1,1,1  
1146,1,1,0,0,0,0,0



187

188

```

0.,0.,0.,0.,0.,0.,0.,0.,0.,0.,
0.,0.,0.,0.,0.,0.,0.,0.,0.,0.,
0.,0.,0.,0.,0.,0.,0.,0.,0.,0.,
0.,0.,0.,0.,0.,0.,0.,0.,0.,0.,
0.,0.,0.,0.,0.,0.,0.,0.,0.,0.,
0.,0.
0
19.7e6,1.579e6,0.925e6,0.276,
0.925e6,0.462e6
24,0.00542
0.,45.,-45.,90.,0.,45.,-45.,90.,0.,45.,-45.,90.,90.,-45.,
45.,0.,90.,-45.,45.,0.,90.,-45.,45.,0.
12.0
41
253,316,570,633,887,950,1204,1267,1521,1584,
1838,1901,2155,2218,2472,2535,2789,2852,3106,
3169,3423,3486,3740,3803,4057,4120,4374,4437,
4691,4754,5008,5071,5325,5388,5642,5705,5959,
6022,6276,6339,6593
0

```

## VITA

Captain James C. Hatfield was born on 7 July 1959 in Albany, New York. He graduated from Pascack Hills High School in Montvale, New Jersey in 1977. Captain Hatfield then attended Purdue University, graduating with a Bachelor of Science in Aeronautical and Astronautical Engineering in 1981; receiving his commission through the 4-year Air Force ROTC program, where he was a distinguished graduate. Captain Hatfield's first assignment was to HQ Foreign Technology Division (FTD), recently renamed the Foreign Aerospace Science and Technology Center, at Wright-Patterson AFB in Ohio. There as a Ballistic Missile Systems Engineer, he was responsible for analyzing the capabilities of two major foreign weapon systems and publishing technical studies for the Defense Intelligence Agency. Also at this time, he attended graduate school part-time at the University of Dayton and received a Master of Business Administration degree. Upon completion of this assignment in 1984, Captain Hatfield went to FTD's Far East detachment at Yokota AB near Tokyo, Japan. There he was responsible for managing the collection of aerospace technologies of interest to the Air Force, as well as, acting as a liaison with the Japanese Air Self Defense Force (JASDF). In 1987, Captain Hatfield was reassigned to Air Force ROTC Detachment 905 at Washington State University in Pullman, Washington. During his four-year tenure as the Commandant of Cadets and senior-level academic instructor, the detachment was awarded two consecutive Air Force Organizational Excellence Awards. In May 1991, Captain Hatfield entered the School of Engineering at the Air Force Institute of Technology.

Permanent Address: 110 Clairmont Drive  
Woodcliff Lake, NJ 07675

# REPORT DOCUMENTATION PAGE

Form Approved  
OMB No. 0704-0188

Public reporting burden for this collection of information is estimated to average 1 hour per response, including the time for reviewing instructions, searching existing data sources, gathering and maintaining the data needed, and completing and reviewing the collection of information. Send comments regarding this burden estimate or any other aspect of this collection of information, including suggestions for reducing this burden, to Washington Headquarters Services, Directorate for Information Operations and Reports, 1215 Jefferson Davis Highway, Suite 1204, Arlington, VA 22202-4302, and to the Office of Management and Budget, Paperwork Reduction Project (0704-0188), Washington, DC 20503.

1. AGENCY USE ONLY (Leave blank)		2. REPORT DATE December 1992	3. REPORT TYPE AND DATES COVERED Master's Thesis
4. TITLE AND SUBTITLE EFFECT OF THICKNESS AND PLY LAYUP ON THE COLLAPSE CHARACTERISTICS OF CYLINDRICAL COMPOSITE SHELLS WITH LARGE CUTOUTS			5. FUNDING NUMBERS
6. AUTHOR(S)  James C. Hatfield, Captain, USAF			
7. PERFORMING ORGANIZATION NAME(S) AND ADDRESS(ES)  Air Force Institute of Technology, WPAFB OH 45433-6583			8. PERFORMING ORGANIZATION REPORT NUMBER  AFIT/GAE/ENY/92D-20
9. SPONSORING / MONITORING AGENCY NAME(S) AND ADDRESS(ES) Dr. R.S. Sandhu WL/FIBCA Bldg 45, Wright-Patterson AFB, OH 45433-6553			10. SPONSORING / MONITORING AGENCY REPORT NUMBER
11. SUPPLEMENTARY NOTES			
12a. DISTRIBUTION / AVAILABILITY STATEMENT  Approved for public release; distribution unlimited			12b. DISTRIBUTION CODE
13. ABSTRACT (Maximum 200 words) This study involved a numerical and experimental investigation of the geometric instability(collapse loads/displacements) of vertically unsupported graphite/epoxy cylindrical shell panels undergoing axial compression. Symmetric quasi-isotropic and cross-ply laminates, with and without 4"X4" centralized cutouts, were investigated for three thicknesses:8,16,and 24 plies. The experimental data was compared to results from SHELL, a geometrically nonlinear finite-element computer program which incorporates a parabolic transverse shear strain distribution through the thickness. Good correlation was obtained for shells with large cutouts between the SHELL numerical data and the experimental results. This research verified that the SHELL program will provide good predictions of the collapse characteristics of shell structures undergoing large displacements and moderately large rotations. It was found that the magnitudes of transverse shear strain increased with increasing panel thickness and increased significantly when a large cutout was placed in a shell. Also, there were indications that under large displacement and moderately large rotation conditions, the collapse of cross-ply shells was more affected by transverse shear strain than the collapse of quasi-isotropic shells.			
14. SUBJECT TERMS Composites, Shells, Cylindrical Panels, Cutouts, Finite Elements, Nonlinear Analysis, Transverse Shear, Geometric Instability, Collapse, Graphite/Epoxy			15. NUMBER OF PAGES 203
			16. PRICE CODE
17. SECURITY CLASSIFICATION OF REPORT Unclassified	18. SECURITY CLASSIFICATION OF THIS PAGE Unclassified	19. SECURITY CLASSIFICATION OF ABSTRACT Unclassified	20. LIMITATION OF ABSTRACT UL